UNIVERSITY OF SOUTHAMPTON

FACULTY OF ENGINEERING AND THE ENVIRONMENT

Materials and Surface Engineering

A dry powder micro delivery device for

multiple material additive manufacturing

by

Srisit Chianrabutra

Thesis for the degree of Doctor of Philosophy

September 2015

UNIVERSITY OF SOUTHAMPTON

ABSTRACT

FACULTY OF ENGINEERING AND THE ENVIRONMENT

Materials and Surface Engineering

Thesis for the degree of Doctor of Philosophy

A DRY POWDER MICRO DELIVERY DEVICE FOR MULTIPLE MATERIAL ADDITIVE MANUFACTURING

Srisit Chianrabutra

This thesis focuses on developing a novel material delivery device for a Multiple Material Additive Manufacturing (MMAM) system using a Dry Powder Printing (DPP) technique developed recently. The goal of the thesis was to study in detail the characteristic of a micro dispensing device utilizing ultrasonic vibration via a piezoelectric transducer, which was designed and constructed to handle a wide range of fine powder materials. The research systematically investigated the nature of the interaction between the device and the materials, which allowed the design and processing parameters to be understood. Experiments were conducted to explain the effects of the printing parameters on printing results so as to discover the basic characteristics of the new dry powder printing device. Moreover, weight measurements of the deposited powder, microscopy and image visualization was used to assess the behavior of the device.

The device developed can successfully provide continuity, consistency and reliability of layer printing of multiple material powders. The results demonstrated that the device is capable of dispensing various types of fine powders, such as metals, polymers and ceramics, with particle sizes of between 14-72 μm. The relative standard deviation of the device is less than 7%. The minimum mass flow rate can be reached at 0.14 mg/s for a cohesive powder such as a copper powder. The maximum moving speed is up to 50 mm/s for a free flowing powder such as a

solder powder. Currently, the precise printing of micro geometries can be achieved up to a diameter as small as 85 μm. Moreover, the study also reveals that the performance of the device mainly depends on the dispensing parameters (e.g. nozzle diameter, nozzle angle, and piezoelectric position), material parameters (e.g. type, particle size, flowability) and process parameters (e.g. moving speed, signal voltage and standoff distance). High resolution printing by the device can be achieved by controlling these parameters. This work has shown that the dispenser can deliver different powders in very precise and small quantities at almost any designated position. This demonstrates the potential of this method for a multiple material delivery system for MMAM in the near future.

Table of Contents

List of tables

List of figures

DECLARATION OF AUTHORSHIP

I, Srisit Chianrabutra declare that this thesis and the work presented in it are my own and have been generated by me as the result of my own original research.

A dry powder micro delivery device for multiple material additive manufacturing

I confirm that:

1. This work was done wholly or mainly while in candidature for a research degree at this University;
2. Where any part of this thesis has previously been submitted for a degree or any other qualification at this University or any other institution, this has been clearly stated;
3. Where I have consulted the published work of others, this is always clearly attributed;
4. Where I have quoted from the work of others, the source is always given. With the exception of such quotations, this thesis is entirely my own work;
5. I have acknowledged all main sources of help;
6. Where the thesis is based on work done by myself jointly with others, I have made clear exactly what was done by others and what I have contributed myself;
7. None of this work has been published before submission, or parts of this work have been published as listed in Appendix C.

Signed: .....

Date: .....

Acknowledgements

Apart from the efforts of myself, the success of this thesis depends on the supports and helps of many others. I take this opportunity to express my deepest gratitude to those who have contributed with their advice and experience to the work in this thesis.

I would like to thank my principal supervisor, Dr. Shoufeng Yang, for the excellent direction, guidance, support, patience and engagement throughout the learning process of this thesis. I also would like to thank Dr.Brian Mellor, who is my second supervisor, for the good advice, useful comments and his patience during the corrections of my thesis. Without their assistances, this thesis would not have been possible.

I would like to acknowledge the important role of the staff of Engineering Faculty, who gave permission to use all required facilities and the necessary equipment to complete the task. Additionally, I sincerely thank the EPSRC Engineering Instrument Pool for providing the loan of a Photron FASTCAM high speed camera. Furthermore, I thank my fellow's postgraduates within my research group at University of Southampton, who were always willing to help and give their best suggestions. It would be lonely without them.

I also would like to thank those people outside the academic word who have been there to always support and encourage me with their best wishes, in particular my wife and my family.

Finally, I would like to thank The Royal Thai Government for supporting this study by providing my scholarship.

Abbreviations

3DP	-	3D Printing
AM	-	Additive Manufacturing
CIJ	-	Continuous Inkjet
DW	-	Direct writing
DMD	-	Direct Metal Deposition
DMM	-	Discrete Multiple Material
DoD	-	Drop on Demand
DPP	-	Dry Powder Printing
EBM	-	Electron Beam Melting
FDM	-	Fused Deposition Modeling
FGM	-	Functionally Graded Material/Functionally Gradient Material
FDMM	-	Fuse Deposition Multi-Materials
LC	-	Laser Cladding
LCVD	-	Laser Chemical Vapour Deposition
LENS	-	Laser Engineering Net Shape
LOM	-	Laminated Object Manufacturing
MMAM	-	Multiple Material Additive Manufacturing
MIP-SL	-	Mask-Image-Projection-based Stereolithography
PJT	-	Poly Jetting Technology
RSD	-	Relative Standard Deviation
SDM	-	Shape Deposition Manufacturing
SMS	-	Selective Mask Sintering

SLS	-	Selective laser Sintering
SLM	-	Selective Laser Melting
SL or SLA	-	Stereolithography
STLG	-	Stereo-Thermal Lithography
UC	-	Ultrasonic Consolidation

Nomenclatures

Θ	-	Angle of repose	(degree)
Θ_w	-	Wall angle/Hopper angle/Hopper inclination	(degree)
ρ_a	-	Initial density	(kg/m^3)
ρ_b	-	Bulk density	(kg/m^3)
ρ_m	-	Mixture density	(kg/m^3)
ρ_t	-	Tap density	(kg/m^3)
σ_1	-	Major principle stress	(N/m^2)
σ_2	-	Minor principle stress	(N/m^2)
σ_C	-	Compacting stress	(N/m^2)
σ_D	-	Developing stress	(N/m^2)
σ_y	-	Unconfined yield stress	(N/m^2)
σ_{Crit}	-	Critical stress	(N/m^2)
ϕ	-	Wall friction angle	(degree)
φ	-	Hopper half-angle	(degree)
δ	-	Internal friction angle	(degree)
μ_w	-	Wall friction coefficient	(dimensionless)
A	-	Surface area	(m^2)
B	-	Outlet diameter	(m)
B_{Crit}	-	Critical outlet diameter	(m)
D_{33}	-	Piezoelectric constant	(dimensionless)
D	-	Outlet diameter	(m)
D_0	-	Hopper orifice diameter	(m)

D_p	-	Particle diameter	(m)
d_f	-	Fine particle diameter	(m)
d	-	Outlet size	(m)
d_c	-	Coarse particle diameter	(m)
d_m	-	Mixture diameter	(m)
d_p	-	Particle size	(m)
F_a	-	Downward force	(N)
F_b	-	Vibration force	(N)
F_f	-	Friction force	(N)
ff	-	Flow factor	(dimensionless)
FF	-	Function flow factor	(dimensionless)
g	-	Gravity	(N/m^2)
G	-	Gravitational force	(N)
h	-	Height	(m)
k	-	Particle shape constant	(dimensionless)
k_m	-	Coefficient mixture particle	(dimensionless)
m	-	Mass	(kg)
$\dot{m}$	-	Mass flow rate	(kg/s)
N	-	Normal force	(N)
Q	-	Mass flow rate	(kg/s)
S_{33}^E	-	Elastic constant	(dimensionless)
S	-	Standoff distance	(m)
U	-	Supplied voltage	(V)
v	-	Velocity	(m/s)

V	-	Volume	(m^3)
w_i	-	Dose mass	(kg)
w_{mean}	-	Mean dose mass	(kg)
X_f	-	Mass fraction	(dimensionless)

Chapter 1:

Introduction

This chapter describes the idea of this thesis. This includes the research motivation, objectives and a short summary of the main development of the thesis. In the last section, the structure and brief contents of this thesis are presented. The details will be given in the following sections.

1.1 Research motivation

In the existing worldwide economy, manufacturers continually develop their processes to remain competitive, reduce cost and compress production times. The customers, who buy the products need high quality, time responsiveness and personalization. The application of manufacturing such as Additive Manufacturing (AM) offers a potential means for achieving these requirements. Various AM techniques that automatically produce complex three dimensional parts from digital data have a dramatic impact on minimising lead times from months to weeks or days or even hours. However, the next generation of AM technology should provide full functionality, offer changeable material systems, and give the entire bonding system at an affordable price [1-3].

Multiple material objects are more interesting and will be highly important in many industrial applications. Multiple Material Additive Manufacturing (MMAM) is a newly developing technology that can fabricate three-dimensional multiple material (heterogeneous) objects. This technology can create multiple material objects and can vary material compositions within the layer [4]. The ability to print multiple materials by an additive manufacturing system can either improve the mechanical properties of the parts or provide additional functions to the 3D printed parts [5]. MMAM technology has the potential to become an important manufacturing resource for next generation technology. This is because single material AM systems cannot fulfil the requirements of some applications that require multiple material objects, such as compliant mechanisms, embedded components, 3D circuits, human tissues, medical compatible implants etc. Currently, most commercial additive manufacturing systems are designed to produce parts from a

single material [6]. Many research institutes and companies have been developing AM technologies to allow more materials to be used in single material AM technology, and to improve the properties of the AM parts and to enhance the capability of the basic process [5].

Powder based materials are very interesting as they can provide a wide variety of material options. In most of the current powder based AM systems, fine powders are spread using a roller onto a powder bed resulting in the impossibility of using multiple materials without cross-contamination [7, 8]. Therefore, it is essential to develop processing technologies that can handle fine powder particles for use in material delivery systems for the MMAM systems. The Dry Powder Printing (DPP) technique is one of the promising techniques available to dispense fine powders [9]. Among the DPP techniques, the ultrasonic dispensing method has many major advantages for depositing fine powders in terms of uniformity and controllability. In addition, this method has the great ability to handle a wide variety of powder materials. However, processing and handling powder materials is very challenging due to their unique properties. To deposit such materials, it is necessary to understand thoroughly the powder flow in the dispensing nozzle.

Only a few studies have been carried out using ultrasonic vibration to dispense dry powders for MMAM [5]. The detailed mechanism of DPP has not been fully clarified and is needed for the technique to be a commercial success. The processing of fine powder in the micrometre size range has proved difficult [10, 11]. This is due to the feature size being driven by the size of the dispenser orifice, a smaller feature size resulting from a smaller diameter orifice. For the production of drops from micrometre diameter size fine powders, the process is difficult to control reliability or sometimes powders cannot be dispensed because of their poor flowability. In this Ph.D thesis, we focus on developing a novel material delivery device for a Multiple Material Additive Manufacturing (MMAM) system using a Dry Powder Printing (DPP) technique developed recently. This innovative method of fine powder printing through a micro orifice will create the possibility of achieving the fabrication of multiple material layers automatically. The existing powder fusion processes, such as Direct Metal Laser Sintering (DMLS), Electron Beam Melting (EBM), Selective Laser Melting (SLM) and Selective Laser Sintering (SLS), might be upgraded to provide the multiple materials bonding in order to offer the additional functionality of multiple material objects in the near future.

1.2 Research objectives

The overall goal of this thesis is to study in detail the characteristics of a micro dispensing device utilizing ultrasonic vibration via a piezoelectric transducer, which is designed and constructed to handle a wide range of fine powder materials (particle sizes between 14-72 μm). The research aims to systematically investigate the nature of the interaction between the device and the material, and so allow the design and processing parameters to be understood. Experiments will be conducted to explain the effects of the printing parameters on printing results so as to discover the basic characteristics of the new dry powder printing device. Moreover, weight measurements of the deposited powder, microscopy and image visualization will be used to assess the behavior of the novel device. The outcomes obtained from many aspects of the studies will be compared and analyzed. The specific objectives are as follows.

1. To develop a new dry powder printing device and to design, fabricate and demonstrate the performance and capability of the new device.
2. To investigate the fundamental behaviour of the device to illustrate its fundamental operating principles.
3. To explore the effects of the design and processing parameters on the performance of the device.
4. To establish the necessary relationships required to provide operational guidelines for the device.

1.3 Research structure

This thesis is divided into six chapters to present all the details of the research motivation, research objectives, research methodology, research findings, data analysis, discussion, conclusion and future work. The structure of the thesis is shown in Figure 1-1 and a brief outline of each chapter now follows.

Chapter 1 introduces the main objectives of this research starting from the motivation. This chapter concludes with the aims of this work and the thesis structure.

Chapter 1

Chapter 2 reviews the current state of knowledge related to Multiple Material Additive Manufacturing (MMAM), powder flow technology and dry powder printing techniques. Technical challenges of the aforementioned topics are also described in this chapter.

Chapter 3 explains the experimental setup for a dry powder printing device and the system used in this research. The details of the design and fabrication of the device are provided. The details of experimental powders are also addressed. Additionally, methods of data collection and procedures to ensure the obtention of repeatable results are discussed.

Chapter 4 presents the results and data analyses of the investigations achieved by experimentation. This chapter deals with the dispensing characteristics and the powder discharge behaviour in dry powder printing. The details of the effects of design and processing parameters on dry powder printing are also discussed. Estimation models for the operational guidelines based on the performance results are developed. Finally, various examples of fine powder printing are demonstrated.

Chapter 5 summarizes the conclusions drawn from the study.

Chapter 6 points out some suggestions and recommendations for possible future work.

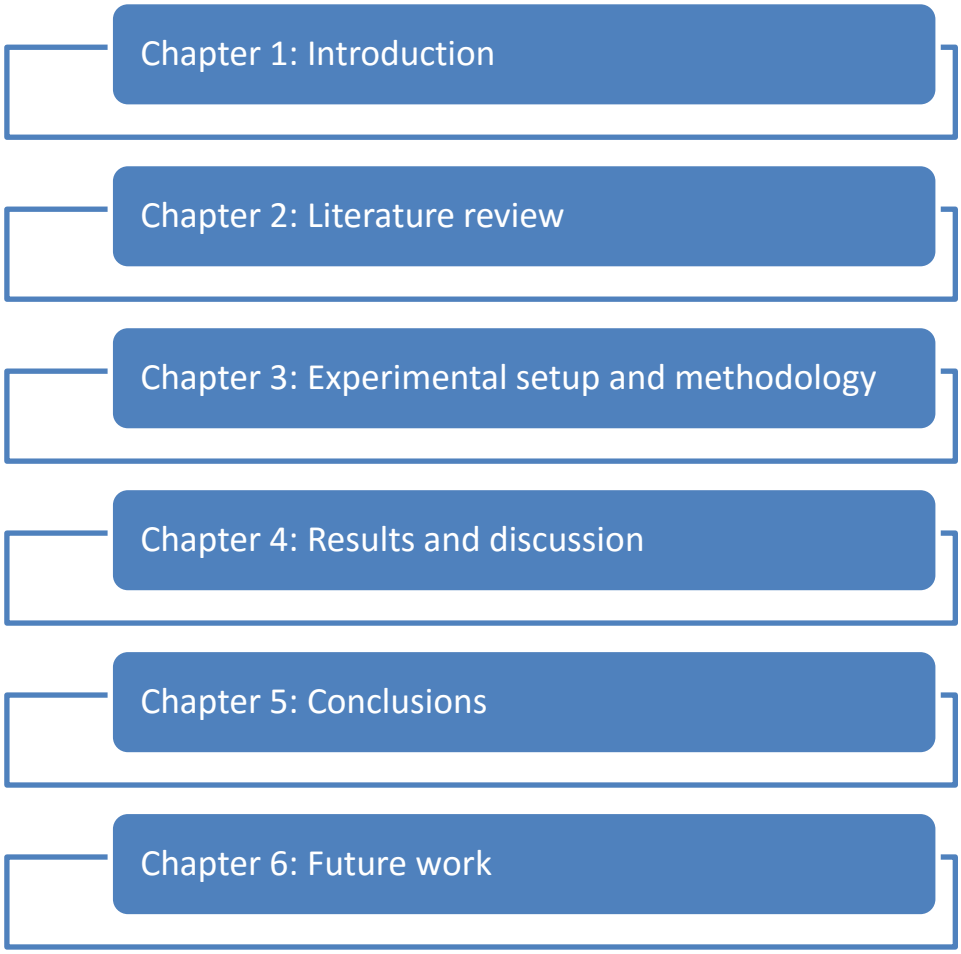

Figure 1-1 Structure of this thesis.

Chapter 2:

Literature review

The chapter describes information from currently published articles related to the process of dry powder deposition. The first section serves as an introduction to Multiple Material Additive Manufacturing (MMAM), which is the main application of this research on developing a novel material delivery device for multiple material powders. This section is based on a recently reviewed paper of which I am a co-author [5]. The second section is on topics related to powder flow, which is the key information in this material delivery system studied. The last section focuses on current research on dry powder printing technology, which is another key element of the novel device being developed.

2.1 Multiple Material Additive Manufacturing (MMAM)

Additive Manufacturing (AM) is the direct manufacture of final components using a technology that builds the product up layer-by-layer from 3D CAD data. AM technology has been developed so as to incorporate multiple materials hence the term Multiple Material Additive Manufacturing (MMAM). These multiple materials may be used to form many structures for example, heterogeneous materials, functionally graded materials and porous materials [12]. These materials have incredible applications in the fields of automotive, aeronautical, and medical manufacturing such as such as compliant mechanisms, embedded components, 3D circuits, human tissues, medical compatible implants etc. The traditional techniques have difficulties in fabricating components which need adjustment of the percentage of materials, control of uniformity or randomisation of primary materials. Therefore, MMAM technology is used to solve those problems.

As described above, AM processes are based on deposition by layers to produce the product. However almost all the current commercial technology can manufacture from only a single material [13], therefore, current AM technologies still require to be improved in terms of quality and performance efficiency. MMAM technology can increase the performance efficiency of AM methodology by adding complexity and increasing the functionality of the machine [14]. The machine

being developed can vary and change the material types or compositions within the layers. This is an exceptional improvement not achievable by the conventional manufacturing processes. MMAM is expected to not only successfully combine multiple materials but also to achieve other objectives for example providing additional functionality, mechanical properties improvement, and design freedom in the final products [12].

The development of MMAM technologies is valuable for various applications, particularly in the embedded component and electronic device industries where MMAM methodology can be used to print all resistor circuits and three dimensional circuits. This technology can reduce production and inventory cost, lead time and product weight.

The purpose of this section of this thesis is to provide an overview of present MMAM technology. In this section, MMAM processes will be classified and described under eight headings namely; photopolymer vat, material jetting, binder jetting processes, material extrusion processes, powder bed fusion processes, directed energy deposition, sheet lamination, and hybrid and direct writing. The technical challenges of MMAM will also be discussed.

2.1.1 Classification and description

Multiple Material Additive Manufacturing (MMAM) is a new technology that can fabricate three-dimensional multiple material (heterogeneous) objects. This technology can create multiple material objects and can vary material compositions within the layer. This is hardly attainable by conventional manufacturing processes [15, 16]. Presently there are many different MMAM technologies under development. Multiple material objects can be classified into two main groups; there are discrete multiple material (DMM) objects and functionally graded material (FGM) objects [7, 17]. Discrete multiple material (DMM) objects are a collection of distinct materials. In a DMM object each part can be clearly differentiated as in tissues from blood vessels of a human organ [18]. Functionally graded material (FGM) objects are composite materials characterized by a continuous change in the microstructural details from one material to another material. FGM can be used to improve structural properties, as thermal or flow gradient structures, or to provide wear and corrosion resistance in high temperature applications [19].

Nowadays, the ASTM International F42 Committees have standardized and classified AM Technologies. They have classified these technologies into seven main categories namely: photopolymer vat, material extrusion, powder bed fusion, directed energy deposition, sheet lamination, material jetting, and binder jetting [20]. Table 2-1 presents an overview of the different AM and MMAM processes based on the ASTM F2792-12a standard.

Table 2-1 AM and MMAM classification [5].

Process	Description	Typical AM techniques	Current MMAM techniques	Materials
Photopolymer vat	Liquid photopolymer is selectively cured using a light source	SL, 2PP	SL	Photo-curable polymers
Material extrusion	Material selectively is dispensed through a nozzle or extruder	Extrusion freeforming techniques (see section 2.4)	Extrusion freeforming techniques (see section 2.4)	Polymers, ceramics, metals
Powder bed fusion	Thermal energy selectively fuses regions of powder bed material	SLS, SLM, EBM, SMS	SLS	Polymers, Metals, Ceramics
Directed energy deposition	Focused thermal energy melts materials as deposited	LENS, DMD,	LENS, DMD	Metals, ceramics
Sheet lamination	Material sheets are bonded together and selectively cut in each layer to create the desired 3D object	LOM, UC	LOM, UC	Metals, Ceramics, Polymers
Material jetting	Droplets of build material are selectively deposited layer by layer	DoD Inkjet printing, PJT	DoD Inkjet printing, PJT	Polymers, metals, ceramics
Binder jetting	Liquid bonding ink is selectively spread to join solid powder material	3DP	3DP	Polymers, Metals, Ceramics

2.1.1.1 PHOTOPOLYMER VAT PROCESSES

Photopolymer vat processes involve selective curing of photopolymers using a light source [20]. In stereolithography (SL), a laser beam or other ultra violet (UV) light source is used to project onto a cross-section of a single slice of the object made from a photosensitive liquid polymer causing the solidification of a layer of the photopolymer [21]. The platform within the vat containing the photopolymer moves the solid part down and the laser cures the next layer of the photopolymer. This process is continued until all the layers of the complete object are created.

Two main SL techniques have been developed depending on the beam delivery system: scanning SL and projection SL.

Maruo et al. [22] used a scanning SL micofabrication process for fabricating optical waveguides from two kinds of photocurable polymers having different refractive indexes. Liu and Bhatia [23] demonstrated the fabrication of 3D hydrogel structures containing living cells with micro scale resolution via multiple steps using a micro patterned photo polymerisation processes. The researchers in W. M. Keck centre for 3D Innovation at the University of Texas at El Paso have developed different MMAM systems based on SL and FDM techniques [24]. They have presented a multiple vat carousel design and alternative machine designs to create 3D multiple material objects using a scanning SL system. In their design, the platform is moved below the surface of a liquid polymer in one of the build vats and then the platform was raised out of the current vat and the vat underneath the platform is rotated to provide access to a different material [25]. To reduce contamination, the process offers a cleaning step where the platform is submerged and cleaned in a cleaning vat before being submerged in a different material vat [26]. Kim et al. [27] developed a process-planning algorithm to improve the processing time by reducing the number of material changeovers, they also used low viscosity polymers without a sweeping process. In medical applications, Arcaute et al.[28] studied the capabilities of scanning SL for fabricating multiple material spatially controlled poly(ethylene glycol) bioactive scaffolds.

The advantages of the multiple materials scanning SL technique are high quality of surface finish and dimensional accuracy. Also, it provides different colours of polymers to embed in medical models and to tailor bioactive and mechanical properties in tissue engineering applications. The system can fabricate multiple material objects with horizontally and vertically oriented interfaces. However, contamination is difficult to eliminate with this technique. A multiple vat system requires a large area to operate the process and consumes time in pumping processes. Additionally draining and cleaning the previous material before changing to another resin vat takes a long time and leads to considerable material waste [27]. In addition, there are some problems that affect the shape of the desired object such as shadowing obstruction of the previously built part, trapped volumes when creating one material inside another, surface tension between two materials, and surface tension with the previous layer [26].

In projection SL, build time is significantly less when compared with scanning SL as a whole layer of the photopolymer is cured once via exposure through a mask. Bertsch et al. [29] proposed that a liquid crystal display (LCD) could be applied as the dynamic mask to generate the pattern expected in each layer in the projection SL process. Later , they proposed that the Digital Micromirror Device (DMD) which is embedded in digital light processing (DLP) projectors could be applied more efficiently as the dynamic mask in the SL process [30]. Stampfl et al. [31] used DMD-based SL, in which visible light is projected from below the resin vat to produce high quality 3D micro-parts. Furthermore, UV light was used by Hadipoespito et al. [32] and Cheng et al. [33] instead of visible light, to cure the resin.

Several advantages would potentially be derived by setting up a multiple material DMD-based SL system. Researchers at the W. M. Keck centre for 3D Innovation developed a DMD-based multiple material SL using a syringe pump system to add a material to a small, and removable vat designed specifically for the multiple material SL system [34]. Multiple material fabrication was accomplished using a material changeover process that included manually removing the vat, draining the current material, rinsing the vat, returning the vat to the system, and finally dispensing a prescribed volume in the vat using the syringe pump. Han et al. [35] also presented an automatic material switching approach by dispensing the solution using a pipette into a custom-made small vat, and subsequently washing out the current solution before changing to the next solution. Based on this technique, they fabricated 3D hybrid scaffolds for heterogeneous tissue engineering. Both the DMD-based systems mentioned were based on top-down projection. Due to the need to drain and clean the first resin from the deep vat before changing to another resin, it took a long time and led to significant material waste. To overcome this problem, researchers at the University of Southern California developed a DMD-based SL system called Multi-material Mask-Image-Projection-based Stereolithography (MIP-SL) which uses bottom-up projection to fabricate 3D multi-material objects faster [14]. Using bottom-up projection the portion of built up material to be cleaned when switching to new material vats was reduced.

To create FGM scaffolds, Researchers from the Centre for Rapid and Sustainable Product Development of the Polytechnic Institute of Leiria (Portugal) have developed a stereolithographic fabrication process called Stereo-Thermal-

Lithography (STLG) [36-38]. This process uses ultraviolet radiation and infrared radiation to initiate the polymerisation reaction in a medium containing both photo- and thermal-initiators. The system also contains a rotating multiple vat that enables the fabrication of multiple material structures.

2.1.1.2 MATERIAL JETTING PROCESSES

Material jetting is the method of inkjet printing or other similar techniques to deposit droplets of build material that are selectively dispensed through a nozzle or orifice to build up a 3D structure [20]. In material jetting processes, liquid material, in the form of a droplet, is jetted and often turns into solid after deposition via cooling, chemical changes or solvent evaporation [39]. Two different modes are mainly used for material droplet creation, namely Drop on Demand (DoD) and continuous inkjet (CIJ). Generally, CIJ systems use fluids with lower viscosity at higher drop velocities than DoD and are mostly used where printing speed is important. In comparison, DoD is used where smaller drop size, and higher accuracy is required and it has fewer limitations on ink properties [40].

For multi-material printing, print heads usually include several separate nozzles which are fed with different materials and are separately controllable. Material jetting processes are capable of printing multiple material and gradient-material structures. Applications of multiple material parts range from parts with controlled hardness and flexibility to parts with differing electrical properties in various regions to tissue-engineered structures with different biological properties in different regions of the part [20].

There are many reports on the printing of multi-material and functionally gradient materials (FGMs). Mott et al. [41] and Wang et al. [42] used a drop-on-demand jet printer and an ink mixing protocol to fabricate a one-dimensional zirconia–alumina FGM. Ibrahim et al. [43] adapted a commercial inkjet printer to fabricate 3D multiple material patterns layer-by-layer. The design, fabrication and performance of a multiple material DoD inkjet system based on a pneumatic diaphragm actuator was described by Xie et al. [44].

Researchers at the National University of Singapore (NUS) conducted a comprehensive study on applying inkjet printing for multiple material printing with a multiple actuating system [45-47]. They used two micro dispensing units

including a solenoid actuating micro-valve and a piezoelectric print head for printing multiple materials.

Material cooling and curing of a photopolymer ink using UV light are the two most common phase transition methods in multiple material inkjet printing. Molten materials can be jetted through a multiple nozzle piezoelectric head and are cooled upon deposition to make high resolution multiple material parts. UV curable photopolymers can also be jetted through a multiple nozzle head and each photopolymer layer is cured by UV light immediately as it is printed, producing fully cured multiple material parts. Two MMAM systems, namely: Connex™ printers by Objet Geometries Ltd. (www.objet.com) and ProJet printers (formerly InVision™) by 3D Systems Inc. (www.3dsystems.com) based on this principle have been commercialized. In ProJet printers, a print head jets two separate materials, an acrylic UV-curable photopolymer-based model material and a wax-like material to produce support structures for the model. With Objet's technology, it is possible to print many different photopolymer materials (over 60 materials) into a single part which have properties ranging from rigid to rubber-like, transparent to opaque and standard to ABS-grade engineering plastics, with a large number of in-between Shore grades and shades. The system is able to create advanced composite materials featuring unique mechanical and thermal properties. However, Objet can only print photopolymer materials, which have limited mechanical properties and other functionalities, compared to metal and/or ceramic materials.

2.1.1.3 BINDER JETTING PROCESSES

Binder-jetting techniques also use nozzles to print material, but instead of printing with the build material, the printed material is "glue", which holds powder together in the desired shape [20]. The 3D printing (3DP) process is the main binder-jetting technique based on inkjet technology and was developed at the Massachusetts Institute of Technology. In this process, droplets of a binder material are deposited over the surface of a powder bed, sticking the powder particles together where the part is to be shaped. This process is followed by lowering the powder bed via a piston and a fresh layer of powder is spread over the previous layer and again binder is deposited over the surface of the new layer. This procedure is repeated to build the whole part.

3DP has demonstrated the capability of fabricating parts of a variety of materials, including ceramics, metals, shape-memory alloys (SMA) and polymers with an array of unique geometries [48-51]. For MMAM, researchers at the Fraunhofer Institute for Manufacturing and Advanced Materials (IFAM) in Bremen, Germany, developed a two-binder system for 3D Printing technology, where one binder is traditional and one is carbon laden [52]. Their goal was to produce gradient strength steel parts by depositing the carbon according to a desired distribution of hardness. Sherwood et al. [53] developed a heterogeneous osteochondral scaffold using the TheriFormTM 3D printing process. Their scaffold parts can vary the material composition, porosity, macroarchitecture, and mechanical properties.

For MMAM, either the print heads need to deliver different binder materials or different powders need to be applied. However, due to the very limited types of binder delivered from the nozzles, the capacity of MMAM using this method is poor, unless the powder bed materials can be changed by another dry powder dispensing technology.

2.1.1.4 MATERIAL EXTRUSION PROCESSES

Material extrusion processes deposit material in the form of a continuous flow, layer by layer to make objects. They are very diverse in concept but can be classified into two main sub-groups: processes based on material melting and processes without material melting. Fused deposition modelling (FDM), multiphase jet solidification (MJS) [54], precise extrusion manufacturing (PEM) [55], precision extrusion deposition (PED) [56] and 3D fiber deposition [57] are AM techniques based on the melting process. Robocasting [58], 3D-Bioplotting [59], Pressure-assisted microsyringe (PAM) [60], low-temperature deposition manufacturing (LDM) [61], and solvent-based extrusion freeforming [62] are the most commonly used AM techniques without material melting.

Two or more extrusion nozzles are often incorporated in extrusion-based AM systems to fabricate multiple material structures. For example, two discrete materials are usually used in the FDM process so that one material may serve as support structure and can be easily removed once the build has been completed. Apart from hardware, an efficient pre-processing tool needs to be applied, Qiu et al. [63] developed a CAD system which generates high quality tool paths for multi-material part fabrication using extrusion-based systems.

Fused Deposition of Multi-Materials (FDMM) is a FDM method developed at Rutgers University to produce a variety of ceramic components composed of up to four materials [64, 65]. Safari's group at Rutgers University [66, 67] produced 3D photonic band gap (PBG) structures from alumina and wax using FDMM. The co-firing of multiple materials ceramics parts is made difficult by different ceramics having different sintering temperatures and shrinkage.

Solvent-based extrusion freeforming is another technique developed to produce bioceramic scaffolds [62]. Composite ceramic pastes such as alumina/silica, and alumina/graphite have been used successfully for the fabrication of 3D lattice structures with fine filaments [68, 69].

Xiong et al. [70] proposed the LDM process, which consists of the non-heating liquefying processing of materials. By integrating multiple nozzles with different designs into the LDM technique gave multi-nozzle low-temperature deposition and manufacturing (M-LDM) and multi-nozzle deposition manufacturing (MDM) [71, 72]. This M-LDM system has been used to build multi-material scaffolds [71].

Researchers at Cornell University, USA have enhanced multi-material freefrom fabrication of active systems by combining a FDM using molten-extrusion and a Robocating process using a robotically controlled syringe in the same machine [73, 74]. Moreover, they have developed a system that can print embedded circuits by combining a FDM to fabricate a structural part and a direct writing (DW) to print conductive circuits on the part [75].

Ang et al. [76] set up a special robotic bioplotting device called rapid prototyping robot dispensing (RPBOD) for the design and fabrication of chitosan-HA scaffolds. The RPBOD system was further improved to include a new manufacturing method, a dual dispensing system. Besides the pneumatic dispenser, a mechanical dispenser which was driven by a stepper motor was set up to deposit the curing medium [77].

The Polytechnic Institute of Leiria developed a variation of FDM called the BioExtruder with the aim of multiple material TE scaffold fabrication [78, 79]. It comprises two different deposition systems: one rotational system for multi-material deposition actuated by a pneumatic mechanism and another one for single material deposition that uses a screw to assist the deposition process.

Highly uniform PCL scaffolds have been made using the BioExtruder but no multiple materials scaffold has been reported.

Schuurman et al. [80] used a hybrid bioplotting approach for the fabrication of solid biodegradable materials (polymers, ceramics) with cell-laden hydrogels that could combine favourable mechanical properties with cells positioned at defined locations of high densities. This approach allows the use of multiple hydrogels, and can thus build constructs containing multiple cell types or bioactive factors. Furthermore, since the hydrogel is supported by the thermoplastic material, a broader range of hydrogel types, concentrations and cross-link densities can be used compared to the deposition of hydrogels alone, thereby improving the conditions for encapsulated cells to proliferate and deposit new matrix [38].

A common problem of material extrusion processes is buckling of the filament because of the high viscosity and low stiffness of the filaments. Therefore, the filaments or material pastes must be stiff enough to withstand the basic pressure required for extrusion through the nozzle [81] . Moreover, this technique has limitations on the minimum size of nozzle and the speed is slow.

2.1.1.5 POWDER BED FUSION PROCESSES

Powder-bed-fusion machines work in a manner similar to binder jetting; however, instead of printing glue onto a layer of powder, thermal energy is used to melt the powder into the desired pattern [20]. Most systems use laser power to melt polymer, metal or ceramic materials. For partial melting, the system is called Selective Laser Sintering (SLS). For full melting, the system is termed Selective Laser Melting (SLM). Another system that uses an electron beam to melt metal powder is known as Electron Beam Melting (EBM). Also, Selective Mask Sintering (SMS) is a slightly different system that uses IR-light through a digitally printed optical mask to melt a thin layer of plastic powder. The process is governed by powder characteristics (e.g. particle shape, particle size, particle distribution) and processing parameters such as energy source, energy power, spot size, scan speed, spacing distance and layer thickness [82-85]. Tolochko et al. [86] studied the effect of laser wavelength on its absorption by powder materials. It was shown that for metal powders laser absorption decreases with increasing wavelength, while for ceramic and polymer powders it increases with increasing wavelength. The laser wavelength should be adapted to the powder material because laser

absorption greatly changes with the type of material. CO_2 lasers are well-matched for polymer powders and oxide ceramic powders, whereas, Nd:YAG lasers are suited for metallic powders [87, 88].

Multiple material powder bed fusion has been investigated in the University of Texas at Austin, USA [7]. They have focused on discrete multiple materials processing that is performed by two different deposition methods; (1) depositing a complete layer followed by iterative selective removal and blind deposition of a secondary material by a counter-rotating roller as in a traditional SLS, and (2) deposition of a primary layer by a roller and depositing a secondary material in the desired location by a nozzle. In this process, a cross-section layer is built by the movement of a laser beam which melts the powder in the working area and the excess materials are selectively removed by electrostatic attraction [8]. This process can produce objects with nearly full density in a single processing step.

Another system has been developed by researchers from the Laser Insitut Mittelsachsen e. V., Germany [89]. The sintering platform has two cylindrical bores for the copper and silver powder supply and one for the building part piston. Two special rakes serve as a blade and a powder reservoir sweeps the powder material in a circular motion onto the platform. This technique is limited to vertical gradients of material. In addition, accurate material feeding systems to recoat multiple materials are difficult to design [90]. After fabrication, it is difficult to recycle the loose powders due to uncontrolled powder dispensing in layers.

Powder bed fusion processes are fit for functional MMAM parts that require a wider range of materials and material properties available from traditional manufacturing methods. It can be used in automotive, medical [91, 92] and aerospace [93] applications that require multifunctional capabilities which other manufacturing methods cannot produce. The process can be speeded up via applying optical mask printing techniques as is used in the Selective Mask Sintering (SMS) process. The reuse of materials also presents an important problem because the current recoating system has a contamination problem when changing between materials. To solve this problem, the material recoating system still requires improvement.

2.1.1.6 DIRECTED ENERGY DEPOSITION PROCESSES

Directed energy deposition uses a laser beam to melt and fuse particles of the powder material delivered from the material deposition head. The X-Y table is moved to shape the cross-section of each desired layer. This process is repeated until all the desired cross-sectional layers of the part are created. There are various types of this technology such as Laser Engineering Net Shape (LENS), Laser Cladding (LC), Direct Metal Deposition (DMD).

Multiple material directed energy deposition employs a nozzle to feed multiple powders and these are melted on a substrate by a laser beam to form fully dense objects. The key feature of this process is the powder feeding mechanism that can change or mix materials when fabricating multi-material structures. A wide range of different metals and alloys such as tool steel, stainless, nickel base superalloys, Co–Cr–Mo alloy and titanium have been deposited using this method [94, 95]. For FGMs, the powder feeders are used to deposit different powders separately and their feed rates are controlled individually to regulate the material composition [96, 97]. Independently controllable multiple powder feeders in the LENS process enable variations of composition and porosity simultaneously in one operation and enable the manufacture of novel implant structures. Functionally graded structures with a hard and wear resistant Co–Cr–Mo alloy coating on a porous Ti_6Al_4V alloy with a metallurgically sound interface have been produced using LENS by Bandyopadhyay et al. [98]. For electronic components and conductive lines, Zeng et al. presented a laser micro-cladding method to fabricate electronic pastes on insulated boards that will be useful in the electronic manufacturing industry and other fields such as MEMS [99].

The key benefit of directed energy deposition is that the system can perform material composition changes during deposition and achieve full density. The system is also suitable for repair applications. With this technology, it is possible to create three-dimensional structures that encapsulate actuators and arrays of sensors without fasteners or connectors [100, 101]. The primary limitation of this process is poor resolution and surface roughness. Part geometries of these processes are limited because they cannot build free-hanging features or internal overhang features which require rigid support, since there are no support materials in these processes. Additionally, build times of these processes can be very long [12, 102]. To develop robust multiple material laser processing, the

effects of various material and processing parameters on the final quality need to be understood. The key material and processing parameters include types of materials, the shape of the desired object, laser input power density, laser scanning pattern, scanning rate, and scanning spacing [103].

2.1.1.7 SHEET LAMINATION PROCESSES

Sheet lamination techniques work by cutting and bonding sheets of material to form an object. The original system used glue or binder to bond paper or plastic sheets and is called Laminated Object Manufacturing, whereas ultrasonic welding of metal sheets is named Ultrasonic Consolidation (UC).

2.1.1.7.1 LAMINATED OBJECT MANUFACTURE (LOM)

This technique involves the lamination of sheet material with each sheet representing a cross-sectional layer of the part. The sheets can be cut by either a knife or a laser and then the layers bonded by gluing or adhesive bonding. For a multiple material LOM processes, the material supply either comes from two different materials or comes from blended multiple materials. LOM of silicon carbide (SiC) and SiC/SiC composites has been demonstrated to produce high performance ceramic parts by [104]. Also, they have developed the Curved-LOM technology which deposits ceramic fiber-reinforced composite green tapes to create a smooth surface with more uniform mechanical properties [105]. Also, many researchers have presented preform tapes made from ZrO_2 [106], Si3N4 [107], Al_2O_3 [108], TiC/Ni [109] and Si-SiC [110] to fabricate functional and structural parts. Gomes et al. have developed water based green tapes of Li_2O–ZrO_2–SiO_2–Al_2O_3 (LZSA) with high tensile strength, which are able to produce complex geometry, defect-free, laminate glass–ceramic materials [111].

The process requires well-prepared material tapes to reduce variations in layer thickness and material content. The laser power has to be carefully controlled to avoid damage to a tape layer below from excessive energy. Additionally, post processing for the reaction bonding process in a pyrolysis cycle is necessary. The separation of the material layers is a major issue of the process. This technique can process ceramic materials that have mechanical, thermal and chemical stability that are suitable for high-performance shielding. The challenge lies in the bonding process to prevent delamination. Controlling sintering parameters is critical and

requires more understanding. Although varying materials between layers can be achieved, the production of high resolution multiple materials in individual layers is very difficult.

2.1.1.7.2 ULTRASONIC CONSOLIDATION (UC)

Ultrasonic Consolidation (UC) is a hybrid fabrication method combining an additive process and a subtractive process. It uses low amplitude ultrasonic frequency energy to bond thin sheet materials to form the objects by means of a rotating sonotrode. Subsequent layers are deposited over the previous layer. The part is finished by a subtractive process such as milling to produce the desired geometry. This process combines additive ultrasonic welding and subtractive contour milling to produce three dimensional objects [112].

The design of multiple material UC is currently under investigation at the Department of Mechanical and Aerospace Engineering in Utah State University, USA. This machine consists of a welding horn (sonotrode) and an automatic foil (sheet) material feeding system [113]. To create 3D multiple material objects, firstly materials are fed by the automatic foil material feeding system and then the process uses ultrasonic vibration at low amplitudes to create solid-state bonding layers of foil materials and build up a 3D cubic object which is machined to a completely 3D object by a milling machine. This technique can process weldable metal materials such as Al, Fe, Ni, Cu and dissimilar combinations such as Al/brass, Al/stainless steel and Al/Ni [114]. Additionally, Siggard et al. [115] have applied this technique to embed USB-based sensors into aluminium sheets to demonstrate the ability to use UC in embedding mechanical and electrical systems. Several important process parameters are controlled such as substrate temperature, vibration amplitude, welding speed, and normal force to achieve adequate bonding [116]. Researchers at Loughborough University reported on the use of a UC process to make smart material structures by embedding fibres such as conductor, dielectric, and nano-meter NiTi shape memory alloy fibres into a metal matrix [117].

The strength of this technique lies in the ability of the process to produce metallic parts at high fabrication speeds with accurate dimensions because solid-state welding and no liquid to metal transition process is involved, so it is easy to control accuracy during the building of the part. When compared to other AM

methods, this process can be performed at lower temperature, temperatures ranging from 22°C to 204°C are possible; the temperature is normally 150°C [118]. Moreover, it uses a machining process to shape the contour of the final object precisely [119]. The main problem of this technique is voids that occur along the interfaces between layers because of foil surface roughness, insufficient or excessive welding energy, and positioning inaccuracies of foil placement [120]. This defect affects the strength of built parts [12]. Also, this technique can use only metal materials and it is inefficient in material usage due to the subtractive process. Furthermore, the system can fabricate multiple material objects but with only vertically oriented interfaces [121].

The sheet lamination processes uses a relatively low processing temperature that is suitable for electronic encapsulation and embedded electronic system applications because it does not provide the protection of the embedded components. The challenge is the process parameter that can achieve a defect-free bonding layer at low temperature. Delamination between bonded layers is a critical problem of this technique. If this problem is overcome this technique will offer benefits for embedded applications.

2.1.1.8 HYBRID AND DIRECT WRITING PROCESSES

Some AM processes do not have high potential for multiple materials processing but they possess good capability to be integrated with other AM or conventional techniques to create an efficient hybrid system. For example, Direct Write (DW) can be integrated with photopolymer vat processes [122] or material extrusion processes [123] or sheet lamination processes [124] to make multiple material objects. Also, integrating processes from different AM techniques, such FDM and UC [125] or FDM and Robocasting [126-128], have shown to be useful in making multiple material objects. Hybrid and DW technologies such as laser chemical vapour deposition (LCVD), aerosol jet printing, Shape Deposition Manufacturing (SDM) and dry powder printing (DPP), have been more successful in the field of multiple materials. A wide range of materials and complexity of parts are the most significant advantages of these processes which make them a possible technology for further developments in the MMAM area.

2.1.1.8.1 LASER CHEMICAL VAPOUR DEPOSITION (LCVD)

LCVD is a 3D direct writing (DW) process that employs a laser beam to convert gaseous reactants into thin solid layers in a selective manner. In the LCVD process, a laser beam is focused to a spot (~1 μm in diameter) via an optical microscope lens and a gaseous reactant comprising the materials to be laid down is fed into a build chamber. The substrate is heated selectively by scanning the laser beam over it at usually 0.5–5 mm/s to dissociate the reactant gas selectively; consequently, a thin layer of the material is set down onto the substrate. In this way, by repeating the laser scan, microcomponents can be made layer by layer. There is a possibility to fabricate multi-material and gradient 3D microstructures by feeding different gases into the build chamber at different times or using a blend of gases with desirable concentrations. Various microparts from a variety of ceramics and metals can be produced by the LCVD process using different reactant gases. Furthermore, a LCVD process can be used to build carbon fibres and multi-layered carbon structures. Duty et al. [129] deposited various materials including carbon, silicon carbide, boron, boron nitride, and molybdenum (Mo) on a range of substrates namely graphite, grafoil, zirconia, alumina, tungsten, and silicon using the Georgia Tech's LCVD system.

There are two extensions to LCVD known as Selective Area Laser Deposition (SALD) and Selective Area Layer Deposition Vapour Infiltration (SALDVI). They can deposit multiple material directly to build objects at low processing temperatures without the use of any secondary low-melting temperature phases [130]. SALD utilizes a laser beam to create a locally heated zone on a substrate enclosed by a reactant gas and SALDVI uses gas precursors and solids in powder form as starting raw materials [131].

The deposition speed of this process is naturally low, usually it is in terms of μm/s [132], so LCVD might be suitable for micro-scale component applications. To obtain a high deposition rate, the surface reaction mechanisms must be understood so that the process parameters can be adjusted accordingly [133]. Furthermore, when using multi-source precursors it is difficult to control the deposition of multicomponent materials because different precursors have different vaporisation rates, and most of precursor gases are toxic, corrosive, flammable and/or explosive [134]. Moreover, it is expensive and problematic to recycle or reuse the gas when the gas in the chamber needs to be different.

2.1.1.8.2 AEROSOL JET PRINTING

Aerosol jet printing is a type of direct writing method which uses a focused aerosol stream, instead of liquid ink droplets as used in inkjet printing, to deposit a wide range of materials. The process was developed and commercialized by OPTOMEC® under the trademark of M3D which represents Maskless Mesoscale Material Deposition. First, a composite suspension is aerosolized in an atomizer to make a dense aerosol of tiny droplets. Then, the aerosol is transported to the deposition head via a carrier gas flow, and within the aerosol head, the aerosol is focused using a flow guidance deposition head, which creates an annular flow of sheath gas to collimate the aerosol. The high velocity co-axial aerosol stream is sprayed onto a substrate layer by layer to create 3D parts [39]. The high velocity of the aerosol stream enables a relatively large separation between the print head and the substrate, typically 2-5 mm, resulting in the ability to print conformal patterns on 3D substrates.

The Aerosol jet printing can deposit a wide variety of materials, including any materials that can be suspended in liquids (such as metals, ceramics, polymers, composites and biological materials), on virtually any 2D planar surfaces or 3D non-planar substrates. Since aerosol jet is a low temperature process and the droplet size is of the order of a few femto-litres, it is a good candidate for biomanufacturing. The kinetic energy of the droplets is so small due to their tiny mass that it will not demolish living cells. Aerosol jet inks can include polymers, ceramics, metals and biomaterials [39]. However, the system to jet materials is complex and it requires certain material viscosities, to be jettable. Moreover, the focal length of the aerosol needs to be long enough to write features.

2.1.1.8.3 DRY POWDER PRINTING

The dry powder printing technique is one of several techniques that has potential for use as the material delivery system in MMAM. The origin of powder dispensing dates from the sand paintings or manual deposition of the Navajo Indians and has been proposed as a material delivery technique for powder materials [135]. Joseph Pegna is a pioneer in the line printing of dry powders [136]. His experiments studied the feasibility of multi-material deposition by generating a single layer of Portland cement and 220-μm spherical glass beads. Santosa et al.

[137] presented experiments on the delivery of powder under 100 μm through a hopper-nozzle to show the influence of orifice diameters and particle sizes on flow behaviour under gravity. In 2004, Kumar et al. [138] proved the concept of multiple dry powder deposition under gravity alone by using low gas pressure-assisted flow and vibration-assisted flow conditions on an X-Y table. Moreover, they predicted the flow rate under gravity of the experimental powders by Beverloo's correlation. In the meantime there have been many attempts to use ultrasonic vibration to dispense dry powder for MMAM. Matsusaka et al. [139] used a capillary tube vibrated by 20 kHz ultrasound to control the micro-feeding of fine powders. Takehiro [140] created a powder feeding device based on an ultrasonic progressive wave. Yang and Evan [141-144] studied the dispensing mechanism, drop uniformity and dispensing nozzles in ultrasonic micro-dispensing. The technique adopted for powder deposition was acoustic flow rate control of powders in which vibration is used to switch powder flow on and off and to control flow rate by changing amplitude [142]. The static valve is closed by the formation of a powder dome at the end of the orifice tube following conventional architectural principles while flow initiation results from the breakage of domes under vibration force [144].

There are several different methods for powder delivery in additive manufacturing: pneumatic and screw methods, volumetric methods, electrostatic methods, and vibratory methods [145]. Among dry powder dispensing systems, the ultrasonic technique of all the vibratory methods has demonstrated more acceptable results as a material delivery system compared with other systems discussed [146]. Many experimental results show that the dispensing system can use a variety of materials such as H13 tool steel [147], copper [11], glass bead [138] and silver [148]. Therefore, the powder dispensing nozzles can be integrated onto the building platform of the material delivery system to feed different types of material.

Although many studies have demonstrated the success of this method, more work is required to investigate and improve it. The material flow rate in dry powder dispensing is not so high which is ideal for high resolution patterning but makes the process slow. Multiple nozzles have been proposed to increase the speed of dispensing [149]. In addition, powder flow is difficult to calculate theoretically and the stability of the process is poor [150]. To meet the requirements in terms of

processing time and dispensing repeatability and powder controllability, developments should be carried out.

2.1.1.8.4 SHAPE DEPOSITION MANUFACTURING (SDM)

Shape Deposition Manufacturing (SDM) is a hybrid layer by layer process that sprays molten material in near net shape onto the substrate, then uses subtractive processes to remove unwanted material [151]. This process was introduced by researchers at Carnegie Mellon University for creating multi-material metal parts (e.g. copper and stainless steel) [152] and was subsequently extended at Stanford university for polymer and ceramic parts [153]. The technology can fabricate multi-material parts by stacking different material layers but there are no multiple materials in the same layer. In SDM, parts or assemblies are built up through a cycle of alternating layers of structural and support material. Unlike most other MMAM processes, SDM shapes each layer of material on a computer-controlled milling machine after it is deposited. This approach allows for tolerances of ± 0.01 mm and avoids the stair-stepping effect of additive processes. The intermittent addition of sacrificial support material allows for the construction of nearly arbitrary geometries and facilitates the inclusion of embedded components [154]. Some researchers use this technique to fabricate multiple material structures that combine rigid materials, compliant materials and integrate sensors and other discrete components [155, 156] that allow components to be embedded, decreasing the damage to sensor components by encasing them within the part structure and removing the need for assembly [157, 158]. However, SDM has not been widely adopted as there are several major obstacles such as the experimental nature of the process, and lack of knowledge about SDM in the design community that must be overcome. The challenge of educating designers about these techniques, however, is not being sufficiently addressed [159].

As a consequence of what has been discussed above, MMAM processes enable new types of design and manufacturing previously impossible while offering cost reduction on specific types of products. Conventional manufacturing technologies still have a justification for their existence and are often a preferable approach in many cases in terms of cost, time, functionality, and reliability. But MMAM technologies can be an effective tool when there is complexity in terms of both shape and material. Choosing the right MMAM process to be used needs a

comprehensive knowledge on capabilities and limitations of each process. A comparison of MMAM systems is presented in Table 2-2.

Table 2-2 Comparison of different MMAM systems [5].

Category	Techniques	Advantages	Disadvantages	Bonding Interface	Materials resolution	Capability	Material solidification and bonding in layers
Photopolymer Vat	Scanning SL	High dimensional accuracy, offering transparent materials, living cells can be incorporated	Only photopolymers, time consuming materials changing, material contamination and waste in process	Between and within layers	Low	Good	Point by point
	DMD-based SL	Same as scanning SL	Same as scanning SL	Between and within layers	Low	Good	Whole layer once
Material extrusion	Material melting extrusion	Fast, no toxic materials, good material properties	Low dimensional accuracy, delamination, weak bonding between dissimilar polymers	Between and within layers	Medium	Good	Line by line
	Material extrusion without melting	Easy and cheap mechanism, no trapped materials, low material waste, fairly high fabrication speed, living cells can be incorporated	Relatively low dimensional accuracy and mechanical strength	Between and within layers	Medium	Good	Line by line
Powder bed fusion	SLS	Wide range of materials, great material properties, high material strength	Thermal stress, degradation, accuracy limited by the particle size of materials, material contamination when changing to other materials, require atmosphere control for metals	Between layers	Low	Fair	Point by point
Directed energy deposition	LENS DMD LC	Wide range of materials, great material properties	Low dimensional accuracy, thermal stress, require atmosphere control, require machining process for finishing the part	Between and within layers	High	Fair	Point by point
Sheet lamination	LOM	Fast process, accuracy in Z-axis is lower than SLA and SLS	Shrinkage, great amount of scrap, delamination, require changeover when changing other materials, require pyrolysis process	Between layers	Low	Fair	Plane
	UC	High dimensional accuracy, fast process, low temperature effects	Wastage of material in the machining process, delamination, only metals, require changeover when changing other materials	Between layers	Low	Good	Plane
Material jetting	Inkjet Printing	Fast process, wide range of materials, materials mixing on droplet scale	Limited to jettable materials, clogging problem, low viscosity prevents build-up in 3D	Between and within layers	High	Very Good	Point by point
	PJT	Fast process, wide range of materials, materials mixing in droplet scale	Limited to jettable photopolymers, clogging problem	Between and within layers	High	Excellent	Multi-Point
Binder jetting	3DP	Low temperature process, Fast process	High porosity, low surface quality, accuracy limited by the particle size of materials, difficult to	Between and within layers	Medium	Poor	Point by point

			remove trapped materials,				
Hybrid & DW	LCVD	High-resolution process, metals and semiconductors	low-deposition rate, toxic/explosive gas might be involved	Between and within layers	Medium	Poor	Point by point
	Aerosol Jet Printing	High resolution, wide range of materials, ability of writing in 3D space, ideal for deposition of biological inks, noncontact, easy material handling	Solvent involved, shield gas may blow off powders when integrated with powder bed systems	Between and within layers	High	Good	Line by line
	SDM	Wide range of materials	Require machining process during fabrication, feature size is limited by cutting tool	Between and within layers	Low	Fair	Line by line
	DPP+binder printing or laser sintering	Wide range of materials, possible complex materials and geometry control	Limited to good flowability powders, overflow problem, low compaction density of discharged powders	Between and within layers	High	Good	Point by point

2.1.2 Technical challenges of multiple material additive manufacturing

Many researchers have been working on MMAM to allow multiple materials to be used in 3D fabrication. Most systems reported in this review still require much effort to commercialize. Among these MMAM techniques, processes such as material jetting and extrusion freeforming techniques have shown very good potential for multiple material manufacturing due to their capability to deposit a wide range of materials through separate nozzles. Additionally, hybrid and DW systems have shown promising results and it can be expected that their use will spread more in the near future. The technological barriers that need to be contemplated in MMAM processes are discussed as follows:

2.1.2.1 Printing materials

MMAM should offer a wide range of materials to expand its range of applications. Some processes, such as material jetting and photopolymer vat, mostly use polymer materials. In material jetting, the materials require good flowability over a restricted temperature range. In the same way, the photopolymer vat process only photocurable polymers. The limitations in material alternatives will restrict the use of these techniques when higher mechanical properties or functionalities are necessary. In addition, some processes, such as sheet lamination (e.g. LOM) material extrusion and aerosol jet printing, need material preparation, which

consumes time, and specific material formulations. These problems will generate production costs resulting in higher cost for end-users.

2.1.2.2 Material contamination

One important problem in MMAM systems is contamination in the material delivery system when changing to different materials. This creates an imperfect and deficient process. Also, the reuse of materials is difficult or impossible. Powder based fusion and photopolymer vat systems always have this kind of problem. In contrast, nozzle based systems or print head based system, for instance material jetting, material extrusion, directed energy deposition and DW, have less material contamination issues.

2.1.2.3 Material usage

As we know the key advantages of AM technology are extremely complex geometries are possible and material is only used where it is needed. However, some processes, such as powder based fusion or photopolymer vat, require large amounts of material in the container compared to the small size of the object made. Medical or jewellery applications, which use high-value or precious materials, require small amounts of material in the process in order to avoid inventory cost and material loss/waste during the process. By using or integrating a new material delivery system like dry powder printing, which is drop on demand, and selective deposition method, it is believed that such processes will offer a huge potential for these industries.

2.1.2.4 Material depositing ability

In MMAM systems, the most important step is to deliver multiple materials. Some MMAM systems such as powder bed fusion and sheet lamination have the ability to deposit different materials between layers. On the other hand, some systems such as photopolymer vat, material extrusion, directed energy deposition, material jetting, binder jetting and DW can deposit different materials between layers and within a layer. However, material extrusion and directed energy deposition has generally limited resolution and poor surface roughness. In addition, binder jetting can change material compositions only by changing binder inks. LCVD is good for different materials but the process is very slow, difficult and it is expensive to

recycle and reuse the gas. SDM has interruptions due to process changeover during the build process and has limited feature size due to the cutting tool. The favoured MMAM system should be able to vary materials in any aspects to make multi-oriented interfaces including the ability to continuously control material composition.

Bearing in mind all above challenges, it appears that dry powder printing can overcome most of the restrictions. Dry powder dispensing systems, especially ultrasonic dispensing, have demonstrated the ability to precisely deposit fine powders. It is believed that using a dry powder printing device incorporated in current powder-based systems or binder jetting systems would provide a method capable of solving the problems indicated as well as increasing their capability to fabricate multiple material objects. However the current resolution of dry powder printing still requires improvement, as it is hard to obtain controllability and reliability when using very fine powder materials.

2.2 Review of powder flow

Powder materials are commonly used in various industries. A lot of products have been in a powder state during part of their manufacturing process. About 40% of the value added in chemical industries is related to particle technology and more than 50% of all products in the market involves powder materials in their production [160, 161]. The flow of powder materials occurs in many industrial processes such as in the metallurgical, agricultural, food, pharmaceutical, and chemical industries. It is essential to understood well how to handle and process these powders. However, the flow behaviour of this material is not well understood [162-164]. Powder flow is complex because powder materials have unique properties and behave differently to solids, liquids or gases [165, 166]. To understand and control the flow of powder materials, it is appropriate to review the most relevant literature. The objective of this section is to identify and discuss some important basic concepts of powder flow and the effects vibration has on powder materials. In the last part of this section, the technical challenges of powder flow will also be discussed.

2.2.1 Powder definition

A powder is a term for solid particles. Generally, the words “bulk solids,” “granular materials,” “particulate solids,” and “powders” are used interchangeably in much of the literature [162]. Powder materials can be characterized by their mean size from large to small. There are broken solids (1,000-10,000 μm), granular solids (100-1,000 μm), fine powders (10-100 μm), superfine powders (1-10 μm) and ultrafine powders (less than 1 μm) as indicated in Table 2-3. This table also includes some of the powder flow characteristics corresponding to their size ranges. However, this table is not precise and these definitions tend to vary in usage from one industry to another.

Table 2-3 Characteristics of particles according to their size ranges [167, 168].

Size (μm)	Shape	Characteristics
1,000-10,000	Broken solid	Free-flowing, but could cause mechanical arching problems during discharge from bins and silos
100-1,000	Granular solid	Easy-flowing with cohesive effects if % of fines is high
10-100	Fine powder	May show cohesive effects and some handling problems
1-10	Superfine powder	Highly cohesive; very difficult to handle
< 1	Ultrafine powder	Extremely difficult (or impossible) to handle

Rao and Nott [162] described a powder as dry powder material when the spaces or voids between the grains are filled with a gas or an air. If the voids are completely filled with a liquid such as water, the material is called a saturated powder. If there is a liquid in some of the voids, and the rest of the voids are filled with a gas, the material is said to be partially saturated.

2.2.2 Factors affecting powder flow

2.2.2.1 Adhesive forces

The occurrence of molecular forces produces a tendency for solid particles to stick to each other and to other surfaces. Adhesion can occur between component particles of a powder and between a particle and a hopper wall [169]. Schulze [170] described that flowability of fine powder mainly depends on the adhesive force between particles. For a dry powder, the major adhesive forces are due to van der Waals interactions and electrostatic forces. The van der Waals forces are determined by particle size and the distance between the particles, and these forces are large if the powder particles are pressed into contact. The electrostatic forces are based on the different electrical potentials of particle surfaces. For a moist powder, the main adhesive forces are due to liquid bridges and capillary pressure. Liquid bridges are formed by small regions of liquid between the particles, and the adhesive force is dependent on the amount of liquid. Capillary pressure provides an additional adhesive force if the pressure is lower than ambient pressure. In powder flow, electrostatic forces frequently can be neglected because their influence is small compared to other adhesive forces.

2.2.2.2 Bulk density

Bulk density is the ratio of the mass of an amount of bulk solid to its volume. Bulk density is less than particle density or solid density, because voids or pores exist between the individual particles of a bulk solid. Bulk density is dependent on the state of compression or compaction of the bulk solid. With increasing consolidation stress, bulk density increases, since the compaction decreases the voids between the particles [170]. Additionally, bulk, packed and poured densities depend on the rate of powder feed into a specific container volume. Thus the rate of powder flow, height of pour, impaction and powder yield strength including physical properties such as particle size, particle shape, particle density and powder cohesiveness influence powder bulk density [171, 172].

2.2.2.3 Particle size

As adhesion occurs at surfaces, particle size will influence the flowability of a powder. In general, fine powders with very high surface to mass ratio are more cohesive than coarser particles which are influenced more by gravitational forces. Particles larger than 250 μm are usually relatively free-flowing, but as the size decreases below 100 μm powders become cohesive and flow problems tend to occur. Mostly, powders having a particle size less than 10 μm are extremely cohesive and difficult to flow under gravity [169]. Generally, it can be stated that with decreasing particle size the strength of a bulk solid becomes greater and, thus its flowability is reduced. However when a fine powder is mixed with a small portion of a finer powder, this will reduce the strength and increases the flowability because the finer powder acts as a flow agent [170].

Normally for fine particles, the flow rate through an orifice rises rapidly with expanding size until a limit is reached, followed by a decrease in flow rate as the particle size is increased further [173, 174]. The lower flow at larger particle sizes is linked to restrictions due to the size of the orifice relative to the particles, while the lower flow for small particles is due to increasing van der Waals, electrostatic and surface tension forces [173, 175].

The tensile strength of a powder, which is regarded as the sum of the adhesive forces at a large number of particle contacts, inversely related to the flow behaviour, has been shown to be inversely proportional to the square of the particle diameter and directly proportional to the bonding force per point of contact [176]. Therefore, the greater the interparticle forces, the higher the tensile strength of the powder and the poorer the flow behaviour. Even though the tensile strength of a powder does not play an important role in powder handling and powders are normally subjected to compressive stresses rather than tensile stresses, it is easy to link the tensile strength and adhesive forces [170].

Powder flow can be considered to be the opposite of powder agglomeration since flow is governed by gravitational forces whilst agglomeration is dependent upon interparticle forces. As gravitational forces decrease with particle size more quickly than the interparticle forces, the latter will become increasingly dominant over the former and hence particles will tend to agglomerate instead of flow. As discussed previously, for particles with a diameter of less than 10 μm, van der Waals forces

will dominate over gravitational forces. Therefore, such particles are often highly cohesive and have poor flowability [177].

2.2.2.4 Particle shape

Particle shape can also affect flow properties due to differences in the interparticle contacts area of a powder. For example, a group of spheres has good flowability due to minimum interparticle contact areas, whereas a group of particle flakes or dendritic particles has poorer flowability due to a very high surface to volume ratio. Particle shape may also affect the flow properties of a powder by changing interparticle and/or frictional forces between the particles. In general, if the particle shape can reduce both interparticle and frictional forces, then it has good powder flow [177]. A reduction in interparticle forces by modifying particle shape alone cannot guarantee improved powder flow. For example, more angular particles have been found to have poorer flow than more rounded particles [178]. This was due to an increased friction coefficient for angular particles as compared with more rounded particles [179], rather than to an increase in interparticle forces for the more angular particles.

2.2.2.5 Particle size distribution

Particle size distribution is the size range of a set of powder particles representative all sizes in the sample of interest. A monomodal distribution is a powder mixture in which all the particles have the same size. Only theoretical monomodal distributions have zero or near zero size variance. All manufactured powders have some degree of size variance [180]. A polymodal distribution is a powder mixture formed by two monomodal distribution or more. Void spaces between coarse particles may become filled with finer particles in a powder with a wide size range, resulting in a more closely packed cohesive powder. For powders with narrow size distributions, flowability increases significantly with increase in particle size, the internal friction angle reduces [181, 182].

2.2.3 Classification of powder flowability

Powder flowability is the ability of a powder to flow from a specific item at a desired degree of flowability [171]. Powder flowability is often regarded as the

inverse of powder cohesion [183], which essentially determines how well a powder flows. Powder flowability is useful in predicting powder handling behaviour. Typically, the characteristic of powder flowability is crucial in the setup and design of powder handling [184]. If the powder flowability is poor, problems may arise in the processes [185, 186]. Generally, powder flowability can be quantified as a range of mobility, from free flowing to non-flowing. The classification of powder flowability is linked to the applications in which the powders are used. For dry powders, the classification can be considered according to their handling conditions, in the deaerated state and in the aerated state [187]. The Jenike's classification is a classification of powders in the deaerated state, whereas the Geldart's classification is the classification of powders in the aerated state. The, Hausner's ratio, Carr's compressibility and angle of repose, may also be used to characterized the flowability of powders. These concepts are discussed in sections 2.2.3.3, 2.2.3.4 and 2.2.3.5.

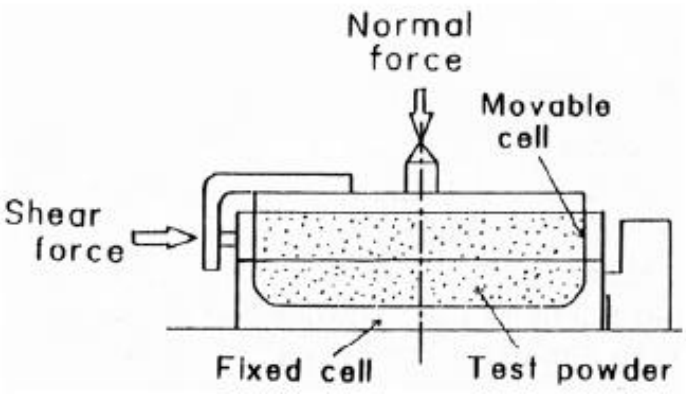

Figure 2-1 Jenike's shear cell tester [188].

2.2.3.1 Jenike's classification

In the deaerated state, the flowability of a powder can be determined from curves derived from a family of yield loci of the powder, which are measured with a shear cell tester (Figure 2-1). The curve represents the relationship between the maximum shear and normal stresses of the consolidated powder samples and is called the yield locus. Each yield locus gives values for the unconfined yield stress (σ_y) and major consolidation stress (σ_c). The ratio of the consolidation stress to the unconfined yield strength is called the flow factor (ff). Figure 2-2 presents a

classification of powders following the proposal of Jenike [189], who classified flowability according to the position of one point of the failure function (FF) at a fixed value of the unconfined yield stress with respect to the flow factor line.

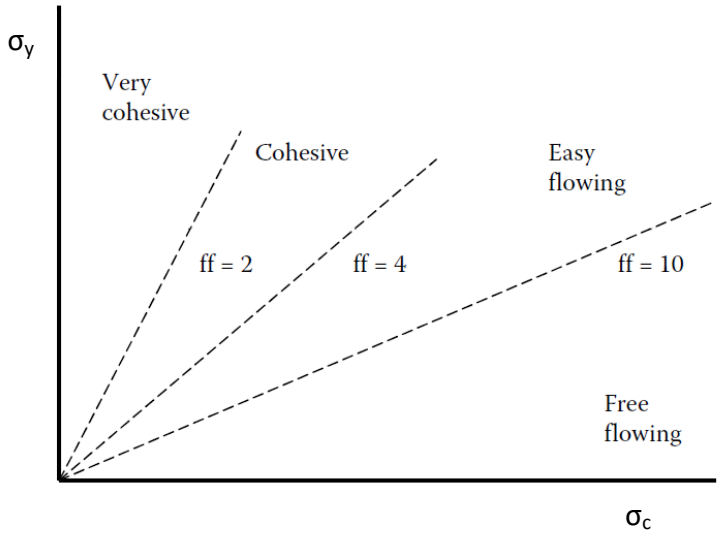

Figure 2-2 Classification of powder flowability according to Jenike [187].

As shown in Table 2-4, the straight line through the origin at a slope 1/ff categorizes the flowabilities of very cohesive, cohesive, easy flowing and free flowing at a fixed value of the unconfined yield strength.

Table 2-4 Classification of powder flowability [187].

Flowability	**ff**
Very cohesive	Less than 2
Cohesive	Between 2 and 4
Easy flow	Between 4 and 10
Free flow	More than 10

2.2.3.2 Geldart's classification

In the aerated state, the classification proposed by Geldart [190] is widely accepted. Geldart's classified the behaviour of powders in a fluidized state into four types of powders. As shown in Figure 2-3, powders can be grouped as A, B, C and D. A powders are known as slightly cohesive and show large bed expansion after minimum fluidization before the initiation of bubbling. B powders are

referred to as sand like and exhibit bubbling at the minimum fluidization velocity with a small bed expansion. C powders are very difficult to fluidize and are known as cohesive. These powders do not form bubbles at the minimum fluidization velocity and have no bed expansion. D powders are called large; these powders can form stable spouted beds, and show large bubbles at the minimum fluidizing velocity. Figure 2-3 illustrates the plot of particle-fluid density difference, which is the difference between particle density and fluid density (or air density), versus particle size according to Geldart's classification.

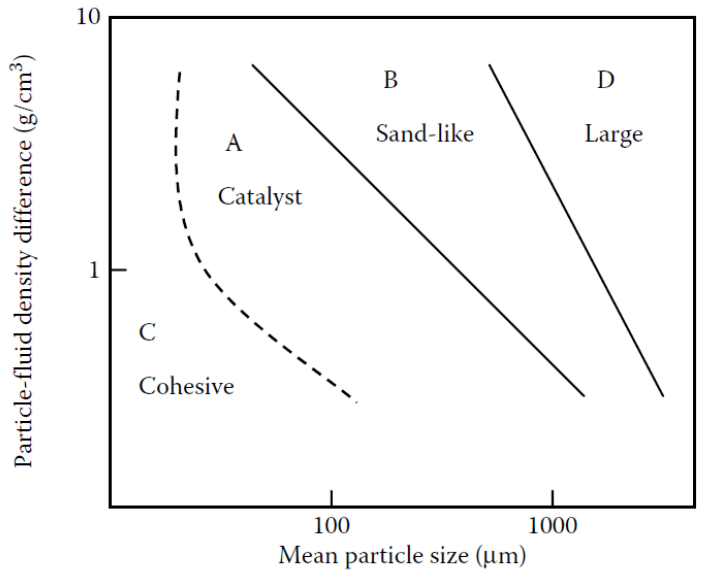

Figure 2-3 Classification of powder flowability according to Geldart [187].

2.2.3.3 Hausner ratio

The Hausner ratio is defined as the ratio of tap density (ρ_t) to aerated density or initial density (ρ_a). This technique is used to characterize the flow of a diversity of industrial powders [168, 191-193]. However, it depends on a lot of parameters, e.g. particle size, particle shape, particle distribution etc., and not always provides reliable results [194]. The classification of flowability is shown in Table 2-5.

$$Hausner\ ratio\ (HR) = \frac{\rho_t}{\rho_a} \tag{2-1}$$

2.2.3.4 Carr's compressibility

Although the Hausner ratio is an acceptable indicator for the prediction of the flowability of powders the ratio may not represent the actual compaction

behaviour [195] a powder may undergo when subjected to industrial powder processing. Powder compressibility can be expressed in alternative ways as defined by Carr [196]:

$$Carr's\ compressibility = 100 \times \frac{\rho_t - \rho_a}{\rho_t} \quad (2\text{-}2)$$

Compressibility in excess of 20% tends to create arches in hoppers while powders with compressibility greater than 40% are difficult to discharge, as shown in Table 2-5.

2.2.3.5 Angle of repose

The angle of the free surface of a pile of powder to the horizontal plane is called the angle of repose as shown in Figure 2-4. The angle of repose has been used as an indirect method of classifying powder flowability because of its relationship with interparticle cohesion [197]. For free-flowing powders, the angle of repose can be used for calculations related to aspects of storage and transport [187]. A standard method for measuring the angle has been reported by the British Standards Institution [198]. Carr [199] and other researchers [200] reported the relationship between powder flowability and the angle of repose as a rough guide to behaviour, as summarized in Table 2.3. The measurement of the angle of repose is quicker and simpler than all the methods mentioned previously, so it is suitable for monitoring the flow behaviour of powder on a practical basis [183]. Nevertheless, the angle of repose can be considered meaningless in many practical applications as an indicators of flowability [201]. Moreover, the angle of repose faces a problem as it is not a constant for a given material and depends on the method of pile formation, however the measurement is consistent when using free to fair flowing and fairly homogenous powders [200].

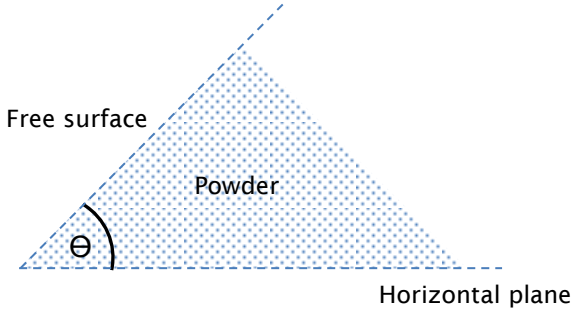

Figure 2-4 Poured angle of repose, Θ.

Table 2-5 Flowability indicators [195].

Description	Angle of repose	Carr's compressibility	Hausner ratio
Very free flow	25-30°	<10%	1.00-1.11
Free flow	31-35°	11-15%	1.12-1.18
Fair	36-40°	16-20%	1.19-1.25
Passable	41-45°	21-25%	1.26-1.34
Cohesive	46-55°	26-31%	1.35-1.45
Very cohesive	56-65°	32-37%	1.46-1.59
Non-flow	>66°	>38%	>1.60

2.2.4 Powder flow through a silo

Silos are vessels used for storing granular materials. Depending on their shapes, silos are also called bins, hoppers, or bunkers (Figure 2-5) [162]. Roberts [202] indicated that the best performance of powder flow in silo design generally comes from symmetric bin shapes. Asymmetric shapes make the prediction of wall loads much more difficult and frequently provide segregation problems with free-flowing materials of various particle sizes. It has been found experimentally that the mass flow rate of coarse materials from silos is approximately independent of the head or height of the material above the exit slot, provided that the head is larger than a few multiples of the size of the exit slot.

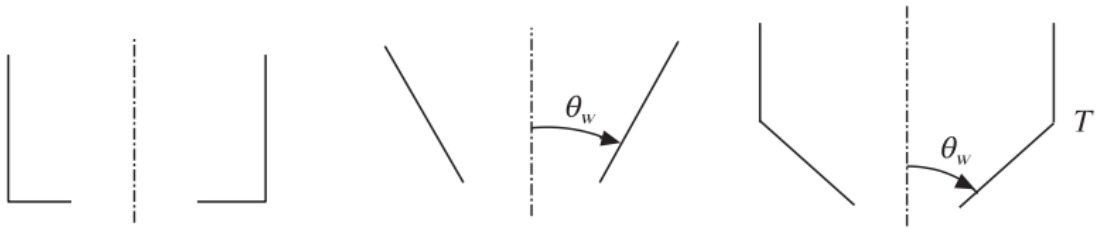

(A) Bin (B) Hopper (C) Bunker

Figure 2-5 Shapes of silos: (a) bin, (b) hopper, and (c) bunker. In (c), T denotes the transition point [162].

The first systematic study of flow in a silo was performed by a Swiss apiculturist Huber-Burnand [203]. Two types of flow patterns were observed around the hopper outlet [162]. When the walls of the silo are steep at a height above the

outlet, the velocity varies smoothly across the hopper (Figure 2-6A). This pattern is called mass flow. In contrast, when the wall angle (Θ_w) is large, there is a core of rapidly moving material bounded by shoulders of material moving very slowly. This flow pattern is called funnel flow or core flow as shown in Figure 2-6B.

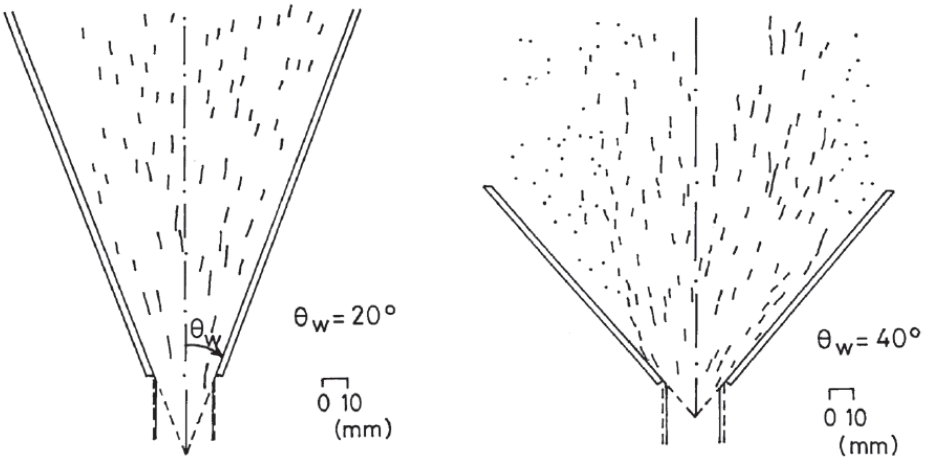

(A) Mass flow, wall angle Θ_w=20° (B) Funnel flow, wall angle Θ_w=40°

Figure 2-6 Flow patterns in (a) mass flow, and (b) funnel flow [204].

Many of the problems related to hopper design can be avoided by designing the hopper to run with a mass flow pattern. However, in cases in which mass flow is not really necessary then funnel flow design may be used. Table 2-6 compares mass flow and funnel flow in hoppers.

Table 2-6 The comparison of mass flow and funnel flow [205, 206].

Flow Profile	Mass flow	Funnel flow
Characteristics	• The entire material is in motion and moves down with a velocity of the same order • The flow pattern is a first-in and first-out type • This is usually achieved in silos equipped with steep smooth hoppers and large outlet diameters.	• The flow pattern is of a first-in last-out type • Stagnant zones reduce the silo capacity.
Advantages	• Most productive flow. • Problems like channelling, hang-ups, flooding of powders	• Suitable for hard abrasive free-flowing materials due to little wall wear.

Flow Profile	Mass flow	Funnel flow
	do not occur. • Stagnant regions are eliminated. • Caking, degrading and segregation are minimised.	
Disadvantages	• A steep hopper angle is required which makes the silo relatively tall • The flowing material contributes to high dynamic wall stress (in particular at a bin/hopper transition) which requires thick silo walls. • Friction between the moving solids and the silo and hopper walls result in erosion of the wall, which gives rise to contamination of the solids by the material of the hopper wall.	• The bulk solid has a tendency to degrade or cake due to stagnant regions. • Piping can occur when non-flowing materials are consolidated and the material still remains stable at the wall after the flow channel was emptied. • Wall stresses are slightly higher than these during filling.

Staniforth [169] noted that powders with very low wall friction angles will empty freely, even from hoppers with very shallow slopes, whereas powders with very high wall friction angles will empty poorly even from steep walled hoppers. In Figure 2-7, two flow patterns are determined by the relationship between wall friction and hopper angle. The wall friction angle is an important factor for the mass flow of a bulk solid and also structural silo design [207]. Wall friction angle often decreases with decreasing wall surface roughness but the influence of surface roughness is less pronounced with very fine grained, cohesive powders (< 50 μm), than with coarse bulk solids [170]. Also, the finer the bulk solid normally the larger the wall friction angle [170].

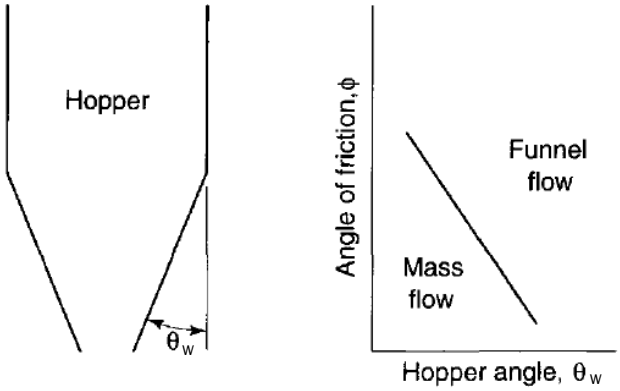

Figure 2-7 Influence of hopper wall angle and powder-wall friction [169].

2.2.4.1 Arching

In mass flow, only the potential problem of arching remains where a stable arch forms above the silo outlet so that discharge stops. The formation of arches occurs over an outlet if the outlet is smaller than a critical value [208-210]. This behavior, which leads to the powder flow ceasing, is one of the most important behavioural characteristics of powders [211]. With noncohesive coarse particles, the cause for mechanical arch formation is the interlocking of solid particles if the particles are large with respect to the opening. For cohesive fine particle, the reason for arching is the cohesive strength caused by consolidation and interparticle forces. The arch is a capable of supporting the weight of powder above [170]. Mechanical and cohesive arches are presented in Figure 2-8. To avoid the formation of a mechanical arch the outlet (dimension B) should be more than four times the maximum particle or gathering size [202]. For a cohesive arch, the outlet should also be big enough to prevent the formation of an arch. The studies of Reisner [212] and Schwedes [213] point out that the minimum hopper orifice size (D_o) to prevent arching should be around 3 to 10 times of the maximum particle dimension (D_p), i.e. D_o/D_p = 3-10.

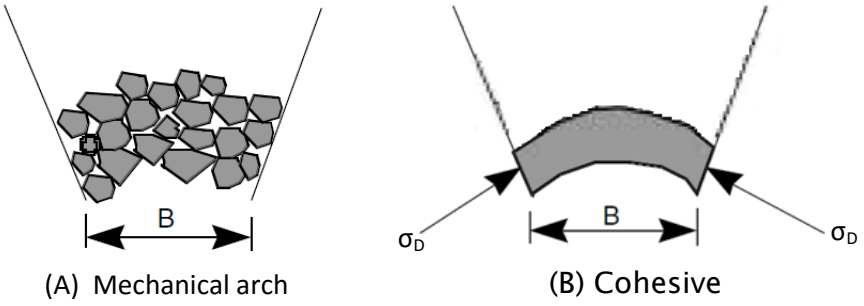

Figure 2-8 Mechanical and cohesive arches [202].

In mass flow design, the aim is to find the hopper half-angle (α) and the minimum outlet (B) to prevent a cohesive arch. Typically, the actual outlet should be larger than the minimum value required for the desired flow rate to ensure that a mechanical arch cannot form. In general, powder is uncompacted when it was firstly deposited in a container. As it flows the powders become compacted under the action of compacting stresses, which lead to powders developing strength. An arch will break and let powder flow by gravity when the strength developed by the powder is less than the stresses acting on the surface of the arch. Figure 2-9 shows the correlation between the strength of powder and compacting stress; the greater the compacting stress the greater the strength [206].

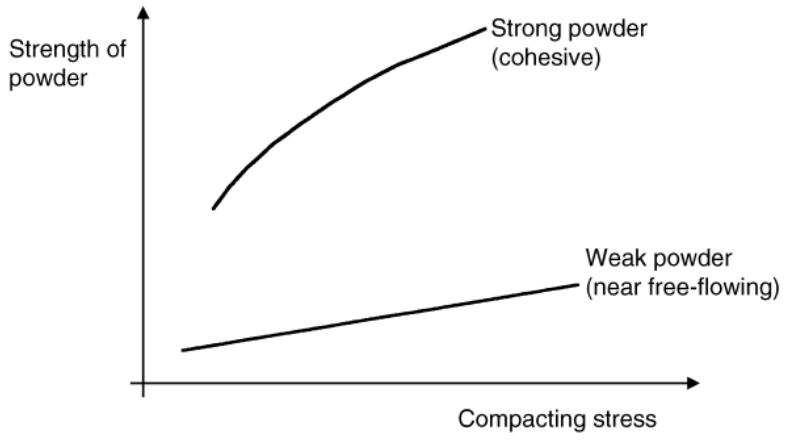

Figure 2-9 Variation of strength of powder and compacting stress for cohesive and free-flowing powders [206].

The flow factor (ff) relates the stress developed in a powder (σ_D) to the compacting stress acting in the container (σ_C). The flow factor is given by:

$$ff = \frac{\sigma_C}{\sigma_D} = \frac{compacting\ stress\ in\ the\ hopper}{stress\ developed\ in\ the\ powder} \quad (2\text{-}3)$$

A high value of ff means low flowability since a high σ_C means greater compaction, and a low value of σ_D means more chance of an arch forming. Suppose that the yield stress (i.e. the stress which causes flow) of the powder in the exposed surface of the arch is σ_y. The stress σ_y is called the unconfined yield stress of the powder. Then if the stresses developed in the powder forming the arch are greater than the unconfined yield stress of the powder in the arch, flow will occur. That is, for flow:

$$\sigma_D > \sigma_y \quad (2\text{-}4)$$

This criterion can be rewritten as:

$$\frac{\sigma_C}{ff} > \sigma_y \quad (2\text{-}5)$$

This may be plotted on the same axes as the powder flow function (unconfined yield stress, σ_y and compacting stress, σ_C) in order to reveal the conditions under which flow will occur for this powder in the hopper. The limiting condition gives a straight line of slope 1/ff . Figure 2-10 shows such a plot. In powder flow function “a” (line a), the powder has a yield stress greater than σ_C/ff and no flow occurs. Where the powder has a yield stress less than σ_C /ff flow occurs as shown in powder flow “c” (line c). Powder flow function “b” (line b) is a critical condition, where the unconfined yield stress, σ_y, is equal to the stress developing at the powder, σ_C /ff . This gives rise to a critical value of stress, σ_{Crit}, which is the critical stress developed on the surface of the arch. If the actual stress developed is less than σ_{Crit}, the powder will not flow. If the actual stress developed is more than σ_{Crit}, the powder will flow.

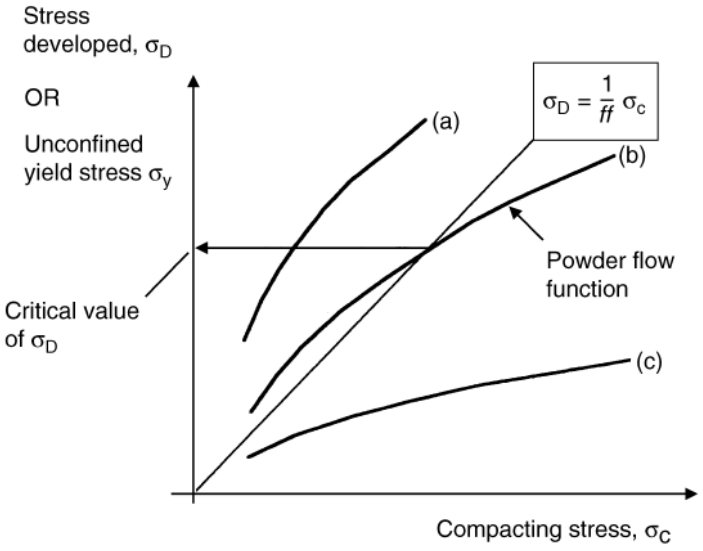

Figure 2-10 Determination of critical conditions for flow [206].

The critical outlet (B_{crit}) is obtained when the stress in the arch (σ_D) equals the unconfined yield stress (σ_y). This condition occurs at the intersection point of the flow function. The critical outlet (B_{crit}) for flow developed by Jenike [189, 214] is defined as:

$$B_{crit} = \frac{\sigma_{crit} H(\varphi)}{\rho_B g} \tag{2-6}$$

Where ρ_b is the bulk density and g is acceleration due to gravity. H(φ) is a factor determined by the slope of the hopper wall (hopper half-angle). The function H(φ) for a conical hopper is not clearly known but may be approximated by the following expression [215]:

$$H(\varphi) = 2 + \frac{\varphi}{65} \tag{2-7}$$

The flow factor (ff) depends on the nature of the powder characterized by the effective angle of internal friction (δ), the nature of the hopper wall characterized by the angle of wall friction (ϕ) and the slope of the hopper wall (φ) characterized by the angle between the sloping hopper wall and the vertical. Therefore, the flow

factor is a function of both powder properties and of the hopper properties. Knowing the flow factor and the powder flow function, the critical stress in the arch and the minimum size of outlet can be determined.

Lozano et al. [216] showed experimental evidence of a two-dimensional symmetrical silo arch structure breaking at the weakest linkage, which is the particle clinging to its neighbours in the arch with the highest angle (ϕ_{max}) as shown in Figure 2-11. The higher the maximum angle the easier it is to break the arch. It always breaks away when the angle (ϕ_{max}) is more than 180˚. Janda et al. [217] found that at intermediate orifice sizes in silo discharge, arches do not arrest the flow and the flow rate has large fluctuations. However, we knows very little about how the transition from flowing to arching/jamming occurs [209] and it requires more investigation to be well understood.

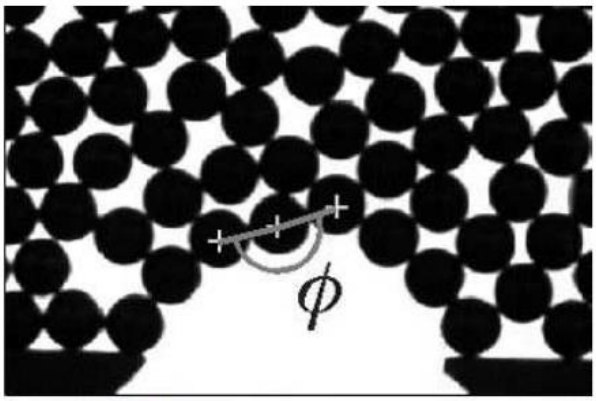

Figure 2-11 Indicating the angle ϕ for one bead [216].

2.2.4.2 Discharge rate

When an outlet is opened, the unrestricted rate of discharge of a powder under gravity is dependent on many parameters such as the powder's properties, the size and shape of the outlet and the hopper inclination [218]. Many equations can be found in the literature developed by empirical or dimensional analysis [219, 220]. Many equations are derived from an analogy to the outflow of liquids under gravity. For a large opened top system, which has an outflow of a distance (h) below the water surface, the velocity (w) of liquid flowing without friction, follows the Torricelli equation [170] :

$$w = \sqrt{2gh} \tag{2-8}$$

In powder materials, the stress is not proportional to height (h) but to the outlet diameter (D). So, the velocity (w) can be written as:

$$w \propto \sqrt{gD} \tag{2-9}$$

To gain the mass flow rate, the outflow velocity has to be multiplied by the cross section (A) and the bulk density (ρ_b):

$$\dot{m} = A \cdot \rho_b \cdot w \propto A \cdot \rho_b \cdot \sqrt{gD} \propto \rho_b \cdot \sqrt{g} \cdot D^{2.5} \tag{2-10}$$

In Equation 2-10, D has to be reduced because the cross section of the outflow is smaller than the real size of the outlet as Hagen [221, 222] proposed. Therefore, a term, kd, being proportional to the particle diameter, d, is subtracted from D.

$$\dot{m} \propto \rho_b \cdot \sqrt{g} \cdot (D - kd)^{2.5} \tag{2-11}$$

The equation presents the basic equation for the estimation of the mass flow rate of free-flowing, coarse powders. For a circular outlet (flat-bottomed silo) and coarse powders Beverloo [208] indicated:

$$\dot{m} = C\rho_b\sqrt{g}(D - kd)^{2.5} \tag{2-12}$$

where C and k are constant parameters; Beverloo found that C = 0.55-0.65 and k = 1.5-3.0. This equation fits very well for big orifices. However, it is not adequate for small orifices where a blockage is possible [209, 223]. Nedderman [222] suggested that Equation 2-12 should be used only for particle diameters in the range 0.4 mm $< d_p <$ D/6, where D is the diameter of the outlet.

The equation for a circular outlet proposed by the British Materials Handling Board [168, 224] for free-flowing coarse powders is :

$$\dot{m} = 0.58\rho_b\sqrt{g}(D - kd)^{2.5}k_\theta \tag{2-13}$$

In Equation 2-13, k is dependent on the particle shape (k=1.6 for spherical particles and k=2.5 for non-spherical particles). The hopper inclination (Θ) is taken into account by the factor k_Θ:

$k_\theta = (tan\theta)^{-0.35}$ for hopper inclinations Θ < 45°

$k_\theta = 1$ for hopper inclinations Θ ≥45°

Until the present, most studies on the discharge rate have focused on monosized particle in silos [225]. Generally, however, there are not many systems that are monodisperse powder. Arteaga and Tüzün [226] investigated the flow of a bidisperse mixture in silos. They modified the equation of Beverloo thus:

$$\dot{m} = C\rho_m \sqrt{g}\,(D - k_m d_m)^{2.5} \tag{2-14}$$

In Equation 2-14, ρ_m is mixture density, k_m is a fitted coefficient mixture particle, and d_m is a mixture diameter,

$$d_m = X_f d_f + \left(1 - X_f\right) d_c \tag{2-15}$$

where d_f is the fine particle diameter, d_c is the coarse particle diameter, and X_f is the mass fraction.

2.2.4.3 Vibratory devices

Typically, fine powder exhibits flow problems such as uncontrolled flow, unsteady flow, limited discharge rate and arching [227]. In some situations, it is preferable to handle fine powders in a fluidized state rather than to only handle them by gravity. Discharge aids or flow promoting devices are used to improve the flow pattern, to increase the discharge rate or initiate flow after arching. Discharge aids can be roughly classified into two groups; 1. Pneumatic discharge aids e.g, air injection and 2. Mechanical discharge aids e.g., knockers, agitators, vibrators [170]. The advantages of a vibratory feeder are its simple construction, low maintenance requirements, and low driving power [168]. By changing the amplitude (electromagnetic drives) or the frequency (all types of drives), the discharge rate can be regulated.

Vibratory devices are widely used to regulate and promote the discharge of powders from storage [228-232]. This method has proved to be an effective technique for handling fine and cohesive particles [233-235]. Many researchers [236-238] indicate that mechanical vibrations decrease the strength of bulk solids and hopper wall friction and increase the ability to flow. Vibrations induced at the silo wall aid to overcome wall friction. Additionally, vibrations quickly increase the stress in the bulk solid. Therefore, if the yield limit is attained, the vibration breaks stable arches. However the design of vibrating devices mounted directly on a silo wall is difficult, because the properties of the silo structure have to be taken into account (e.g., wall thickness and stiffness), and a (conical) hopper is particular stiff

close to its outlet (small radius of curvature) where stable arches are mostly formed.

Vibration promotes fine powder flow by reducing both unconfined yield strength and wall friction as examined by Roberts [239]. Xu and Zhu [240] pointed out in their study that vibration can reduce the tensile strength of the particle bed; vibration can overcome the interparticle forces of fine powders and improve their fluidization. Roberts [239] assumed that the effect of vibration decreases with increasing fineness and compressibility of the powders, because the latter increases the absorption of the vibrations. Intermittent vibration is regularly used for dome breaking. If continuous vibrations are used during discharge, the steady flow of powders will also be influenced by the vibrations [228].

Valdes and Santamarina [232] studied the maximum orifice to particle size ratio (D/d) for which arching is attainable. Their results showed that the arching thresholds (δ=D/d) is dependent on particle sphericity, roundness and surface roughness. Three regimes were identified: a stable arch structure occurs when D/d > δ_{min}, an intermittent arch structure and destruction occur when δ_{min} > D/d > δ_{max} and no arch when D/d > δ_{max}. They pointed out that the intermittent regime is sensitive to external vibrations, which is useful as vibration aids can be used to promote the destruction of the arch. They also noted that bridge sizes can reach 5 times the orifice to particle size ratio in a two dimension system. They suggested that it is easier to prevent arch formation than to destabilize formed arches. Janda et al. [229] studied the outflow of a small-orifice hopper continuously vibrated by a piezoelectric device. They found that vibrations did not significantly affect the flow rates both in the continuous and the intermittent system. They pointed out, however, that the flow rate significantly increases with the vibration amplitude.

2.2.5 Technical challenges of powder flow

Although powder materials are commonly used in various industries, powder flow in powder handling is not well understood. Similarly, vibratory aids used to initiate flow require more studies. Additionally, the goal of the hopper design process is the determination of the hopper slope necessary for mass flow and the minimum outlet size to prevent flow problems due to arching. Arching is one of the important problems in silo discharge and should be avoided. However, arching is the most important powder flow behaviour to use in dry powder printing. The

formation of an arch causes powder flow to stop. Without this mechanism, dry powder printing using ultrasonic vibration cannot regulate the start and stop cycle of a dispenser. Moreover, reports from the literature on micro dosage with small orifices are few and almost entirely use vibration to maintain continuous flow and prevent aching in powder flow. Our study will be focused on using vibration to control the flow of a fine powder through a small orifice size, and it is this which provides technical challenges.

2.2.5.1 Discharging mechanism of a micrometre-scale orifice using ultrasonic vibration

There is extensive literature and studies on bulk powder flow and discharge of powders from hoppers [222, 241]. However, there have been limited studies on the type of powder flow that occurs when vibrating is affected to a micrometre-scale orifice. Additional, almost all conventional hopper designs are for large scale storage, and thus of limited advantage when small flow rate is required. Previous studies on vibratory devices have mainly concentrated on a large hopper with an orifice size on a millimetre scale and frequency of amplitude less than 1,000 Hz. For example, the vibration parameters used in the experiment described in Fayed [238] were 200 Hz frequency and 0.01 mm amplitude, when particle sizes 425 to 2400 μm. Therefore, there is a need for a study of the flow process of fine powders through a small orifice assisted by an ultrasonic vibratory device. The details of the discharging process and the way in which the powder flows under this vibration involving a complex interaction between an ultrasonic transducer and a capillary tube is interesting and is worth investigating.

2.2.5.2 Effects of process parameters on discharge through a micrometre-scale orifice using ultrasonic vibration

High quality and reliable results for fine powder flow in a vibratory system requires an understanding of the effects of various process parameters, powder properties, and design configurations. These affect the flow behaviour. There is much knowledge on powder handling and powder flow to discover, especially when designing a new processing device. This knowledge can then be applied to other applications using a similar technique such as in pharmaceutical, powder handling

or additive manufacturing sectors. Therefore, any progress in the understanding of fine powder material behaviour could have an impact on these industries. In particular, the handling of the fine powder materials is an essential step during operations in many industrial processes.

2.3 Dry powder printing using vibratory assistance

Many studies have proved that MMAM can be possible in powder-based additive manufacturing such as in inkjet printing [42, 242], selective laser sintering [7, 243-245] and selective laser melting [246-248] . The most important benefit of powder-based AM is it can be used to process almost any material [249-251]. If the materials are compatible with each other, the bonding interface will have sufficient strength and a strong structure will be acheived [252]. Therefore, dry powder printing can be extended to layering patterns in powder-based additive manufacturing and be a good candidate for use in the preparation of multiple material layers.

In 1995, Matsusaka et al. [139] was the first group to apply an ultrasonic vibration to the microfeeding of fine powders. They tested seven different powders, whose size range varied from 0.4 to 40 μm. The dispensing device combined a capillary tube and a piezoelectric transducer which was used to generate ultrasonic vibration. Both were installed in a water bath used to transmit the vibration, as shown in Figure 2-12. They pointed out that a thin layer of micro-vibrated particles near the wall was the key for powder discharge. The study showed the possibility of a micro-feeding system for dispensing various fine powders in both continuous operation and intermittent operation. However, they only focused on a micro-discharge application.

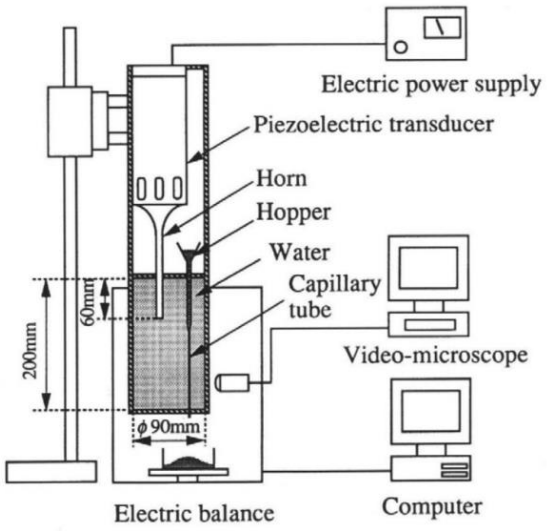

Figure 2-12 Experimental facilities in "Micro-feeding of fine powders using a capillary tube with ultrasonic vibration" [139].

Matsusaka et al. [253] built a simple device from a DC motor generator and a tube which could dispense submilligram doses of dry powders, as shown in Figure 2-13. They found that the particles near the wall vibrated at random and almost moved down as a lump of powder. Furthermore, they found that the powder flow rate increased with the vibration frequency and the critical frequency for powder flow was inversely proportional to the square root of the vibration amplitude. However, their work did not concern printing applications.

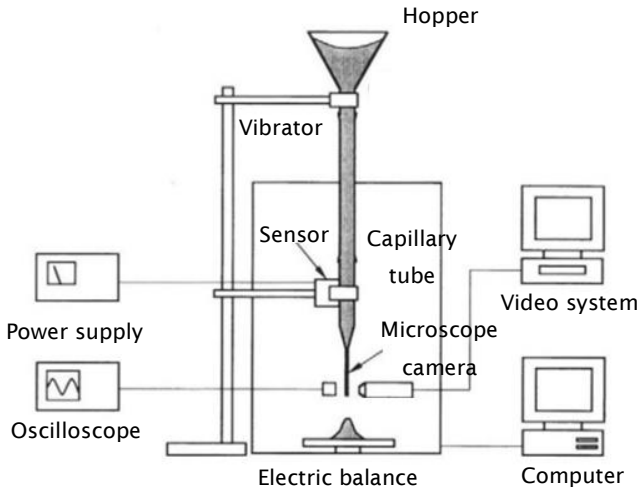

Figure 2-13 Experimental facilities in "Micro-feeding of a fine powder using a vibrating capillary tube" [253].

Li et al. [254] constructed a microdeposition device incorporating laser micromachining for developing a micro rapid prototyping system, as shown in Figure 2-14. The microdeposition device combined a piezoelectric plate coupled to a glass capillary through a tight fitting aluminium block. They observed that irregular shaped powders flowed move poorly than spherical powders. The minimum line width possible was almost the same as the inner diameter of the capillary tube. The results show a twisted and broken line resulting from the powder spinning inside the capillary. The diagram of micro-feeding mechanism in their work showed that the motion of the powder particle had orbited around the tube before coming out of the capillary tube. However, no experimental evidence was presented to support this.

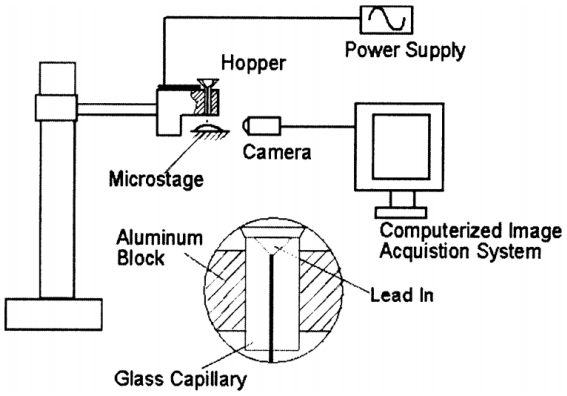

Figure 2-14 Experimental facilities in "Micro rapid prototyping system for micro components" [254].

Yang and Li [11] continued their previous works to understand the feeding mechanism of an ultrasonic microfeeding device. They indicated that ultrasonic waves could feed ultra-fine powder through micro capillary tubes because: (1) the vibration can break the stable dome structure and (2) the travelling wave can push the powder out of the tube. Their study showed that the powder density at the tip was higher than the density inside the hopper. This was attributed to the ultrasonic waves. They pointed out that thermal effects in the piezoelectric plate significantly affect the capability of this powder feeding device. The flow rates will decrease when the voltage applied to the PZT plate is greater than a certain value. In this study, they also showed a picture of the rotating powders in a hopper to confirm their conclusion. Moreover, they presented a printed line track with a width of less than 100 μm. However, all their printed results had the match-head effect at the start and stop.

Yang and Evan[255] developed a dry powder dispensing device using acoustic vibration to demonstrate the dispensing of a H13 tool steel powder via music waves. The dispensing device combined a glass capillary attached via a steel rod connecting a sub-woofer speaker, as shown in Figure 2-15. This study showed a new method of creating a miniature capillary valve without relative moving parts. However, it did not reveal useful information on the effects of control parameters and examples of the dispensing results.

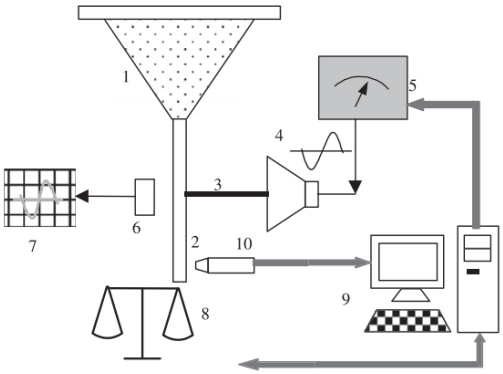

Figure 2-15 Experimental facilities in “Computer control of powder flow for solid freeforming by acoustic modulation” [255].

Kumar et al.[138] presented a concept for multiple material additive manufacturing using miniature hopper-nozzles designed for depositing multiple material patterns. They used a piezoelectric strip actuator contacting the nozzle exterior at the tip of a nozzle to control powder flow, as shown in Figure 2-16. They demonstrated the concept of multiple material printing and proposed simple equations for line width and line height. They showed many complex patterns. However, the minimum feature size was too big to be of interest in high resolution applications of additive manufacturing.

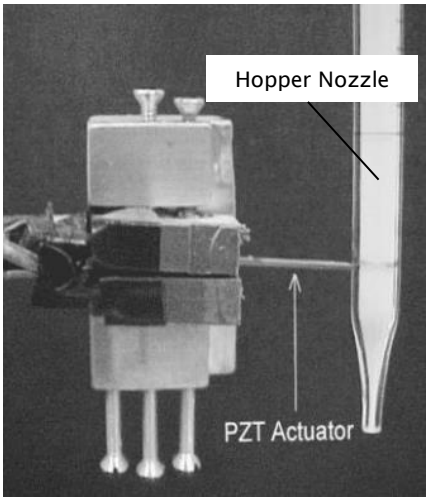

Figure 2-16 Experimental facilities in "Direct-write deposition of fine powders through miniature hopper-nozzles for multi-material solid freeform fabrication" [138].

Yang and Evan [256] developed a device built from an ultrasonic generator and a 280- μm-orifice glass capillary in a water tank that can dispense samples of dry powder of mass down to 0.05 mg, as shown in Figure 2-17. In this work, they combined the device with a motion control system to print fine dots of 12-μm WC. They reported that they could successfully print Fe powder and Hydroxyapatite powder. However, this work only demonstrated dot prints, which were generated by intermittent 24 kHz pulses.

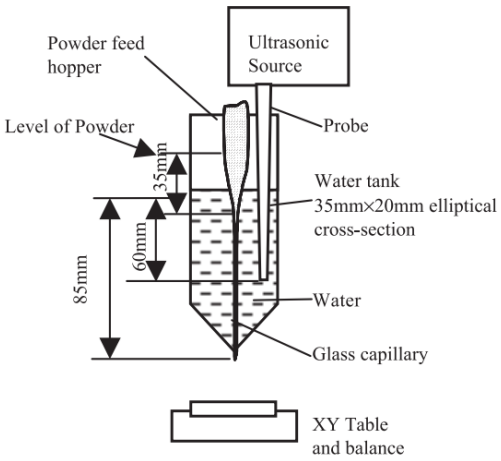

Figure 2-17 Experimental facilities in "A dry powder jet printer for dispensing and combinatorial research" [256].

Yang and Evan [257] developed acoustic control of powder dispensing, by means of a device with a stainless steel rod and a glass capillary of diameter 450 μm. The rod was mounted on a sub-woofer speaker given the reproduction of low-pitched audio frequency. This speaker generated the vibration movement used to start or stop dispensing from the glass capillary, as shown in Figure 2-18. They proposed the relationship between tube radius and particle radius affected jamming of the particles. However, the experimental powder had a wide distribution of particle diameters and was different from the proposed model based on monosize particles.

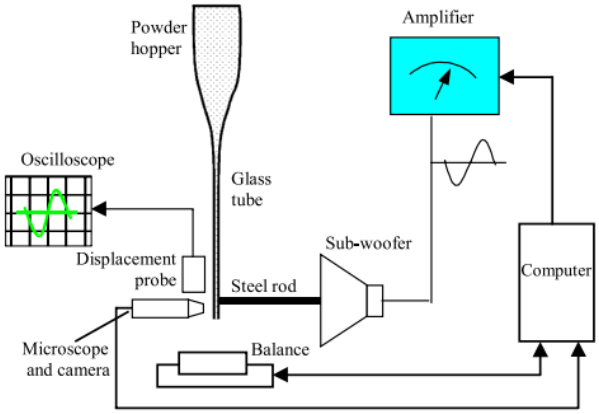

Figure 2-18 Experimental facilities in "Acoustic control of powder dispensing in open tubes" [257].

Yang and Evan [258] investigated the factors affecting the initiation of powder flow. This work was focused on the potential energy of static powder in a dispenser and the kinetic energy of a lateral input. They pointed out that large pulses tended to release more domes, causing a big gap requiring more time to fill and resulting in an over-run mass. Furthermore, they showed the over-run mass is a function of pulse acceleration. This work can used to understand the variation between dosages. However, this showed inadequate details related to multiple material printing applications.

Yang and Evan [259] developed a dual powder delivery device for programmable mixing dry powders by using an acoustic vibration technique, which used a steel rod mechanism generating vibration movement from a sub-woofer speaker, as shown in Figure 2-19. The study showed the possibility to produce Functional Graded Material (FGM) layers. Furthermore, they proposed equations to estimate mass flow rate, track width and minimum moving speed. However, they did not

show the comparison between the experimental results and the estimated values. Moreover, the minimum feature size was too large, which is not interesting for Additive Manufacturing applications.

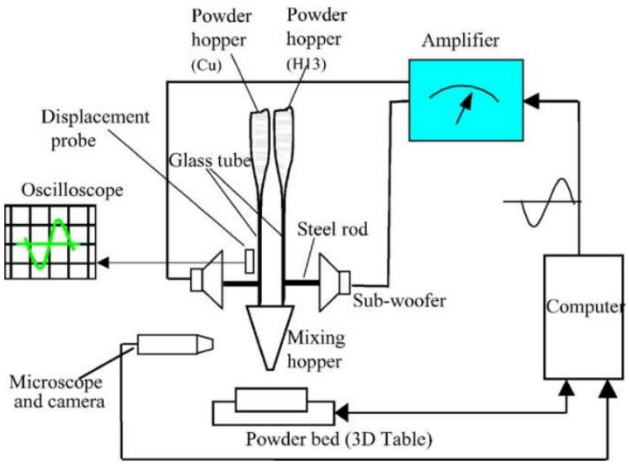

Figure 2-19 Experimental facilities in "A multi-component powder dispensing system for three dimensional functional gradients" [259].

Lu et al. [9] studied on ultrasonic microfeeding for fine powder. The experimental facility comprised a computer, an analogue waveform generator, a piezoelectric ring, a glass nozzle, a water tank and a microbalance, as shown in Figure 2-20. The study showed that particle structures can be divided into three types: arching, plugging and blocking. The dose mass was affected by nozzle diameter, transmission fluid depth, waveforms, voltage amplitude, frequency and oscillation duration. They pointed out that powders which are cohesive and low density tend to block the capillary tube. The relatively less cohesive and high density powders forming arching structures allowed dispensing. All of this study focused on microfeeding behaviour.

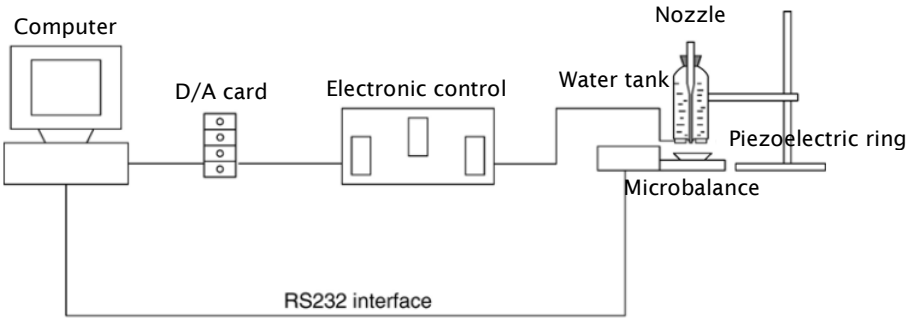

Figure 2-20 Experimental facilities in "Studies on ultrasonic microfeeding of fine powders" [9].

Lu et al. [260] carried out a study on the dose uniformity of an ultrasonic microfeeding device. They believed that dose uniformity is the important indicator to evaluate the microfeeding of fine powder. If the deviation of dose mass is small, it means the device is highly reliable. The study demonstrated the dot printing capability of WC powder achieving 42 DPI or 0.6 mm pitch on plain paper. They pointed out that the minimum dose mass is related to the strength of a stable dome structure and the nozzle diameter. Moreover, the signal voltage and oscillation time affect the dose mass as well as the uniformity. Additionally, they described the different dose forms columnar rod (H13), cluster (WC) and discrete particles (glass bead). However, the conclusion about the dose forms of WC and glass beads, where the angle of repose of both powders was relatively close, was not clear.

Lu et al. [261] investigated the design configuration of their dispensers. The experimental results from four design types showed that all configurations can dispense dry powder. They pointed out that perpendicular vibration using water as the transmission medium is effective and can deliver powder with a relative standard deviation (RSD) of 10%. Vibration with nominally a progressive wave using direct connection is also suitable for microfeeding and can attain a RSD of 5%. However, in the study, they did not conclude which design is the optimum design.

Qi et al. [262] constructed an ultrasonic powder-feeder device using an amplitude transformer rod contacting the capillary tube, as shown in Figure 2-21. They concluded that capillaries with cone angles in the range 30-60° result in stable feeding. Furthermore, they claimed the powder in a tube forming an arch may provide stable feeding. They indicated that the flow rates increase as the amplitude increases and noted that the amplitude has a small effect on flow rate when the orifice diameter is less than the certain number. The signal voltage should be greater than certain value to make flow stable. In this work, the minimum feature size was relatively large when compared with general applications in additive manufacturing.

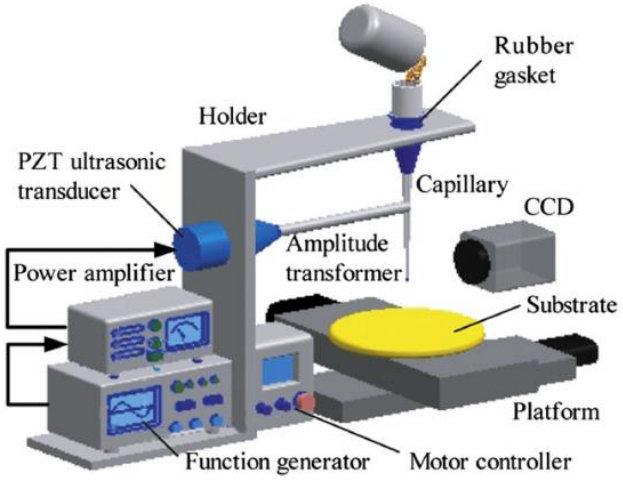

Figure 2-21 Experimental facilities in "Stable micro-feeding of fine powders using a capillary with ultrasonic vibration" [262].

Chen et al. [263] constructed a precision filling system for pharmaceutical powders using a vibrating capillary. They investigated the effects of parameters such as capillary diameter, frequency and amplitude on flow rate. A small hopper was mounted on the aluminium capillary assembled on a piezoelectric linear actuator, as shown in Figure 2-22. They pointed out that the orientation of vibration produced different results and should be taken into account. Moreover, they concluded that; the flow rate can be controlled by changing the input signal, frequency is more important effect than amplitude, and moderate vibration (800 Hz to 1200 Hz) and amplitude between 2-7 Volts lead to better dosing performance. In this study, they did not focus on additive manufacturing applications.

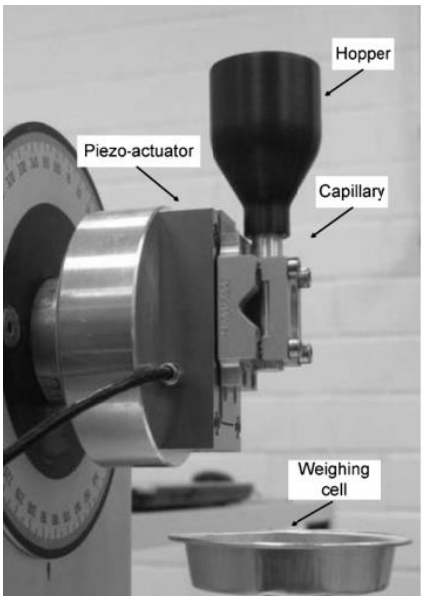

Figure 2-22 Experimental facilities in "Development of a micro dosing system for fine powder using a vibrating capillary. Part 1: The investigation of factors influencing on the dosing performance" [263].

Roper et al.[264] used ultrasonic powder deposition to fabricate graded dielectrics within a structural composite. The micro-dispenser was constructed using a glass tube and a piezoelectric ring shown in Figure 2-23, which was based on the previous work of Yang et al. [11, 255-259, 265]. In this study, they only focused on the fabrication of electromagnetic materials and controlled the pulse width to vary dot weights.

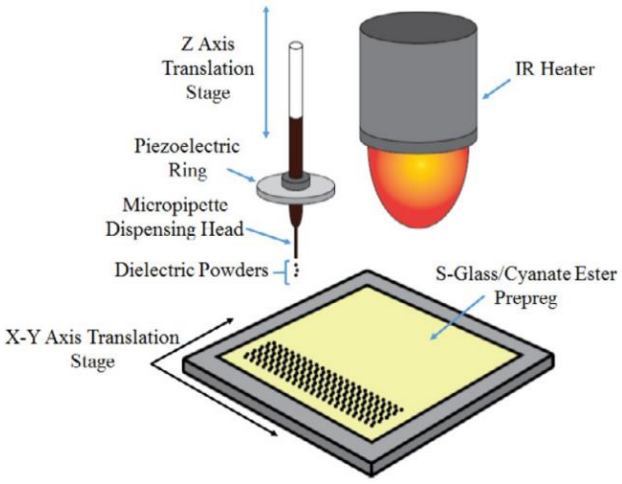

Figure 2-23 Experimental facilities in "Additive manufacturing of graded dielectrics" [264].

Stichel et al.[266] investigated the powder layering process in Laser Beam Melting. They developed capillary steel nozzles and used a vibrating excitation method. In this work, the experimental powder was only polyamide 12. They studied the effects of frequency, amplitude, mass flow rate and printing strategy. However, the printing results for single-layer patterns were relatively coarse and may not be acceptable.

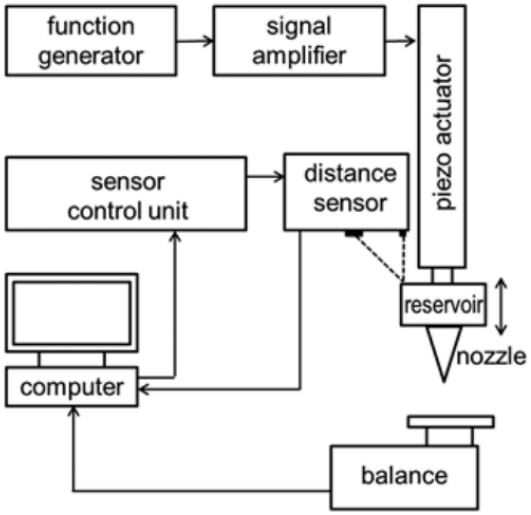

Figure 2-24 Experimental facilities in "Powder layer preparation using vibration-controlled capillary steel nozzles for Additive Manufacturing" [266].

The field of vibration-assisted dispensing of powders has been extensively researched in recent years as detailed the review by Yang [265]. Much progress has been made in recent years to achieve fine and dry powder printing, as summarized in Table 2-7. However, it is not sufficient for commercialization. Many early dry powder printing systems were large and required space to install. To develop the device it has to make sure that their characteristics meet the requirements. The construction should have the appropriate dimensions, strong and reliable enough to handling the printing powders.

Table 2-7 Studies on dry powder printing using a vibrating capillary.

Year	Author	Design Configuration		Material	Operation details					Studied parameters
		Vibration source	Transmission medium		Frequency	Minimum Flow rate	Orifice size	Minimum Feature size	Printing conditions	
1995	Matsusaka et al. [139]	Piezoelectric horn	Water	Fly-ash (5 μm), Alumina (1-40 μm), Alumina (3-10 μm, spherical), Antimony trioxide (4-7 μm), Silicon carbide (0.4 μm), Kanto roam (2 μm), Calcium bicarbonate (2 μm)	20 kHz	0.2 mg/s	0.58-1.26 mm	N/A	N/A	nozzle diameter, time, electric power
1996	Matsusaka et al.[253]	DC motor	Direct contact	Alumina (6 μm, irregular) , Alumina (20 μm, irregular) , Alumina (10 μm, spherical) , Fly-ash (15 μm, spherical)	760 Hz	0.2 mg/s	0.4-1.6 mm	N/A	N/A	nozzle diameter, frequency, amplitude
2002	Li et al.[254]	Piezoelectric plate	Direct contact	Cu (3 μm) , Stainless steel (3 μm)	49 kHz	10 μg/s	125 μm	119-378 μm	moving speed = 1-4 mm/s, standoff distance = 85-170 μm	voltage
2003	Yang and Li [11]	Piezoelectric plate	Direct contact	Copper (3 μm) , Iron (3 μm) , Invar (<22 μm)	44.9-46.65 kHz	10 μg/s	50 – 125 μm	≈80 μm	N/A	voltage
2003	Yang and Evan [255]	Speaker	Steel rod	H13 (< 212 μm)	40-4,000 Hz	≈ 8 mg/s	450 μm	N/A	N/A	nozzle displacement, waveform amplitude, waveform and frequency
2004	Kumar et al.[138]	Piezoelectric strip	Direct contact	Glass bead (38-45, 90-106 μm), Ti-6Al-4V (75-125 μm), PA6 (10-100 μm)	13 kHz	2.5 mg/s.	0.5-2.0 mm	0.8 mm	N/A	frequency, particle size
2004	Yang and Evan [256]	Piezoelectric horn	Water	WC (12 μm)	24 kHz	0.05 mg.	280 μm	300-400 μm	N/A	nozzle diameter, nozzle-hopper profile, vibration amplitude, vibration pulse width, level of powder in

Year	Author	Design Configuration		Material	Operation details					Studied parameters
		Vibration source	Transmission medium		Frequency	Minimum Flow rate	Orifice size	Minimum Feature size	Printing conditions	
										hopper, the amount of water and the depth of the probe in the water
2004	Yang and Evan [257]	Speaker	Steel rod	H13 (180-212 μm)	20-200 Hz	< 1 mg.	450 μm	N/A	N/A	nozzle diameter, amplitude, mechanical damping and particle size distribution
2004	Yang and Evan [259]	Speaker	Steel rod	H13 (90-105 μm), Cu (63-212 μm)	50-300 Hz	6-35 mg/s.	380-600 μm (Mixing hopper 800 μm)	≈ 1 mm	moving speed = 10 mm/s, standoff distance = 2-5 mm	rod size, frequency, waveform and reciprocal amplitude
2005	Yang and Evan [258]	Speaker	Steel rod	H13 (150–212 μm (13.2%); 106–150 μm (14%); 75–106 μm (15.6%), 38–75 μm (26.5%) and 29.2% less than 38 μm)	100-300 Hz	N/A	450 μm	N/A	N/A	Number of pulses and reciprocal amplitude
2006	Lu et al. [9]	Piezoelectric ring	Water	H13 (<22 μm) , WC (12 μm), Glass bead (42 μm), TiO2 (0.18 μm), MgO (0.1 μm), Starch (10 μm), Carbonyl iron (1.1 μm)	44.9-46.65 kHz	N/A	0.21-1.35 mm	N/A	N/A	amplitude voltage, water depth, frequency, wave form and oscillation period
2007	Lu et al. [260]	Piezoelectric ring	Water	H13 (<22 μm) , WC (12 μm), Glass bead (42 μm)	44.9-46.65 kHz	0.2 mg	0.2-0.35 mm	N/A	N/A	amplitude voltage and oscillation period
2007	Lu et al. [261]	Piezoelectric ring	Water/Direct contact	H13 (22 μm) , WC (12 μm)	39.5-47 kHz	0.1 mg	0.35-0.40 mm	N/A	N/A	design configuration, frequency and oscillation period
2011	Qi et al [262]	Piezoelectric rod	Direct contact	Cu (20-80 μm) , Zn (30-100 μm) , Fe (50-120 μm)	20 kHz	2-20 mg/s	150-360 μm	~0.5 mm	moving speed = 1-10 mm/s	powder structure on feeding, nozzle diameter, displacement of the transformer and nozzle amplitude
2012	Chen et al. [263]	Piezoelectric plate	Direct contact	Inhalac 70 (206 μm) , Inhalac 120 (135 μm) ,	800-1500 Hz	1-10 mg/s	0.5-2.0 mm	N/A	N/A	frequency, amplitude, the design of the capillary (angle of cone)

Year	Author	Design Configuration		Material	Operation details					Studied parameters
		Vibration source	Transmission medium		Frequency	Minimum Flow rate	Orifice size	Minimum Feature size	Printing conditions	
				Inhalac 230 (77 µm) , Respitose SV 003 (66 µm) , Flowlac 90 (136 µm)						
2014	Roper et al.[264]	Piezoelectric ring	Direct contact	HiK powder (dielectric powder) (30-250 µm)	42 kHz	1 mg	~0.5 mm	~3 mm	N/A	N/A
2014	Stichel et al.[266]	Piezoelectric rod	Direct contact	Polyamide (40-90 µm)	150-970 Hz	0.8-2.8 mg/s	705,1041 µm	850-1150 µm	13.3 mm/s	Amplitude, frequency, mass flow rate, hatch distance

2.4 Technical challenges of dry powder printing

As evidenced by Table 2-7, dry powder printing is a promising technique for a multiple material delivery device for the next generation of additive manufacturing. Little work has been done specifically on multiple printing using the dry powder printing method; however, some studies have shown that this technique may be a reasonable technique to use for material delivery device for MMAM. There are some technical challenges requiring investigation.

2.4.1 Reliability and repeatability

The device must be designed to emphasize reliability and repeatability in use. To achieve this, possible concerns of variations must be identified and minimised. From the literature, there are a few studies on this area. This characteristic is relatively important and useful for actual applications in additive manufacturing.

2.4.2 Compact and robust design

Yang et at.[9, 11, 118, 141, 142, 145, 245, 255-261, 265, 267-269] have provided much useful information. Their ultrasonic dispensing device with a water tank design can dispense various fine powders. However, we know powder flow is influenced by moisture. In this design, the powder discharged may be exposed to

water vapour or leakage during storage or processing and may cause problems. Moreover, many previous designs require a large space to install the system. To install many types of powder materials, the design should be compact and easy to install. Additionally, the device should be robust and insensitive to variations. In other words, it should have an output with a small standard deviation or the device should provide the design parameters that can minimise response variations.

2.5 Summary

From the literature, only a few studies on printing have been identified. There are many things to be explored such as the time delay of fine powder through the orifice, effect of different powders on dispensing, effects of dispensing parameters on mass flow rate, effects of nozzle design parameters on a dispensing device, fine powder spreading behaviour from the orifice, effects of printing parameters on a quality of printed track etc. Moreover, high quality printing results and images of a dry powder printing has never been reported in the literature. Similarly, the stable dome structure of fine powders in a micrometre size nozzle orifice, the flow characteristics of various powders, the spreading of powder after impact on a substrate have not been reported. Additionally, the guidelines and relationships to achieve the optimum results for printing patterns are required. All of the above concerns will be addressed in this thesis. More knowledge of dry powder printing will help us to understand the behaviour of fine powder flow through a micro orifice and lead to applications of this technique in other areas.

Chapter 3:

Experimental setup and methodology

This chapter details the materials and the experimental setup for a dry powder printing device, including the measurement and the calculations used in this research. The descriptions of dispenser fabrication, material preparation and material dispensing facilities used for the study are given.

3.1 Dispenser fabrication

3.1.1 Previous dispenser

A Dry Powder Printing technique requires a dispenser device to delivery fine powder particles. The dispenser device in this research is based on the earlier work of Yang. et al. [9, 11, 118, 141-147, 245, 255-261, 265, 269, 270]. They developed an acoustic micro-dosing device that utilized vibration energy to control the flow of fine powder from a glass nozzle by activating a piezoelectric transducer mounted at the bottom of an outer vessel filled with water as shown in Figure 3-1. The exact dimensions and details of the original design are illustrated in Appendix A.

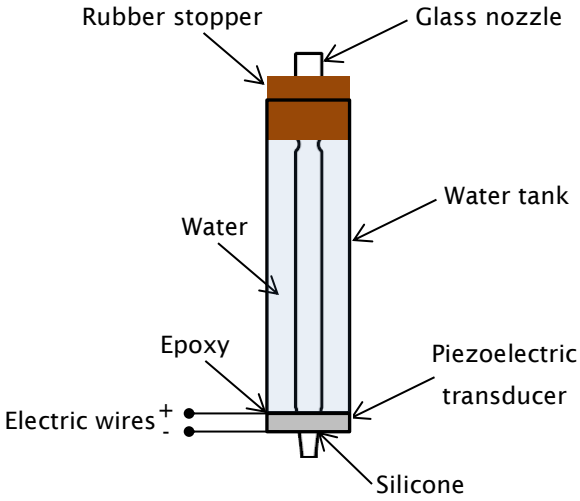

Figure 3-1 The construction of the original piezoelectric dispenser.

In the original design of this device, the dispenser consisted of a borosilicate glass nozzle, a piezoelectric transducer (ϕ25 mm.), a water tank, a rubber stopper and

two wires. The piezoelectric transducer was mounted at the bottom of the water tank with epoxy adhesive. The conical section of the glass nozzle was placed into a premade hole at the bottom of the water tank and sealed with a silicone adhesive sealant. To fully cure, the sealant required approximately six hours. Two flat wires were bonded at the top and the bottom of the transducer. The tank filled with water, which helps vibration propagation utilizing cavitation [9, 271], was closed with the rubber stopper which held the glass nozzle.

The previous design had a relatively big size. Sometimes a small installation space is inevitable which cause difficulty. In addition to the size, the function of the water tank creates another issue. Firstly it is not understood how effective it is in transmitting vibration and secondly this design also has a problem with water leakage from the water tank.

3.1.2 New dispenser

To make the dispenser more compact, the new significantly different design uses the smallest size of a standard piezoelectric ring (ϕ10 mm.), instead of the big piezoelectric ring (ϕ20 mm.), directly attached to a glass nozzle without the outer vessel filled with water. Figure 3-2 shows the new design of the piezoelectric dispenser. In our experiments, the dispenser consists of a glass nozzle, a piezoelectric transducer and two wires. Two flat wires were soldered to the top and the bottom surfaces of the piezoelectric transducer. The transducer is installed around the glass nozzle at a certain distance from its end by using epoxy adhesive. The details of the new design are shown in Appendix A.

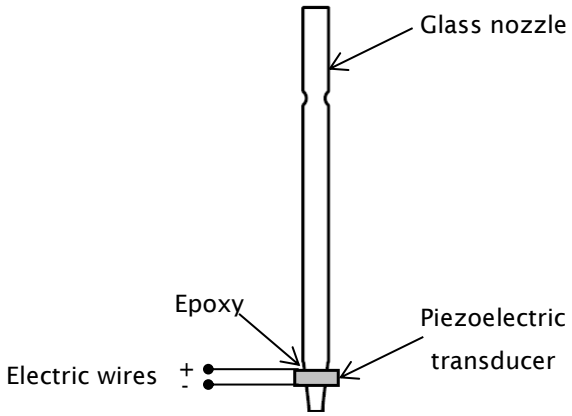

Figure 3-2 The construction of the new piezoelectric dispenser.

Comparing the design of the old and the new printing device one of the advantages of the new device is its smaller size. It is compact and can be installed in a small working chamber such as the small space in the traditional SLS/SLM system. Moreover, the new design has eliminated the water tank resulting in removing the water leakage possibility. The dispensing results of the device will be discussed in Chapter 4. The new design has fewer components, and therefore will consume less fabrication time, needs less maintenance, and provides higher reliability and maintainability with a minor cost compared to the former design described in section 3.1.1. Therefore, using the new design as a new material delivery device allows the problems associated with the previous device to be overcome.

3.1.3 Glass nozzle fabrication

Glass nozzles consisting of a small orifice, the size of which was used to regulate the powder dispensing process, were utilized in the study. Optimally constructed fine powder nozzles in the 60 to 400 μm range, with a smooth surface such as from glass, are not off the shelf components. Therefore, hand-made glass nozzles were fabricated with various geometries suitable for the experiments to be performed and to minimise experimental cost. Thus all glass nozzles in this study were made by myself.

One simple technique of making a micro scale orifice was to heat a glass tube and draw it while hot in a way that produces a taper cone with an included angle from 15˚ to 80˚. The closed tip was then broken off and ground back until the orifice size was of the desired diameter. The advantage of this method was no complicated equipment was needed and it was cheap. The disadvantages were lack of reproducibility of the exact shape and diameter.

The thin glass tubes used for the dispenser were converted from glass pipettes (Borosilicate glass Pasteur pipettes, 2.5 ml, total length 150 mm, outside diameter 7 mm, thickness 0.55 mm, FB50251, Fisher brand). The tips of the pipettes were heated and carefully drawn to reduce the size of the nozzles. Then the tip was gradually ground by SiC papers (Struers, Denmark) to the desired diameter. This range of nozzle tips diameters gave start/stop switching and flow rate control for the powder samples. Figure 3-3 shows the nozzle on the pipette and after drawing down the glass.

Figure 3-3 Glass pipettes used for the nozzle in the dispensing device.

To obtain an axially symmetric nozzle on a glass pipette, the pipette was attached to a low-speed (~40-100 rpm) rotating chuck while heating via a propane hand torch as shown in Figure 3-4. If too much heat was applied to the rotating glass pipette, the cone was long and had a sharp angle; low heat produced a short and wide angle. One can pull the lower end of a glass pipette to control the shape of the nozzle tip. This work was labour intensive and required trial and error to get the right cone angle. With the right flame set and the right distance, the desired results could be obtained. A detailed discussion of fabricating glass nozzles can be found in Lee [272].

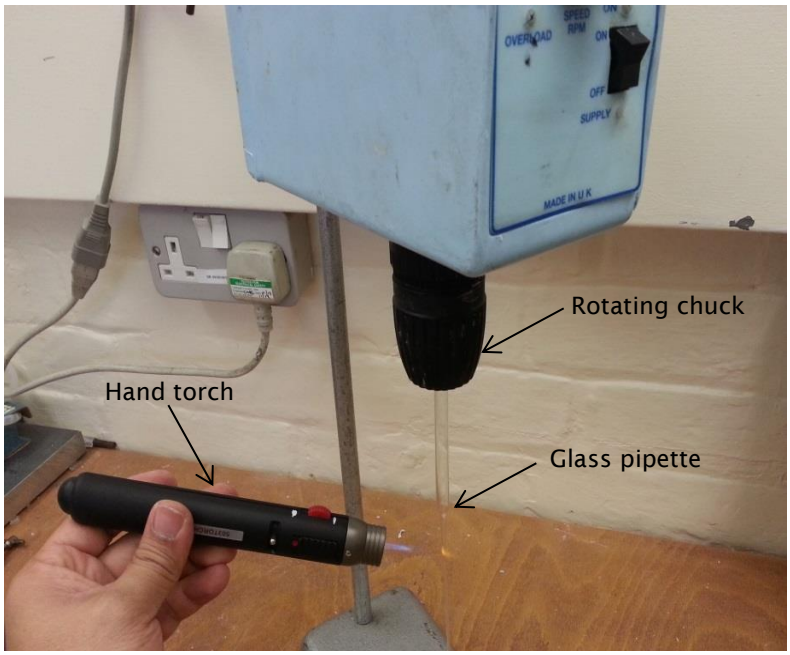

Figure 3-4 Setup for fabricating a glass nozzle using a rotating chuck.

After drawing many glass nozzles, a microscope was used to measure the angle of the nozzles (Figure 3-5A) and then to select a nozzle of the desired angle for grinding back (Figure 3-6A). The glass nozzle was ground on abrasive paper (800-

4,000) until the desired diameter of its orifice was reached (Figure 3-6B). For coarse grinding, 800-grit paper was used until the tip was open. After that, 1,200-grit paper was used to remove small amounts of glass until the desired diameter was reached. Finally, 4,000-grit paper was used to smooth the surface of the tip.

(A) Setup for angle measurement

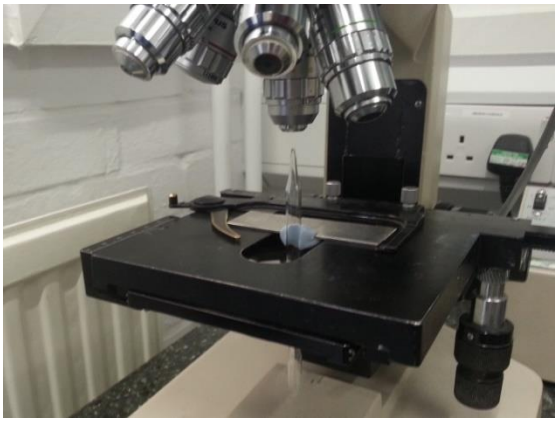

(B) Setup for diameter measurement

Figure 3-5 Setup used to measure the angle (A) and the diameter (B) of the nozzle.

For the sharp nozzle angles, the orifice diameter could be changed rapidly. Thus, it was necessary to stop grinding and check frequently. This fabricating process was an inexpensive method for making a micro-dosage dispenser but it was very difficult to fabricate reproducible nozzles.

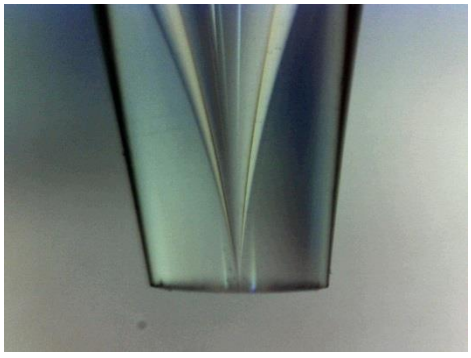

(A) Closed end

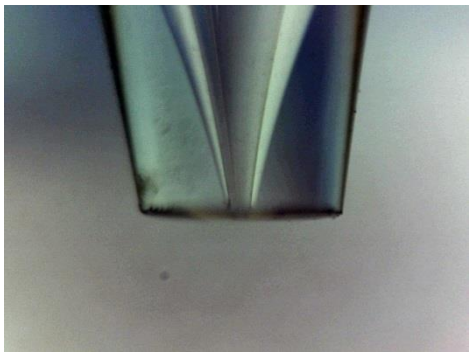

(B) Open end

Figure 3-6 Photographs of the tip of a drawn pipette: (A) Closed end and (B) Open end.

The method of determining the nozzle diameter was to mount the nozzle vertically on a microscope (Figure 3-6B) and use imaging software to measure the diameter (Figure 3-7).

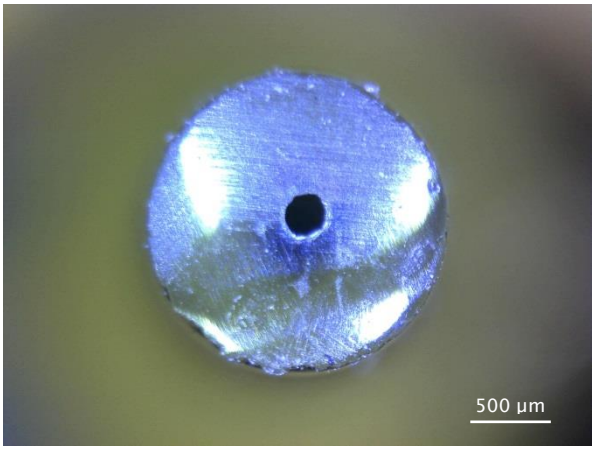

Figure 3-7 The 250-micrometre diameter orifice of the glass nozzle.

3.1.4 Piezoelectric transducer

A piezoelectric transducer converts electrical potential into mechanical force. When a voltage is applied to the piezoelectric transducer, deformation of the piezoelectric material is originated. This deformation creates vibration, the level of which is normally proportional to the voltage applied. Ceramic lead zirconate titanate (PZT) piezoelectric transducers were bought from MPI Co., Switzerland. The dimensions were 10 mm outside diameter, 5 mm inside diameter and 3 mm thickness. The resonance frequency of the piezoelectric transducer was 153 kHz. The specification and performance characteristics of the piezo are presented in Appendix B. The piezoelectric transducer produced powder deposition by vibrating the glass tube in the region where the transducer is located. This produced pulses that transmitted the vibration energy from the glass nozzle to the powder in the orifice region. The vibration energy was high enough to relocate the position of the powder particles and disturb the stable dome structure until the dome was broken and then the powder was discharged (as detailed in section 4.1.1 of Chapter 4).

Soldering wires to the piezoelectric element could surpass the Curie temperature of the piezoelectric material, which was 320˚C, and could depole the element. Furthermore, this can thermally debond the silver conductive coating of the piezoelectric. Therefore, the soldering temperature was set below 300˚C. Additionally, Lee [272] recommended that the best solder should have 3% silver content to minimise leaching of the coating of the piezoelectric transducer.

3.1.5 Assembly of a dispenser

A piezoelectric transducer was mounted around the glass nozzle using an Araldite (Huntsman, USA) epoxy, which is a two-part adhesive supplied in a syringe, and has a fast curing time. The surface of the glass nozzle was clean, dry, free from dirt and grease before attaching the transducer. Following the instructions from the supplier, equal volumes of resin and hardener were dispensed onto a clean surface. The two components were mixed by stirring for 30 seconds. Then, the freshly mixed epoxy was carefully applied to both the surface of the glass nozzle and the piezoelectric transducer. Then the nozzle was inserted into the transducer over the intended region. More epoxy was applied to the end of the transducer and the assembly maintained in position until the adhesive had fully cured. The complete dispensers are presented in Figure 3-8.

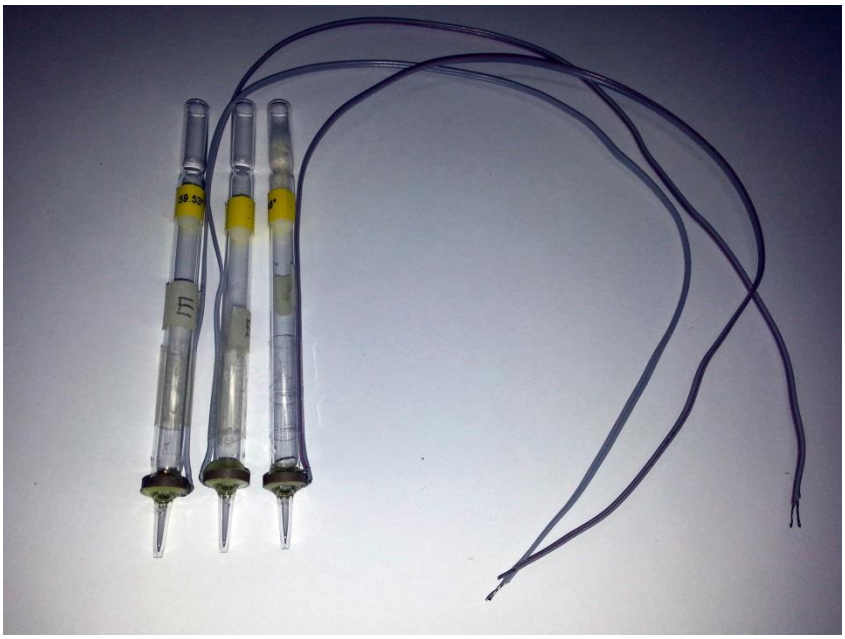

Figure 3-8 The complete dispensers.

All of the nozzles used in this research were carefully made and assembled. Nevertheless, as made by hand, the shape of the dispensers cannot be exact. There was an approximate error of ±2.5˚ for the nozzle angle, ±5 μm for nozzle diameter and ±2.5 mm for position of the piezoelectric from the desired values.

3.2 Material preparation and measurement

Ten fine powders were selected for the study as shown in Figure 3-9. The selected powder materials were copper (Osprey Metals, Neath, Wales), solder (Sn63Pb37, IPS (Suzhou) New Materials Co. Ltd., China), 316L stainless steel (Osprey Metals, Neath, Wales), tungsten carbide (Sandvik, Conventry, UK), alumina (Al_2O_3, BA Chemicals Ltd., Buckinghamshire, UK), CoCr (Concept Laser GmbH, Lichtenfels, Germany), 420S45 stainless steel (Osprey Metals, Neath, Wales), glass bead (Whitehouse Scientific Ltd., UK), and Glass-filled Nylon (DuraForm® GF, 3D Systems Corp., USA) in the size range 14-72 μm and their details are shown in Table 3-1. These materials were selected to cover metals, polymers and ceramics with different densities, particle sizes and particle shapes used in AM systems. Below is the general procedure used for the experimental powders.

3.2.1 Powder storage

The materials studied in this research were dry powders. As dry powders might absorb moisture or degrade, the experimental powders were thus kept in tight packages impervious to air and moisture and stored in a laboratory at 20±5 C° and 35±10 % RH.

3.2.2 Powder sieving

The particle size of the experimental powders is an important factor in a dry powder printing process. The size of the powder affects the test results. It was essential to sieve the experimental powders before testing to remove any contaminants in the powders which might interrupt a discharging process. The sieving was done by manual sieving. With one sieve two fractions, a fine and a coarse one, are gained. More sieves can be used to obtain a size range of powders. To screen the contaminants of the experimental powders before testing, in this study, the 100-μm sieve size was used before filling the powder into a dispenser, i.e. all particles dispensed passed through a 140 mesh sieve.

3.2.3 Apparent density

Apparent density or poured density or bulk density is the mass per unit volume of an untapped powder sample and includes the interparticulate void volume. This density depends on the density of the powder particles and the spatial arrangement of the particles in the powder bed. The apparent density is expressed in grams per millilitre (g/mL) and also in grams per cubic centimetre (g/cm^3). The apparent density is dependent on the preparation, storage and handling of the sample. The particles can be packed and may result in a changed bulk density. The apparent density of powders was determined by measuring the volume of a known mass of powder sample that had been passed through a sieve. A 5-mL graduated glass cylinder was used to measure the volume of powder sample. The powder samples were poured directly from the top of the graduated glass cylinder until the powder was 1 mL at eye level. A precision balance is then used to measure the mass of the powder sample. Thus the apparent density can be determined as:

$$\rho_A = \frac{m}{V} \tag{3-1}$$

Where V is the known volume from the graduated glass cylinder and m is the measured value from the precision balance. The average of 3 determinations was used to represent the apparent density of the sample powders.

3.2.4 Angle of repose

The angle of repose is the angle at which a powder sample can be piled without collapsing. This angle is widely used to classify the cohesiveness of powder materials. The angle of repose was measured in this study using our dispenser as a funnel test. The tip of the dispenser was placed 10 mm above a substrate. In the test, a powder sample was deposited on a horizontal ceramic plate for 5 seconds at a signal voltage of 2 Volts. The powder moved over the accumulated pile until the movement stopped. To measure the angle of repose, a Supereyes portable microscope (Shenzhen D&F Co., Ltd., China) was used to capture the front view of the conical pile and the angle was measured with ImageJ software (National Institutes of Health, USA). It was repeated three times in each sample. The angle of repose (α) of powders measured in this study is illustrated in Figure 3-9. The

average of three determinations was recorded to represent the angle of repose of the sample powders and is shown the value in Table 3-1.

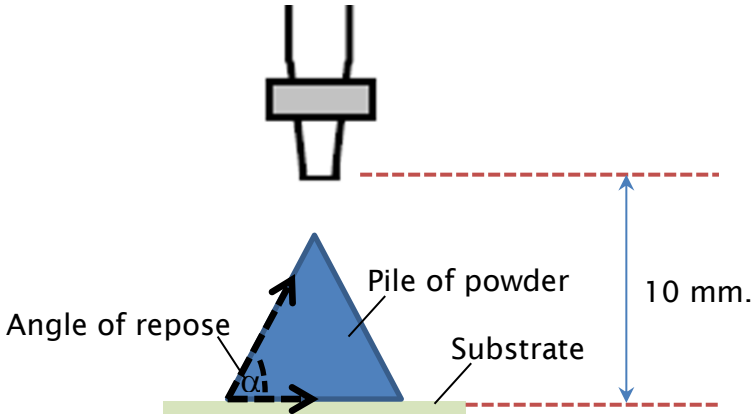

Figure 3-9 Angle of repose.

According to the flowability indicators in Table 2-1, powder flowability based on angle of repose is free-flowing from 31-35˚, fair from 36-40˚, passable from 41-45˚ and cohesive 46-55˚. The minimum value of angle of repose shown in Table 3-1 is 33˚, corresponding to the glass powder, and the second lowest is 35˚, corresponding to the solder powder. Therefore, these powders were determined to be free-flowing. The maximum value of the angle of repose presented in Table 3-1 was 52˚, corresponding to the copper powder and the second highest was 51˚, corresponding to the alumina powder. Thus, these powders were considered cohesive.

3.2.5 Particle size distribution

The size distributions of all material powders were analysed by using a light scattering size analyser (Malvern Mastersizer 2,000, Malvern Instruments Ltd., UK) to confirm that the size ranges were within specification. The analyser uses laser diffraction to determine the size distribution of the particles by measuring the angular variation in the intensity of the scattered light as a laser beam passes through a dispersed particulate sample. The small particles scatter light at large angles and large particles scatter light at small angles. The angular scattering intensity data is analysed to calculate the size of the particulate sample, which created the scattering pattern [273].

3.2.6 Particle morphology

The materials studied in this research had different morphologies such as spherical and irregular shapes. In order to determine the particle properties such as particle size, particle shape, surface morphology and particle agglomeration, a LEO 1455 VP scanning electron microscope (SEM) was used to observe the external appearance of the experimental powders. Prior to the observation, non-conductive powders such as glass bead and glass-filled Nylon were sputter coated with a thin electrically conductive gold film. Accelerating voltages from 1kV to 30 kV can be used in SEM. In our samples, the SEM was mostly operated at an accelerating voltage of 7 kV. Figure 3-10 presents the images of the experimental powders using the Scanning Electron Microscope (SEM) and the relevant features are summarized in Table 3-1.

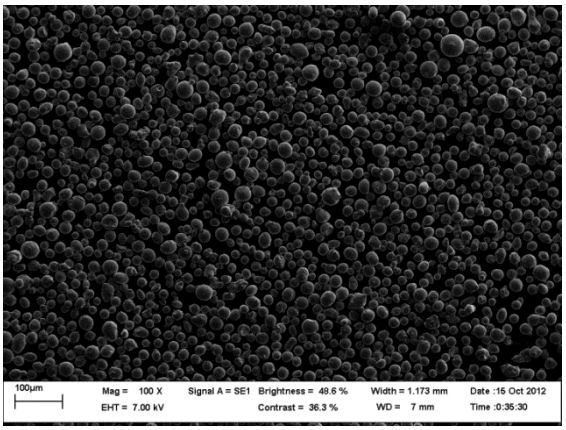

(A) 316L SS

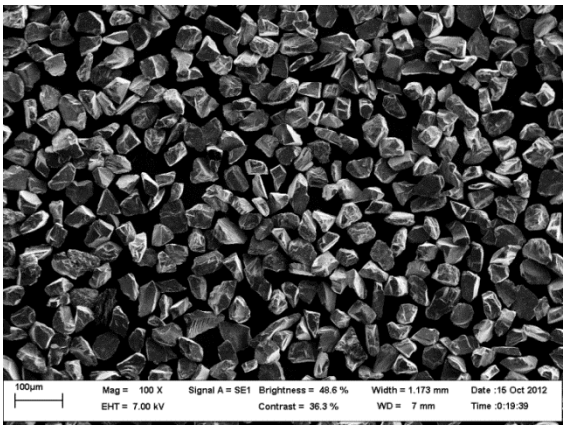

(B) SiC

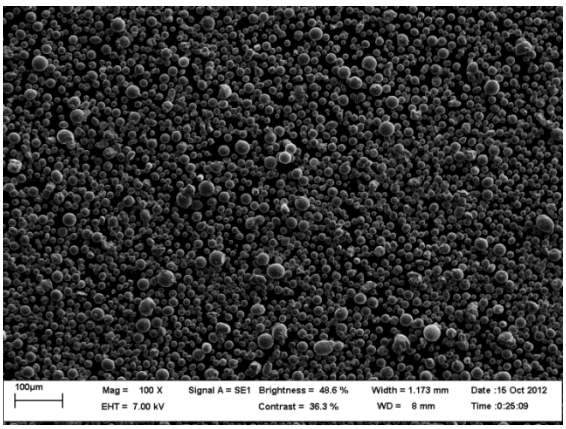

(C) CoCr

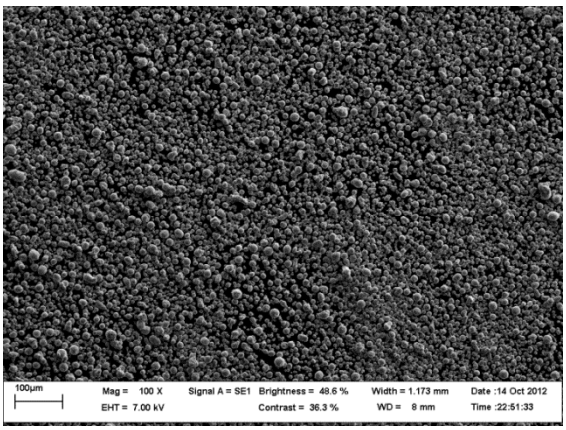

(D) Cu

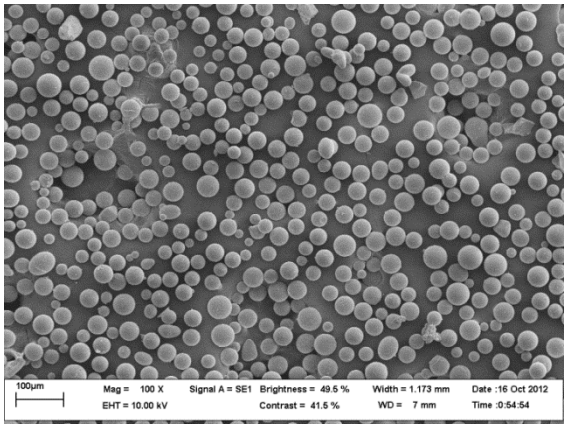

(E) Glass

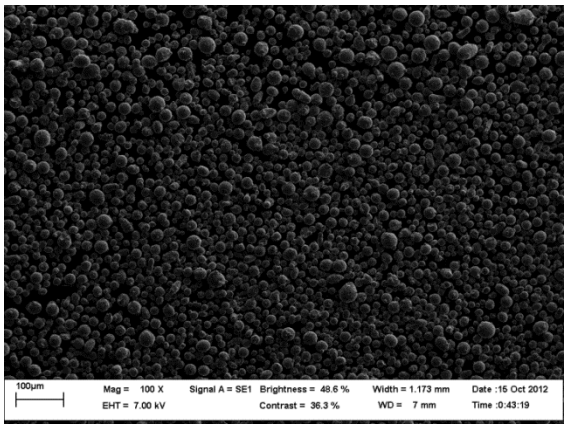

(F) 420S45 SS

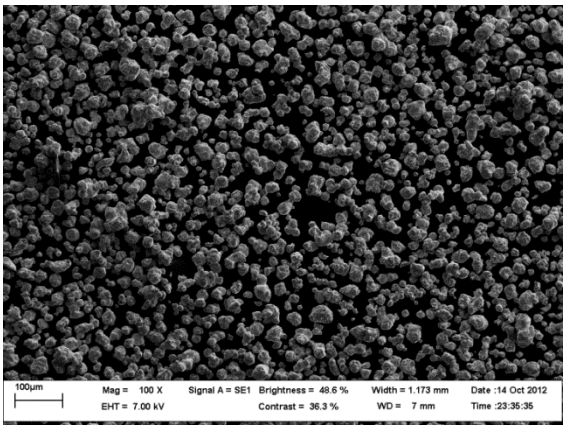

(G) WC

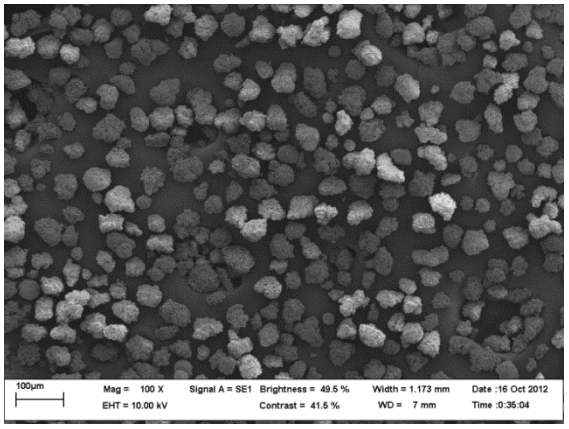

(H) Al_2O_3

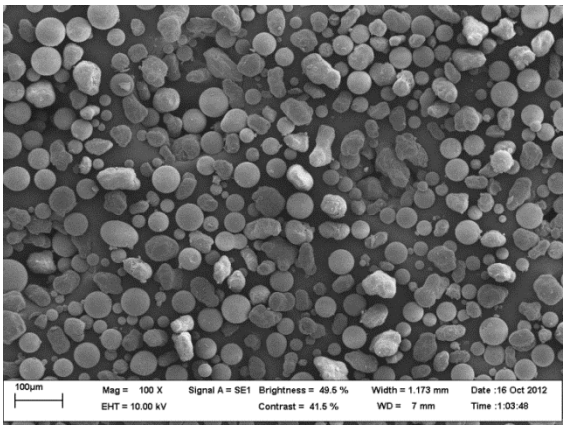

(I) Glass-filled PA

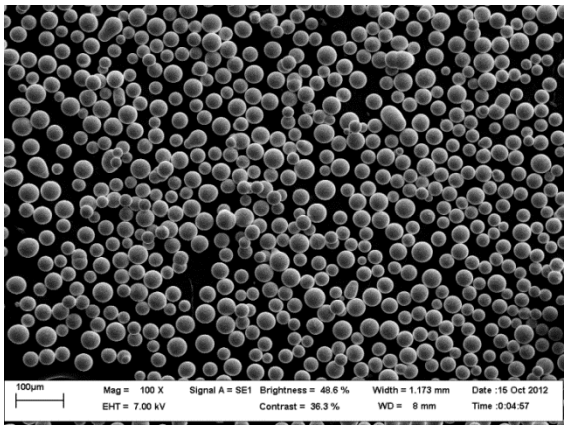

(J) SnPb

Figure 3-10 The images of the experimental powders using the Scanning Electron Microscope.

Table 3-1 Physical characteristics of the experimental powders.

Powder	Particle density (kg/m3)	Angle of Repose (degree)	D_{50} (μm)	Particle shape
Cu	8940	52±0.5	14	Spherical
SiC	3220	46±0.5	54	Irregular
Al_2O_3	3970	51±0.5	52	Spherical
Glass	2300	33±0.5	41	Spherical
CoCr	8290	48±0.5	18	Spherical
SnPb	8400	35±0.5	35	Spherical
316L SS	7890	46±0.5	32	Spherical
420S45 SS	7740	50±0.5	20	Spherical
WC	15500	45±0.5	35	Irregular
Glass-filled PA	1490	42±0.5	72	Spherical, irregular

3.3 Material dispensing facilities

The material dispensing facilities in this research are presented in Figure 3-11. These facilities were used to investigate the dry powder printing process that will be explained in section 3.5. The purpose of these facilities was to control the dispensing and the environmental conditions in the process.

3.3.1 Glove box

Most dry powders are sensitive to environmental conditions, particularly temperature and relative humidity. In order to control the specific atmospheric conditions of the experiments, a glove box (COY Laboratory Products Inc., Michigan, USA), which provides a leak-tight environment, was used. The glove box can maintain temperature and moisture either below and/or above ambient conditions. This glove box has an automatic monitoring system which controls temperature and relative humidity at set values. The glove box comprises a main chamber, a hinged pass through door, a transfer chambers and two glove ports.

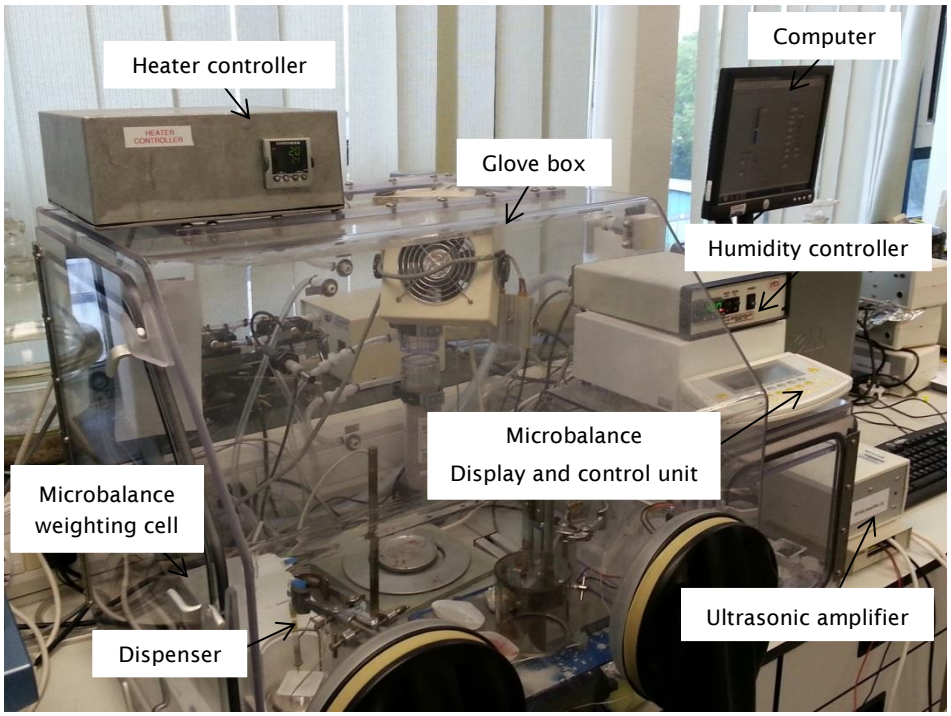

Figure 3-11 Material dispensing facilities.

3.3.2 Temperature controller

To control the temperature inside the glove box, a heater controller was installed. The controller takes an input from a temperature sensor placed inside the glove box and has an output that is connected to a heater and fan. The circulation fan is used to ensure uniform temperature in the glove box.

3.3.3 Humidity controller

A humidity controller (Electro-tech System Inc., Philadelphia, USA) was installed in the glove box to control the moisture content. It started and stopped the pump that activated the humidification and dehumidification apparatus when the moisture level deviated from the user-set point. The dehumidification consists of desiccant cartridges installed at the rear of the chamber and a pump that circulates air from the glove box through the desiccant. The humidification consists of a water chamber mounted in the interior of the chamber, water reservoir and a water pump located on the exterior of the glove box. The circulation fan is used to ensure appropriate uniform humidity throughout the glove box.

3.3.4 Microbalance

A Sartorius SE2 microbalance (Sartorius AG, Germany) was used in this study. The microbalance consists of a weighting cell and a display and control unit; it has an accuracy of 0.1 μg and has a weighing capacity of 2100 μg. The weighting cell is placed inside the glove box. It has a weighing pan which is positioned beneath the dispenser to measure the weight of powder dispensed. The display and control unit, which is placed outside the glove box, receives mass data by means of the communication port (RS232) of the weighing cell and sends data to a computer via a printer port. In this way, the signal from the balance is recorded and processed by the computer. After that, mass flow rate is calculated.

3.3.5 Ultrasonic amplifier

The ultrasonic amplifier was used to magnify the pulse wave signal sent to activate the piezoelectric transducer of the dispenser. This pulse signal causes deformation of the piezo leading to vibration assisted discharge. This amplifier uses a Sonic Systems driver board (Sonic Systems Ltd, UK). The driver is capable of delivering 50 Watts of output power in the frequency range 40 to 153 kHz. This board requires a 24 Volts DC supply capable of 3 Amps continuous current.

3.3.6 Computer and software

A computer and a LabView (National Instruments, Texas, USA) program allow the operator to input parameters that were suitable for the nozzles and powder materials. The LabView program in this study was developed by X. Lu and S. Yang at the Queen Mary University of London, it was used to generate the desired signal for driving the piezoelectric transducer of the dispenser [269]. There were two main parameters that were set in the LabView program. One was the wave amplitude of the signal voltage which regulated the strength of the piezoelectric deformation. Another one was the pulse width which specified the time duration of the ultrasonic vibration as shown in Figure 3-12. The LabView program also received the real-time data signal from the microbalance of the mass of powder dispensed.

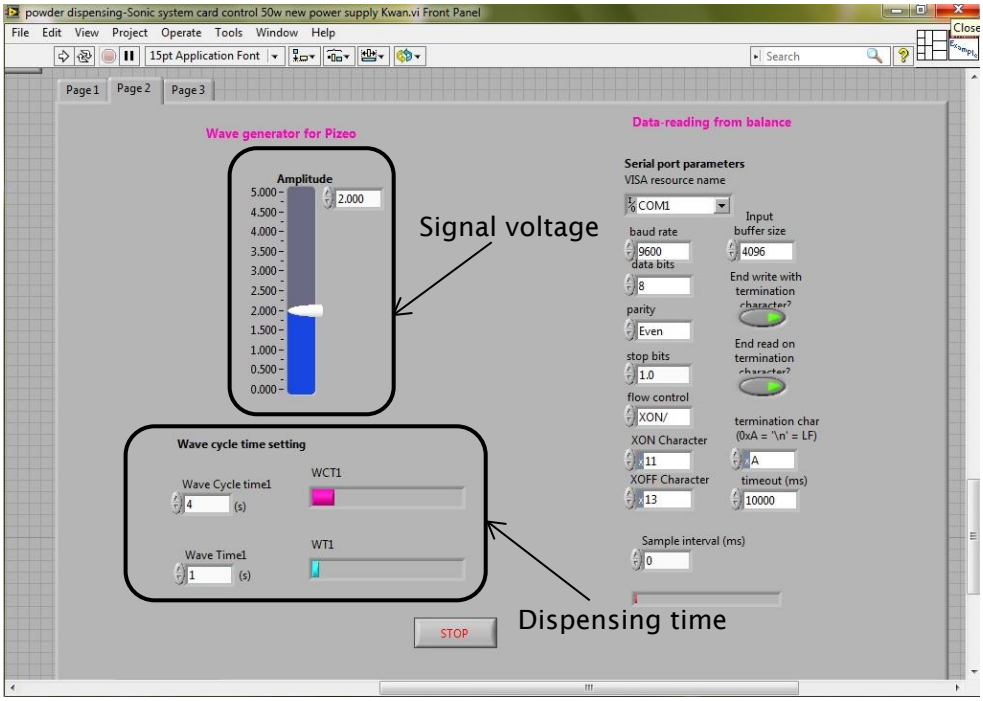

Figure 3-12 LabView control parameter interface.

The dispensing device could adjust the time duration by controlling the duty cycle, which is the proportion of the time during which a piezoelectric transducer operated (the dispensing wave cycle). This is shown schematically in Figure 3-13. The duty cycle can be presented as a percentage. To calculate a duty cycle, the signal's pulse width and wave cycle time were required. The following equation is used for calculating the duty cycle as a percentage of the wave time to the wave cycle time as shown in Equation 3-2:

$$\text{Duty Cycle} = \frac{\text{Wave time}}{\text{Wave cycle time}} \times 100 \qquad (3\text{-}2)$$

The wave time was the time that the device was turned on to dispense the powder, and the wave cycle time was the total time taken for a signal to complete an on-off cycle.

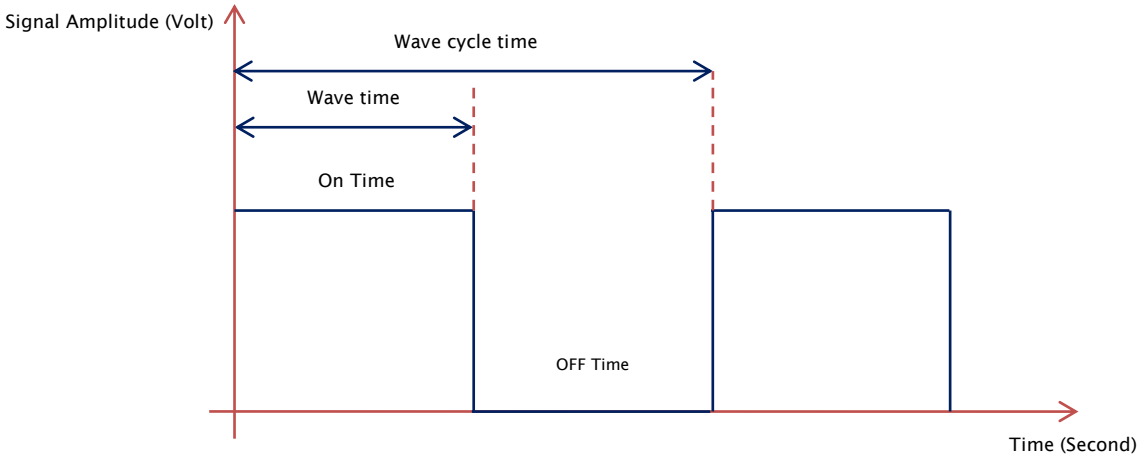

Figure 3-13 Schematic description of the signal parameters.

3.3.7 Dispensing evaluation

Mass flow rate and relative standard deviation (RSD) were employed to evaluate the dispensing results. The RSD was used to evaluate the dose uniformity as shown in Equation 3-3:

$$\mathrm{RSD} = \frac{\sqrt{\frac{1}{n-1}\sum_{i=1}^{n}(W_i - W_{mean})^2}}{W_{mean}} \times 100\% \qquad (3\text{-}3)$$

where n is the number of samples, W_i is the ith dose mass and W_{mean} is the mean dose mass. For RSD, a small number shows better consistency of powder dispensing from dose to dose.

3.4 Precautionary requirements

For our observations, clogging and semi-blocking were common problem. They mainly resulted from big contaminants or fibres in the powder inside the nozzle (as shown in Figure 3-14). These problems caused unstable flow of the powder. These problems always took place when relatively small-diameter nozzles (when compared with mean particle diameter) were used for dispensing. Therefore, the use of larger-diameter nozzles to reduce the chance of blockage minimises this problem. However, this solution could not guarantee a stable flow rate in powder

dispensing. Thus, it was necessary to ensure that the powders were sieved to screen contaminants before dispensing. To avoid the nozzle failing to discharge properly during the experiments, the dispensers required carefully intermittent checking and cleaning after 10 – 15 minutes of printing. This was achieved by wiping across the nozzle orifice with a lint-free cloth or blowing with dry air. Additionally, particles floating in the air or particles falling from the equipment occasionally can cause the problem by interrupting the dispensing process. In an ideal situation, the testing process should be carried out in clean room to avoid clogging or blocking from the unintentional particles. In some cases, the problem cannot be observed by eye; thus, a high magnification camera should be introduced to investigate and monitor this problem.

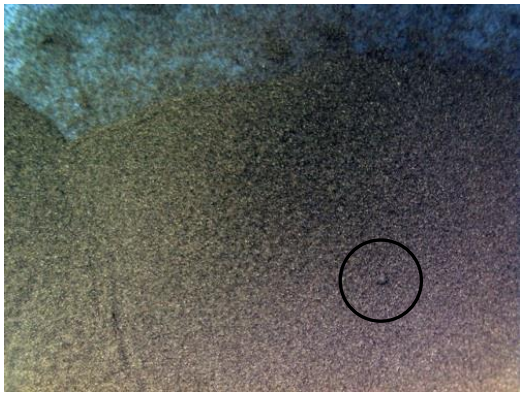

A) Agglomeration.

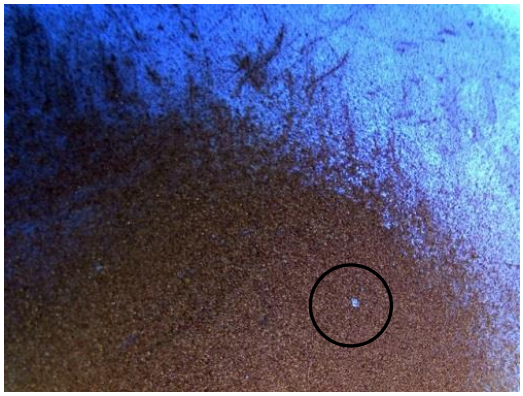

B) Contaminant particle.

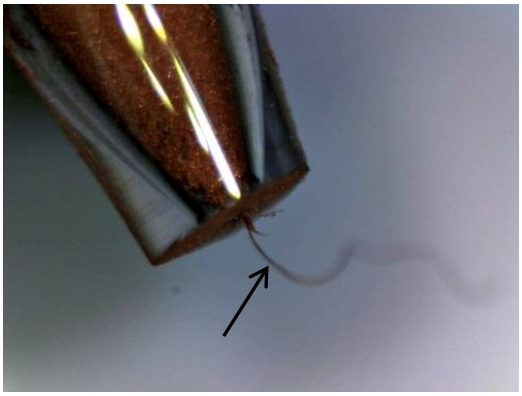

C) Contamination (fibre).

Figure 3-14 Causes of blocking from observations.

3.5 Scope of experiments

This research consisted of many experiments to study the effect of the many variables on powder dispensing. All of the experiments will be summarised in this section. Each experiment had some different procedures and parameters but the tests were on the same set of dry powder printing devices. In the following chapters all experiments will be presented in detail.

3.5.1 Investigating the behaviour of dry powder dispensing generation

This investigation observed the behaviour of fine powder flow through the dry powder printing device. All of the experiments were carried out under ambient conditions. There were two studies in this investigation. First was the generation of doming and the collapse of the stable dome structure of the solder powder. Second was the time delay in starting and stopping dispensing. The dispensing device was constructed of a transparent pipette glass, which allowed the users to observe the movement within the device. The dispensing characteristics were captured by a high speed camera. Furthermore, video imaging was used to investigate directly the relationship between the data output and the specific movements of the powder particles within the device.

The experimental set up of dispensing generation is shown schematically in Figure 3-15. The experimental apparatus consists of two computers, an analogue waveform generator (NI 6733 DAQmx card, National Instruments Corporation Ltd. Berkshire, UK), a power amplifier (50w, Sonic Systems Ltd, Somerset, UK), a hand-made glass nozzle (Pasteur glass pipette, Fisher Scientific International Inc., New Hampshire, USA).) attached to a piezoelectric ceramic ring (SPZT8-100-50x20, MPI Co., Switzerland) by an adhesive epoxy (Araldite Rapid Syringe-Epoxy Extra Strong, Huntsman Corp., USA) and a high speed video system (Photon Fastcam SA-3 monochrome system, Photron USA, Inc.) operating range of 1,000-4,000 fps to observe the flow behaviour of the discharging powder. The images were recorded at a rate of 1,000 – 4,000 frames per second (fps) and analysed via digital image processing (Photon Fastcam Viewer, Photron USA, Inc.).

The computer No.1, a dispensing controller, generates a rectangular signal wave at a set signal voltage to activate the piezoelectric ring on the glass tube. The high

speed camera captured the flow of powder deposited from the nozzle after vibration from the piezoelectric transducer and transferred the data to the computer No.2 through Gigabit Ethernet (RS-422). The signal from the computer No.1 was split into two signals. One was the standard amplified output signal that was sent to the piezoelectric ring to activate vibration for discharging the powder inside the nozzle. The other signal was the TTL (Transistor-Transistor Logic) signal, which had the same frequency as the standard output signal, to command the trigger of the video recording system via the computer No.2.

To capture the high magnification images of the flow of the powder as it was discharged in the experiment, the high-speed camera was attached to a c-mount adapter on a Leica Monozoom 7 (Leica Microsystem Inc., USA). This macroscopic lens was installed close to the dispenser. Image processing software, ImageJ, was also used to adjust and analyse the images.

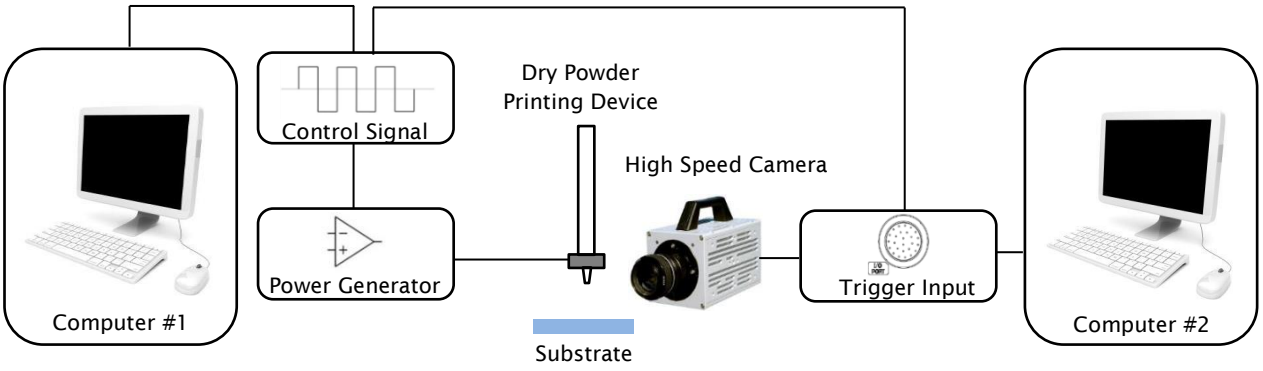

Figure 3-15 Schematic diagram of dispensing generation study.

To capture the images with a high speed shutter speed, the system required adequate lighting. This was achieved by two halogen lamps (650 W, Osram, Munich, Germany) installed in front of the nozzle device and a white-paper screen was place at the back of the nozzle as illustrated in Figure 3-16. The distance between the light sources and the dry powder printing device was about 1m to avoid disturbance from hot air generated by the light source. These investigations concentrated on the powder profile in the vertical and horizontal directions during dispensing. The images were taken against a white background with the high speed camera set to high resolution (512 x 512 Pixels). The position of the lights remained approximately constant throughout the experiment. In additionally, a

linear-scale reference was recorded for measurement purposes after the setting up of the experimental facilities was completed.

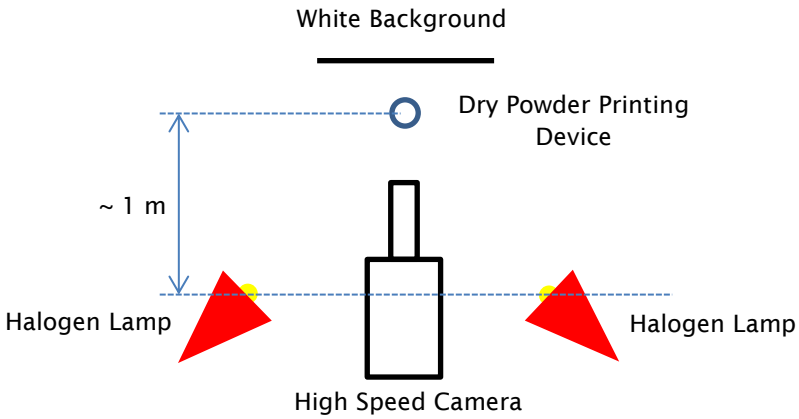

Figure 3-16 Schematic diagram of the light sources used for flow visualization (Top view).

3.5.1.1 Powder flow generation

In order to study the behaviour of dry powder dispensing, the solder powder that had spherical particles 35-μm in diameter was observed by the high speed camera. The design of the dispenser (Figure 3-17) used in this study had a nozzle diameter of 250 μm. The nozzle angle was 75˚. A piezoelectric transducer was attached to the glass pipettes at a distance of 12 mm from the nozzle tip (piezoelectric position). The signal voltage used was fixed at 2 Volts. The sequence of images captured from the starting dispensing to stopping dispensing of the solder powder from the glass nozzle was recorded. The magnified images around the powder dome were also captured. Also, analysis of the dome structure was conducted. The behaviour of powder discharge from the device was explored and is discussed in section 4.1.1 of Chapter 4.

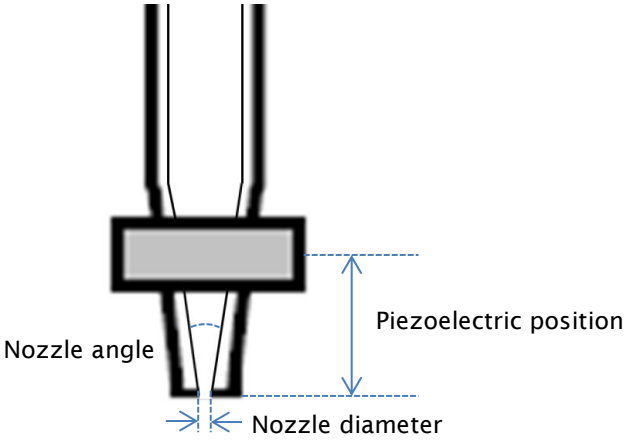

Figure 3-17 Design parameters and their reference levels for the experimental nozzle.

3.5.1.2 Time delay

For this study, the time delay of the dry powder printing device was tested with an example of a cohesive powder (copper powder) and a free-flowing powder (solder powder). These two spherical powders were chosen for detailed examination because they are common metal powders that are used in relatively large quantities in electrical-circuit applications, which is one potential application of multiple material additive manufacturing. The solder powder and the copper powder were spherical particles 35 μm and 14 μm in diameter respectively. To measure the duration time of the starting time delay, the dispenser was filled with the selected powder. Then the magnified images of powder dropping were captured using the high speed camera. Finally, the images were used to observe visually the nature of the discharge. The parameters studied are given in Table 3-2.

Table 3-2 Study parameters and their reference levels for the time delay experiment.

Parameters	Level
Nozzle Diameter	150 μm , 450 μm
Nozzle Angle	45˚, 65˚
Powder	Solder, Copper

To study the time delay, the response of the dry powder printing device was tested by switching the pulse signal of the ultrasonic controller on and off. TTL (Transistor-Transistor Logic) signal, which had the same frequency as the standard output signal, was used to start the recording of the high speed camera. In other words, the camera started recording when the pulse signal was ON, which was used as the starting point to measure the time delay of the dispensing. A pulse signal was applied to the dispenser with a wave cycle of 1 second and a wave time of 2 seconds. The results from the study with the parameters of Table 3-2 were based on conducting the experiment ten times. These results were compared and the discussion is presented in section 4.1.2 of Chapter 4.

3.5.2 Investigating the characteristics and design parameters of dry powder dispensing

There were five studies in this investigation to examine the characteristics and design parameter of the dry powder printing device. Figure 3-19 presents a schematic diagram of the dispensing study for the dry powder printing device. The apparatus employs the same computer control and amplifier as described in section 3.5.1. To assess the mass flow rate, a microbalance with a data transfer system is installed in this experimental setup. The experimental apparatus includes the computer, the analogue waveform generator, the power amplifier, experimental nozzles and a microbalance (2,100 mg ± 0.1 µg, Sartorius AG, Germany). All of the experiments required to assess mass flow rate were carried out in the glove box. The temperature was 20±2.5 ˚C. The relative humidity was also controlled at 35-45% to avoid disturbances caused by liquid bridge forces, which become relevant when the relative humidity reaches a value of 67-75% [274-276].

The computer was used to generate the level of the signal voltage and switching on/off of the signal voltage. The power amplifier generated a rectangular wave signal at a set signal voltage with a 40±3 kHz frequency to activate the piezoelectric ring on the glass tube. The microbalance recorded the weight of powder deposited from the nozzle by the vibration of the piezoelectric transducer and transferred the data to the computer through a serial port (RS232).

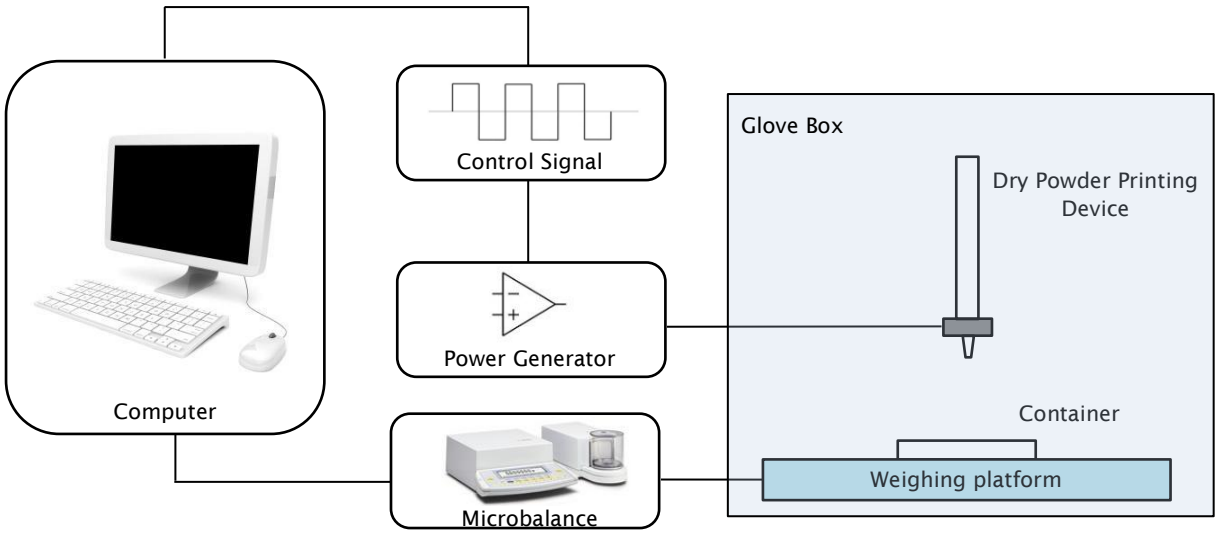

Figure 3-18 Schematic diagram of dispensing study.

For controlling the start and stop of the dispenser, the wave cycle time was 4 seconds with 1 second of ON time (pulse duration) and 3 seconds of an OFF time. In all experiments (except for the experiment in section 3.5.2.1), the dispenser was loaded with 3 grams of powder, i.e. approximately 30% of the full capacity of the dispenser. The data for dose mass were sampled at 60 points from the start to the stop of dispensing. To avoid the influences of unstable dosing during the beginning of dispensing, 20 points in a run-in region were not used and 40 points in a stable region were employed to calculate the dispensing mass (The justification of this suggestion is discussed in section 4.2.1). The weight of the particles discharged from the nozzle was automatically measured at constant time interval (1 s) by the digital microbalance. The relationships between the mass flow rate and the sequential number of dispensing were obtained by digital processing.

3.5.2.1 Powder dispensing profile

For the first study, the characteristic of the mass flow rate from the beginning of dispensing to material run out was observed. The experimental powder used was the copper powder. The particle diameter was 35-μm and the particle shape was spherical. The nozzle diameter used in this study was 350 μm. The nozzle angle was 65°. The position of the piezoelectric ring was 16 mm from the nozzle tip. The

signal voltage used was fixed at 2 Volts. The dispenser was loaded with up to 2 grams of powder. The data collection began at the start of dispensing and continued to the end of dispensing when the powder ran out. The analysis and the discussion on the mass flow rate profile from the dispensing device are shown in section 4.2.1 of Chapter 4.

3.5.2.2 Effect of different powders on mass flow rate

For the second study, the mass flow rate for different powder materials was explored. The solder powder and copper powder were used to evaluate the mass flow rate. A nozzle design with a diameter of 250 μm, a nozzle angle of 75° and the piezoelectric ring positioned of 12 mm from the nozzle tip were used in this study. The signal voltage was set at 2 Volts. The tests were repeated 4 times for each powder. The mass flow rate and RSD of these experimental powders were compared. The effect of different powders is discussed in section 4.2.2 of Chapter 4.

3.5.2.3 Effect of nozzle design and signal voltage on mass flow rate

For the third study, the effect of dispensing parameters on mass flow rate was investigated. The parameters selected were based on the literature review in Chapter 2 and the levels of the parameters were selected from our experience. Four dispensing parameters were considered to be controlling factors; signal voltage amplitude, nozzle diameter, nozzle angle and piezoelectric position. Each input parameter was studied at 2-levels to see the effect of each control factor, a low level represented by -1 and a high level represented by +1. Table 3-3 shows the list of the variable parameters and their levels. A 2^4 full factorial test was performed and it was repeated three times in each trial condition. The experimental powder used was the copper powder. The results from this study are analysed and the discussion is presented in section 4.2.3 of Chapter 4.

Table 3-3 Study parameters and their reference levels for the nozzle design and signal voltage experiments.

Parameters	Levels	
	Low	High
Signal voltage	0.5 Volt	2.0 Volt
Nozzle angle	45˚	65˚
Nozzle diameter	180 µm	270 µm
Piezoelectric position	10 mm	20 mm

3.5.2.4 Effect of nozzle diameter on mass flow rate

For the fourth study, whose purpose was to determine the influence of nozzle diameters on mass flow rate, two different powders namely the solder powder and the copper powder were selected. The signal voltage was set at 2 Volts. During the test, the same dispenser, successively ground to vary the nozzle diameter sizes, was used. The nozzle angle was 66˚. The piezoelectric transducer was attached to the glass tube 12 mm from the tip when the nozzle diameter was 110 µm. The sizes of the nozzle diameters were varied as shown in Table 3-4. Their mass flow rates were recorded and the results were examined. The results for the two experimental powders were compared and the discussion is presented in section 4.2.4 of Chapter 4.

Table 3-4 Study parameters and their reference levels for the nozzle diameter experiment.

Parameters	Details
Nozzle Diameter	110, 200, 255, 280, 320,375, 400 (µm)
Material	Solder, Copper

3.5.2.5 Effect of signal voltage on mass flow rate

For the fifth study, whose aim was to find the effect of signal voltage on mass flow rate for the dry powder printing device, the solder powder and the copper powder were again selected. The signal voltage was varied to see its effect on the mass flow rate. The levels of the signal voltage were changed in the range of 0.5-5 Volts

as shown by the steps in Table 3-5. A nozzle design with a diameter of 250 μm, a nozzle angle of 75˚ and a piezoelectric position of 12 mm from the nozzle tip were used in this study. The comparison of the two experimental powders and the discussion are detailed in section 4.2.5 of Chapter 4.

Table 3-5 Study parameters and their reference levels for the signal voltage experiment.

Parameters	Details
Signal voltage	0.5,1.0, 1.5, 2.0, 2.5, 3.0, 3.5, 4.0, 5.5, 5.0 (Volt)
Material	Solder, Copper

3.5.3 Investigating the characteristics and processing parameters of dry powder printing

This investigation explored the characteristics and processing parameters of the dry powder printing device. There were two main objectives in this investigation. The first objective was to dispense and observe ten different powders and to demonstrate the capability of the device by printing a variety of samples. They were both a single material in a layer and multiple materials in a layer. The second objective was to study the processing parameters of the device. The standoff distance and moving speed were varied. These results were to analyse and discuss the material deposition rate and the feature size of the printing track deposited. Problems affecting printing quality are presented and finally, the operation guidelines are developed. This is detailed in section 4.3 of Chapter 4.

The experimental apparatus includes a computer, an analogue waveform generator, a power amplifier, a motion controller, experimental nozzles and an XYZ movement. The computer contained a digital to analogue card controlling the Z column and X-Y table, which were driven by servo motor (Parker Hannifin, supplied by Micromech, Braintree, UK). The motion controller and a 6K4 card controlled the axes and the printing device through LabView and Motion Planner program. The experimental setup is as shown schematically in Figure 3-19.

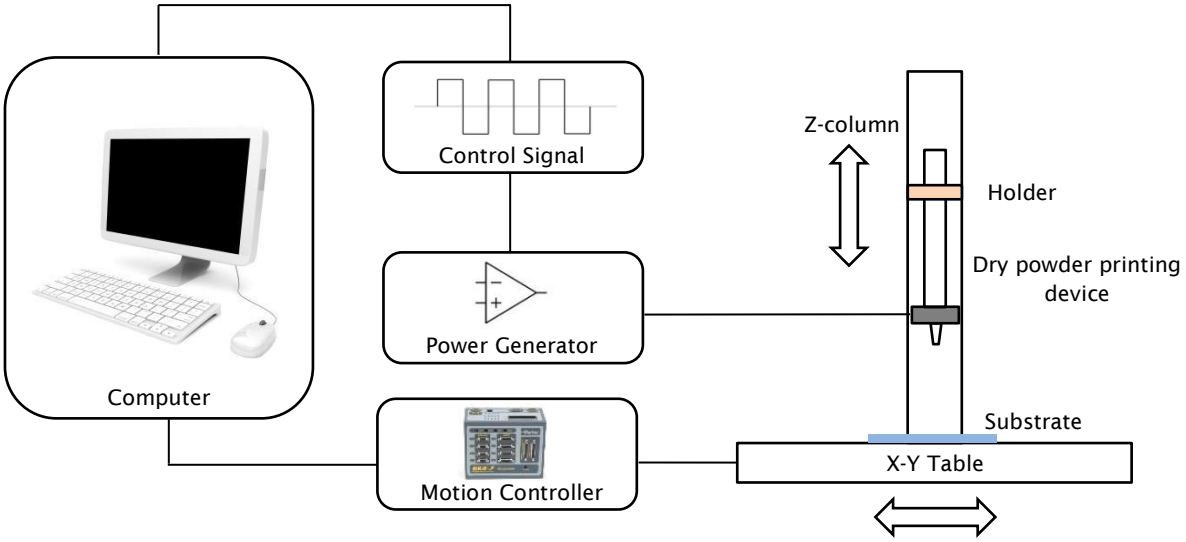

Figure 3-19 Schematic diagram of printing study.

The position of dry powder printing was controlled by an XYZ positioning system for traditional Cartesian coordination. The XYZ stage utilizes a workspace of 400 x 400 x 150 mm. The XYZ movement provided a positional accuracy of ±25 μm. The X-axis and the Y-axis moved a substrate on the platform in a horizontal plane. The Z-axis carried the dry powder printing device in a vertical direction. The substrate was placed on the X-Y platform below an independent Z-axis that the printing device incrementally moved up and down. After setting the vertical level, the printing system mounted on the Z-axis was immobile during the deposition of each layer. A photograph of the printing axes is shown in Figure 3-20.

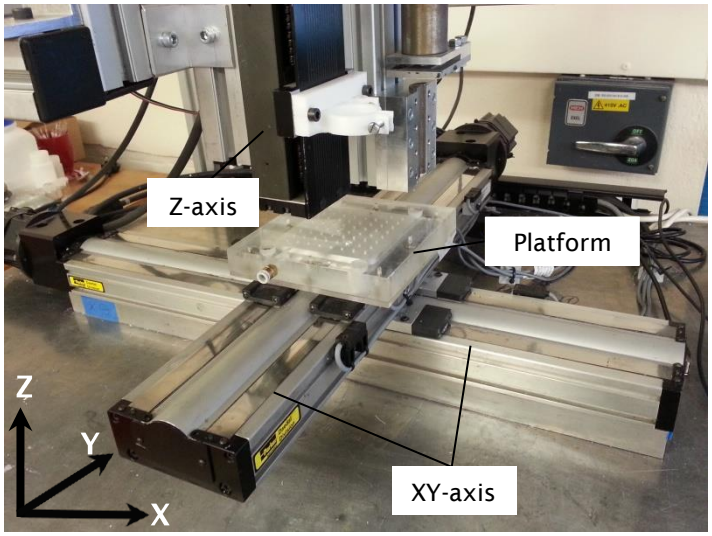

Figure 3-20 The axes and platform of the dry powder printing system.

To create a pattern layer by powder printing, this study required the X-Y table to move the substrate in relation to the nozzle. The X-Y table must be synchronized to print properly the desired drop pattern on the substrate. The use of the automatic X-Y movement allows printing of the material in various patterns depending on the programing. To prepare the test geometries, firstly the geometries were made by SolidWorks software (Dassault Systemes SolidWorks Corp., Velizy, France). After making the CAD model, the model was converted to DXF format and imported to CompuCAM solftware (Parker Hannifin, supplied by Micromech, Braintree, UK) to generate the tool path and commands for the X-Y table. The communication between the X-Y table and the dispensing device was managed by the Motion Planner software (Parker Hannifin, supplied by Micromech, Braintree, UK). The software ran the tool path programme and commanded the driver of the X-Y table. At the same time, the computer sent a command to interface Labview software to generate a signal to control the piezoelectric transducer of the printing device. In the single-material printing study, the system was mounted with one device on the Z axis (Figure 3-21). Three printing devices were assembled on the Z axis for the multiple material printing study (Figure 3-22). In order to assess the printed pattern, an optical microscopy was used (Olympus digital microscope, BX41, Olympus Corp., Tokyo, Japan). All of the experiments were carried out under ambient conditions; temperature was in the range 23-28 ˚C and relative humidity was in the range 36-45%.

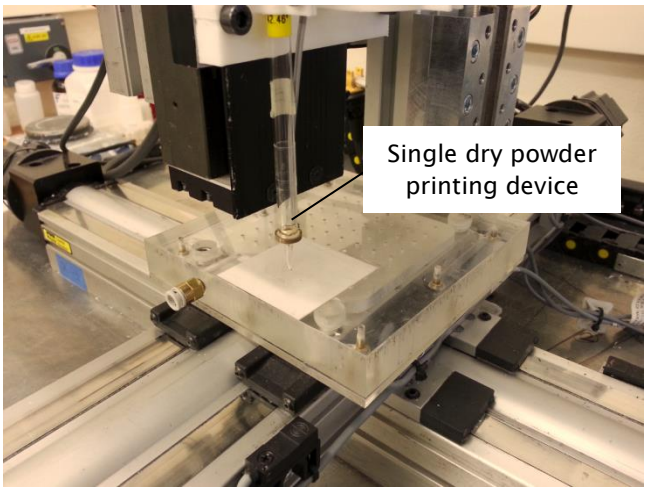

Figure 3-21 The set up for a single-material printing study.

Figure 3-22 The set up for a multiple-material printing study.

3.5.3.1 Printable powders

In this study, the powder materials were copper, solder (SnPb), 316L stainless steel, tungsten carbide, alumina (Al_2O_3,), cobalt-chrome (CoCr), 420S45 stainless steel, glass bead, and glass-filled nylon. The size range was 14-72 μm and their details were shown in Figure 3-10 and Table 3-1. To determine the flow pattern characteristics, the experimental powders were captured with the high-speed camera at 1,000 frames per second. The experiment was similar to the procedure outlined in section 3.5.1. All experiments used an identical dispenser with the same dispensing conditions. The design of the dispenser used in this study had a nozzle diameter of 250 μm. The nozzle angle was 75˚. The piezoelectric position was 12 mm. The signal voltage used was fixed at 2 Volts. The flow patterns of the powders were compared and discussed. All details are shown in section 4.3.1 of Chapter 4.

Also, to compare the difference in printing results from the ten powders, single-material printing onto a flat substrate was studied. Single-material printing samples were fabricated with the developed device to produce a dot, a straight line and a spiral line. All printing used a moving speed of 10 mm/s. After printing the samples onto the substrate, the results were analysed with the optical microscope. To evaluate the feature size, the track width of the tracks was analysed by imaging

software. The results for the powders were compared and discussed. All details are shown in section 4.3.2 of Chapter 4.

3.5.3.2 Effect of signal voltage on spray angle

This experiment investigated the effects of signal voltage on spray angle during powder particle discharge from the dry powder printing device. The solder powder and the copper powder were used in this investigation. The flow characteristics of the experimental powders were observed by the high speed camera to obtain information on the spray angle of the powder stream. The recording ability of the camera was between 1,000 and 4,000 fps, and the camera was focused on the nozzle orifice to record powder flow while dispensing the powders from the device. Different combinations of signal voltage, nozzle angle, nozzle diameter and powder material were tested. ImageJ software was then used to contrast appropriate low and high thresholds to aid analysis and measurement. These images were measured to estimate the average spreading angle of the powder stream for each combination. The detail of the setup facility was described in section 3.5.1 and the control values are given in Table 3-6. The comparison of the results is illustrated and discussed in section 4.3.2.1 of Chapter 4.

Table 3-6 The printing parameters of spray angle experiment.

Parameter	Details
Material	Solder, Copper
Nozzle design	1) 150-μm/12˚/12mm 2) 250-μm/12˚/12mm 3) 250-μm/75˚/12mm
Signal Voltage	0.5, 1.25, 2 Volts

3.5.3.3 Effect of dry powder printing parameters

There were three studies in this section. The copper powder was used in the experiments. The first study was to test the accuracy of the expected length. A series of tracks were printed with different lengths, from 1 to 10 mm, with 1-mm incremental step. The second study was to explore the effect of moving speed and standoff distance (the distance of the tip of the nozzle to the top of the substrate). The details are shown in Table 3-7. The third study was to examine the effect of

moving speed, which is relative speed between the nozzle and the substrate. The copper powder was printed with a standoff distance of 200 μm and moving speeds of 5, 10, 15, 20 and 25 mm/s. A nozzle design with a diameter of 250 μm, a nozzle angle of 75˚ and a piezoelectric position of 12 mm from the nozzle tip was used in this study. All experimental results were captured with the optical microscope and the image process program measured the dimensions. The results for the powders are presented and discussed in section 4.3.2 of Chapter 4.

Table 3-7 The parameters selected for moving speed and standoff distance experiment.

Parameter	Details
Standoff distance	150, 250, 350 (μm)
Moving speed	1, 5, 10 (mm/s)

3.5.3.4 Demonstration of dry powder printing

In order to demonstrate the capability of the device, the best resolution for single material printing was presented. Also, a sample of dry powder printing on an existing object was assessed. Furthermore, multiple material printing from three different powders (stainless steel powder, tungsten carbide powder and copper powder) was set up and presented. The experimental setup used for the printing was the same as the previous experiments. Finally, the operational guidelines for the device are summarized and discussed. All details are reported in section 4.3.3 to 4.3.6 in Chapter 4.

3.6 Summary

In conclusion, this chapter illustrates the improved device and the material preparations necessary to carry out each experiment in our research. Furthermore, the new dry powder printing device was introduced and compared with the previous design. Chapter 4 presents the results and discussion of all experimental results.

Chapter 4:

Results and discussion

In this chapter, the results obtained from the experiments using the novel dry powder micro dispensing device are presented and discussed. First, dry powder flow generation is observed. Then, the behaviour of powder dispensing in the device is examined. After that, the effects of printing parameters are investigated and powder pattern printing is demonstrated. All of our study focuses on a comprehensive understanding of the behaviour and the control of the process in this device.

4.1 The behavior of dry powder generation

In this section, the study was to examine the behaviour of dry powder generation through the device. The generation of doming and the collapse of the stable dome structure were observed. Then, the time delay in starting and stopping dispensing were investigated.

4.1.1 Powder flow generation

This investigation was to observe the flow of fine powder through a novel device under ultrasonic vibration. Spherical solder powder with a mean particle size of 35 μm was loaded in a dispenser with a nozzle angle of 75˚, a nozzle diameter of 250 μm and a piezoelectric position of 12 mm. A high speed camera was used to capture the images at a frame rate of 1,000 fps. The signal voltage applied in the study was 0.5 Volts. Once the dispenser was filled, particles freely flowed from the orifice until a stable dome structure was formed (Figure 4-1). After that, the device was used to dispense the powder 20 times with 1-second vibration. To capture the powder flow, the trigger of the high speed camera started after sending a pulse signal to the dispenser and stopped after the signal was turned off for 1 second.

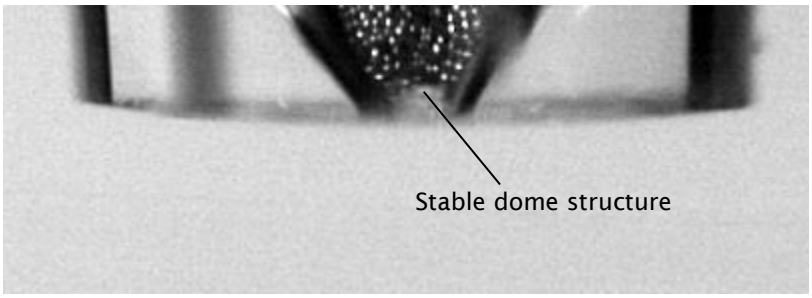

Figure 4-1 Dome structure of a fine powder above a micro orifice (250 μm).

Figure 4-2 shows the sequential images captured by the high speed camera at 0.01 second increments from the start of dispensing (B) to the cessation of dispensing (G) when the powder forms a new stable dome structure (H-J) inside the glass nozzle. As can be seen, during dispensing, the vibration from the piezoelectric transducer transmits energy through the glass tube to particles around the dome structure and the result is to break the dome structure and so achieve flow of the powder. On switching off the vibrations, particle-particle and particle-wall friction lead to the formation of domes causing powder flow to arrest in the nozzle.

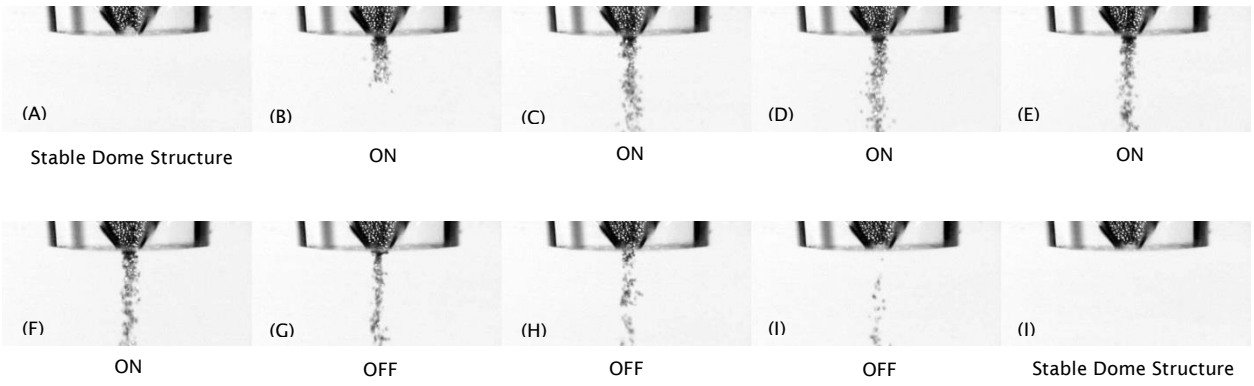

Figure 4-2 Sequence of images captured from the start of dispensing to the cessation of dispensing of a fine powder from the glass nozzle (the signal voltage = 0.5 Volts, the time step = 0.01 seconds).

Information obtained in previous work using ultrasonic dispensing indicated that the forced vibration regulates flow and the mass flow rate of powder [11, 139, 253, 255]. The powder flow starts when vibration starts and the flow stops when vibration stops. However, in the previous studies, the flow behaviour of powder

through the orifice was little mention. In this study, the observations were obtained using the high speed camera, which show clearly details of the starting and stopping process while the dry powder dispensing device is working.

The powder was dispensed by the ultrasonic dispensing system using a glass nozzle as a funnel and a computer control system. Powders were dispensed through the orifice by breaking the stable dome structure by activating a voltage signal pulse to the piezoelectric transducer attached to the dispenser. The stable dome structure of the powder particles functioned as a control valve in the dispensing process. When the device was activated by piezoelectric vibration, powder particles were dilated and the void spaces between particles were increased. Consequently, particle interlocking, the adhesive force and the friction force between particles were weakened. The stable dome structure collapsed and the "control valve" opened and powder flow finally started. When the vibration signal was stopped by inactivating the piezoelectric transducer and the rest of the powder particles formed a new stable dome structure and as a result the flow stopped or the control valve was closed.

From the experimental results, the control of powder flow was simplified into 2D pictures to illustrate the flow mechanism through the device, as shown in Figure 4-3. Brown particles form a stable dome structure supporting the other particles inside the dispenser, and so the particles are unable to discharge under gravity, as shown in Figure 4-3(A). By disturbing the dome with external force from ultrasonic vibration, in Figure 4-3(B), the supporting dome could be easily broken.

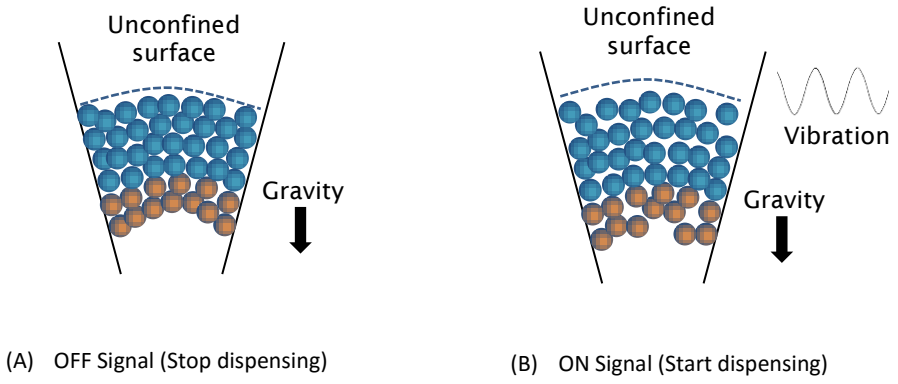

Figure 4-3 OFF and ON signals to control powder flow.

As the bulk powder inside the dispenser was exposed to external vibration, the unconfined surface of the powder could expand and the degree of compaction

decreased. The stable dome structure starts collapsing when the particles moved upward and the voidages between the particles increased. This collapse allowed powder flow through the orifice. This indicates that the key mechanism of this device is the formation of a stable dome structure across the orifice, which acts as a natural control valve. The stable dome structure is broken by the mechanical energy that is transmitted through the container wall to the stored powder. This mechanical energy comes from the ultrasonic vibration of a piezoelectric transducer.

At first, the powder particles formed a stable dome structure above an orifice under the force of gravity, known as a jammed stage. In this jammed stage, the powders together act as a solid and the velocity of individual particles was zero. After applying external force from the ultrasonic vibration, the dome structure collapses and then the powder particles flow through the orifice. When the external force is stopped, the velocities of particles drop and they even come to a complete stop. At this stage, a new stable dome structure is formed again.

The powder flow controlled by ultrasonic vibration can be broadly explained by the arching analysis proposed by Lu et al.[277] This explanation is based on the equations introduced by Li [278] and Jing [279]. The assumption of this model is (1) the powder is composed of an arched layer, the major principal stress (σ_1) is tangential to the arched layer and the minor principal stress (σ_2) is normal to the arched layer. (2) The major principal stress and the minor principal stress belong to the Mohr circle locus of the powder in the container. (3) The voidage of the powder is considered constant and the minor principal stress on the bottom surface of an arched layer is equivalent to zero.

A stable dome structure is balanced by three forces as follows:

$$G + F_a = F_f \tag{4-1}$$

where G is the gravitational force due to the mass of particles, F_a is the downward force on the top of the arced layer and F_f is the friction force from the wall of the container.

The relationship between the gravitational force and the mass of particles of the arched layer is given by:

$$G = \rho_b g A h \tag{4-2}$$

where ρ_b is the bulk density of the powder, g is the gravitational acceleration, A is the surface area of the arch layer and h is the height from the tip of the nozzle to the top of the arched layer.

The downward force on the top of the arched layer is given by:

$$F_a = \pi R^2 \sigma_2 \tag{4-3}$$

where R is the radius of the nozzle and σ_2 is the minor principal stress that is normal to the arched layer.

The relationship between the friction force on the wall of the container and the major principal stress and the minor principal stress is presented as follows:

$$F_f = 2\pi Rh\left[\frac{\sigma_1-\sigma_2}{2}\sin(2\beta)\right] = \mu_W N \tag{4-4}$$

where β is the angle between the major principal stress and normal to the wall of the container, μ_w is the wall friction coefficient and N is the normal force to the wall.

Lu et al.[277] pointed out that the arched layer collapses when the three forces are unbalanced by external vibration. The powder above the arch can move downward when the ultrasonic vibration is activated as the resultant force is bigger than the friction force. This behavior can be explained by the following equation:

$$\rho_b gAh + \pi R^2 \sigma_2 > F_f = 2\pi Rh\left[\frac{\sigma_1-\sigma_2}{2}\sin(2\beta)\right] = \mu_W N \tag{4-5}$$

In addition, the high speed camera used in this investigation revealed the jamming of particles to form the arch above the orifice. In Figure 4-4, the results from the images captured at different stopping times are presented. These images show that the positions of a stable dome structure are different when the device was

turned off several times. It can be clearly seen that the stable dome positions are random in each cycle and the difference of the tip of the ach to the nozzle orifice varied from 94-188 μm.

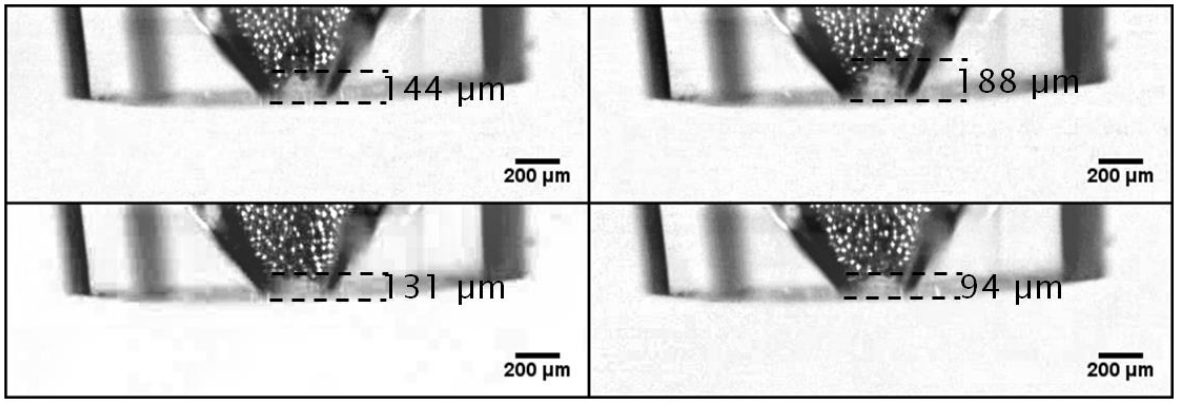

Figure 4-4 The images of stable dome structures at different stoppages via the high speed camera.

If the position of the stable dome structure with respect to the nozzle orifice changes, a variation of dispensing will occur. The variation of dome forming position is thus one of the main causes of mass flow rate fluctuations. Consequently, the relative standard deviation (RSD) of mass flow rate will depend on the variation of the dome position. Moreover, this variation in dome position could also affect the time delay in starting and stopping dispensing.

Similar results have been obtained by Tang and Behringer [280] , in a 2D hopper flow study (particle size = 5.3 mm). They always found that there was a stable arch across the outlet when jamming occurred and the shape of the arches could not be predicted. The effect of a dome position on mass flow rate can be expressed by the following equation proposed by Oldal et al.[281]:

$$W = \frac{\pi}{6}\rho\sqrt{2g\delta(d-d_p)^5} \tag{4-6}$$

where W is the mass flow rate, ρ is the bulk density, g is the gravitational acceleration, d is the outlet size, d_p is the particle size. δ is the arch shape coefficient that depends on the powder, which is the ratio of the arch height to the outlet diameter. Equation 4-6 indicates that the mass flow rate is affected by the arch shape coefficient. When the arch height is changed, the coefficient also changed. Therefore, the variation of mass flow rate can be explained by the randomness of the different dome positions.

4.1.2 Time delay

In a powder deposition process, the capability to control the powder dispensing ON and OFF responsively is an important feature of a powder handling system [282]. From the literature in Chapter 2, no study was found the on time-delay of dry powder printing using a vibration-assisted system. To explore this issue, the response of the dry powder printing device was tested by switching the pulse signal of the ultrasonic controller on and off. The high-speed camera was used to record the dispensing. Photo Fastcam Viewer was used to analyse the time delay of each experiment. In the study, the solder powder with a mean particle size of 35 µm and copper powder with a mean particle size of 14 µm were used in four dispensers with; (1) nozzle diameter of 150 µm, nozzle angle of 62˚ and piezoelectric position of 18 mm, (2) nozzle diameter of 450 µm, nozzle angle of 66˚ and piezoelectric position of 12 mm, (3) nozzle diameter of 270 µm, nozzle angle of 45˚ and piezoelectric position of 10 mm, and (4) nozzle diameter of 270 µm, nozzle angle of 65˚ and piezoelectric position of 10 mm. All tests were carried out with a signal voltage of 2 Volts. The test was repeated ten times to evaluate the time delay.

Figure 4-5 presents multiple bar charts of the time delay for different nozzle diameters for each powder. By visually comparing the heights of the paired bars for each start and stopping stage, we can observe that the average value of the time delay of the stopping stage is higher than the starting stage. It is also seen that the time delay of the starting stage for both powders is relatively similar for the different nozzle diameters. However, in the stopping stage, the time delay for the different nozzle diameters for each powder is very different. It is also interesting that the time delay for the stopping stage of both powders is similar for the 150-µm nozzle diameter. In contrast, the time delay for the stopping stage for the 150-µm nozzle diameter shows a huge different between the copper powder and the solder powder.

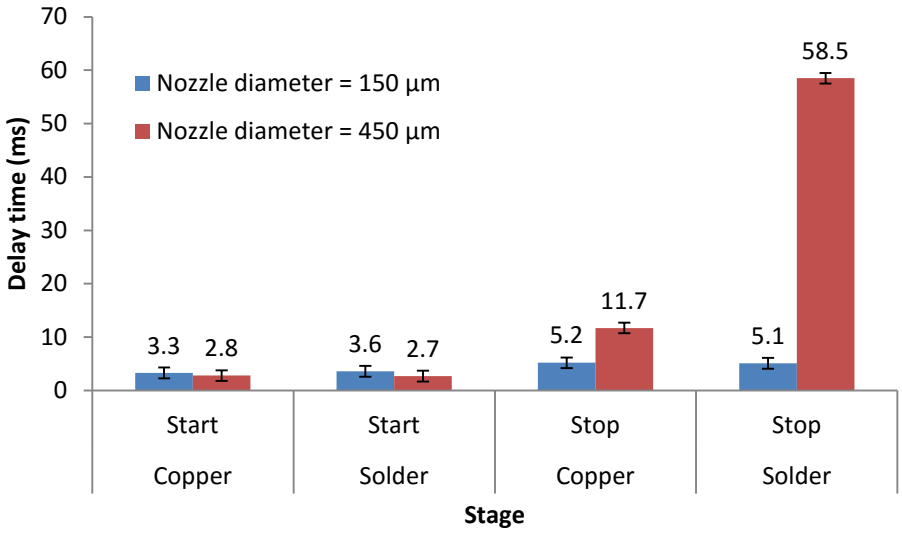

Figure 4-5 Delay time for copper and solder powders with a 150-µm nozzle and a 450-µm nozzle (the nozzle angle = 62˚ and 68˚).

Figure 4-6 shows the bar charts for the time delay for different nozzle angles for each powder. There are no differences in the time delay for both powders at the starting stage. However, for the stopping stage, the highest average time delay is for the narrower nozzle angle. The charts also show that the time delay for the stopping stage for the solder powder is longer than for the copper powder.

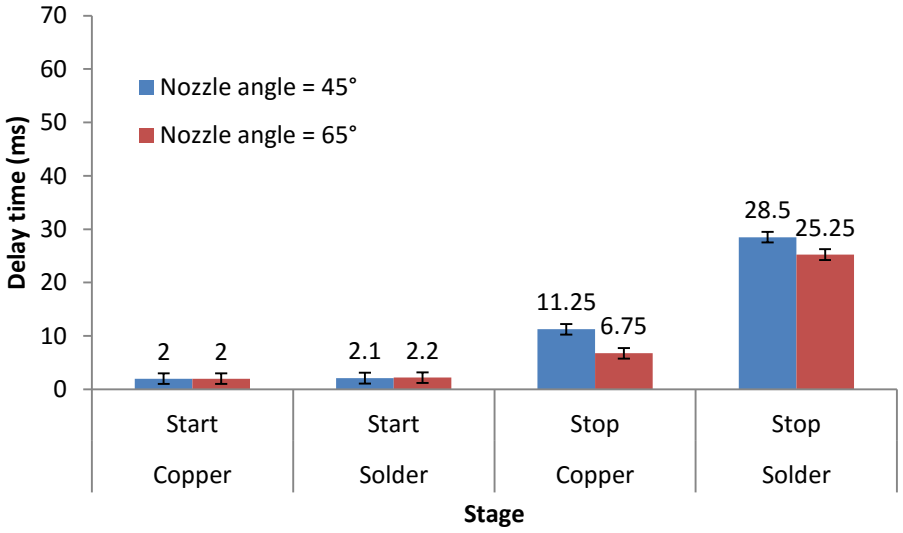

Figure 4-6 Delay time for copper and solder powders with the 45˚ nozzle and the 65˚ nozzle (the nozzle diameter = 270 µm).

From the above results, it can be seen that the time delay for the starting stage is shorter than for the stopping stage. The reason is that when the pulse signal stops, the particles in the nozzle stop oscillating and a new stable dome structure forms when the particles return to equilibrium. At that point, the particles under the free-fall arch region are dispensed and this continues until there are no more particles. The time delay of the solder powder was noted to be longer than the copper powder. The time delay of the copper powder was shorter because it is more cohesive. This cohesiveness can generate a higher wall friction force resulting in a faster time to reform a stable dome structure. For the solder powder that the time delay was long because it has better flowability and it less cohesive. We can conclude that a powder with low flowability leads to a longer stopping delay time. For different nozzle angles, the time delay for the 45˚ nozzle angle was longer than for the 65˚ nozzle angle. Generally, for a steep wall hopper angle, the particles move faster than on a shallow angle. Therefore, for a steep angle, the particles require more time to achieve zero movement and balance the forces to achieve a new stable dome structure. This could be the reason why the time delay for the 45˚ nozzle angle was longer than the 65˚ nozzle angle. For different nozzle diameters, the time delay for the 150-μm nozzle diameter was shorter than for the 450-μm nozzle diameter. It is believed that in order to form a new stable dome a wider nozzle diameter requires more time than a narrower nozzle diameter. The particles above the orifice need contacts to support the stress from the particles around the stable dome structure. If the nozzle diameter is big, more time is required to get the particles closer and achieve contacts to form the dome structure. Thus a large nozzle diameter leads to a longer time delay. Interestingly, in Figure 4-5, the time delay for the starting stage is slightly different for both powders for the different nozzle design conditions. However, the distance between the piezoelectric transducer and the tip of the nozzle for the 150-um diameter nozzle (18 mm) is longer than for the 450-um diameter nozzle (12 mm). Thus the piezoelectric position may influence to the time delay for the starting stage. The longer distance between the dome structure and the source of the vibration requires more time for the vibration to travel to the dome. Hence as the piezoelectric position increases, the time delay for the starting stage becomes longer.

A precise on-off control would be beneficial for accurate dispensing and printing from the device. Figure 4-7 presents a schematic of the control signal and the

actual discharge of powder through the device. In the ideal situation, the device should immediately respond to the control signal to discharge the powder when the signal is turned on and turned off. However, there are the time delays on both turning on and turning off signal. In this illustration, we assumed that the delay from the electronic and electro-mechanical components in the control system was very small and could be neglected. For the on-delay time, we could conclude that it arises from the time the vibration wave take to travel from the piezoelectric transducer to the powder inside the glass tube. Next, the vibration transfers to the particles around the stable dome structure. Finally, the particles relocate and the stable dome structure collapses. The off-delay time arises from the time the particles take to form a new stable dome structure after the control signal is turned off and then, the time the free-flowing particles under the stable dome structure take to discharge completely.

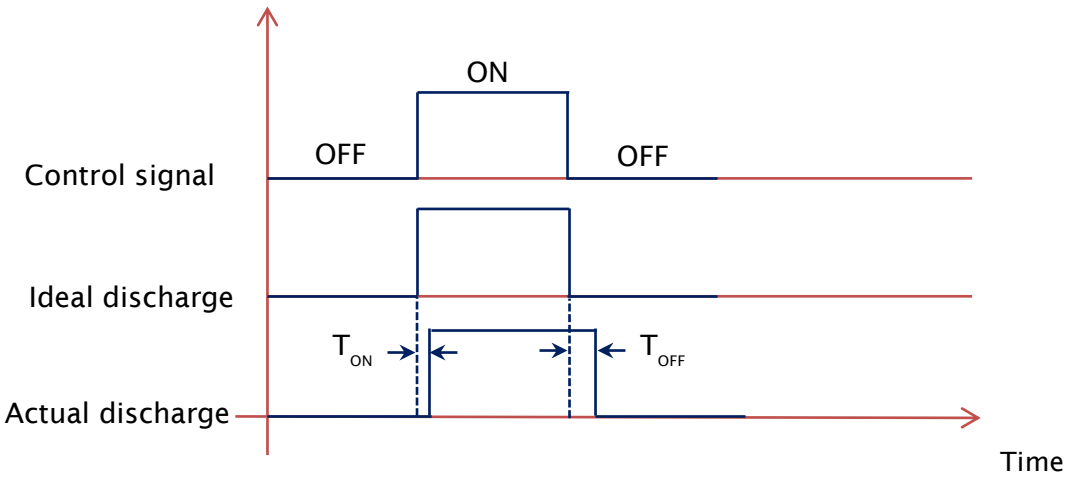

Figure 4-7 Schematic of the comparing an ideal ON/OFF response and that found in practice.

This information can be used to correct the time delay during the printing operation of the device. Figure 4-8 and Figure 4-9 describe the effect of the time delay in powder dispensing on the accuracy of a printed track. The discharged powder could take a few milliseconds to reach the substrate due to the on-delay time, including the time the particles take to reach the substrate due to gravity that can be estimated from the free falling object equation:

$$t = \sqrt{\frac{2S}{g}} \tag{4-7}$$

where t is the time for falling particles to reach the top of the substrate, S is the standoff distance, g is the gravitational acceleration.

The printed powder could be deposited some position after the programmed start point as shown in Figure 4-8. When the control signal is turned off, the powder flow does not stop suddenly. Therefore, at the end point, the additional powder is deposited as presented in Figure 4-9. This additional powder will cause a problem called a match-head effect that will be discussed in section 4.3.2.6. From this study, the time delay could be mainly dependent on the powder type and the nozzle design parameters such as nozzle diameter, nozzle angle and piezoelectric position. Also, the standoff distance is another variable. To solve this problem software be built into the controller to compensate for the on/off delay times and thus improve positional accuracy.

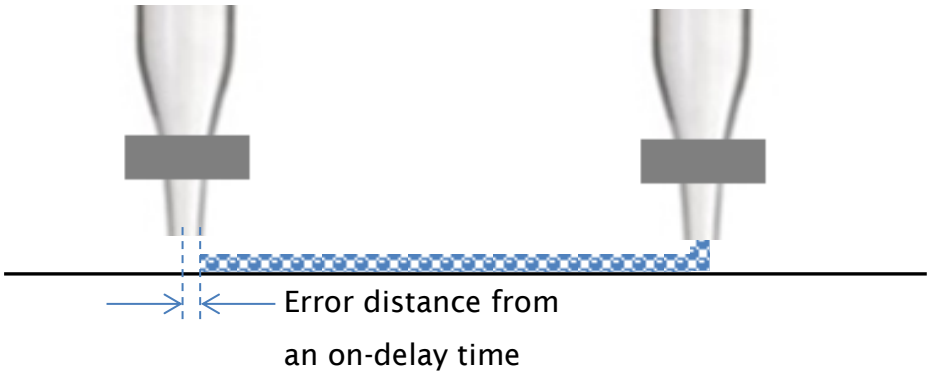

Figure 4-8 The effect of an on-delay time in powder printing.

Figure 4-9 The effect of an off-delay time in powder printing.

In summary, the delay time of the starting stage through a micro orifice is shorter than the delay time of the stopping stage. The reason is because after stopping the signal activation, the free-falling particles under a new stable dome structure need time to flow out of the orifice. Widening the nozzle angle would reduce the delay time of the starting and stopping stage. Also, reducing the nozzle diameter would enhance the ability to form a new stable dome structure leading to a decrease in the time delay. Furthermore, decreasing the piezoelectric position can decrease the time delay. In addition, the cohesive and adhesive property of a powder also influences the time delay of starting and/or stopping through a micro orifice. A more cohesive powder can shorten the time delay in powder dispensing. To improve the responsiveness and controllability of powder dispensing in the device, we can suggest that a design nozzle with a wide nozzle angle, a small nozzle diameter and a short piezoelectric position can improve the time delay at the start and the finish of dispensing.

4.2 Characteristics and design parameters of dry powder printing

In this section, a set of experiments was carried out to examine the dispensing characteristics of the dry powder printing device. The influence of the design parameters and other parameters such as a nozzle diameter, a nozzle angle, a piezoelectric position and a signal voltage were also examined.

4.2.1 Powder dispensing profile

To observe the characteristics of powder dispensing from the beginning of the start of dispensing to material run out, the mass flow rate as a function of the time of copper powder dispensing was determined. The dispenser used a 350-μm nozzle diameter with a nozzle angle of 65° and a piezoelectric distance of 16 mm. Figure 4-10 shows the mass flow rate as a function of time from start to run out for the copper powder. The graph of powder flow is characterized as a bathtub curve. The mass flow rate is high in the run-in stage or initial stage and then decreases to a steady stage. This stage is characterized by a constant mass flow

rate. Finally, the mass flow rate greatly increases and then decreases again until the powder runs out.

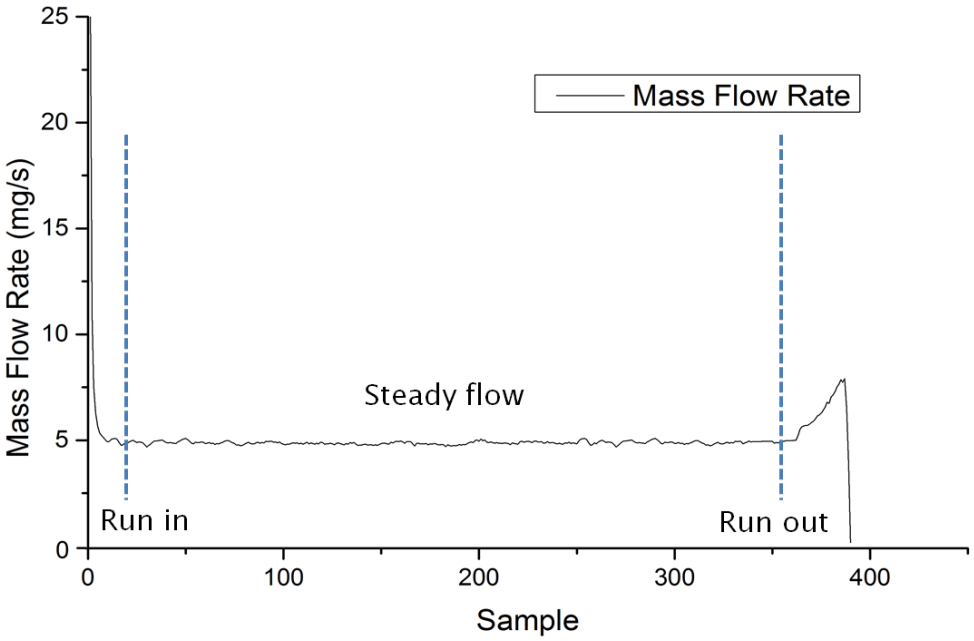

Figure 4-10 The mass flow rate graph observed in a copper powder dispensed from start to run out (the nozzle diameter = 350 μm, the nozzle angle = 65˚, the piezoelectric position = 16 mm and the signal voltage = 2 volts.).

At the start of dispensing, the bulk density of the powder has been affected by the pouring process and the particles have settled under gravity. They tend to be loosely packed. During this period, a high mass flow rate occurs because the powder had not compacted resulting in a low compact stress and thus it easily flows. The stable dome structure was easily broken and as a result the amount of powder flow per unit time was high. After the piezoelectric transducer started working, the particles inside the device were oscillated and they became closely packed. However, the bulk density is also increased via the vibratory packing process. Therefore, the mass flow rates rapidly decreased due to compaction of the powder and then gradually decreased with dispensing time. The compaction created low mass flow rates. This is because the stable dome structure was hard to break and the particle velocity was reduced due to close packing. Thus, the particles might take a longer time to discharge. After the powder has been shaken for a period of time its bulk density reaches a nearly constant value and the mass flow rate reached a steady value. In the steady stage, the mass flow rate gives the most wanted condition for dispensing because it provides a steady mass flow rate.

At this stage, we believe the device can provide consistent dispensing because the particles are packed near the limit of the powder compressibility. Dispensing reliability with a constant mass flow rate can be expected in this stage. At the run-out stage, i.e. the final stage before the dispenser was empty, the mass flow rate dramatically increased again because the bulk density was reduced owing to the powder mass above the orifice having been removed. Consequently, the mass flow rate reduces significantly until the powder in the dispenser runs out. At this stage our device behaves similarly to the fluidized powder in a silo that is uncontrollable flow resulting in flushing or flooding when it nearly runs out [227]. This result suggests that before the mass flow rate becomes high when reaching the run-out stage, the dispenser should be refilled to maintain the steady mass flow rate of dispensing. This explanation generally agrees with the study reported by Harnby et al. [283]. They pointed out that changes in bulk density can be very sensitive indicators of changes in the structural strength of a loosely compacted powder and hence of its flow characteristics.

4.2.2 Effect of different powders on dispensing

Powder flowability affects the performance of the dry powder printing device. Different powders have different flowability and they can influence dispensing in a different way. In this study, a solder powder and a copper powder of 14 μm and 35 μm mean particle size respectively were used to examine the effects of different powders on powder dispensing. The dispenser used was a 250-μm nozzle diameter with a nozzle angle of 75˚ and a piezoelectric distance of 12 mm. The signal voltage was fixed at 2 Volts. All of the experiments were repeated 4 times. The pulse repetition period (wave cycle) was 4 seconds combined with 1-second ON time (pulse duration) and 3-seconds OFF time.

4.2.2.1 Mass flow rate

The mass flow rate is generally affected by powder flowability. The mass flow rate of the copper powder and the solder powder was measured. To calculate the average mass flow rate of the experimental powders, data for dose mass were sampled at 90 points from the start to end dispensing and 20 points before the stable region were removed to avoid the effects of starting dispensing.

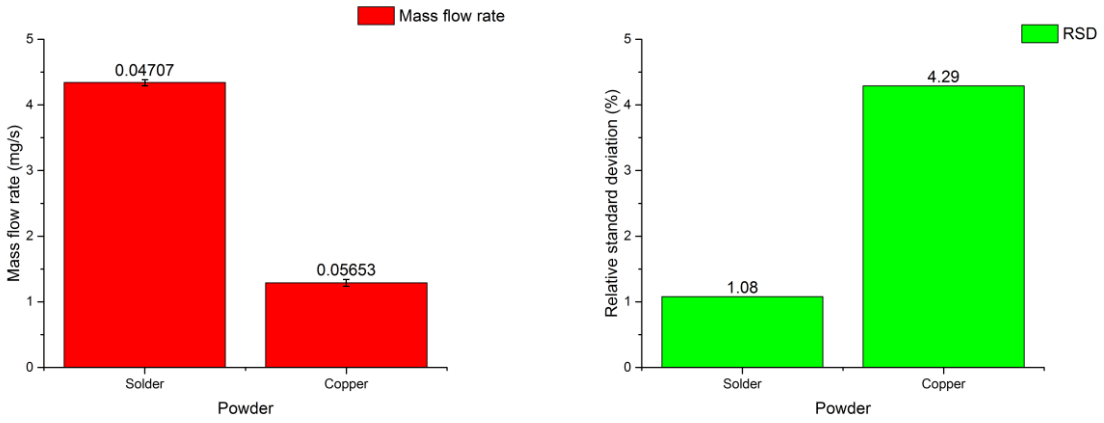

A) Average mass flow rate.

B) Average relative standard deviation.

Figure 4-11 The average mass flow rate (A) and the average relative standard deviation (B) of the solder powder and the copper powder.

Figure 4-11 compares the mass flow rate of solder powder and copper powder of a mass flow rate and their relative standard deviation. The average mass flow rate of the solder powder was obviously much higher than that of the copper powder, 4.36±0.047 mg/s and 1.29±0.057 mg/s respectively , as shown in Figure 4-11A. The difference in the mass flow rates of different powders results from the difference in their flowability. As we can see from their angle of repose given in Table 3-1 of Chapter 3, the flowability of the copper powder is poorer than the solder powder. Also, the size of the copper powder was smaller than the solder powder. Generally, a smaller particle size is more difficult to discharge than larger particles [265] because they have more surface area relative to their mass which causes friction, adhesion, and cohesive force generated by the van de Waals force and electrostatic effects [284]. Thus high flowability powders can give higher mass flow rates than low flowability powders.

The average relative standard deviation (RSD or the sample standard deviation expressed as a percentage of the mean) of the solder powder was much lower than that of the copper powder, 1.08% and 4.29% respectively (as shown in Figure 4-11B). The difference in the relative standard deviation for different powders might be because of the difference in their uniformity. The powder uniformity was analyzed by using a Malvern Mastersizer 2000 particle size analyzer (smaller values indicate better uniformity). The uniformity of the copper powder was 0.396 and the solder powder was 0.136. This meant the size distribution of the solder

powder was narrower than the copper powder, which was confirmed by the SEM images in Figure 3-9. This completely agrees with the findings of Liu et al. [181]. They pointed out that powder flowability is significantly influenced by the particle size and size distribution; flowability increases with increasing particle size and narrower size distribution.

Many dry powder printing devices from previous studies have suffered from unstable feeding of powder, especially when using a small nozzle diameter and cohesive powders. The mass flow rate of the experimental powders from the current device was found to be highly stable and reliable. The device showed less than 5% RSD.

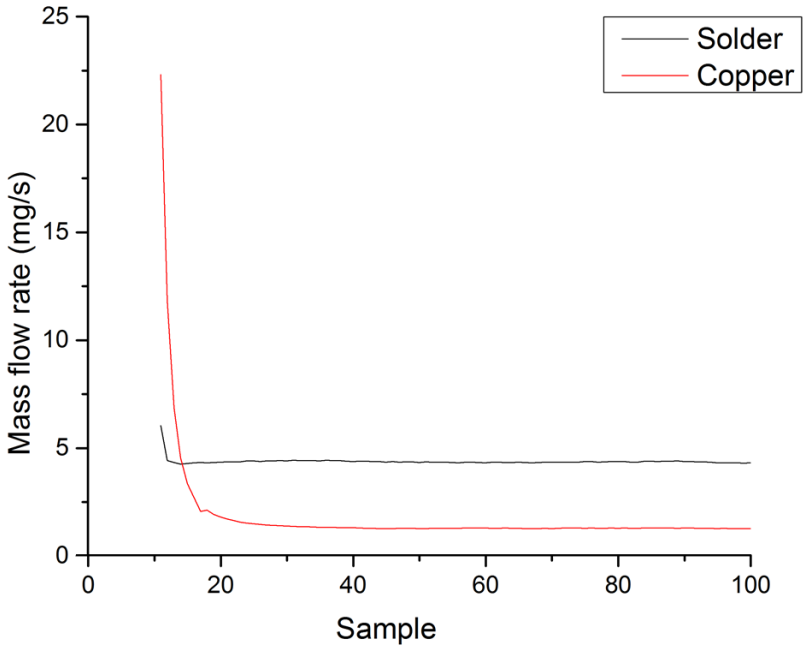

Figure 4-12 The average mass flow rate of the copper powder and the solder powder.

Figure 4-12 shows the results of the average mass flow rate obtained from the two powders with the same dispenser as a function of the serial number of the dose. Each curve presents the average of four measurements from the dispensing of ninety samples. The mass flow rates are highest at the start of dispensing and then noticeably decrease until reaching a steady value. The run-in stage showed a difference between the two powders. The mass flow rate of the solder powder reaches the steady value around 10-sample number. While the copper powder reaches the steady value around 20-sample number. The run-in time of the solder powder was shorter than the copper powder.

This result shown in Figure 4-12 indicates that the mass flow rate at the run-in stage decreases because the bulk density of the powder increases. This is because of compaction of powder due to the vibration of the piezoelectric transducer. The compaction of the powder increases the mechanical strength and the bulk density of the powder. Generally, for a free-flow powder such as the solder powder, the compressibility is small, which means that the bulk density and tapped density would be close. In contrast, a cohesive powder, which is high compressible, has a larger difference between the bulk density and tapped density. Thus the run-in stage of a poor flowability powder is longer than that of a good flowability powder. Our result is in good agreement with the experiment carried out by Chen et al.[285], who mentioned that the time period to reach a constant state of packing varies from powder to powder depending on their flow properties.

These two graphs can be used to illustrate a general trend concerning the steady stage of the mass flow rate in the device. In the study, the results show that with the higher flowability powder, solder, the steady stage is reached faster than for the copper powder which has a poorer flowability. This reflects the fact that the compressibility of a cohesive powder such as the copper is higher than that of a free-flowing powder such as the solder. Therefore, a cohesive powder requires a longer time period to reach the steady stage than a free-flowing powder. It can therefore be concluded with ultrasonic vibration, the density of the powder inside the nozzle was increased. The change of the bulk density of the powder in the dispenser after vibrating equalizes the powder density. This produces a stable mass flow rate in powder dispensing. To obtain stable results in powder printing, therefore, preparation of the powder prior to dispensing is recommended. The dispenser should be blocked and vibrated with a pulse duration of one second for 20 cycles for the copper powder (or other cohesive powders) and 10 cycles for the solder powder (or other free-flowing powders). This will produce a uniform density, i.e. equalize the density, in the dispenser. This suggestion is included in the operational guidelines in section 4.3.3.

4.2.2.2 Dispensing repeatability and stability

Continuous dispensing of the fine powder through a micro orifice tends to be unreliable because of the complex properties of friction, cohesion and adhesion of the fine powders. To demonstrate the repeatability and the stability of dispensing of the device, four sets of dispensing results are shown in Figure 4-13. The four

profiles of mass flow rate versus sequential samples for each powder reveal similar profiles for both experimental powders. As can be seen, each profile has a consistent pattern but there is a difference between materials. These two graphs show that the flow rate of both powders is relatively stable after their run-in stage.

One of the important indicators for evaluating the repeatability of dry powder printing or micro-feeding is dose uniformity. If the deviation between dose masses is large, it indicates inconsistency dispensing. Calculations indicate the relative standard deviation of the solder powder is 1.08% and 4.29% for the copper powder. This means the amount of each dose mass tends to be very close to their mean dose mass. These two sets of graphs confirm that the device can provide identical dispensing characteristics every time that it performs under normal conditions.

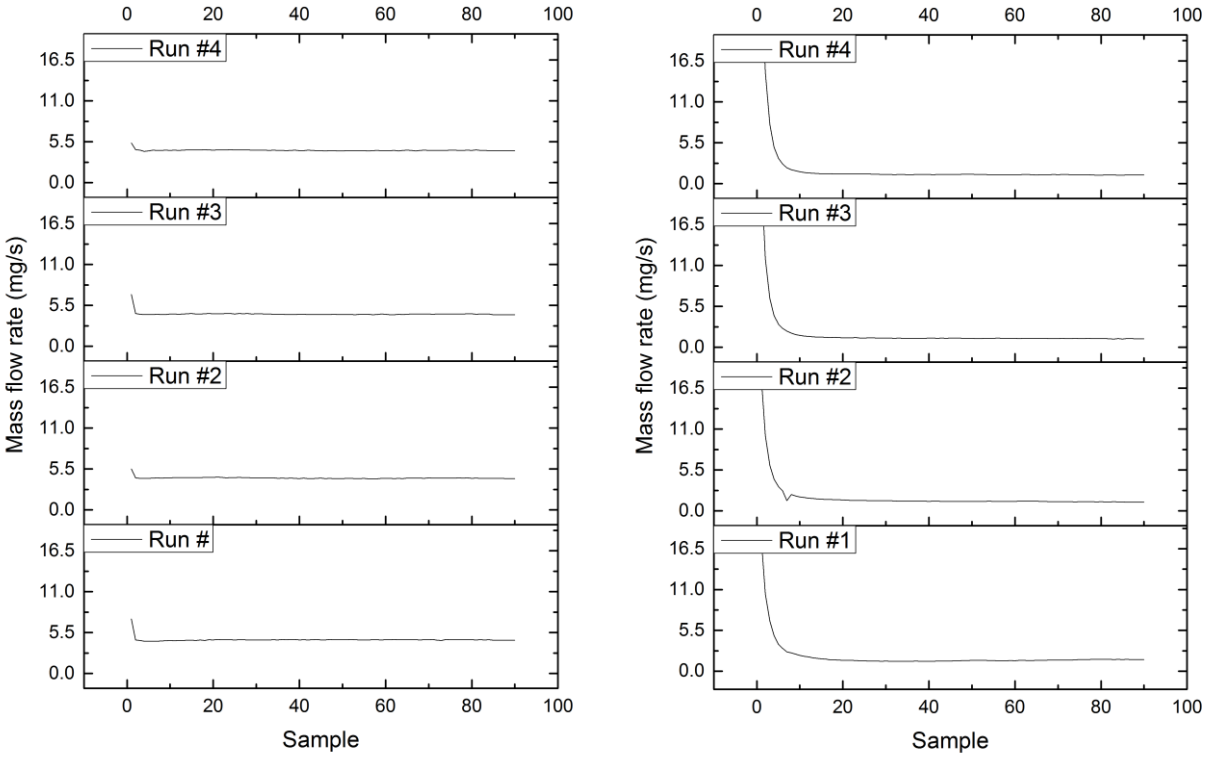

(A) Solder powder. (B) Copper powder.

Figure 4-13 The mass flow rate profiles of the solder powder (A) and the copper powder (B).

Continuous dispensing without the device stopping or blocking is important for successful operation. From our observations, big contaminants or fibers mixed in the powder inside the nozzle could be the causes of clogging and semi-blocking. These problems produced unstable flow of the powder during dispensing. Thus it

is necessary to ensure that the feedstock powder is sieved to screen contaminants before dispensing. The problem is more severe when relatively small-diameter nozzles, when compared with mean particle diameter, were used to dispense. The use of larger-diameter nozzles reduces the chance of blockage. Additionally, particles floating in the room or particles falling from the equipment occasionally entered the dispenser. This problem could also disturb the dispensing process.

4.2.3 Effect of nozzle design and signal voltage on mass flow rate

The mass flow rate from the device is one of the major processing characteristics that plays an important role in determining the speed of deposition of the layers. Experiments were designed to reveal how the input parameters of the device such as nozzle diameter, nozzle angle and piezoelectric distance including signal voltage, affect the mass flow rate. Sixteen experiments were conducted and the design layout of these experiments with their corresponding mass flow rates is shown in Table 4-1. All the results in the table have RSD less than 7%.

Table 4-1 Design layout of the experiment with response values.

Trial	Nozzle Diameter	Nozzle Angle	Piezoelectric position	Signal Voltage	Flow rate (mg/s) # 1	# 2	# 3
1	180	45	10	0.5	0.74	0.78	0.77
2	180	45	10	2.0	1.68	1.65	1.69
3	180	65	10	0.5	0.43	0.41	0.52
4	180	65	10	2.0	1.05	1.00	0.96
5	180	45	20	0.5	0.45	0.45	0.51
6	180	45	20	2.0	0.61	0.54	0.51
7	180	65	20	0.5	0.34	0.36	0.37
8	180	65	20	2.0	0.87	0.97	0.85
9	270	45	10	0.5	1.7	1.66	1.75
10	270	45	10	2.0	3.4	3.46	3.51
11	270	65	10	0.5	1.17	1.23	1.21
12	270	65	10	2.0	2.19	2.16	2.02
13	270	45	20	0.5	1.31	1.26	1.29
14	270	45	20	2.0	2.01	1.97	1.9
15	270	65	20	0.5	1.21	1.23	1.2
16	270	65	20	2.0	1.28	1.27	1.24

The data were analyzed to identify how the input parameters affected the mass flow rate. The plot of mean mass flow rate obtained using Minitab software is presented in Figure 4-14.

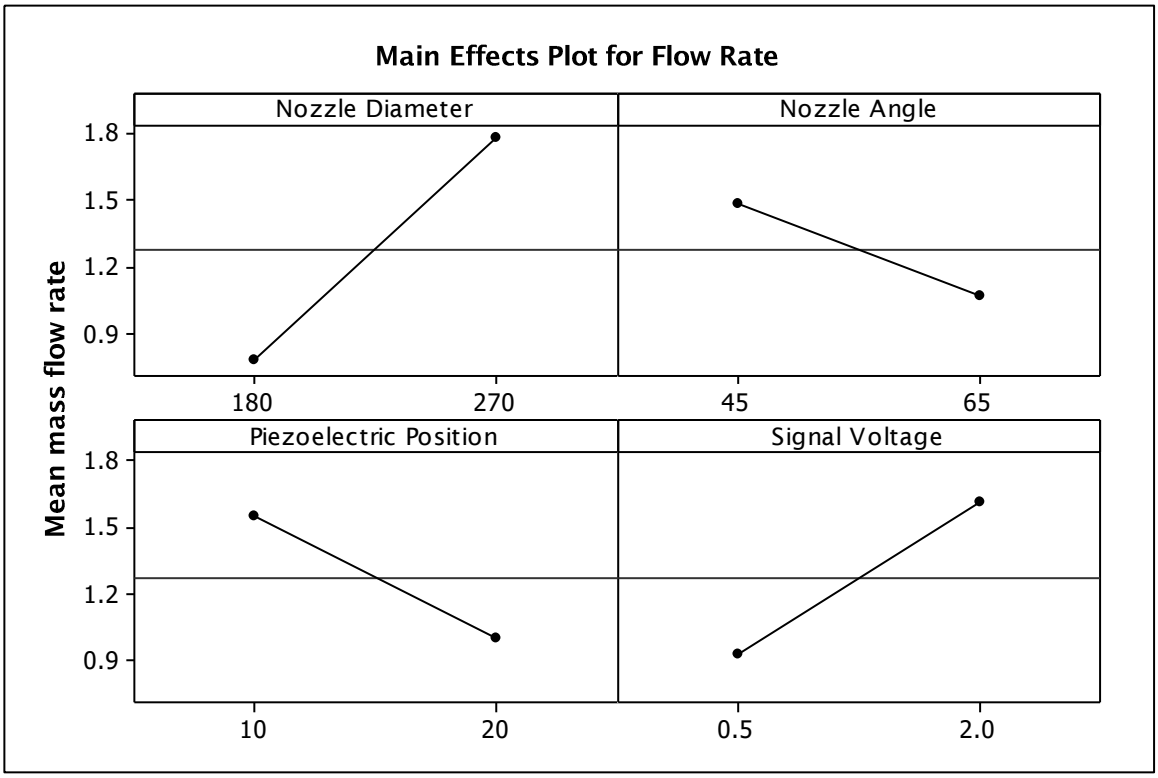

Figure 4-14 Main effects plot on mass flow rate.

Figure 4-14 gives the main effects plot of the mean results from Table 4-1. Nozzle diameter, piezoelectric position and signal voltage have a significant impact on the mean mass flow rate. The 270-μm diameter nozzle produces a higher mean mass flow rate than the 180-μm diameter nozzle. The 65˚ angle nozzle creates a lower mean mass flow rate than the 45˚ angle nozzle. The 20-mm piezoelectric position gives a smaller mean mass flow rate than the 10-mm piezoelectric position. The 2-Volt signal voltage produces a higher mass flow rate than the 0.5-Volt signal voltage. The two most significant impact parameters are the nozzle diameter and the signal voltage. The lowest impact parameter is the nozzle angle. The nozzle diameter and the signal voltage show a positive relationship with the mass flow rate. In contrast, the piezoelectric position and the nozzle angle show a negative relationship with the mass flow rate. The relationships may not be linear.

4.2.3.1 Nozzle diameter

The effect of nozzle diameter on the mass flow rate is shown in the graph in the upper left of Figure 4-14. The mass flow rate increases with increasing nozzle diameter. The nozzle diameter shows a high impact on the mean mass flow rate. This is because an increase in nozzle diameter allows the volume of powder exiting from the nozzle to increase and as a result the mass flow rate becomes higher. In the literature in Chapter 2, the mass flow rates were normally found to very depending on the nozzle diameters.

4.2.3.2 Nozzle angle

From the graph located in the upper right of Figure 4-14, an increase in the nozzle angle decreases the mass flow rate. From the literature review, many studies on gravity flow in silos [286] found that with an decrease in hopper angle, powder flow can improve. Mass flow occurs when the sloping hopper walls have a low enough friction and are steep enough for particles to slide along the wall. Generally, the friction force between particles and the wall of the nozzle is affected by the nozzle angle. Thus, a narrower nozzle angle could provide a higher mass flow rate than a wider nozzle angle. These results indicate that the dispenser with a narrower angle has smaller particle-wall friction force than the dispenser with a wider angle. Consequently, a nozzle design with a narrow nozzle angle can be advantageous for cohesive powders and increase the mass flow rate from the device.

4.2.3.3 Piezoelectric position

As can be seen from the lower left of Figure 4-14, the distance of the piezoelectric ring from the nozzle tip (piezoelectric position) shows a negative relationship with the mass flow rate. In dry powder printing using ultrasonic dispensing, the main mechanism of powder discharge is to break the stable dome structure of the powder above the nozzle orifice through vibration. Therefore, the compacting stress can overcome the unconfined yield strength (the stress which causes flow) of the powder in the stable dome structure. The mean mass flow rate decreased when the piezoelectric position was increased. This arises because if the vibration source is closer to the stable dome structure, the higher vibration could break the

dome structure more effectively and make the powder come out easier. In addition, the smaller distance between the vibration source and the stable dome structure can reduce the transmission loss of the vibration energy. From the findings, it can be concluded that the mass flow rate increases with the decrease in the piezoelectric position. To improve the mass flow rate, we can suggest that the piezoelectric transducer should be externally mounted to a glass tube as near as practical to the dome forming position.

4.2.3.4 Signal voltage

The graph in the lower right of Figure 4-14 shows that a higher amplitude signal voltage can create a higher mass flow rate. The primary reason is that a higher signal voltage can provide a higher excitation voltage to the piezoelectric transducer. The piezoelectric transducer was inserted on the glass tube above the orifice, and attached by epoxy, to create the ultrasonic pulse necessary for powder dispensing. Generally, when the power amplifier takes the higher signal the higher resulting output voltage, which is coupled to a piezoelectric transducer, will increase the excitation voltage and change the electric field to mechanical deformation. The signal voltage was used to control the deformation of the piezoelectric. An increase in voltage caused the piezoelectric deformation to increase. Due to this reason, the piezoelectric transducer can generate more vibration. From this, it can be expected that increasing the level of the signal voltage causes an increase in vibration and this can increase the mass flow rate from the device. However, from our observation, it should be noted that if the piezo is not well attached to the nozzle, it will reduce the vibration and so it reduce the mass flow rate.

From this study, the nozzle diameter, the nozzle angle and the piezoelectric position, and the signal voltage influenced the mass flow rate. The design parameters are important when making the device because they cannot be adjusted during the dispensing or printing process. The results indicated that the nozzle diameter had a major effect on the mass flow rate. The signal voltage had much greater effect on mass flow rate than the piezoelectric position and the nozzle angle. The nozzle angle had less effect than the piezoelectric position. Our results were similar to the results of Lu et al.[9] who showed that the nozzle diameter had a larger effect on mass flow rate than the signal voltage.

Thus the mass flow rate increases with increasing nozzle diameter and increase in signal voltage. Whereas, the mass flow rate is decreased when increasing the piezoelectric position and the nozzle angle. Therefore, changing the nozzle diameter is important for improving the mass flow rate (or powder deposition rate). However, in powder printing applications, a small nozzle diameter is needed for high resolution results. Therefore, optimization of the mass flow rate can be achieved by modifying other parameters when the nozzle diameter is restricted.

4.2.4 Effect of nozzle diameter on mass flow rate

In order to find the effect of nozzle diameter on the mass flow rate for different powders, experiments with the solder powder and the copper powder were conducted. In this study, two sets of experiments for mass flow rate were conducted on the device for nozzle diameters of 110, 200, 255, 280, 320, 375 and 400 μm. This nozzle had a nozzle angle of 66° and a piezoelectric position of 12 mm. All the tests in this study had a signal voltage of 2 Volts. Table 4-2 shows the results of mass flow rate for the two selected powder tested with this range of nozzle diameters. The RSD of the results presented in the table was less than 7%.

Table 4-2 The mass flow rate for copper and solder powders from a range of nozzle diameters.

Nozzle Diameter(μm)	Mass flow rate (mg/s)	
	Copper	Solder
110	0.36	0.39
200	1.71	3.32
255	2.40	5.80
280	3.03	8.46
320	4.22	11.53
375	6.18	21.38
400	7.20	26.74

The results in Table 4-2 and Figure 4-15 show unsurprisingly that the biggest nozzle with a diameter of 400 μm can dispense the highest mass flow rate. The nozzle with 110-μm diameter has the lowest mass flow rate. The mass flow rates increase with nozzle diameter. At the smallest nozzle diameters, the mass flow rates of the two powders are similar. Throughout the range of these nozzle diameters, the solder powder has a higher flow rate than the copper powder. A

free-flowing powder such as the solder powder has higher flowability and thus greater mass flow rate than a cohesive powder such as the copper powder.

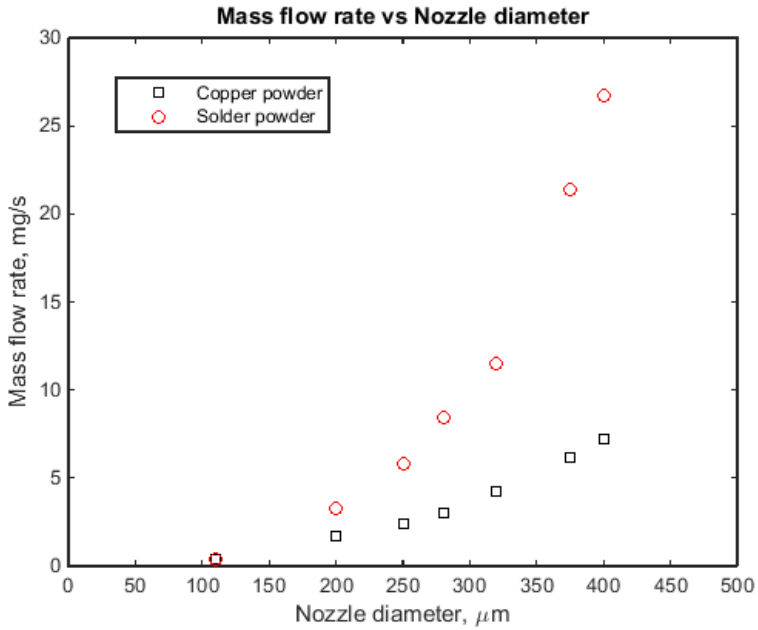

Figure 4-15 Mass flow rate as a function of nozzle diameter for copper and solder powders (the nozzle angle = 66˚, the signal voltage = 2 Volts).

Figure 4-15 shows that the mass flow rates for both powders increase rapidly with the nozzle diameters. By visually comparing the results for the solder and the copper powder, it can be seen that the nozzle diameter has more effect on a free-flowing powder than on a cohesive powder. For the solder powder, the mass flow rate increases sharply because the nozzle diameter is very close to the maximum diameter in which the dome can form and the dispensing cannot be controlled if it is beyond this size. We found that the discharge of the solder powder was uncontrollable at a nozzle diameter of 450 μm (~13 times that of the maximum particle diameter). However, the copper powder had wider range of the nozzle diameter for controllable discharge and the nozzle diameter can be increased further until the mass flow rate increases rapidly. We found that the copper powder was uncontrolled at a nozzle diameter of 940 μm (~67 times that of the maximum particle diameter) for a nozzle angle of 30˚. However, if the nozzle angle were wider, the nozzle diameter could be larger. From this result, it can be concluded that a cohesive powder (the copper powder) has a wider range of nozzle diameters for uncontrollable discharge than a free-flowing powder (the solder powder).

To estimate the mass flow rate, Beverloo created the basic equation for free-flowing coarse powder. The equation is given by:

$$Q = C\rho_B\sqrt{g}(D_0 - kd)^{2.5} \quad (4\text{-}8)$$

Q is mass flow rate of particles (g/s), C is an empirical constant, ρ_B is bulk density of powder (g/mm^3), g is acceleration due to gravity (9,810 mm/s^2), D_0 is hopper orifice diameter (mm), k is an empirical constant for particle shape, and d is the mean particle diameter, C and k are dimensionless constants and the values are 0.58 and 1.6 respectively as reported by Beverloo et al. [208]. Usually the discharge coefficient is in the range of 0.55<C<0.65 and the shape factor is in the range of 1<k<2 [220, 287]. This equation fits very well for big orifices. However, it is not adequate for small orifices where a blockage is possible [209, 223]. Nedderman [222] suggested that Equation 4-8 should be used only for particle diameters in the range 0.4 mm < d_p < D/6, where D is the diameter of the outlet.

By using the curve fitting tool of Matlab software (MathWorks, Massachusetts, US) to fit the experimental data with Equation 4-8, the values of C and k can be calculated after defining the mean particle size and the bulk density of each powder. The bulk density of the solder powder and the copper powder was estimated by assuming the bulk density inside the dispenser is equal to the tap density. Then, the tap density can be estimated by using Hausner ratio at 1.15 and 1.4, from Table 2-5 in Chapter 2, for the solder powder and the copper powder respectively.

Table 4-3 Constant values of C and k for the experimental powders.

Powder	Tap Density (g/mm^3)	Constant Value		R-square
		C	k	
Solder	5520	0.80	2.159	0.9942
Copper	6580	0.09	-2.012	0.9979

Table 4-3 gives the values of the constant C and K (with 95% confidence bounds) for the solder powder and the copper powder respectively. The goodness of fit (R^2) is 0.9942 and 0.9979 for the copper powder and the solder powder respectively. For the solder powder, the value of C from this study was bigger than the value shown by Beverloo et al. (0.8 vs 0.55-0.65) For the copper powder, the value of C

from the study was much smaller than the value obtained by Beverloo et al. (0.09 vs 0.55-0.65). The difference might be due to the particle sizes of this study (14 and 35 μm) and the nozzle diameters (110-400 μm) being smaller than the particle sizes and the nozzle diameters of Beverloo et al. (1.6-3.0 mm, 3-30 mm). Furthermore, the Beverloo's equation is often recommended only for free-flowing coarse powders.

Consequently, for the selected powders, the mass flow rate could be estimated by the following equation.

Solder:

$$Q = 1.382 \times 10^{-5} \times (D_0 - 75.57)^{2.5} \quad (4\text{-}9)$$

Copper:

$$Q = 1.888 \times 10^{-6} \times (D_0 + 28.16)^{2.5} \quad (4\text{-}10)$$

For Equations 4-9 and 4-10, the unit of Q is mg/s and the unit of D_0 is μm.

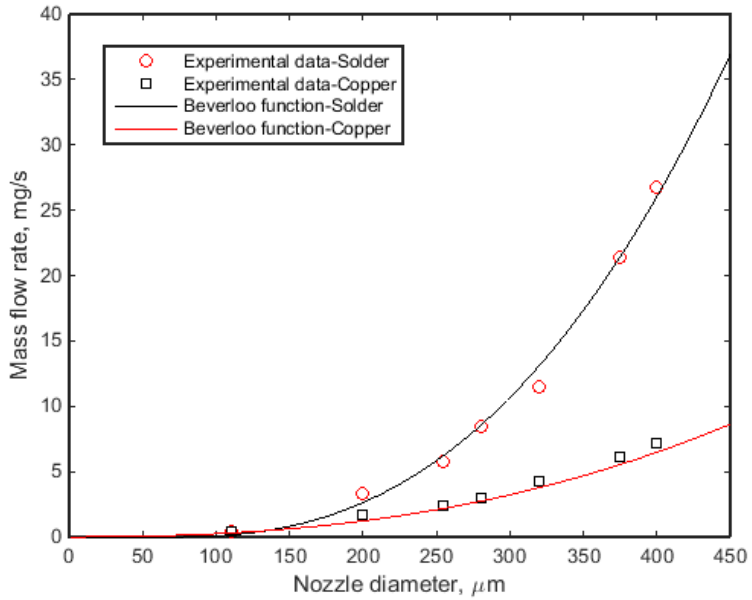

Figure 4-16 Comparison between Beverloo function and the experimental results.

The graph in Figure 4-16 shows the plot of mass flow rate against nozzle diameter for the equations based on Beverloo's function and the experimental data. The

experimental results can clearly be fitted by the equations. Therefore, we can conclude that the Beverloo's equation can be modified to predict the mass flow rate for this device. However, Equation 4-8 cannot be used when the nozzle diameter is less than roughly 76 μm. Also, Equation 4-9, cannot be used when the nozzle diameter is too small to dispense the powder. Therefore, to guarantee the estimation of mass flow rate, we recommend using these equations for the nozzle diameters in the range 110 and 400 μm.

The lower limit of the nozzle diameter should large enough for the particles to not to block or clog it. Dry powder cannot be discharged from a capillary whose nozzle diameter is too small when compared with the maximum particle size of the powder to be discharged. In our observations, we found that a cohesive powder such as the copper powder had a minimum nozzle diameter of 45 μm (~3 times that of the maximum particle diameter) and a free-flowing powder such as the solder powder had a minimum nozzle diameter of 110 μm (~3 times that of the maximum particle diameter). The upper and the lower nozzle diameters thus differ from powder to powder. Nozzle diameter is also particularly important as it affects spot size or a resolution of a printing process. In order to reduce the track width, the nozzle diameter should be as small as possible. In our study, we found that a cohesive powder like the copper powder had a practical range of nozzle diameters between 4-42 times that of the maximum particle diameter, where their RSD was less than 10%. For a free-flowing powder like the solder powder, a range of nozzle diameters were between 3-12 times that of the maximum particle diameter.

Doming is the most important powder flow behaviour in dry powder printing. A stable dome structure is a self-supporting structure that occurs after the particles converge toward the conical section of the dispenser. The formation of a dome causes powder flow to stop. Without this mechanism, dry powder printing using ultrasonic vibration cannot regulate the start and stop cycle of a dispenser.

Figure 4-17 illustrates schematically the three different types of controllability in powder dispensing. For the immovable type (

Figure 4-17A), the powder cannot exit the dispenser because the powder clogs and/or the strength of the dome structure is too large to break via the vibration generated from the piezoelectric transducer. For the controllable type (

Figure 4-17B), the powder can form a stable dome structure that our device was able to break via piezoelectric vibration. For the uncontrollable type (

Figure 4-17C), the powder was not cohesive enough to create a stable dome structure. So, the powder flowed continuously until the powder ran out and the device could not control the powder flow. Yang et al.[258] found that good control in their devices with nozzle diameter to the particle size ratio of 2-5 could be achieved for several metal powders and ceramic powders with particle size less than 100 μm can be achieved.

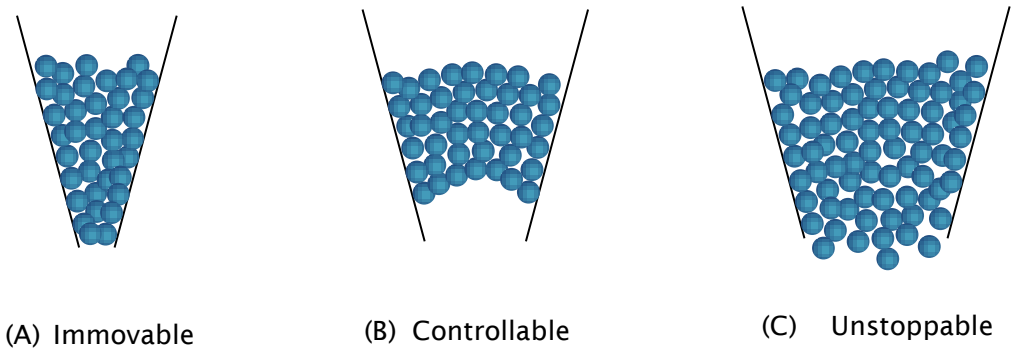

Figure 4-17 Simplified pictures of the effect of nozzle diameter on discharge controllability.

4.2.5 Effect of signal voltage on mass flow rate

In our device, the mass flow rate can be regulated by the vibration generated by the signal voltage, which controls the deformation amplitude of the piezoelectric transducer. Generally, when the signal voltage is increased the vibration intensity is enhanced. To examine the effect of signal voltage on mass flow rate for our device, the level of signal voltage was varied between 0.5 and 5 Volts by steps of 0.5 Volts. The experimental powders were solder powder and copper powder. For all experiments, a nozzle design with a nozzle diameter of 250 μm, a nozzle angle of 75˚ and a piezoelectric position of 12 mm were selected.

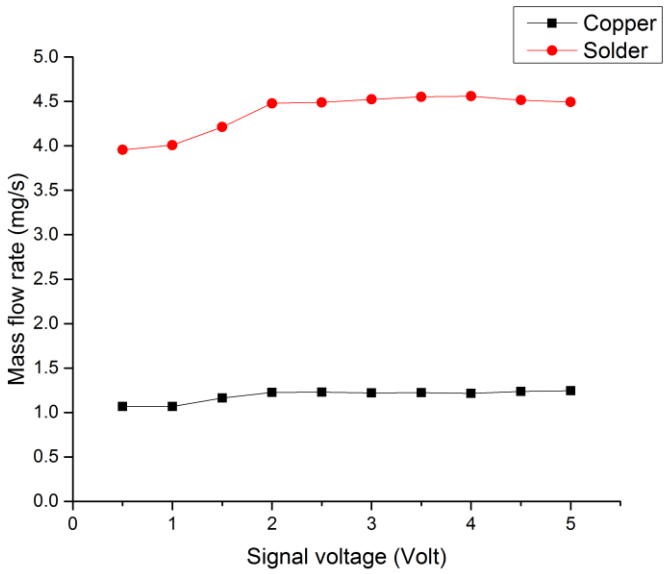

Figure 4-18 The mass flow rate for copper and solder powder at various signal voltages (the nozzle diameter = 250 μm, the nozzle angle = 75˚, the piezoelectric position = 12 mm).

The graphs in Figure 4-18 show the mass flow rate of copper and solder powder with different signal voltages supplied to the device. The maximum mass flow rate of both powders is obtained when the signal voltage reaches 2 Volts. Between a signal voltage of 2 and 5 Volts, the mass flow rates of both powders are quite constant. The solder powder has the mass flow rates higher than the copper powder. This might indicate that the piezoelectric transducer seems to have a working range up to 2 Volts. Once the vibration, as influenced by the signal voltage, has reached a certain value a higher signal voltage could not generate more vibration and thus a different mass flow rate. Normally, a piezoelectric transducer has limited material deformation and it will deform the same amount, saturate, above a certain voltage. In addition, the mass flow rate of different powders is improved by increasing the signal voltage in different ways. A good flowability powder is more sensitive to a higher signal voltage than a poor flowability powder. It can be concluded that the device can increase the mass flow rate when a voltage to up 2 Volts is supplied. Therefore, this signal voltage range can be used to adjust the mass flow rate for this device.

The controllability by signal voltage in the working range (up to 2 Volts) of our device might be explained by the equation developed by Loverich [288]. The vibration force generated via a piezoelectric block is given by the following equation:

$$F_b = \frac{d_{33}A}{S_{33}^E h}U \quad (4\text{-}11)$$

where F_b is the maximum vibration force, d_{33} is the piezoelectric constant, S_{33}^E is the elastic constant, A is the area of the piezoelectric block, h is the height of the piezoelectric box and U is the voltage supplied to the transducer. As seen in Equation 4-11, when the supplied voltage is increased, the vibrations force increases. This agrees with our findings when the voltage varies from 0.5 to 2 Volts.

4.3 Characteristics and processing parameters of dry powder printing

Many of the powder micro dispensing studies that have been carried out to date have used several materials and discuss the relationship between the control parameters of their devices and the uniformity of the dispensed dose. However, they rarely focus on the printing parameter to use in a powder layering process. This investigation aimed at characterising the printing behaviour and establishing the relationship between processing parameters in order to prepare an operation guideline for printing multiple powder material. The key characteristics of powder printing are the quality of the printed track. Some of those parameters which control this, such as moving speed, standoff distance, spot size are described below.

4.3.1 Printable powders

The flowability of a powder is the most important property for the selection of printing powders. Bradley et al. [289] pointed out that a very simple way to know the flowability is to squeeze the material powder. If it is cohesive, it will form a ball. In contrast, if it cannot form a ball and is like dry sand, it is free flowing. We found this also be true. In addition, if SEM images of the powder show no

agglomerations but rather discrete particles this is also a good indication of a printable powder.

However, fine powders have difficulty discharging freely through a nozzle due to adhesion to the internal wall of the glass tube and cohesion between powder particles. In order to determine the printability of powder, a variety of powder materials were tested. All of the results came from the same dispenser geometry, i.e. a 250 μm nozzle diameter with a nozzle angle of 75˚. The piezoelectric transducer was attached 12 mm from the orifice and the signal voltage was 2 Volts. The experimental powders are discharged from the dispenser into a container and the flow pattern characteristics were captured with a high- speed camera at 1,000 frames per second.

The images presented in Figure 4-19 reveal the drop characteristics of the experimental powders. The different powder drop forms could be classified in two different types: A) cluster particles and B) discrete particles. The drop forms are presented schematically in Figure 4-20. The copper (Cu), alumina (Al_2O_3) and 420S45 stainless steel (420S45 SS) powders had the three largest angles of repose among the experimental powders (as shown in Table 3-1), partly owing to their greater cohesion. They formed the cluster-particle drop type. The other experimental powders formed the discrete-particle drop type. The solder (SnPb), silicon carbide (SiC) and tungsten carbide (WC) produced the discrete-particle drop with very large spray angles. The glass bead, alumina (Al_2O_3), 316L stainless steel (316L SS) and glass-filled nylon (Glass-filled PA) fell as the discrete-particle drop with smaller spray angles.

(A) SnPb

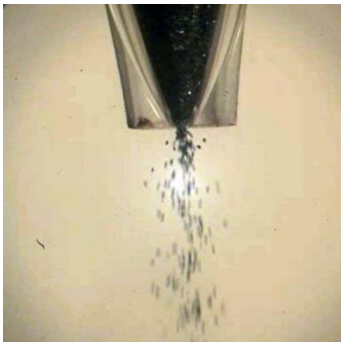

(B) SiC

(C) WC

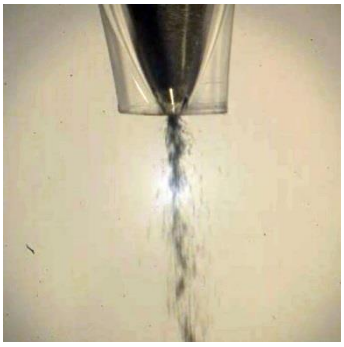

(D) 316L

(E) Glass

(F) Al_2O_3

(G) Glass-filled PA

(H) 420 S45

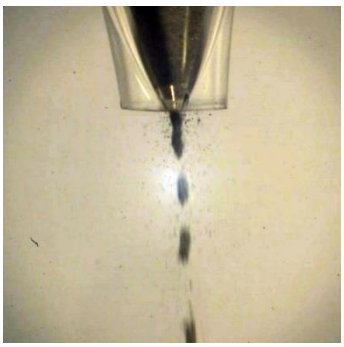

(I) CoCr

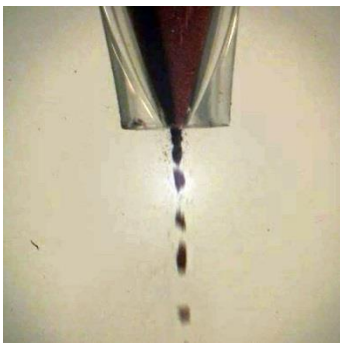

(J) Cu

Figure 4-19 Images showing the drop characteristics of different powder materials under the same dispensing condition.

It can be seen that the flowability determines the drop forms of powders. The more cohesive powders tend to discharge as cluster particles, while the less cohesive powders tend to discharge as discrete particles. The scale of the interparticle forces significantly increases when the particle size becomes smaller. These forces could make the individual particles stick to each other and form agglomerates, which lead to the cluster-particle drop. Other related studies [9, 260, 267, 285] showed that in dry powder dispensing the powder drops in three different forms: 1) rod particles, 2) cluster particles and 3) discrete particles. These authors pointed out that the rod-particle drop usually occurred with very cohesive powders. Previous works [9] and our own experience indicated that it is difficult to obtain stable flow with rod or plug drops and hard to control dispensing. Thus, for dry powder printing applications, we suggest that this type of drop form is not suitable for printing. Additionally, the findings indicate that our device is able to print powders with particle size from 14 to 72 μm and angle of repose below 52˚. Furthermore, the printable powders tend to form the drop as cluster particles and discrete particles.

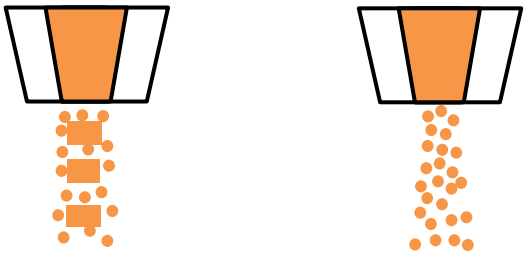

A) Cluster particles B) Discrete particles

Figure 4-20 The two different types of drop forms.

Based on the particle's density and mean particle diameter all the experimental powders, except for copper, fit into groups A and B of Geldart's classification presented in Figure 4-21, The copper powder is located on boundary A and C. Group A powders are ideal for conveying in sliding bed flow, Group B powders are easy to fluidize and they rapidly de-aerate while Group C powders are difficult to fluidize and are cohesive [195, 290]. By locating the ten experimental powders into the Geldart's chart, we can conclude that in almost cases, the powders used in this study were free-flowing powders or not extremely cohesive powder.

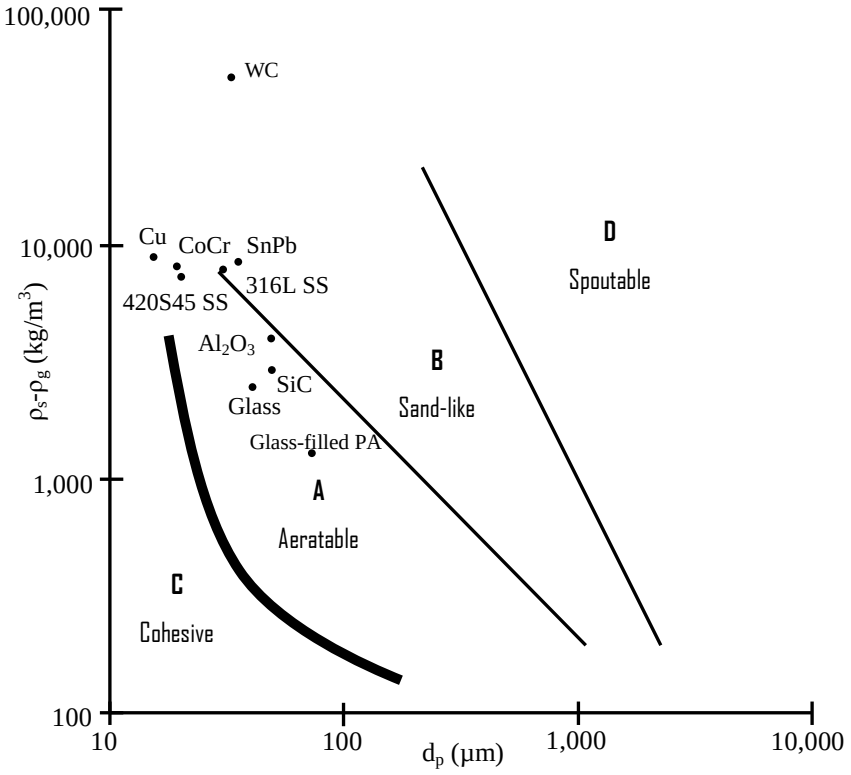

Figure 4-21 Experimental powders shown in Geldart's classification.

(ρ_s-solid density, ρ_g-gas density, d_p- mean particle diameter)

In summary, a very wide range of powder materials has been printed by our device. It is possible to print a polymer material such as glass-filled nylon and ceramic materials such as glass bead, silicon carbide and alumina. The metals consist of copper, solder, 316L stainless steel, 420S45 stainless steel, tungsten carbide and cobalt chrome. Dry fine powder particle within the range 14 to 72 μm can be practically printed without any problem.

4.3.2 Dry powder printing

In order to assess the capability of the device for various powders, a dot, a straight line and a spiral line were used to evaluate the printing characteristics. To demonstrate layer printing, a nozzle was placed above a CNC table which had XYZ-positioning movement in both horizontal and vertical directions. All of these results came from the same dispenser geometry, i.e. a 250 μm nozzle diameter with a nozzle angle of 75˚ and a piezoelectric position of 12 mm. Throughout this

study, the experiments were carried out with an applied signal voltage of 2 Volts, a standoff distance of 200 μm and a moving speed of 10 mm/s.

As can be seen in Figure 4-22, the ten experimental powders detailed in Table 3-1 were successfully printed on a ceramic substrate. Uniform track width and height were achieved for all powders. It should be noted that the appropriate control of parameters for each experimental powder can markedly improve the printed results. As detailed in section 4.3.1, the powder drops for dry powder dispensing occurred as cluster-particle drops and the discrete-particle drops. All powders in the discrete-particle drop group showed large coverage areas of satellite particles located around their main track in contrast to most powders in the cluster-particle drop group. The main track width and satellite diameter of the tracks were measured and are presented in the multiple bar chart of Figure 4-23.

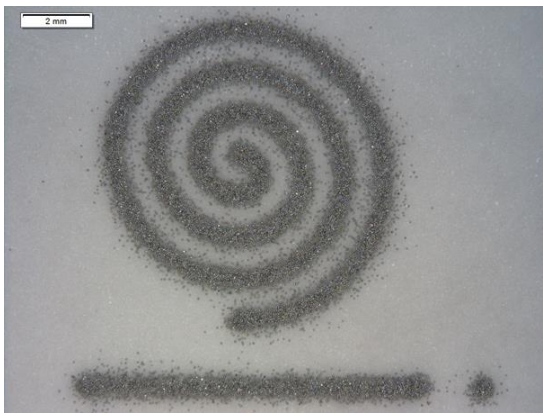

SnPb

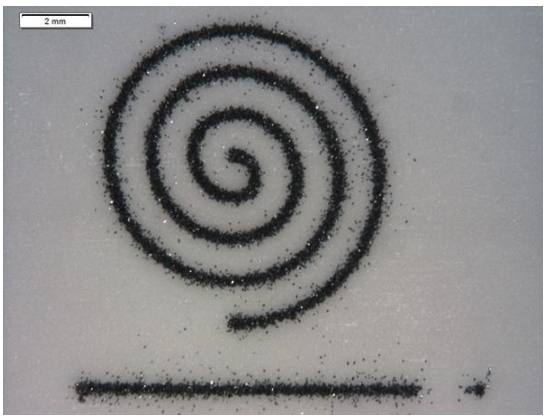

SiC

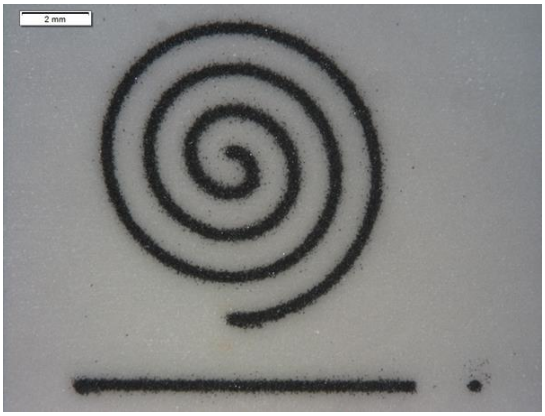

WC

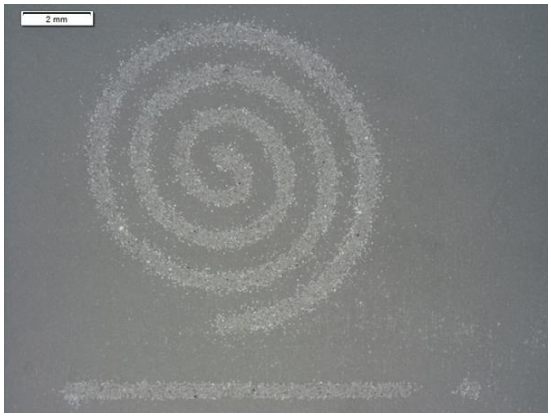

Glass

Al_2O_3

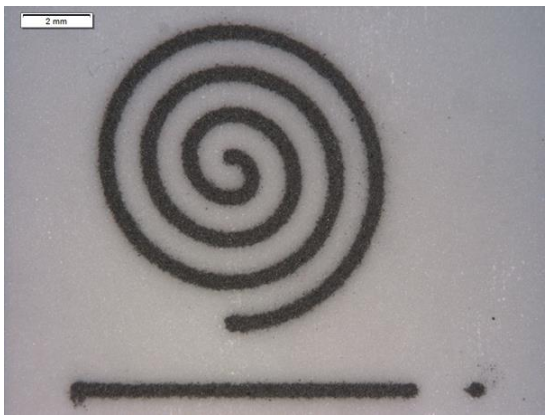

CoCr

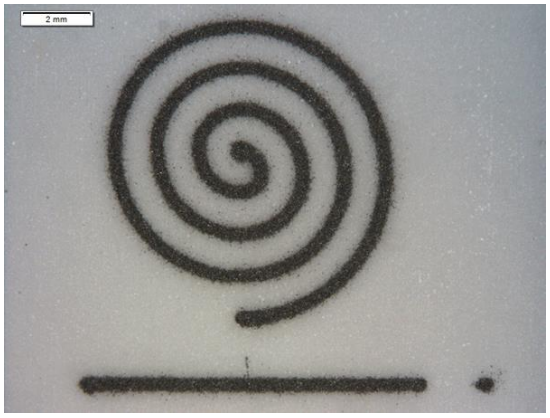

316L SS

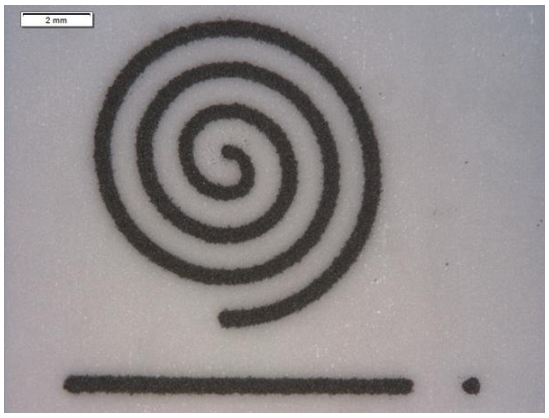

420S45 SS

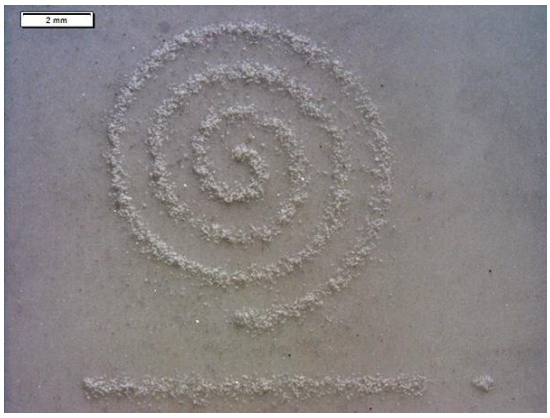

Glass-filled PA

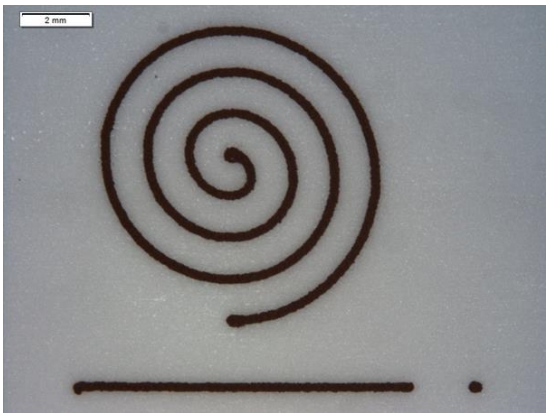

Copper

Figure 4-22 Single material printing of various powders.

It can be seen that the copper (Cu), alumina (Al_2O_3) and silicon carbide (SiC) have the three smallest main track widths. The solder (SnPb), glass bead and S45 stainless steel (S45) show the three biggest main track widths. For the satellite diameter, the three largest are the solder (SnPb), glass bead and silicon carbide (SiC). The three smallest are the copper (Cu), S45 stainless steel (S45) and cobalt chrome (CoCr). The track widths and satellite diameters were a function of the drop form. Furthermore, most cohesive powders show small track widths and small satellite diameters. In contrast, most free-flowing powders show large track widths and huge satellite diameters.

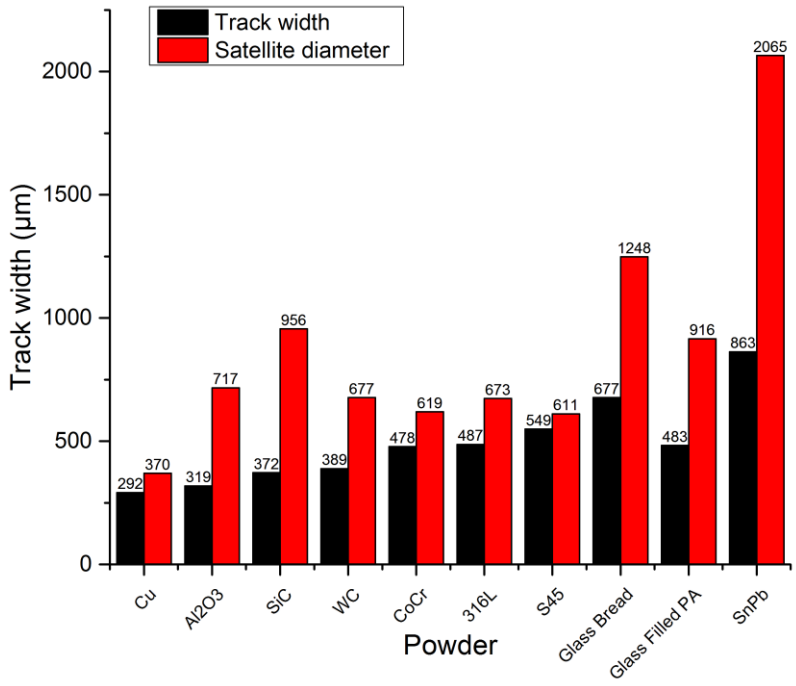

Figure 4-23 The main track width and satellite diameter of printed powders.

4.3.2.1 Spray effect

As detailed in section 4.3.1, the powder drop can present in three drop forms: 1) rod particles, 2) cluster particles and 3) discrete particles. In this investigation, we focused on the spray angle that is normally found with the cluster-particle drop and the discrete drop. However, up to now, most researchers have reported only the drop types and have seldom focused on the effect on this behaviour. This dispensing characteristic can affect the track width and part quality in dry powder printing. If the tip of a nozzle is far from a substrate, the spray of a powder during

dispensing with the discrete particle pattern will be larger with the cluster particle pattern. Consequently, the track width of the dispensing line will depend on the distance between the tip of the nozzle and the substrate. This discussion will be presented in section 4.3.2.3.

In order to investigate the effects of signal voltage on spray angle, the solder and copper powders were used. Three nozzles were used; 1) a nozzle diameter of 250 μm, a nozzle angle of 75˚ and a piezoelectric position of 12 mm., 2) a nozzle diameter of 150 μm, a nozzle angle of 15˚ and a piezoelectric position of 12 mm., 3) a nozzle diameter of 250 μm, a nozzle angle of 15˚ and a piezoelectric position of 12 mm. The signal voltages were varied from 0.5 to 1.25 in steps of 0.75 Volts. A high speed camera was used to record the powder stream at 4,000 frames per second. ImageJ software was used to analyse the captured images.

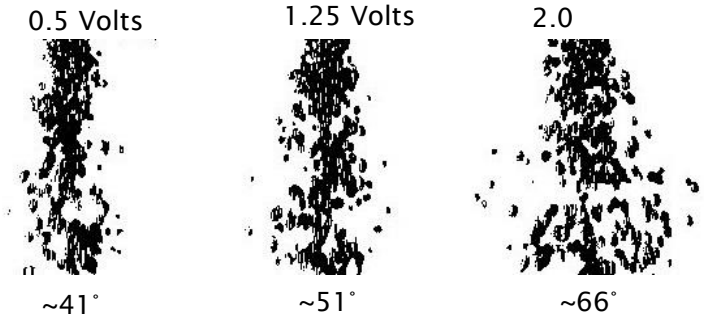

(A) Nozzle diameter = 250 μm, Nozzle angle = 15˚

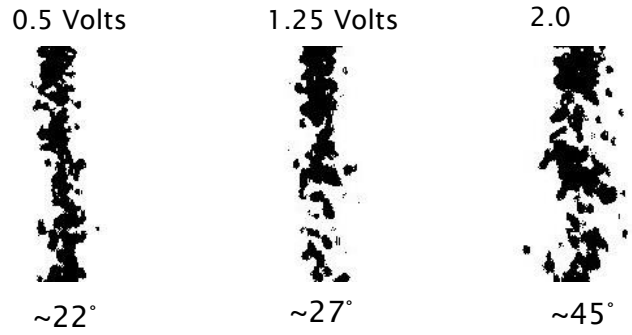

(B) Nozzle diameter = 250 μm, Nozzle angle = 75˚

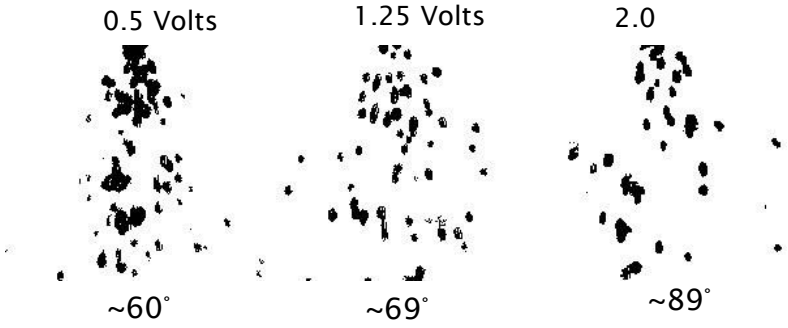

(C) Nozzle diameter = 150 μm, Nozzle angle = 15˚

Figure 4-24 Powder streams of solder powder from three different nozzles at signal voltages of 0.5, 1.25 and 2.0 Volts.

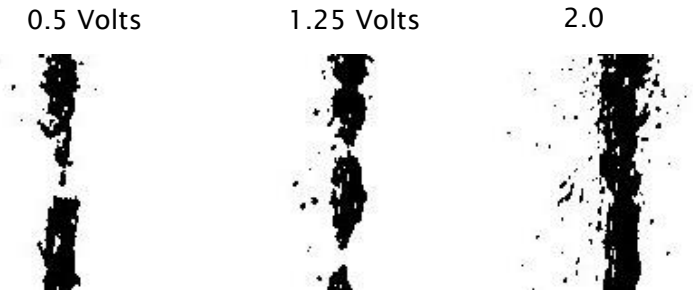

(A) Nozzle diameter = 150 μm, Nozzle angle = 15°

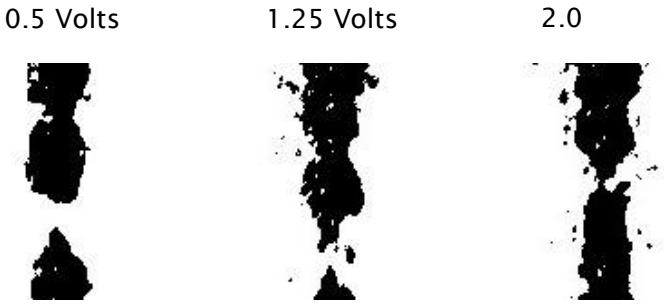

(B) Nozzle diameter = 250 μm, Nozzle angle = 15°

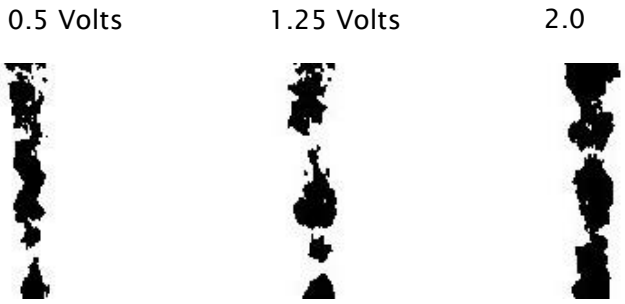

(C) Nozzle diameter = 250 μm, Nozzle angle = 75°

Figure 4-25 Powder streams of copper powder from three different nozzles at signal voltages of 0.5, 1.25 and 2.0 Volts.

Figure 4-24 and Figure 4-25 show powder streams of the solder and copper powder from three different nozzles. The spray angle of the solder powder has a larger angle than the copper powder. The powder streams of the solder powder

show large spray angles as the signal voltage increases. The largest spray angle occurs for a nozzle diameter of 150 µm and nozzle angle of 15˚. For the same nozzle diameter of 250 µm, a nozzle angle of 15˚ has a larger spray angle than the nozzle angle of 75˚. For the copper powder, the powder streams have relatively small spray angles. However, a lot of satellite particles are presented around the main powder stream at high signal voltage for a nozzle angle of 15˚ and the nozzle diameter of 150 µm. For the nozzle angle of 75˚, the powder stream shows a weaker powder stream than the nozzle angle of 15˚ for the same nozzle size. The maximum number of satellite particles occurs around the powder stream of the nozzle with an angle of 15˚ and diameter of 150 µm. For a nozzle diameter of 250 µm and nozzle angle of 75˚, the satellite particles are not readily apparent. In addition, from our observation, we found that the copper powder could start dispensing at 0.20 Volts for a nozzle diameter of 250 µm and nozzle angle of 15˚, whereas, a nozzle diameter of 250 µm and nozzle angle of 75˚ required a signal voltage of 0.30 Volts to start dispensing. However, the solder powder with a nozzle diameter of 250 µm and nozzle angle of 15˚ required a signal voltage of 0.15 Volts. A nozzle diameter of 250 µm and angle of 75˚ required a signal voltage of 0.20 Volts to start dispensing. The RSDs of all samples dispensed were bigger that 10% resulting in unstable flow and inconsistency of the mass flow rate. Chen et al. pointed out that the strength of dome structures vary from powder to powder. Thus, the vibration to break the dome structures and initiate powder flow is different [285].

This study revealed that a narrower nozzle angle has a bigger spreading angle than a wider nozzle angle for the same nozzle diameter. Also, a bigger nozzle diameter has a smaller spreading angle than a smaller nozzle diameter with the same nozzle angle. It can also be concluded that the spray angle increases with increasing signal voltage. A large spray angle is found for free-flowing powders than for cohesive powders. These results are in agreement with the work reported by Kumar et al. [138]. However, this is the first time we found and reported that the nozzle angle has effect on the spray angle of powders. For our study, the copper powder showed a very small spray angle but large amount of satellite particles around the main powder stream for a small nozzle diameter, narrow nozzle angle and high signal voltage. This might be due to the velocity of the particles near the wall of the dispenser being high resulting in enhancement of the electrostatic field around the tip of the nozzle.

Lu et al. [9] pointed out that gravity force and vibration energy are the main driving force for powder flow in dry powder dispensing using ultrasonic vibration. However, in our dry powder printing device, we believe that excessive vibration energy directly affects the powder spray angle. Therefore, the optimal vibration energy should be large enough to provide uniformity of powder flow, but it should not too large to generate the spray angle effect. This finding suggests that the minimum signal voltage causes the minimum spray angle. To reduce the effect of spray angle, the signal voltage should be decrease until the minimum value that provides uniformity of powder dispensing is reached. From our observations, we suggest that the relative standard deviation (RSD) of powder dispensing should be less than 10% or small enough to get consistent printing results.

4.3.2.2 Spread effect

The behaviour of powder as it is deposited on a substrate is interesting. However, the research in the literature in Chapter 2 rarely concerns the behaviour of powder drops on the substrate from landing to the end-stage. In the powder printing process, ensuring the printed powder lands in a selective location is very important. To understand the process that occurs when the printed powder lands on the substrate, a high speed camera was used. There were two types of substrate used in this study. One was a ceramic plate that is relatively smooth but rigid and powder tend to bounce when fall on such the substrate. The other was a nylon powder sintered object that is relatively rough but relatively soft and powder less tends to bounce on such the substrate. Copper powder and Solder powder were used. A high speed camera with a zoom lens was used to observe the impact of the powders dropping on the substrates. A nozzle diameter of 150 μm, nozzle angle of 15° and piezoelectric position of 12 mm was used. The signal voltage was 0.25 Volts. The printing time used to create a powder drop was 100 ms.

Figure 4-26 shows images of the two powders dispensing onto the ceramic and nylon substrates, from the start at 0 ms to the final stage at 140 ms. At time=20 ms, the three sets of images show the spreading of a first layer after impacting the substrate. If the same standoff distance is used, we can predict that the copper powder has a smaller spreading width than the solder powder. When comparing the spreading width of the solder powder on the two substrates, it can be seen that the spreading width on the sintered nylon substrate is smaller than on the ceramic substrate. At times from 40 to 120 ms, the three sets of images show

powder piling up on the substrates and the particles of the top of each pile moving outward from the main pile. At time=140 ms, the three sets of images show the final stage for each powder. The copper powder deposit has a hemispherical shape (Figure 4-27A), the solder powders on the ceramic and sintered nylon substrate have a conical shape (Figure 4-27B and Figure 4-27C). It can be seen that the pile of each powder reflects their angle of repose. In addition, video recording from the high speed camera revealed that the solder powder bounced more on the ceramic substrate than on the nylon substrate.

When the surface roughness is high, the spreading of the powder particles was decreased by friction forces. Thus the spreading width depends on the friction between powder and substrate. High friction could cause less spreading. Poor flowability and high surface roughness decreases the spreading effect. Good flowability powders attain larger diameter drops than poor flowability powders. Also, smooth surfaces produce larger diameter drops than surface with high roughness.

Furthermore, a powder drop spreads after impacting on a substrate could increase if the speed of drop particles is high. They may have large spread distance and/or bouncing. This effect leads to poor control of powder printing tracks resulting in low resolution printing. The bouncing and spreading of the powder could be controlled or prevented by using a small standoff distance or selecting a highly absorbable substrate. For this reason, this dry powder printing could be integrated in a powder bed system because then it could print into a loose powder layer with less spreading. The results showed a larger diameter when a longer standoff distance was used and hence standoff distance is an important parameter to control. The final shape of the deposited powder reflects its angle of repose and its flowability.

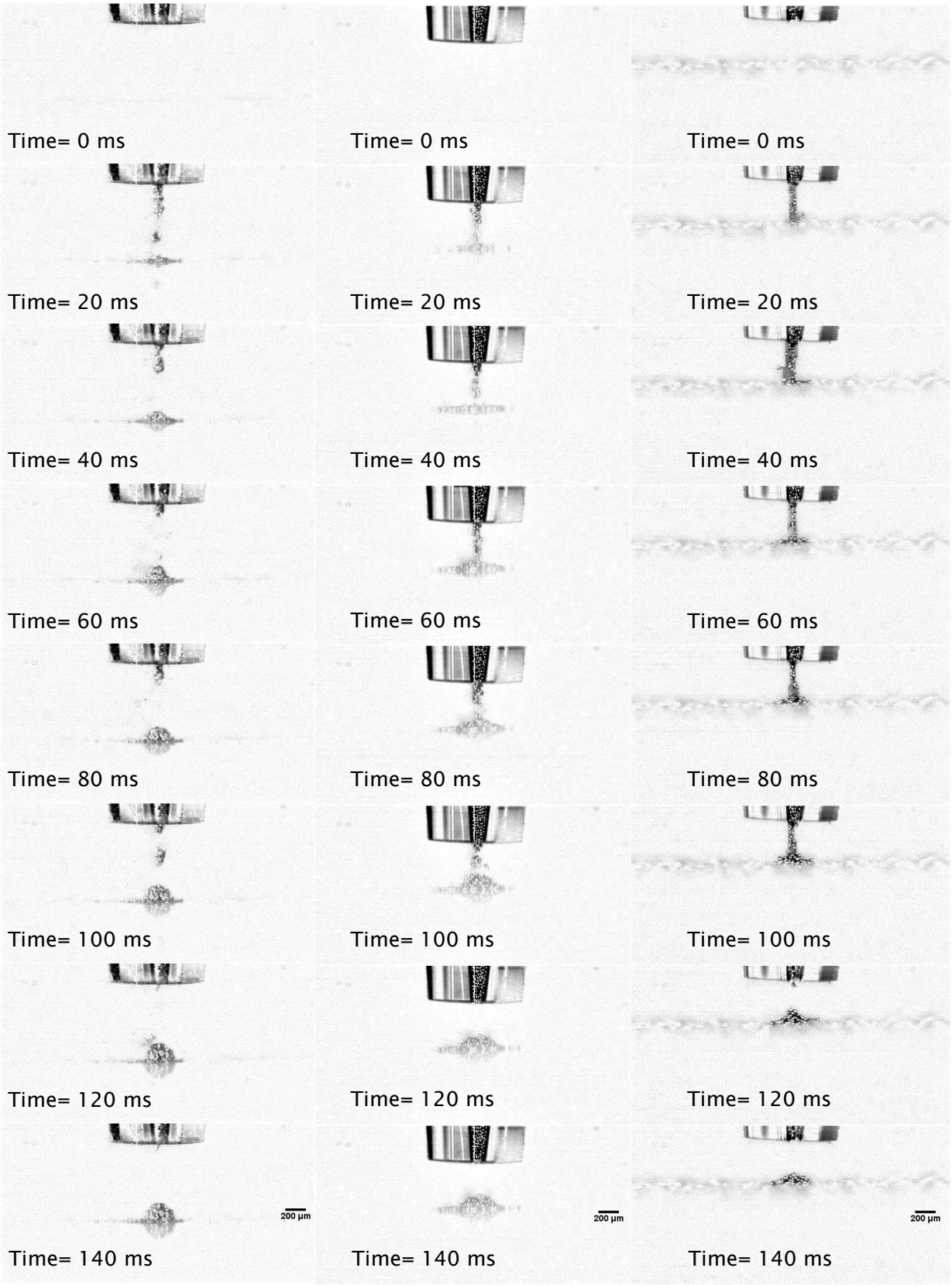

(A) Copper powder on a ceramic substrate.

(B) Solder powder on a ceramic substrate.

(C) Solder powder on a sintered PA substrate.

Figure 4-26 Sequential images of a powder dropping, time step = 20 ms.

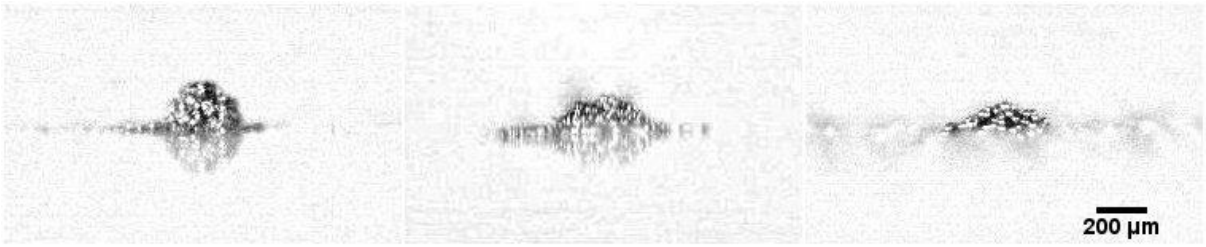

(A) (B) (C)

Figure 4-27 Images of a powder track: (A) copper powder on a ceramic substrate, (B) solder powder on a ceramic substrate and (C) solder powder on a sintered nylon substrate.

Our experiments is in complete agreement with that of Kumar et al.[138] who pointed out the relationship between angle of repose and line spread. Therefore, in order to produce high resolution results in dry powder printing, this issue must be taken into account. Ideally, the system should be controlled a drop and immediately adhere to the substrate with minimal spreading. Spreading can be inhibited by optimizing the distance between the nozzle and the substrate (the standoff distance) and improving the printability by having high surface roughness.

4.3.2.3 Standoff distance

Standoff distance is the distance of the tip of the nozzle to the top of the substrate. From the previous discussion, printed powders normally spread out and the spray angle depends on the signal voltage. Therefore, in order to print a small line width, the standoff distance should be as small as possible. Figure 4-28 illustrates the print results associated with high and low standoff distances. The image on the left shows wide printed lines and a small powder height, while the image on the right shows narrow printed lines and a high powder height.

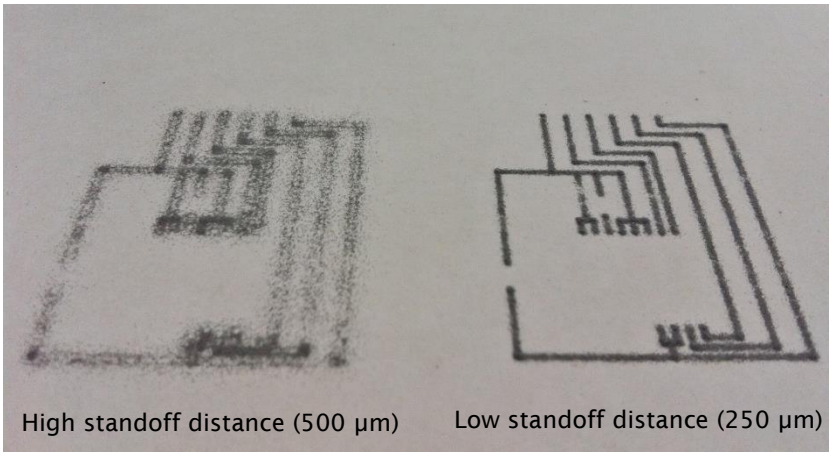

Figure 4-28 The effect of different standoff distances on tracks in solder powder (the moving speed = 10 mm/s).

Thus in order to decrease the track width and increase the resolution of powder printing, the standoff distance between the nozzle tip and the substrate should be as small as possible. However the standoff distance should also be taken into account the moving speed and mass flow rate to avoid the nozzle hitting the powder track while feeding the material. Moreover, the lower limit to standoff distance depends on the moving speed as the standoff distance must be sufficient to avoid powder blocking the flow between the tip of the nozzle and the top of the substrate.

In order to assess the effect of the standoff distance on the track width of printed line, varying standoff distances and moving speeds were tested. The nozzle diameter used was 250 μm and a signal voltage was 2 Volts. Figure 4-29 shows that the tracks produced all moving speeds with a 125-μm standoff distance contacts the tip on the nozzle resulting in compression of the printed lines. Thus the line heights of all printed lines are equal to the standoff distance. At the 625-μm standoff distance, there are no contacts between the tip and the printed lines at all moving speeds. For the moving speed of 5 and 10 mm/s, there are also no contacts to the printed lines at the 325-μm standoff distance. However, at the moving speed of 1 mm/s, the printed line is slightly lower than the printed line at the 625-μm standoff distance. The reason is it might interrupt the powder flow at the outlet. The results confirm that decreasing a standoff distance too much causes the nozzle to hit the powder track.

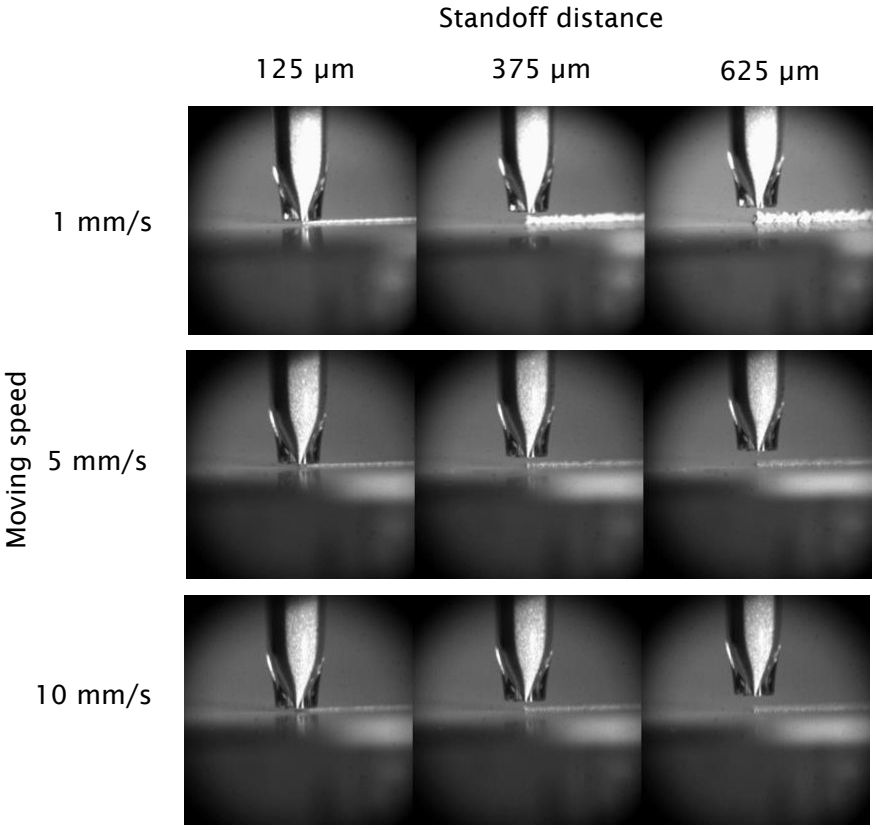

Figure 4-29 Images obtained from a high speed camera for copper powder dispensing with different moving speeds and standoff distances.

4.3.2.4 Material Deposition Rate (MDR)

The material deposition rate (MDR) is the amount of powder per unit time that prints from the device, which is equal to the mass flow rate. It directly influences the layer thickness and the build speed. High material deposition rate results in thick layers and fast build time. The MDR is equal to the volume flow rate multiplied by the apparent density of the printed powder. As we assume that the printed powder was a loose powders, the MDR can be calculated by using the equation below:

$$Q = \rho_a \times h \times d \times v \tag{4-12}$$

where h is the layer thickness (m), Q is the mass flow rate (kg/s), ρ_a is the apparent density (kg/m^3), d is the track width (m) and v is the moving speed (m/s).

Both the volume deposition rates and the layer thickness are affected by the mass flow rate and the moving speed. However, this is simple model to estimate the

parameters in MDR and in the real situation, the cross-sectional shape of the printed track is not a rectangular. The shape of the printed track is shown in section 4.3.2.2.

The layer thickness of a printed layer is a key requirement for AM applications. This thickness could be controlled by varying the mass flow rate and the moving speed. Generally, there are two methods to know the layer height, one direct method and the other indirect. The powder height can be directly measured from the printed track by an optical microscope or a laser or optical scanner. This method is straightforward, but it is difficult to move the sample to the measuring equipment because the printed powder is a loose powder and it is difficult to maintain the powder shape when handling. As an indirect method, the powder height can be estimated from:

$$h = \frac{Q}{\rho_a \times d \times v} \tag{4-13}$$

4.3.2.5 Moving speed

The material deposition rate is a key factor in determining the speed of layer printing. Generally, layer printing should be fast, which could be met by increasing the moving speed. From our study, the mass flow rate can be adjusted by varying the nozzle diameter, nozzle angle, piezoelectric position and signal voltage. However, the nozzle diameter, nozzle angle and piezoelectric position cannot be adjusted after construction of the nozzle. However, from our study, the signal voltage can be adjusted over a small range and so able the mass flow rate, but it can produce the spray angle effect. Therefore, the most effective control parameter is the moving speed. To determine the effect of moving speed, 10-mm printed lines were produced by copper powder with different moving speeds at a fixed standoff distance. The standoff distance was 200 μm. The nozzle diameter used was 250 μm and the signal voltage was 2 Volts.

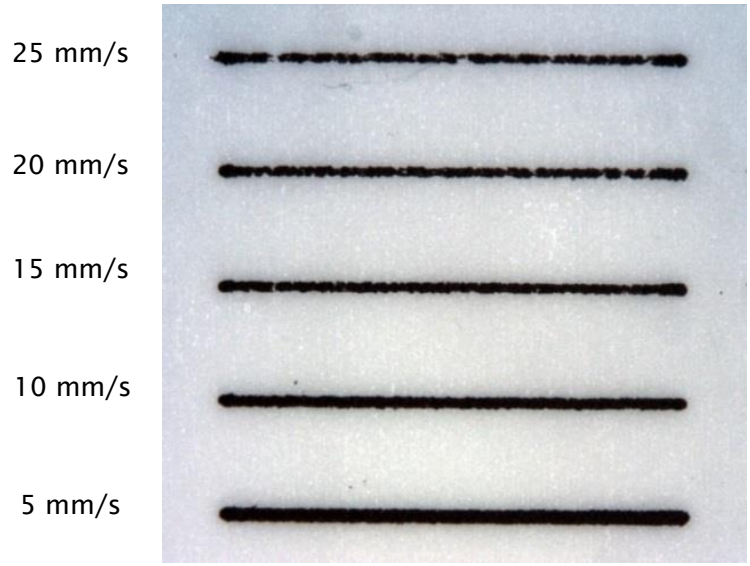

Figure 4-30 Printing results for copper powder obtained from different moving speeds.

Figure 4-30 shows that the copper line printed with a moving speed of 5 mm/s is thickest. The copper printed with moving speeds of 10 mm/s and 15 mm/s were complete and fine. However, the edge of the former line is better and the line width of the later is thinner. Printing with moving speeds of 20 mm/s and 25 mm/s cannot create complete printed lines. This indicates that the maximum moving speed should be less than 15 mm/s to obtain a complete and continuous line. In order to achieve a small line width, the minimum moving speed should be faster than 5 mm/s. For a free flowing powder such as the solder powder, the moving speed for good printing results was in the range of 10 mm/s to 50 mm/s.

The results show that with a slow moving speed the line will be thicker and higher. From our observation, moving speed is critical to the quality of powder printing. A fast moving speed increases the printing speed of the build process and causes a thin layer. However, the moving speed should not be so fast as to produce a discontinuity in the printed line. In contrast, a slow moving speed increases both the width of the line and the line height because the printed powder will gather on the top and then spread out from the main track. Moreover, a very slow moving speed can cause blockage of the dispenser if the height of the powder is greater than the standoff distance. In addition, we found that at high moving speed for a large nozzle diameter that is near the upper limit of the ratio of the nozzle diameter to the particle size, powder printing was not controllable due to the inertial force of the accelerating force acting on particles inside the device.

4.3.2.6 Match-head effect

The match-head effect is a large dot at the starting point of a printed line. This dot is bigger than the average size of the printed line and its shape looks like a match head. A match-head occurs on printed lines when the printing is in the run-in stage since the mass flow rates are so high. The investigation in section 4.2.2 indicated a high mass flow rate in the run-in stage. Therefore, in the run-in period, the mass flow rate tends to be high and this causes the printed line to have a match-effect every time. In addition, the study in section 4.1.2 found that in the finishing point of a printed line has the effect of an off-delay time and can also create the match-head effect.

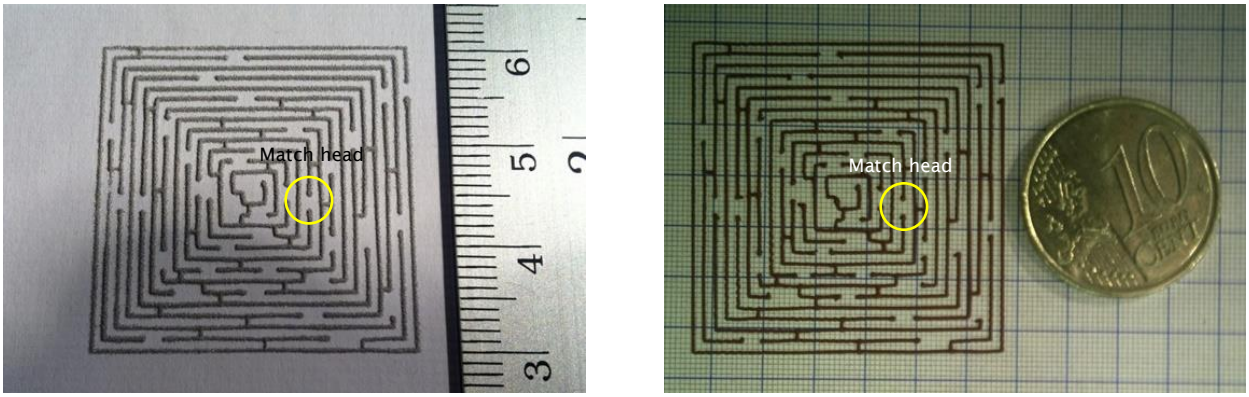

(A) Solder powder (B) Copper powder

Figure 4-31 Printing patterns of solder powder (A) and copper powder (B).

The match-head effect of different powders is shown in Figure 4-31 which are examples of powder printing without equalizing the bulk density of powder inside the nozzle. In Figure 4-31A, there are a few match heads at the end and the start of each individual solder-printed line, whereas, in Figure 4-31B, the copper-printed pattern, is it can be clearly seen that there are many match heads at the end and the start of each individual printed line. The match-head effect in the copper powder is more noticeable than for the solder powder. One cause could be the compressibility of the solder is poorer than the copper resulting in the packing density of the solder not varying much during discharge. So, the initial drops when switching on are closed to the average drops. This match-head effect was small size when a free-flowing powder, such as the solder powder, was dispensed.

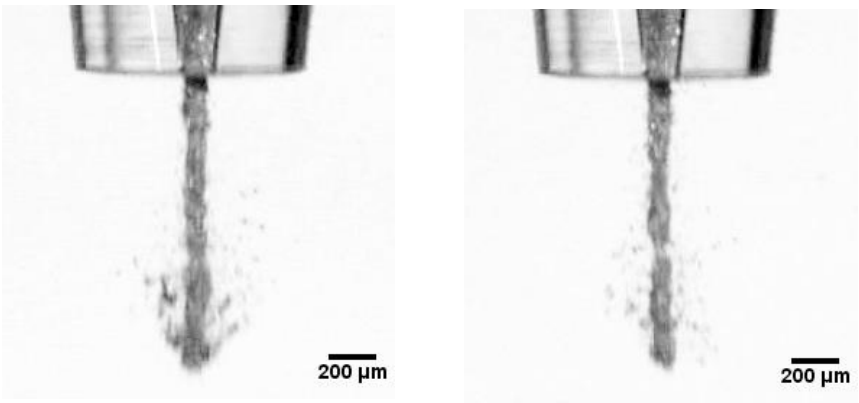

(A) Before equalizing (B) After equalizing

Figure 4-32 The comparison between before equalizing (A) and after equalizing (B) of copper dispensing.

Thus match-head effect could continue to occur until the bulk density of the powder is nearly constant value or the mass flow rate is reached to the steady stage as detailed in sections 4.2.1 and 4.2.2. It can be concluded that cohesive powders tend to have more chance to form the match-head effect than free-flowing powders. Therefore, equalization of the bulk density of powders after filling a dispenser is needed, especially for cohesive powders.

The result suggests that the nozzle should be vibrated for 20 seconds before dispensing the first track so as to pack the copper powder inside the container before printing. Figure 4-32 shows a comparison of powder dispensing before equalizing and after equalizing the copper powder. The start size of the powder stream vibrated until the bulk density was close to constant was smaller than the powder stream without vibrating. From the range of the experiment powders studied in our work, the match-head effect can be avoided by dispensing the powder inside the dispenser 10 to 20 times to equalize the bulk density to a constant density. However, another alternative is to block the orifice and then vibrating 10 to 20 times without discharging.

This match-head effect was also found in a study by Yang [268]; their printed patterns affected from the match-head effect. Lu et al [9], recommended to wasting the first three dispenses to obtain steady feeding of their device. Ludovico et al. [291] found that at high moving speed, the deposition at the start and the stop point was greater than the central part of the printed track because acceleration is required go from zero speed to the desired moving speed at the

start point and deceleration is required to slow down from the constant moving speed to a zero movement at the end point. If the target speed is high, the acceleration time and the deceleration time have to fit with the performance of the motor axes. Moreover, high acceleration and deceleration makes abrupt changes. This can affect the unintentional discharge of the powder around a stable dome structure. This means the acceleration and deceleration can affect the match-head effect on printed lines. However, in this study, we did not found the acceleration and deceleration problem for the match-head effect.

4.3.2.7 Satellite effect

Satellites are a distribution of particles around the main powder particles discharged from an orifice. Satellites blur the edge of a printed line as shown in Figure 4-33. A nozzle design with a diameter of 80 µm, a nozzle angle of 60˚ and a piezoelectric position of 10 mm from the nozzle tip was used in this printing. Additionally, a signal voltage of 2 Volts and a standoff distance of 150 µm were used. Undesirable satellite particles can be clearly observed by the optical microscope. These satellite particles could cover an area over three times that of the main drop size. Figure 4-33B shows the printed result from a moving speed of 5 mm/s and Figure 4-33C shows the printed result with a moving speed of 1 mm/s. Generally, for slow moving speed, the satellites form the thicker layer and the effect can be clearly seen. This effect also reduces the resolution of the printed line.

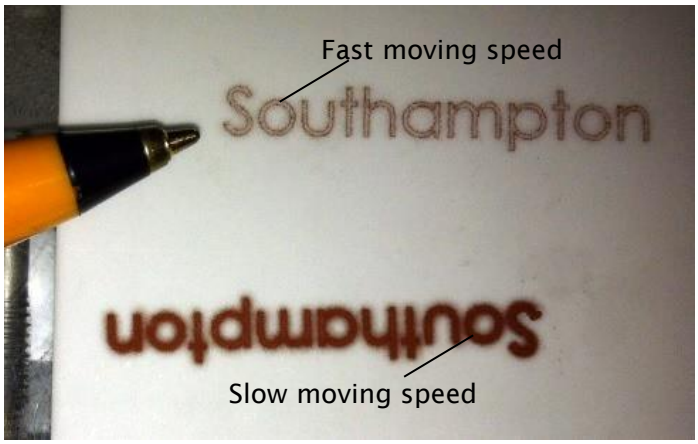

(A) Printing samples of copper powder at different moving speed

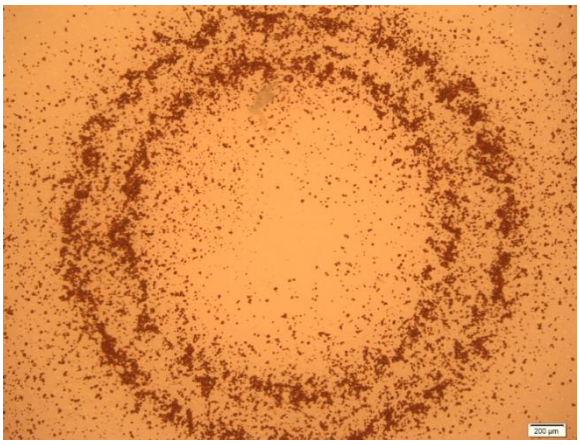

(B) Fast moving speed (5 mm/s)

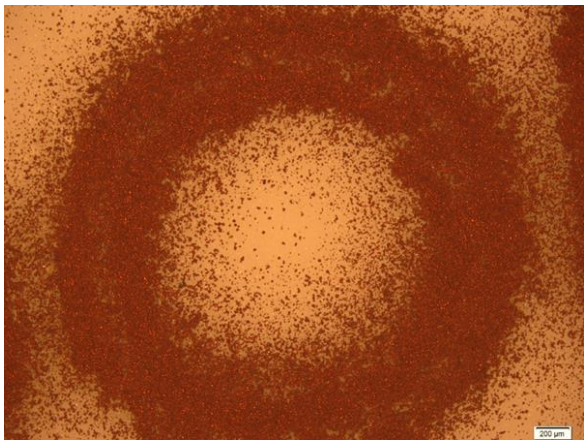

(C) Slow moving speed (1 mm/s)

Figure 4-33 The printing results of a 80-µm diameter nozzle moving with 5 mm/s (A) and 1 mm/s (B).

In Figure 4-33B and Figure 4-33C, satellite drops are presented between the main drops. These satellite particles could be produced by air currents induced by the table movement. This satellite phenomenon has also occurred in liquid-based printing using an inkjet nozzle as reported by Castrejon-Pita et. al [292]. From the study in section 4.3.2.1, a high signal voltage tends to create satellite drops more than low signal voltage by reason of the spray angle effect. In multiple material printing, the satellite drops can travel and contaminate close by material tracks resulting in the unintentional mixing of the materials. To avoid the satellite problem, the signal voltage can be reduced for a given nozzle diameter. The satellite problem can be avoided by using the proper combination of signal voltage and nozzle diameter. Moreover, the air currents in the working space should be minimised.

4.3.2.8 Dot-size effect

The accuracy of powder printing is important for creating complex geometry patterns. In order to test the accuracy of the expected track length, a series of tracks were printed with different lengths, from 1 to 10 mm with a 1-mm incremental step. The actual lengths of the tracks were measured and errors were found. Figure 4-34 shows the dot-size effect diagram and indicates a possible cause of the error of the expected length. Because the reference point in a printed track is the centre of the powder dot at the starting point and finishing point, there is an error of a half of starting point and a half of ending point which makes

the expected length longer by around the dot size of powder. In order to accurately print, we suggest that compensation of the dot size effect should be considered.

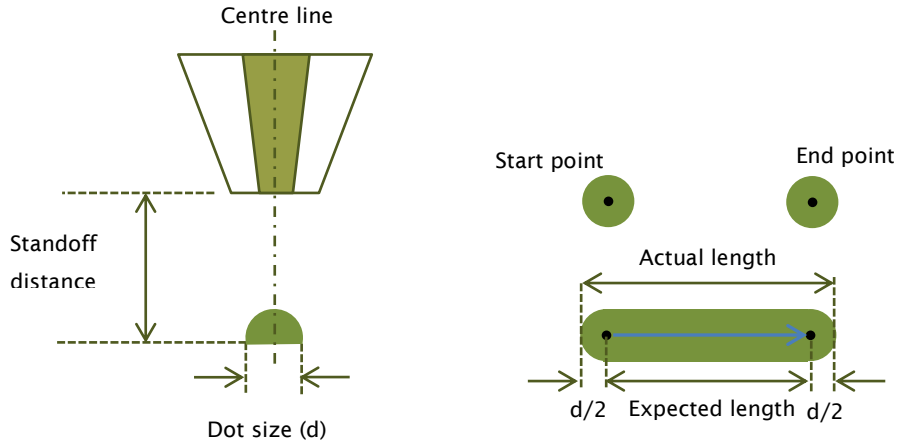

Figure 4-34 Effect of dot size on expected length.

4.3.2.8 High printing resolution

For line printing and pattern printing applications, the resolution of printing is an important quality. Printing quality includes a smooth, continuous sharp edge and accurate position of the powder drops on the substrate. The resolution of layer geometry is limited by track width and track height. A narrower printed line enhances resolution and increases the accuracy of the printed layers. Decreasing the thickness of a powder layer is a promising approach for improving the resolution in the z-axis direct as it reduces the stair-step appearance between layers. Resolution is a trade-off between track size and production rate. The device with a small nozzle diameter will print tiny lines slowly, whereas a large nozzle diameter will print large areas quickly. When the nozzle diameter decreases, limitations will occur from blockage through the nozzle orifice. On the other hand, when the nozzle diameter increases, limitations will occur from unstable dome structure above the nozzle orifice. However, by reducing track width by controlling the nozzle diameter, pattern layers of more complex geometry can be applied.

For our device, the way to increase resolution, such as dot size or linewidth, is by decreasing the nozzle diameter. However, particle size and the flowability of powders limit the choice of nozzle diameters. The particle size has to be smaller

than the nozzle diameter because of nozzle clogging as detailed in section 4.2.4. To obtain satisfactory quality and consistency of powder printing, a careful control of processing parameters was required. In our work, smaller powder drops could be printed by optimizing signal voltage, standoff distance and moving speed.

The dot diameter or track width is a key factor for high resolution powder printing. An ideal dot diameter is equal to the nozzle diameter. From our observations, however, we found that the dot diameter was slightly bigger than the nozzle diameter on account of the effect of the spray angle, the standoff distance and the spreading width. A high signal voltage and/or the high standoff distance resulted in a larger dot diameter. Also, the dot diameter was slightly enlarged when the powder impacted the substrate. Furthermore, the spot diameter tended to increase when the flowability of the printed powders was good. Therefore, the track width was minimised by careful adjustment on all the above parameters. However, it is also important to minimize track height for high resolution printing. The track height can be approximated from Equation 4-13. However, the major limitation of track height is the particle size of the powder and the mass flow rate that depends on the dispenser used. In order to achieve high resolution track width, we can suggest that, a low signal voltage, a wide nozzle angle, a small nozzle diameter and a small standoff distance are used. Nevertheless, to assure reliability and consistency of powder printing with these control parameters, the RSD of powder dispensing should be determined and it should be less than 10%. For high resolution track height or layer thickness, the moving speed should be high.

4.3.3 Fine line pattern

High quality printing powder is very crucial to create regular layers. Therefore, the best combination of printing parameters to create a smooth and regular powder track should be sought. Small or large feature size may be needed depending on the requirements. If a small feature size is required, the printed track should be minimum. To demonstrate the feasibility of dry powder printing through our device, the printing parameters were adjusted to fabricate fine-line pattern on a substrate. To evaluate the resolution of printing, copper powder with a particle size of 14 μm was used. A dry powder printing device with a nozzle diameter of 60 μm, a nozzle diameter of 65° and a piezoelectric position of 15 mm was used. During the printing process the standoff distance of the deposition nozzle from

the substrate was 150 μm, the moving speed was 5 mm/s and the signal voltage was 0.5 Volts (at the mass flow rate of 0.14 mg/s). Figure 4-35 shows the printed spiral lines of the copper powder on a ceramic substrate. The current work revealed that a 60-μm diameter nozzle can be used for printing the copper powder and hence a printed line with a track width as fine as 85 μm was achieved.

Figure 4-35 Samples with a track width of less than 100 μm.

A uniform printed track was achieved and line was continuous and repeatable. This study shows that our device can print a wide range of fine powders and can certainly be a material delivery method for handling multiple material powders. The results indicated that the current device performed significantly better than previous models in term of resolution and consistency. From the literature in Chapter 2, almost all printed feature have had a relatively large track width or dot size. The layer printing quality from the current device, in term of track consistency, track continuity and size feature, was far superior to previous work. With a printing resolution of 85 μm, the process has shown its potential as a micro-manufacturing technique for the deposition of powder materials.

4.3.3 Operational guidelines

The device was able to provide controllability and consistency in powder printing. Currently, this device operated at room temperature and was easy to control and simple to operate. From our study, we found that the primary factor that has to be considered early in the printing process was powder flowability. This property had to be assessed before designing and making the nozzle. This flowability can refer to the ability of the powder particles to discharge from an orifice and form sufficient particles for a printed line. Free-flowing powders allow an easy breakup

of the stable dome structure above the orifice of a printing device with smaller vibration. However, the printed particles can easily spread after impacting the substrate. In contrast, a cohesive powder has poor flowability and causes resistance to flow inside the device. High flowability powder benefits the consistency and reliability of the printing process. Nevertheless, they exhibit the spray effect when the dome structure is broken with the excessive vibration. Additionally, the free-flowing powders exhibit the spreading effect after impacting a substrate. This is depended on the standoff distance and the surface properties of the substrate. Our study has demonstrated the importance of the angle of repose. The accepted angle is mostly lower than 52˚. However, a lower angle is usually preferable. Table 4-4 gives a summary of the technical capabilities of the device.

Table 4-4 Technical capabilities of the device.

Feature	Range
Printable powder	Free flowing powder to cohesive powder
Angle of repose	< 52˚
Minimum RSD	< 7%
Minimum mass flow rate	0.14 mg/s
Minimum feature size	< 100 μm
Moving speed	~ 5 - 50 mm/s
Standoff distance	~100 - 500 μm

In order to support future operation of the dry powder micro delivery system, a summary of the operational guidelines from this study is shown in the flowchart of Figure 4-36. Firstly, it is very important to understand the basic requirements of the printed features by checking the smallest feature size or geometries in a pattern layer. Then, the particle size and the angle of repose of the desired powder can be used to evaluate the printability of the powder. In this step, the operator can decide whether the requirements can be met by the device. Once the desired powder is chosen, the procedure for making the device is straightforward. Initially, the proper nozzle diameter needs to be selected. From our study, the minimum nozzle diameter should be four times the biggest particle diameter and half the maximum nozzle angle should be less than the angle of repose of the printed powder. The smallest nozzle diameter provides the finest resolution when printing

a pattern. This nozzle diameter can be used to roughly define the track width. Then, the dispenser is constructed as detailed in section 3.1.3. After that, in order to test the dispenser, the simplest method is to fill it with powder and try manually tapping the tip of the glass tube. If powder can be discharged from the tube, then the assembly of a piezoelectric transducer can be undertaken. If the powder cannot be discharged, then change to a smaller nozzle angle glass tube with the same nozzle diameter. If the smallest nozzle angle cannot dispense the desired powder, the powder cannot be used with the target feature size.

After the desired powder has satisfied the restriction of nozzle diameter, the signal voltage supplying the piezoelectric transducer for creating the vibration has to be determined. Adequate vibration is required at all times to process the powder properly. The optimal signal voltage needs to be big enough to break the dome formation with minimum the spray effect, but it must higher enough to provide reliability and consistency of powder flow. Currently, the voltage has to be adjusted on the device with the given powder by visually observing the powder stream with a microscope and measuring the RSD of the mass flow rate by a microbalance. Our experience suggests that the optimised signal voltage should have no spray effect on the powder stream and it should provide an RSD below 10%. On the other hand, correct setting of the voltage can be also verified by measuring the printed size on a substrate. Once the proper signal voltage for the powder has been found, then the table speed or moving speed is defined. Next, the printed line has to be examined. In this step, the continuity and consistency of the printed line is visually assessed. To be able to print a layer pattern, a 2D pattern is created by using CAD (Computer Aided Design) software. Then a CAM (Computer Aided Manufacturing) system generates a tool path command from the CAD model. In this step, the line width or dot size will be defined for the radius compensation in the CAM program. Finally, a substrate needs to be setup on a machine platform and the centre of the nozzle aligns to the reference point on the substrate. Then, the pattern printing is produced via the program.

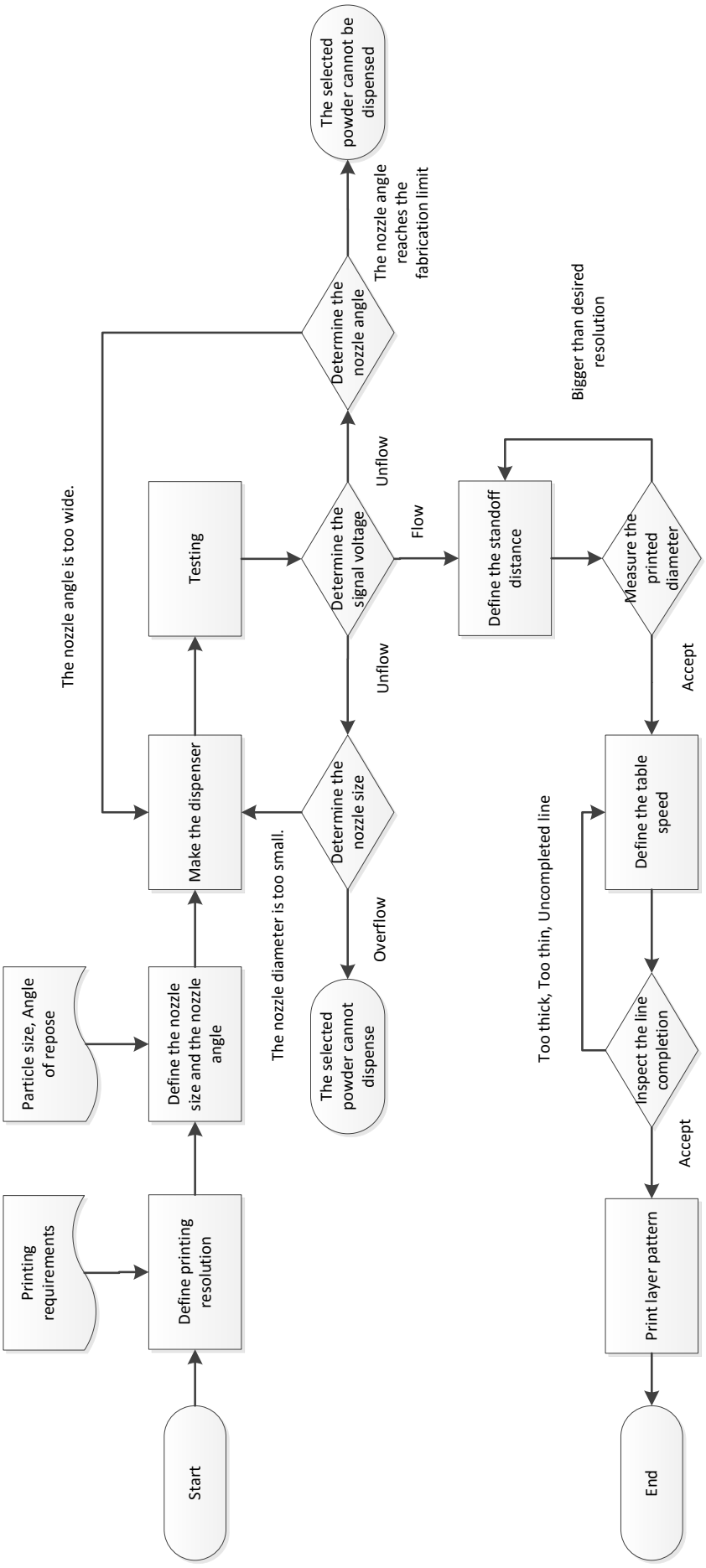

Figure 4-36 Flowchart of the operational guidelines for dry powder printing.

4.3.4 Powder printing over an existing object

The developed device is also capable of printing powders over existing objects. To demonstrate this, the dry powder printing device was setup to print the solder powder on a 3D-printed object. Firstly, the test geometries were made by SolidWorks and converted to DXF format for generating the nozzle tool path via CompuCAM. Then, the centre of the orifice was aligned to the reference point on the existing part by moving the XY table and setting the reference by Motion Planner. This procedure allowed accurate positioning for powder printing. The dry powder printing device used a nozzle diameter of 250 μm and a nozzle diameter of 65˚. Figure 4-37 shows the printing of circuit lines into the slot of an existing object. The width and depth of the slot was 0.5 and 0.5 mm respectively. Uniform and consistent results and height were achieved in all slots. The deposition could locate solder powder in the desired positions without problems.

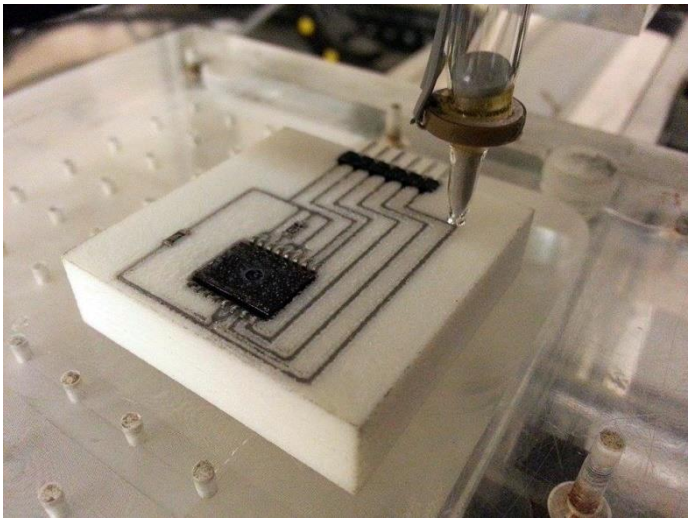

Figure 4-37 Printing of solder powder tracks on a 3D-printed object.

This example was the printing of conductive tracks for an electronics component. By using the proper parameters, the technique was good enough to print powder without undesired powder being deposited outside the slots of the nylon object. In other words, there was no bridging of printed powder between tracks, which could be a problem for conductive track applications. This demonstration proves that it is possible to deposit powder material on an existing object. When this conductive powder printing is combined with a bonding system in the future, this capability could be used to enhance the functionality of existing objects by integrating

electrical or mechanical components in the fabrication of functional electric devices and circuitry.

4.3.5 Multiple material printing

Multiple material printing is more difficult than single material printing because the conditions are more complicated during deposition. Factors such as powder spreading, stability of all printing nozzles and cross-talk problems have to be considered. Therefore, we have demonstrated the feasibility of using our dry powder printing device to produce a multiple material layer which formed a complex pattern. For the demonstration, a complex pattern with a width 60 mm and length 60 mm were fabricated using three different powders. The first powder was a copper powder with a mean particle size of 14 μm. The other two powders were 420S45 stainless steel powder and tungsten carbide powder with mean particles size of 20 and 35 μm respectively. Three separate dispensers mounted on the Z axis were used to print the three different powders which allowed the creation of a multiple material layer. A flat surface substrate was placed on the precision x-y stage that was synchronised by the motor controller. Three nozzles having diameters of 270, 230 and 300 μm, were used to print copper, stainless steel and tungsten carbide respectively. The mass flow rates at the signal voltage of 0.5 Volts were 0.74 mg/s, 2.19 mg/s and 5.88 mg/s for the copper, stainless steel and tungsten carbide respectively.

Firstly, the single nozzle printing conditions were determined. To test the individual printing nozzles, a spiral track was printed. A 500 μm-grid paper substrate was placed relative to the printing nozzle using the XYZ movement. The results of printing a single layer of the copper, stainless steel and tungsten carbide powders are presented in Figure 4-38. The track width of the copper, stainless steel and tungsten carbide were 0.25, 0.35 and 0.48 mm respectively. Uniform track width and height were achieved for all powders.

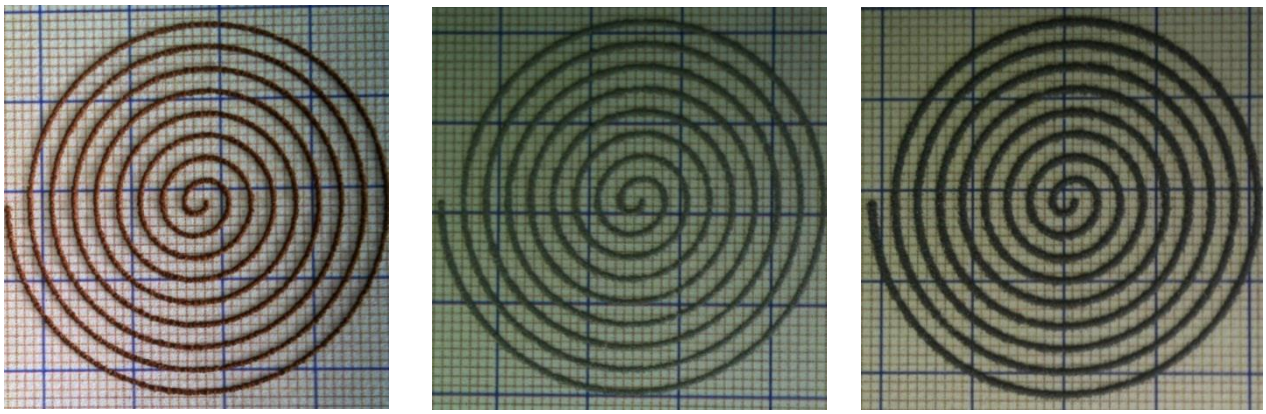

(C) Copper powder (A) Stainless steel powder (B) Tungsten carbide powder

Figure 4-38 Single material printing: (A) copper, (B) stainless steel and (C) tungsten carbide.

After establishing the optimal conditions of each nozzle, the three sets of optimal parameters from the previous process were used to produce a fine pattern. The standoff distance used was 300 μm and the signal voltage activating the piezoelectric transducer was fixed at 0.5 Volts. The moving speeds were 10 mm/s, 12 mm/s and 18 mm/s for the stainless steel, copper and tungsten carbide respectively. Then, the operation was extended to multiple material printing by using multiple nozzles. Each nozzle was filled with a different powder. In order to precisely set the printing position under the three nozzles, the drop position of each nozzle was defined with respect to the reference point of the XYZ coordination. In our setup, we selected the drop position of one nozzle to be the reference point for the X and Y axis. Then, for the Z axis, we referenced the top of a substrate to be the reference point. Finally, the drop positions of the other two nozzles were established with respect to the reference point.

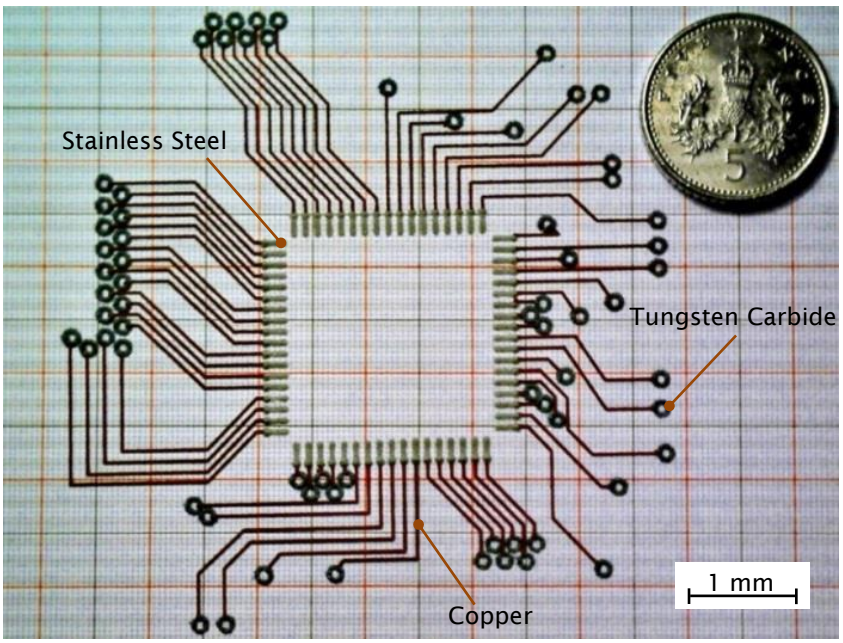

Figure 4-39 Multiple material printing pattern.

Figure 4-39 shows a circuitry pattern printed from three different powders. The demonstration shows that the multiple powder material printing system can successfully produce multiple materials in one layer. The printing nozzles were able to produce the patterns with consistency and reproducibility. Uniform and fine printed lines were produced. The pattern has the desired geometry and printing quality. In our investigation, however, it was found that a bigger nozzle diameter tended to have a cross-talk problem and also suffered from accidental dispensing from the vibration caused by high-velocity movement which can affect the controllability of powder dispensing. This problem was not investigated but it certainly needs attention. Nevertheless, this could be overcome by mounting the device in a system with smooth movement and adequate damping.

This work shows that this device can fabricate multiple material layers that traditional material delivery methods cannot create. The device can print powder in selective areas by a non-contact method and can provide accurate printing of various powders. The material preparatory steps of this device are few because the printed powder only requires sieving before printing. Different materials can be printed simply by adding a new dispenser to the system. Utilising a nozzle based method, powder materials can be delivered between and within layers to make flexible material location in a part. Using separate nozzles to print powder material in selective areas is an accurate, efficient and easy method which avoids

contamination between materials. The device has few components resulting in less maintenance and an economical cost.

This developed device differs from traditional powder delivery methods, which layer powder by a blade or a roller, in the following two main respects. First, there is no contact between the powder material and the device. Conventional recoating methods often use a roller or a blade to sweep the powder layer to deposit the material. This method can give rise to contamination by contact with a powder-transfer roller. Our nozzle-based technique can create multiple material layers without having to worry about contaminant material problem, because there is no direct contact with the powders. Therefore, powder contamination can be avoided when printing multiple materials. Second, it allows selective-area deposition due to precise control on the placement and amount of the powder material dispensed. Our method can define the location of different materials in one layer. Multiple material objects fabricated with the blade/roller method can only create different materials in a vertical direction (planar layer) by changing the material when recoating the upper layer. Furthermore, our method can eliminate material wastage by printing only the desired layer material, which is a major benefit when printing high value powder materials. With this printing system, multiple material patterns can be easily produced by powder deposition. The position and material type are defined by programing. 2D multiple material layers can be fabricated by using sequential printing with a single nozzle or using multiple nozzles with a single setup.

Although our device has many advantages, it is limited to 2D structures because the printed track is a loose powder. In addition, the device must be installed vertically because it mainly deploys gravity and piezoelectric vibration to discharge material. Moreover, the printing speed of our method is generally lower than the traditional method. However, multiple nozzle arrays could also be used to deposit materials simultaneously and so achieve a higher deposition speed. We believe that using this dry powder dispensing system integrated with current powder-based additive manufacturing systems, such as laser sintering, laser melting or binder jetting, would increase their ability to produce multiple material parts. Also, in the future, if the development of a melting/solidification system combined with our material delivery device is successful, MMAM will offer a new paradigm in this manufacturing technology. Finally, because of the above advantages including the low cost of this equipment to commercialization will be rapid.

4.4 Summary

The fabrication of multiple material objects using additive manufacturing is a challenge, especially for powder-based fusion processes. However, a material delivery system for providing multiple material layers is still needed. There are no proper platforms because of the difficulty of printing layer in a wide variety of powder materials. The developed dry powder printing method using a piezoelectric transducer attached to a glass tube nozzle was able to print several powder materials. It is able to cope with metals, ceramics and polymers. The device showed improvements in terms of accuracy, stability and consistency in powder dispensing. Compared with all previous studies, our device demonstrated the ability to print various materials (10 types) and offered the smallest feature size (up to 85 μm). The benefits of this device are many, such as a wide range of materials, high accuracy and reproducibility of the layering process, less material contamination via separated nozzles and minimal material wastage through selective area deposition. This device can be used in printing free-flowing powder to cohesive powder with a particle size from 14 to 72 μm. Furthermore, material preparation is minimal. Additionally, the device has uncomplicated components and minimum cost. Therefore, we strongly believe our device is a clear improvement on dry powder printing methods. In this thesis, several important issues in the development of our new device have been examined. Weight of powder deposited measurements, microscopy and high-speed images of powder flow in the developed device provided valuable information on the behaviour and characteristics of powder dispensing and powder printing. This thesis provides additions to fundamental knowledge related to this method and results are useful for developing a multiple material delivery method for incorporation in a powder-based AM processes.

Chapter 5:

Conclusions

This chapter gives the key conclusions and contributions from this research. The objective of this thesis was to develop a novel dry powder micro delivery device for multiple material additive manufacturing (MMAM) using an ultrasonic dispensing technique. This device can successfully provide continuity, consistency and reliability when layer printing multiple material powders. Additionally, there were a series of investigations to understand the behaviour of fine powder flow through the micro-scale orifice of this new device. The work also included demonstrating the printing results with various sizes and types of material powders. The final objective was to develop the guidelines and fundamental equations to achieve good results for powder printing patterns.

In the literature review chapter, firstly fundamental information on MMAM was presented. Then, a powder flow theory was introduced and finally, reviews of recent developments in Dry Powder Printing (DPP) were presented. Therefore, the advances made in these related fields could be understood. In the experimental chapters, details of the construction of the dispensing device were explained. Also, a description of material preparation, experimental facilities and methods used in the investigations was given. In the results and discussion chapter, all details of the investigations were presented, analyzed and discussed.

This thesis is one of the first works devoted to a multiple material delivery device using a dry powder printing technique based on vibration causing fine powder to flow through a micro orifice. In terms of the thesis objectives, we have achieved the development of a device for printing multiple materials. The current results show that dry powder deposition is a reliable dispensing process and leads to better control over uniformity and gives a highly precise powder pattern in a layer. This work suggests opportunities for greater understanding of the knowledge and developments in both powder handling and dry powder printing technologies.

The major goal of this thesis was to establish a multiple material delivery device for printing fine powder materials. The main accomplishments of this thesis are as follows:

1. A new material delivery device of fine powder printing from a micro orifice has been developed and analysed. Also, the performance of the device has been demonstrated.

2. In-depth experimental investigations of the effect of design and processing parameters on powder flow and powder handling have been performed.

3. A generic approach for the determination of suitable parameters that ensure reliability and consistency in the printing process has been illustrated. Approximate equations and guidelines for operating the device have been established as well.

The main conclusions in each of the above areas of achievement are summarized in the following sections.

5.1 Multiple material delivery device

1. A novel dry powder micro delivery device, which is made of a borosilicate glass pipette directly attached to a piezoelectric transducer, was developed and built. This current device was improved by reducing its size to be more compact and easier to construct and maintain by decreasing the numbers of components of the device. Additionally, the device has a water-free design that removes the possibility of leakage and prevents the powder inside the device suffering from humidity problems.

2. Experimental printing tests were carried out to validate the novel device for functionality. The programmable-moving platform integrated in the device has allowed the reliability and repeatability of producing multiple material layers with fine powders to be demonstrated. Experimental powders with a particle size above 14 μm were able to be dry powder printed via the device. This result of our study can open opportunities to customize the material of the printing layers for AM technology.

3. Our powder delivery device can offer a uniform and stable powder delivery function under the control of an automatically moving platform (printing resolution less than 100 μm). Additionally, to print multiple material layers, this device adopts a modularised design. If there are more than one type of

powder materials, more powder nozzles can be added correspondingly. Furthermore, our study shows that dry powder printing, driven by ultrasonic vibration, can be exploited for fine powder printing of many types of powder materials. The use of a wider range of materials and creating multiple layers thus become possible.

4. This printing device was developed to handle a wide range of materials with high repeatability (less than 7% RSD) including dispensing an accurately controlled powder quantity (up to 0.14 mg/s). A powder printing platform was built by integrating the device on a computer numerical controlled table to demonstrate the feasibility of producing single multiple material layers, which would lead to showing the capability of the multiple material delivery method for providing multiple material objects in the near future.

5.2 Powder flow through a micro orifice

1. The stable dome structure of the experimental powders above the orifice of the device was observed and it was found that this structure prevents free flow under gravity. The dome structure in this study can be formed within the ratio of nozzle diameter to the mean particle size diameter of 3 to 67 depending on the flowability of the powder. The study indicated that the ratio for cohesive powders is higher than the ratio for free-flowing powders.

2. The collapse of the dome structure occurs by repositioning the particles in the nozzle. For our device, it was found that the collapse requires a different signal voltage level for each type of experimental powders, differing in material flowability, to generate the required vibration energy from the piezoelectric transducer. Image data taken by a high speed camera has shown that the particles around the stable dome structure move upwards before collapsing.

3. For the hopper-like design shape of the micrometer-scale orifice in our device, the design parameters of the device, such as the nozzle diameter and the nozzle angle were found to affect the powder flow. The micro nozzle diameter is one of the crucial factors for the mass flow rate just as it is for large-scale nozzle diameters in general industries. The results have shown an agreement with powder flow in large-scale hoppers and similarly

present mass flow rates following Beverloo's equation. For the nozzle angle, it was found that wide nozzle angles allow the delay time of start/stop dispensing to be shortened, so this angle can improve the controllability of powder flow in a hopper-like shape.

4. To obtain a steady mass flow rate of the powder flow, the bulk density of the powder has to be equalized until a constant packing density is achieved. Additionally, variation of weight fluctuations can occur during the dispensing process. The positions of a stable dome structure were found to influence the mass flow rate and the consistency of powder flow.

5.3 Dry powder printing using piezoelectric dispensing

1. Our dry powder printing (DPP) device uses the stable dome structure of the particles above an orifice to act as the mechanism to stop powder flow. The device employs an ultrasonic vibration source to start powder flow through a micro orifice. It is possible to produce multiple material layers from the fine powder materials with various particle sizes between 14 and 72 μm. Furthermore, this device is relatively compact and has few components in its construction. This technique, also, can be employed at room temperature with simple material preparation.

2. The device is a useful material delivery method for layering complex profiles and produces high resolution features in a wide range of powder materials. The device is also suitable for precise printing of micro geometries. The micro features have very small diameters (up to 85 μm) and can be produced with high accuracy and reliability. A powder with good flowability allows a high reproducibility in dry powder printing, which gives the printed results produced more consistency and reliability.

3. The performance of the device mainly depends on the dispensing parameters (e.g. nozzle diameter, nozzle angle, and piezoelectric position), material parameters (e.g. type, particle size, flowability) and process parameters (e.g. moving speed, signal voltage and standoff distance). The fundamental relationships established for dry powder printing are able to serve as the operational guidelines for the device.

4. The level of the signal voltage affects the mass flow rate, which is directly proportional to the material deposition rate. In this thesis, the mass flow rate was able to be increased by increasing the voltage between 0.5 Volts and 3 Volts. In addition, a low input voltage can minimise the spray angle of the powder stream profile and thus the track width of a printed line. Furthermore, the property of powder flowability directly influences this spray effect. For powders of different flowability, a cohesive powder has less spray effect than a free-flowing powder.

5. An increase in standoff distance results in enlarging the spray angle and so affects the track width of the printed lines. Therefore, a small standoff distance should be considered as a printing parameter. The resolution of the printing track will be improved when implementing a smaller standoff distance. However, when the standoff distance is less than the minimum distance, the nozzle tip will smear the printed track and leads to an imperfect printed line. When these parameters are properly defined, the printed results will exhibit high resolution features and complete printed tracks.

5.4 Limitations of study

There were some limitations that our study has faced. We can classify there into three major issues; (1) powder flow property testing equipment, (2) nozzle fabrication method and (3) powder bonding facility. These limited the ability to fulfill all our goals. The details are as follows.

Firstly, our powder flow property testing equipment is limited since our research group was established less than 4 years ago. Therefore, our group still requires many up to date facilities to utilize in the research experiments. The most important equipment is a powder flow tester, which is generally used in testing the flowability of powder material. In our study, we compared the flowability of experimental powders by using the angle of repose and also the mass flow rate from the same orifice. With a powder flowmeter, we would be able to analyse many important properties such as flow function, cohesive strength, wall friction, internal friction, adhesion etc. All of these parameters lead to in-depth analysis and allows more relationships between the intrinsic powder properties and the

behaviour of the dispensing process to be established. Some recommended solutions are to collaborate with other universities that have powder testing facilities or to invest in equipment such as a powder flow tester and/or a powder rheometer.

Secondly, the limitation of the glass nozzle fabricating method; currently experimental nozzles are handmade. To create a specific nozzle angle, we had to draw many pipette tubes to give different nozzle angles and then pick the nozzle that had the angle closest to the desired angle. After that, we manually ground the closed-end orifice to open the orifice to the required diameter and regularly examined it by an optical microscope to check the actual size of the nozzle diameter. This process was very time consuming and limited the levels of variable parameters examined. If we had an automatic machine or a method to produce our test nozzles, which could reliably control the shape and size of the glass nozzle, future experiments could be conducted more quickly.

Finally, multiple layer printing cannot be explored due to lack of a bonding facility. The bonding system needs a powder fusion technique that is not commercially available. In our case, companies cannot provide a machine even if we could afford the construction budget. Moreover, it is a relatively expensive investment. This issue meant that this investigation has examined only single layer printing. Therefore, we were not able to study multiple layer printing, which would be needed during the MMAM process. An adhesive bonding facility such as in adhesive ink-jet printing, maybe could be integrated in this system for multiple layer studies. However, this bonding technique is not suitable for creating functional 3D objects but its use for exploring the multiple layers is acceptable.

In conclusion, we have identified and explained the importance of the limitations. Suggestions to overcome these limitations in future studies were also given. If we can overcome these limitations, it will allow greater depth and lead to a rapid expansion in this field in the future.

5.5 Summary

This thesis has described a new device for printing a wide variety of powder materials with particle sizes of between 14-72 μm. We believe that the results and the conclusions obtained from this study will set the foundations for further

research in other powder systems. In particular, the system handles fine dry powder through a micro orifice activated by ultrasonic vibration. Although the dry powder printing device in this thesis was originally conceived as a material delivery device for a layering process, the features also have the potential to provide the foundations of a generic powder handling process. Our device can deliver powder in very precise and manner in small quantities at almost any location within a designated working space. Furthermore, two-dimensional layering can position amounts of different powder materials to desired positions on a substrate. Moreover, it has the possibility to be used to form fully three-dimensional objects by integrating this delivery system with a material bonding system.

Chapter 6:

Future work

Fine powder handling is receiving attention in academia and is a fundamentally important issue in many industrial applications. Dry powder printing is also of interest and is being explored by several researchers. This technique has its challenges and more work needs to be carried out to understand it better. However, the findings of this thesis inspire further work on using this dry powder micro delivery device. A number of issues must be solved to allow the development of a multiple material delivery system for incorporation in MMAM technology. These issues provide work for future research in this area that needs to be pursued to make the system feasible. At least four research areas can be identified. These areas include:

- Developing a MMAM machine and a nozzle fabrication technique,
- Improving the efficiency of the current device,
- Investigating the other parameters of the device and
- Extending possible applications.

The following sections discuss each of these areas in more detail.

6.1 Developing a MMAM machine and a nozzle fabrication technique

6.1.1 Developing the MMAM machine

Multiple Material Additive Manufacturing (MMAM) is a relatively new research area where many issues remain to be investigated. The most important direction for future research is designing the complete system and creating a prototype MMAM machine that integrates dry powder printing in the machine. To develop the complete machine the following conceptual design is proposed.

The flowchart in Figure 6-1 shows the conceptual design of the MMAM machine. The multiple material objects are created a layer at a time by combining a recoating system and a dry powder printing device. A layer created from one type of powder is spread out in a powder bed. Then a vacuum head automatically removes the material from selected areas. After that, a second powder print head deposits another material in these selected areas. After finishing powder deposition in a one layer, the layer is bonded by a laser fusion technique. This laser fusion device comprises a CO_2 laser for polymeric materials and a fibre laser for metal and ceramic materials. The powder bed is then moved down and another layer of powder is recoated and deposited in position. The process repeats layer by layer until the object is completed.

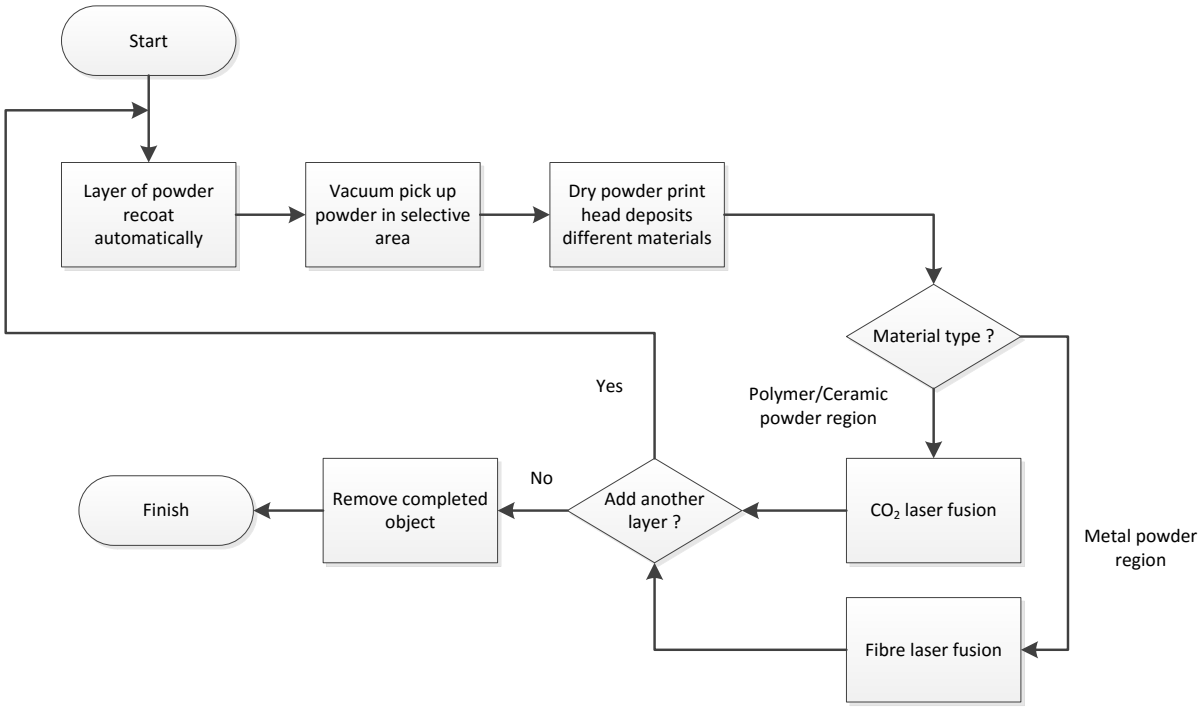

Figure 6-1 Flow process chart of the MMAM fabrication process.

To perform laser fusion bonding of multiple material objects, an idea for developing a full functional system to automatically fabricate the multiple materials parts is presented in Figure 6-2. There are six key components in this system: 1) a CO_2 laser with a galvanometric scanning system; 2) a fibre laser with focusing optics; 3) a dry powder printing system; 4) a powder vacuum system; 5) a sintering chamber with an inert gas atmosphere; 6) an XY gantry; and a powder bed delivery and levelling system.

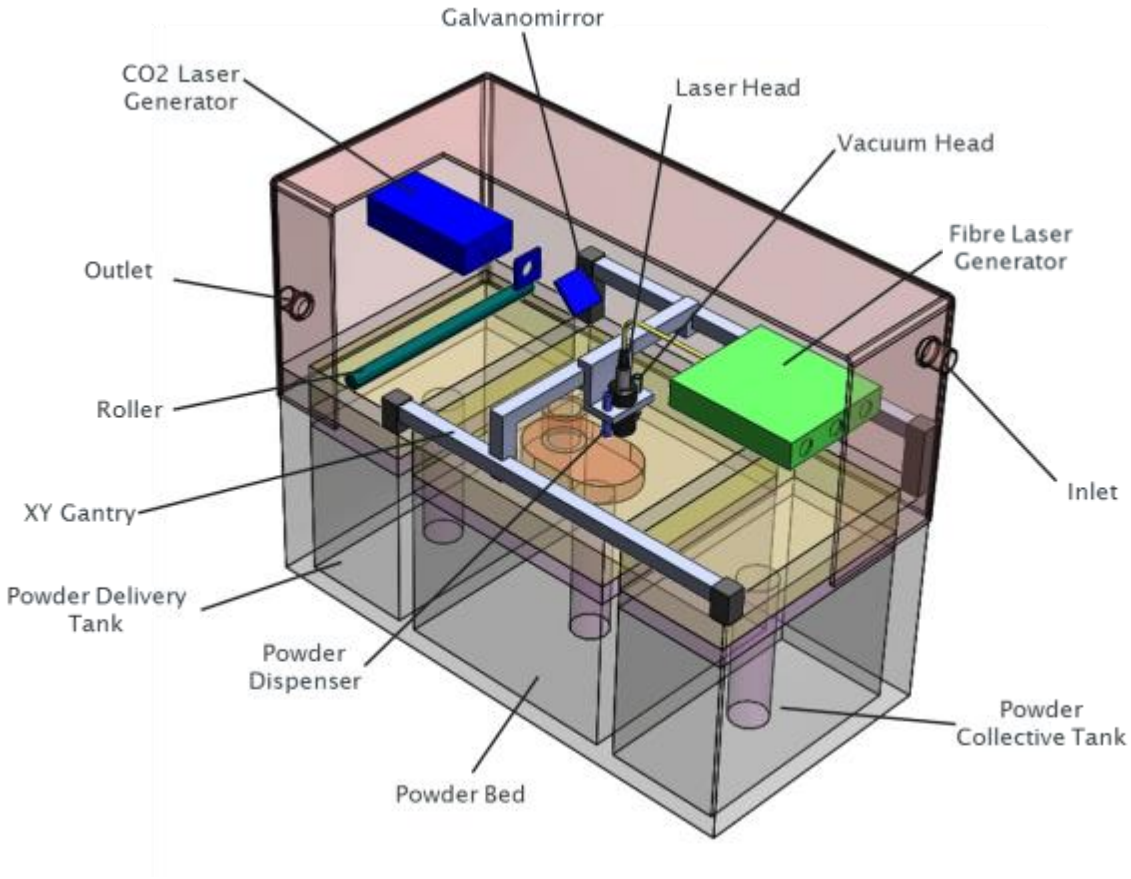

Figure 6-2 MMAM machine design.

Key components:

1) CO_2 laser with a galvanometric scanning system

The CO_2 laser delivers a coherent heating beam which is scanned over the powder bed in the X-Y directions by a galvanometric mirror and fuses adjacent powder particles to form a solid object. A polymeric material, such as nylon, is suitable for fusing with this laser type.

2) Fibre Laser with focusing optics

The fibre laser is designed to process metallic materials, because it has a shorter wavelength than a CO_2 laser and has a lower reflection loss than a CO_2 laser. The movement of a XY gantry allows the fibre laser head to fuse metal powders in selective regions.

3) Powder vacuum system

The powder vacuum system uses a vacuum head as a material removal system which eliminates material selectively to generate a cavity into which a DPP device dispenses a different material in the layer. This vacuum head is installed in the tool holder on a XY gantry.

4) Dry powder printing system

The dry powder printing (DDP) system is used to print powders in selected areas. The powder is dispensed by the application of vibration energy, controlled by a computer, from a glass capillary. The DPP head is attached onto a holder located on a XY Gantry to create 2D patterns in an X-Y direction.

5) Sintering chamber with an inert gas atmosphere

Eliminating oxidation during the sintering process is very important for proper process control. An enclosed chamber is an ideal solution for laser fusion in a controlled atmosphere when working with oxygen sensitive materials. Inert gases such as Nitrogen, Helium and Argon could be easily maintained in this system. Additionally, this chamber is designed so that the working temperature inside can be regulated.

6) XY gantry

To provide repeatability and high throughput, the X and Y axes are manipulated on a XY gantry that uses servo motors to drive ball screws to provide linear movement. The gantry is designed to move the DPP head, the fibre laser head and the vacuum head. The platform is designed to provide access to the working area from all four sides of the system.

7) Powder bed delivery and levelling system

This system combines a powder-spreading roller, a powder bed, powder delivery tank and an excessive powder tank mounted on individual pistons. The powder is spread from the powder delivery tank to the powder bed by movement of the counter-rotating roller over the built surface. The piston in the powder delivery system moves up to prepare the feed material, while a piston in the powder bed moves down to accommodate the new layer of powder. The excessive powder

from the powder bed is swept by the roller into a collection tank installed on the other side of the platform.

6.1.2 Developing the fabrication technique for making a glass nozzle

At this stage, our experimental nozzles are fabricated from glass and made by hand. Consequently, achieving high accuracy and high repeatability for the nozzle diameter or nozzle angle was very difficult. Therefore, an automated grinding system should be introduced for fabricating the nozzle diameter. A method to produce the desired angle for the nozzle is also required.

6.2 Improving efficiency

6.2.1 Using a precision metal nozzle

The approach involving the discharge of fine powder through a hand-made glass nozzle has proven to be versatile but is not ideal. Moreover, the transparent property of the glass nozzle allows powder flow to be easily observed. However, nozzles made from metals have not been examined an in-depth study. In a feasibility study, we have used a commercial metal nozzle attached to a piezoelectric ring and dispensed 14-μm copper powder (Figure 6-3). The results showed that a metal nozzle can be used to handle the powder in the same way as a glass nozzle. In general, the use of metal nozzles should be investigated since they are expected to be a good solution for reducing set-up time and improving nozzle consistency. Furthermore, the roughness of the nozzle wall surface affects powder flow resistance as the flow of powder particles inside a dispenser through an orifice is controlled by how the powder particles interact with the wall surface. Thus this needs to be studied.

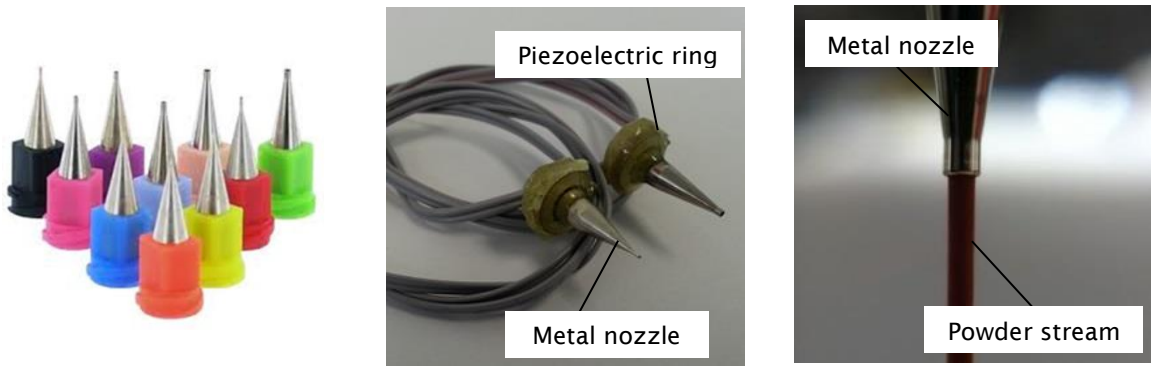

(A) (B) (C)

Figure 6-3 Metal nozzle: (A) Precision metal nozzles, (B) Metal nozzle dispenser and (C) Copper powder dispensing through a metal nozzle.

6.2.2 Improving the throughput of dry powder printing

The current results show that dry powder deposition is a reliable dispensing process and leads to uniform and precise powder patterns in a layer. However, the mass flow rate from nozzle printing is low and thus the processing speed is slow. To increase processing speed an array-nozzle system should be considered as a way to increase the speed of material dispensing. This can also offer the opportunity of depositing different materials at the same time. Furthermore, increasing the diameter of nozzle, which is one of the solutions to this problem, should be investigated.

To develop an array-nozzle a possible design of the nozzle component is offered in Figure 6-4. The nozzle array consists of a powder compartment, glass nozzles, piezoelectric rings and rubber rings. The rubber rings act as a vibration absorber to avoid cross talk between nozzles. Our experiments showed that an array-nozzle prototype could dispense without unintentional discharge from nozzles. However, the design of a future array system should seriously consider cross talk caused by nozzles switching on and off resulting in unintentional discharge from nozzles that are switched off due to excessive vibration from nozzles that are switched on. This issue is highly relevant and more study is necessary.

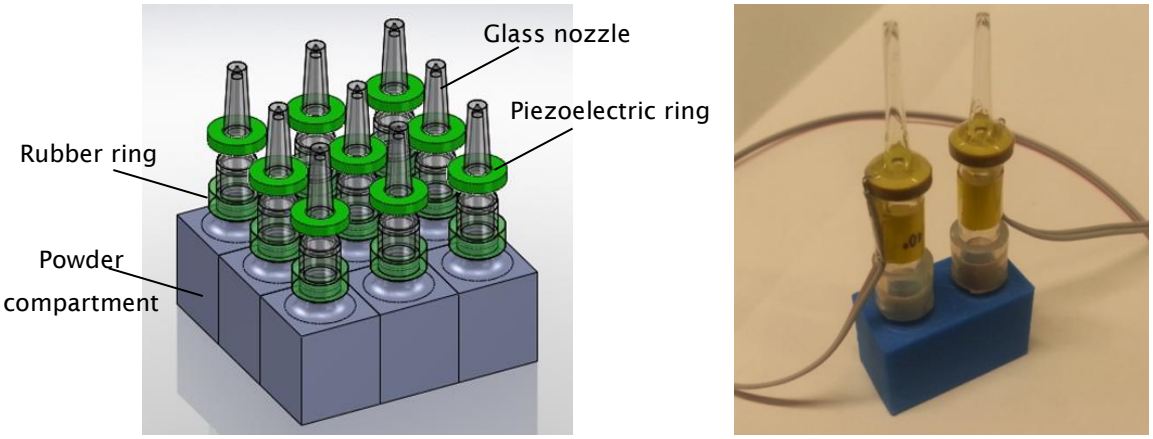

(A) 3x3 Array nozzle design (B) 1x2 Array nozzle prototype

Figure 6-4 Array nozzle; (A) 3x3 array nozzle design and (B) 1x2 array nozzle prototype.

There are advantages and disadvantages to printing different sizes of printed track. Printing a smaller track width means it will take longer to build entire on layer, but allows for better precision and higher resolution. Larger nozzle diameters lead to shorter production times, but lower resolution. To increase the processing speed and enlarge the printable area, we have developed a new design of nozzle. It has a 10-mm slot nozzle head over which a nylon sieve mesh with 120-μm opening was positioned, the head being inserted in a flat-bottom glass tube (12-mm outer diameter, 9.5-mm inner diameter) attached to a piezoelectric ring (SPZT-4 A3544C-W, 35mm x 15mm x 5mm, MPI Co., Switzerland). In our feasibility study, this technique generated a track width of up to 12-mm with 14-μm copper powder, as shown in Figure 6-5. Further work could be carried out on nozzle head design.

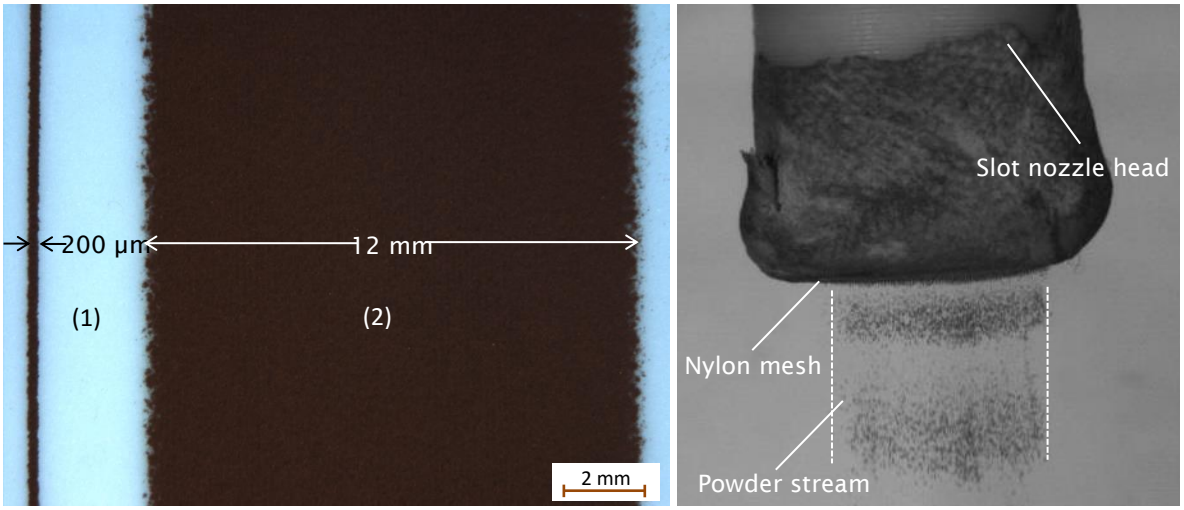

Figure 6-5 Copper powder tracks generated by (1) an original nozzle and (2) a slot nozzle and (B) the slot nozzle components.

6.2.3 Developing a closed-loop control system

In this thesis, an open-loop system, which cannot correct for errors due to changes in printing parameters, was used. To precisely control powder dispensing and correct for variations of mass flow rate is important. Therefore, closed-loop operation should be integrated into the system. To achieve this requirement, we propose three possible solutions for future work. The first solution is that weight sensors should be installed on the platform on the top of the moveable table so that in-process checks can be carried out to confirm that the printing process is being correctly performed. If the mass flow rate is not consistent, the closed-loop control will intelligently adjust the input parameters, such as the amplitude of the signal voltage, to instantaneously compensate for the error. The second solution is to install a vision system to measure the track width and height of the printed powder on the substrate and thus provide on-line feedback to adjust the mass flow rate. The last solution is to monitor the position of the location of the stable dome inside the nozzle orifice by using a vision system. As mass variations at the start and finish of printing come from variation of the dome location, as described in Chapter 4, a closed-loop system monitoring the dome position can be used to predict the mass flow rate and adjust the speed of the moving table to compensate for variation in mass volume of the printing powder.

6.3 Investigating other parameters

6.3.1 Investigating effects of high working temperature

All studies in this thesis were carried out at room temperature; the device running below 30 ˚C. The effects of dispensing in a higher temperature environment on the mass flow rate and the quality of printed lines have not been studied. At higher temperature, the flowability of powder materials inside the dispenser can be affected. Studies should be carried out at working temperatures, to validate whether the device can provide reliability and consistency of mass flow rate at these temperatures. To study this, the device can be installed in a heating chamber to determine the mass flow rate during dispensing at high temperature. However, the advantages and the disadvantages of the process should receive more investigation. Additionally, this investigation can explore the durability of the components of the device if a higher operating temperature is used.

6.3.2 Investigating the optimisation of the design and printing parameters

This thesis has highlighted the effect of the important design and printing parameters. The experimental studies have partially revealed how the input parameters can affect the mass flow rate of the device. Guidelines for the printing process have been established. However optimisation of the printing process was not studied. An optimization study would allow us to better select parameters based on the intended outcome. Further studies are clearly required in this area. Moreover, the nozzle diameter, the nozzle angle and the piezoelectric position were not explored in detail. Thus an extensive parametric study is required. Taguchi and/or design of experimental methods could be used to screen the key factors. Then, a response optimization technique could be used to find the combination of input parameters that provides the optimal response.

6.3.3 Investigating very cohesive powders

The key challenge for additive manufacturing is to create high definition features with high surface quality. One important feature is the thickness of material layers.

To improve the surface quality, the layer thickness should be as thin as possible. Therefore, the material powder should have the smallest particle size possible. However, dry powder printing depends upon the flowability of the feed stock materials. The smaller the particle size used, the lower the flowability. Low flowability is also the main problem when dispensing sticky or cohesive materials. In this thesis, the smallest particle size used in the experiments was 14 μm. Handling ultrafine powders, where the particle size is less than 10 μm, is very challenging. Moreover, further investigation of very cohesive powders should be undertaken to find the capability boundary of the device. To study this environmental control should be considered. The preparation of materials used before dispensing has to be strictly controlled. Humidity and electrostatic effects should be investigated and their effects on inter-particles force and the adhesive force between particle and wall, which determine the response of the powder to ultrasonic vibration, should be carefully explored. In addition, the present study did not address in detail the effect of particle shape, particle size and particle size distribution on flow. As these particle parameters can influence flow they should be the subject of further study.

6.3.4 Investigating three-dimensional dome structure modelling.

The stable dome structure is of key importance to the device. The doming mechanism needs to be further studied. In this thesis, an optical high speed camera has been used to observe the doming behaviour during dispensing. However, only two dimensional images taken from the front of the dispensing device were obtained. These results showed the dome structure of the particles in contact with the glass nozzle and do not give the 3D profile of the dome. Microcomputed tomography (MicroCT) could be used to evaluate the three-dimensional stable dome structure of the powder particles above a nozzle orifice. This equipment will reveal the exact shape of the dome structure based on x-ray absorption differences. The results could be incorporated into the dispensing model to better account for the effect of the control parameters such as a nozzle angle, nozzle diameter and particle parameters.

6.3.5 Investigating life-expectancy estimation

Life expectancy is the length of time a device would reliably be expected to work properly. The long term performance of the printing device can be affected by a number of factors: damage of the orifice from wear by the powders, deterioration of the adhesive attaching the piezoelectric device to the capillary, cracking of the piezoelectric, humidity, or some combinations of these factors. To determine the life expectancy of the device tests should be performed using the actual conditions experienced by printing in real-world situations. Using experimental data collected in this manner the life-expectancy estimation can be investigated.

6.3.6 Investigating multi-layer printing and printing strategy

In the present study, only single-layer printing was demonstrated. To achieve a fully functional MMAM system, multi-layer printing should be studied in the future. This work will provide more information on the multiple material delivery process by using the technique described in this thesis for creating powder layers. Furthermore, the overall printing strategy is critical for both printing quality and reduction of printing time. Therefore, different strategies of printing movement should be investigated and compared. To minimise the printing time and maximise printing quality, an optimization study involving all the process parameters and the printing patterns should be undertaken.

6.3.7 Investigating the effects of vibration energy

The vibration transmitting property of a nozzle material is one of the most important factors in the dry powder printing device. Because the measuring equipment limitations this thesis did not address this factor. To do this a direct-contact vibration sensor such as an accelerometer, which can measure the acceleration of a vibrating object, could be used. Alternatively, a non-contact vibration sensor such as a 3D laser vibrometer, which can measure three linear velocity components at a point on a vibrating structure, could be employed. After varying the input parameters (e.g. signal voltage, frequency, etc.) of the device, the response data could be collected. Then, the relationship of the vibration energy to the input parameters can be explored.

6.4 Extending possible applications

6.4.1 Smart material applications

The most straightforward application is to use the printing device to fabricate a new multiple material object. When applying such a printing technique, the objects could have new advantageous characteristics. For example, magnetorheological elastomers (MREs) or magnetosensitive elastomers are smart materials whose mechanical properties can be controlled by an external magnetic field. Typically, MREs are prepared by a curing process for polymers mixed with iron powders. However, the current process for mixing the powder is manual. Dry powder printing can be integrated into the fabrication process. Using this technique, the patterning of the iron powder within the matrix material can easily be intricate and flexible. Another application of smart materials is a Frequency Selective Surface (FSS) structure which contains conductive material on the surface, which is designed to absorb or reflect electromagnetic fields based on frequency. To show the conceptual idea of using dry powder printing for this application an example of a 3D structure that has metallic copper powder within the surface dispensed by 3D printing is presented in Figure 6-6.

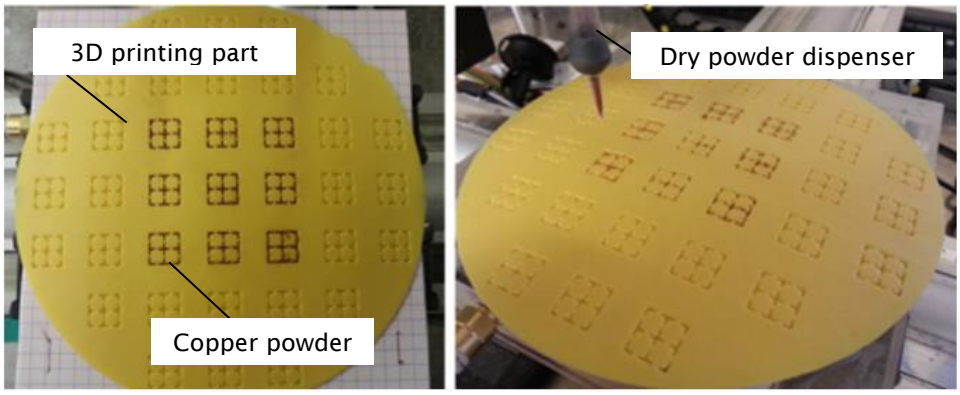

Figure 6-6 Copper dispensed into the cavities on a 3D structure.

6.4.2 Material mixing system for Functionally Graded Material (FGM)

In order to prepare the powder layers for a FGM using the device described in this thesis, the material delivery system needs a device to accurately mix powders so as to provide the correct powder concentration gradient. In this thesis, the dry powder printing device has demonstrated its ability to precisely control and deliver an accurate dose mass of the experimental powders. The gradient can be varied by controlling the duration time of the dispensing period. One method to achieve this is shown in Figure 6-7 where additional dispensers have been incorporated into a material mixing system. This simple idea may use a primary dispenser combined with secondary dispensers. This system will determine the material composition of the layer by controlling the secondary dispenser. This system may require two or more powder dispensing devices for simultaneously depositing different powders so as to change the composition and/or concentration gradient. To achieve this system as described, the control of powder deposition must be improved by adding feedback systems and this must be addressed.

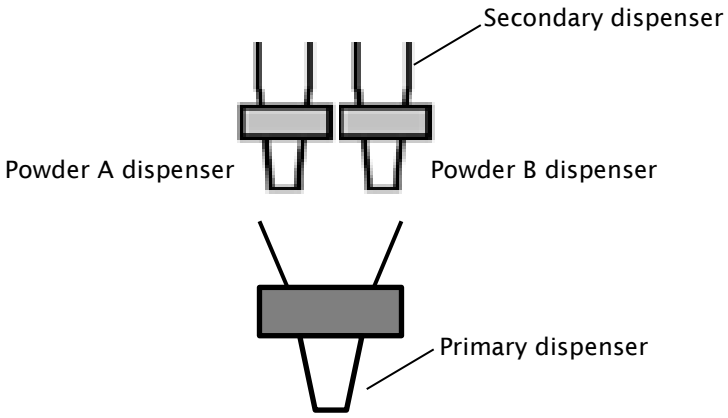

Figure 6-7 Dry powder mixing system for FGM.

6.4.3 Combining liquid printing and dry powder printing in a single device

Presently, no printing device has the handling capability of both liquid and solid materials in a single device. However, the device described in this thesis can dispense liquids such as water and alcohol. In Figure 6-8, an example of water dispensing from the original un-modified dry powder printing dispenser is shown. This finding should be further investigated to provide an explanation for this phenomenon. The knowledge gained from the study can be used to suggest new applications in the future.

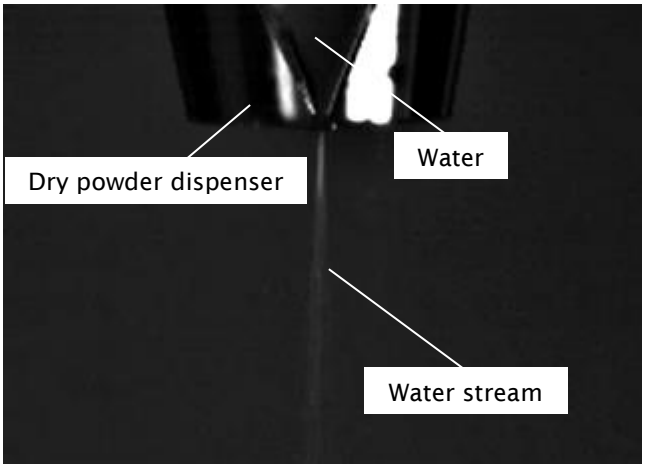

Figure 6-8 Liquid dispensing via a dry powder dispenser device.

Appendices

Appendix A : Drawings

Appendix B : Piezoelectric details.

Appendix C : Publications.

Appendix A : Drawings

ITEM NO.	PART NUMBER	DESCRIPTION	QTY.
1	Piezoelectric Diameter 20	SPZT8-200-100-50	1
2	Glass Pasteur Pipette	FB50251Fisher Brand	1
3	Water tank	Borosilicate glass tube 17 mm	1
4	Rubber stopper	Rubber stopper/Bung No.15	1

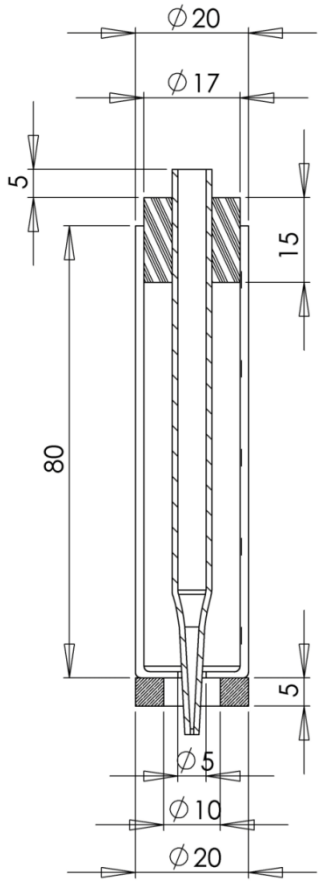

SECTION A-A

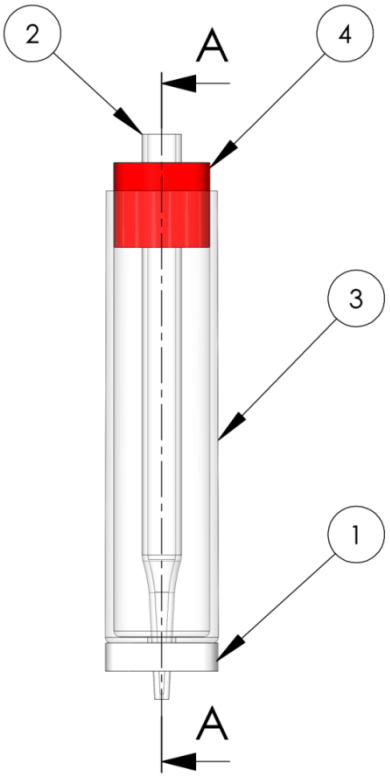

View: First angle projection	Organisation: University of Southampton	
Unit: millimetre	Part Name: Original piezoelectric dispenser	A4
SCALE:1:1	SHEET 1 OF 1	

ITEM NO.	PART NUMBER	DESCRIPTION	QTY.
1	Piezoelectric Diameter 10	SPZT8-100-50-20	1
2	Glass Pasteur Pipette	FB50251Fisher Brand	1

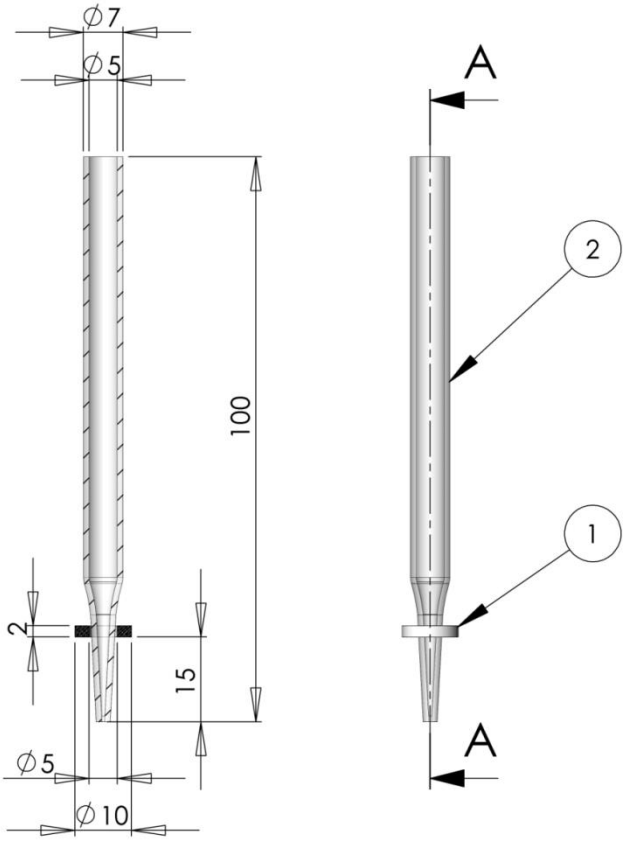

SECTION A-A

View: First angle projection	Organisation: University of Southampton	
Unit: millimetre	Part Name: New piezoelectric dispenser	A4
SCALE:1:1	SHEET 1 OF 1	

Appendix B : Piezoelectric details

The specification and performance characteristics of the piezoelectric elements represented in Chapter 3 are shown below. These piezoelectric rings were supplied by M.P. Interconsulting company from Switzerland.

Piezoelectric Elements: Material SPZT-8

Feature	Original design	New design
Code	SPZT8-200-100-50	SPZT8-100-50-20
Shape (mm)	Φ20*Φ10*5	Φ10*Φ5*2
C±12%(PF)	416	260
tgδ (%)	<0.3	<0.3
FS±3% (kHz)	76	153
ΔF (kHz)	5	11
R_m(Ω)	18	10
Coupling factor Kt/Kr%	≥46	≥46
Curie point T_C°	320	320
Q_m	≥ 800	≥ 800

Appendix C : Publications

Journal paper:

1. Vaezi, M., Chianrabutra, S., Mellor, B., & Yang, S. (2013). Multiple material additive manufacturing–Part 1: a review: This review paper covers a decade of research on multiple material additive manufacturing technologies which can produce complex geometry parts with different materials. Virtual and Physical Prototyping, 8(1), 19-50.

Conference paper:

1. Chianrabutra, S., Mellor, B., & Yang, S. (2014), "A dry powder material delivery device for multiple material additive manufacturing", in The 25th International Solid Freeform Fabrication Symposium, at University of Texas at Austin, USA, 36-48.

Poster:

1. Chianrabutra, S., Mellor, B., & Yang, S. (2012), "Multiple material patterns fabricated by 3D printing using a dry powder direct-write technology", in The 19th Joint Annual Conference of CSCST-SCI (2012) at University of Reading, UK.
2. Chianrabutra, S., Mellor, B., & Yang, S. (2014), "Material delivery device for multiple material additive manufacturing using a dry powder printing technology", in The 2014 Materials Research Exchange at Ricoh Arena, Coventry, UK.

Papers in preparation:

1. Multiple material additive manufacturing–Part 2: dry powder printing, Virtual and Physical Prototyping.
2. The study of flow and discharge behavior of dry powder printing using piezoelectric dispensing, Powder Technology.

Virtual and Physical Prototyping, 2013
Vol. 8, No. 1, 19–50, http://dx.doi.org/10.1080/17452759.2013.778175

Taylor & Francis
Taylor & Francis Group

Multiple material additive manufacturing – Part 1: a review

This review paper covers a decade of research on multiple material additive manufacturing technologies which can produce complex geometry parts with different materials

Mohammad Vaezi, Srisit Chianrabutra, Brian Mellor and Shoufeng Yang*

Faculty of Engineering and the Environment, University of Southampton, Southampton, SO17 1BJ, UK

(*Received 11 February 2013; final version received 18 February 2013*)

Interest in multifunctional structures made automatically from multiple materials poses a challenge for today's additive manufacturing (AM) technologies; however the ability to process multiple materials is a fundamental advantage to some AM technologies. The capability to fabricate multiple material parts can improve AM technologies by either optimising the mechanical properties of the parts or providing additional functions to the final parts. The objective of this paper is to give an overview on the current state of the art of multiple material AM technologies and their practical applications. In this paper, multiple material AM processes have been classified and the principles of the key processes have been reviewed comprehensively. The advantages and disadvantages of each process, recent progress, challenging technological obstacles, the possible strategies to overcome these barriers, and future trends are also discussed.

Keywords: additive manufacturing; multiple material objects; multiple material additive manufacturing; 3D printing; rapid prototyping

Nomenclature

2PP-Two Photon Polymerisation
3DP-Three Dimensional Printing
BioLP-Biological Laser Printing
DLP-Digital Light Processing
DoD-Drop on Demand
DPP-Dry Powder Printing
DMD[1]- Directed Metal Deposition
DMD[2]- Digital Micromirror Device
DW-Direct Writing
FDM-Fused Deposition Modelling
FDMM-Fused Deposition of Multi-Materials
EBM-Electron Beam Melting
LCVD-Laser Chemical Vapour Deposition
LDM-Low-temperature Deposition Manufacturing
LENS-Laser Engineering Net Shape
LC-Laser Cladding
LOM-Laminated Object Material
M-LDM-Multi-nozzle Low-temperature Deposition
MDM-Multi-nozzle Deposition Manufacturing
MIP-SL-Mask Image Projection-based Stereolithography
MJS-Multiphase Jet Solidification
MMAM-Multiple Material Additive Manufacturing
PAM-Pressure-assisted Microsyringe
PED-Precision Extrusion Deposition
PJT-PolyJet Technology
RP-Rapid Prototyping
RPRD-Rapid Prototyping Robot Dispensing

*Corresponding author. Email: s.yang@soton.ac.uk

SDM-Shape Deposition Modelling
SMS-Selective Mask Sintering
SL-Stereolithography
SLM-Selective Laser Melting
SLS-Selective Laser Sintering
STLG-Stereo Thermal Lithography
UC-Ultrasonic Consolidation

1. Introduction

Due to the daily increase in complexity of industrial manufacturing, international competition and market globalisation, there is demand for higher flexibility and greater efficiency and traditional manufacturing processes may not be able to meet all the requirement of today's products. Additive Manufacturing (AM) processes that are based on layer-by-layer manufacturing are identified as an effective approach to overcome these challenges. However, most current commercially available AM systems have been designed to produce parts from a single material (Wohlers 2011). Current AM technologies still need to be improved in terms of part quality and part performance in comparison to traditional manufacturing. Part quality is being dealt with by greater machine control and by applying cutting edge high precision technologies while part performance can be boosted using multiple material systems (Zhou *et al.* 2011). The emerging Multiple Material Additive Manufacturing (MMAM) technology can enhance the performance of AM parts by adding more complexity and functionality. Using MMAM technologies it is possible to improve part performance by varying material compositions or type within the layers; this is not achievable by conventional manufacturing processes. In fact, MMAM represents a whole new paradigm and range of opportunities for design, functionality, and cost effective high value products.

There are a lot of benefits from producing parts with multiple materials and that is why MMAM technology is a fast growing area and several MMAM systems have been investigated and developed to meet today's product demands. As mentioned earlier, the reasons for applying multiple material strategies might be much more than just achieving the purpose of combining the additional materials and other purposes, such as mechanical properties improvement, providing additional functionality and design freedom, traceability and security in the resulting part, are being explored (Gibson *et al.* 2010).

There are many applications that can potentially benefit from the development of MMAM technologies. Additional materials may provide the desired properties in strategic locations around the parts. For examples, thermal conductivity in conformal cooling channels, mechanical properties such as high hardness, high temperature resistance properties in turbines engines and thermal insulation coatings, optical properties in laser telecommunication systems, dielectric and magnetic properties in antenna and metamaterials, chemical properties in fuel cells and batteries, sonic properties in acoustics systems, etc. Moreover, the MMAM process allows the inclusion of embedded components such as resistors, sensors, and other electronic devices. Using multiple materials has the potential for printing three dimension circuits and all-printed resistor-circuits that can reduce lead time, production cost, inventory cost, and reduce product weight. In particular, medical and dental fields require high performance biomedical objects or implants (e.g. artificial hip joints, tissue scaffolds, and bone structures) with desirable properties for biomedical applications. However, traditional manufacturing processes might not meet all requirements and are not economical enough in most cases because of the intricate shapes and internal configurations needed of biomedical models with their delicate material variations. In tissue engineering (TE), different materials and cells need to be precisely placed throughout the scaffolds to elicit the specific desired cell responses. Such control will likely lead to an enhanced generation of new, functional tissue (Bartolo 2011). MMAM is a flexible technology that allows for such multi-material biofabrication of hybrid three-dimensional (3D) structures.

A large number of general reviews and books on additive manufacturing processes have emerged over the past three decades which varied considerably in scope and methods of classification (Pham and Dimov 2000, Gebhardt 2003, Tay *et al.* 2003, Hopkinson *et al.* 2006, Liou 2007). Chua and co-authors' book (2010a) has kept tracing the development of Rapid Prototyping (RP) technology and its applications in industry and has now been revised in the third edition. Fundamentals such as the STL (STereoLithography) file format and the working principle behind the various systems are clearly explained and illustrated. Wholer's report is updated every year and provides broad and timely information though with less academic depth (Wohlers 2012). Some reviews and books have been presented in the fields of medical AM (Gibson 2006, Bartolo and Bidanda 2007, Bidanda and Bartolo 2007, Bartolo *et al.* 2012, Melchels *et al.* 2012).Vaezi *et al.* (2012) presented a comprehensive review on 3D micro-additive manufacturing technologies and their recent developments toward 'rapid micromanufacturing'. Gibson and co-authors have a short chapter in their recently published book (Gibson *et al.* 2010) which provides a review on multiple material additive manufacturing. Oxman (2011) addressed variable property rapid prototyping in which functional components can be produced by dynamically mixing, grading and varying the ratios of material properties. The authors of this paper wish to provide a broader and updated review on MMAM, by providing a comprehensive list of key MMAM from most of MMAM methods published in literature, and a discussion of the advantages and limitations of each method and their potentials.

Table 1. AM and MMAM classification.

Process	Description	Typical AM techniques	Current MMAM techniques	Materials
Photopolymer vat	Liquid photopolymer is selectively cured using a light source	SL, 2PP	SL	Photo-curable polymers
Material extrusion	Material is selectively dispensed through a nozzle or extruder	FDM, robocasting, bioplotting	Extrusion freeforming techniques (see section 2.4)	Polymers, ceramics, metals
Powder bed fusion	Thermal energy selectively fuses regions of powder bed material	SLS, SLM, EBM, SMS	SLS	Polymers, metals, ceramics
Directed energy deposition	Focused thermal energy melts materials as deposited	LENS, DMD[1],	LENS, DMD[1]	Metals, ceramics
Sheet lamination	Material sheets are bonded together and selectively cut in each layer to create a desired 3D object	LOM, UC	LOM, UC	Metals, ceramics, polymers
Material jetting	Droplets of build material are selectively deposited layer by layer	DoD Inkjet printing, PJT	DoD Inkjet printing, PJT	Polymers, metals, ceramics
Binder jetting	Liquid bonding ink is selectively spread to join solid powder material	3DP	3DP	Polymers, metals, ceramics

2. Classification and description

Some authors (Gibson *et al.* 2010) have considered MMAM objects to include those produced from 1) Discrete multiple materials 2) Composite materials and 3) Porous materials suitable for secondary material infiltration. However in this review we will not consider a process to be MMAM if in such process either a) the raw materials are pre-mixed or composited before the AM or b) the second materials is integrated by infiltration or coating or other non-AM post processing methods, because in these processes the compositional variation cannot be freely controlled by computer and program.

To achieve this, different materials or chemicals need to be physically delivered to any spatial location in 3D during the additive manufacturing. In some processes, for example direct 3D printing in Objet, or in the Fused Deposition Modelling (FDM) process, the materials are delivered to the platform dot-by-dot or line-by-line in liquid or semi-liquid form using nozzles. So in these processes, multiple nozzles could be easily integrated into the system to achieve multiple material fabrication. However, in other processes, for example SL, Selective Laser Sintering (SLS), Selective Laser Melting (SLM), Laminated Object Material (LOM), because the materials are delivered as a whole layer by scraper or as a solid sheet, it is very difficult to make MMAM using the configuration of the currently available equipment. New material delivery systems must first be developed in these systems to deliver multiple materials, before further laser sintering or fusion or reaction.

The main scope of this paper is to provide a comprehensive review of the key AM processes which are currently used effectively for fabrication of true discrete multiple material parts. Addressing composite materials is not within the scope of this article since they have been already addressed in the literature (Kumar and Kruth 2010), although some significant work on composite materials will be pointed out.

The field of AM encompasses a variety of unique processes, with varying characteristics, which were previously categorised by several researchers. Recently, AM technologies have been standardised and classified by the American Society for Testing and Materials (ASTM) International Committee F42 on Additive Manufacturing Technologies. The committee has classified AM processes and their variants into seven main categories including: photopolymer vat, material extrusion, powder bed fusion, directed energy deposition, sheet lamination, material jetting, and binder jetting (Stucker 2011). MMAM technologies can be classified in the same way and are described in this paper. However, a combination of different methods could overcome some limitations of a single method MMAM and this will be discussed later in this paper. An overview of the different AM and MMAM processes, and their typical materials based on the recent ASTM standard is provided in Table 1.

It should be noted that several AM techniques have been modified to work at a small scale to deposit passive electronic structures and components (conductors, insulators, resistors, antennas, integrated circuit (IC), etc.). These techniques are often known as Direct Writing (DW) techniques and, for instance, use electronic 'inks' that contain nanoparticles or other additives that result in electronic properties after drying, thermal decomposition, or other post-treatment. By combining DW techniques with other AM techniques it becomes possible to create multi-functional 3D-embedded electronic structures on a layer-by-layer basis that combine structural, thermal, electronic, and other functions into a single component (Stucker 2011). Although components such as resistors and ICs are not directly fabricated by AM methods, and not likely to be made in the near future, here we still count them as MMAM. In some instances multiple AM techniques are combined within the same machine or AM is combined with subtractive techniques such as Computer Numerical Control (CNC) machining or laser cutting. These hybrid techniques are basically used to bring new possibilities. Hybrid and DW systems suitable for multiple material printing will also be discussed in this paper.

2.1 Photopolymer vat processes

Photopolymer vat processes involve selective curing of predeposited photopolymers using some types of light source (Stucker 2011). Stereolithography (SL) is the main photopolymer vat technique in which a laser beam or other ultra violet (UV) light source is used to project a cross-section of a single slice of the object onto a photosensitive liquid polymer which solidifies each layer of the photopolymer. The platform within the vat containing the photopolymer moves the solid part down and the laser traces out the next layer of uncured photopolymer. This process is repeated until all the layers of the complete structure are created. Two main SL techniques have been developed depending on the different beam delivery system: scanning SL and projection SL.

Maruo *et al*. (2001) demonstrated the use of a scanning SL microfabrication process (termed the Multi-polymer IH process) for fabricating optical waveguides with two kinds of photocurable polymers having different refractive indexes. Fabrication of 3D hydrogel structures containing living cells with micro scale resolution has been reported by Liu and Bhatia (2002) via multiple steps using a micro patterned photo polymerisation process. The W. M. Keck Centre for 3D Innovation at the University of Texas at El Paso is a premier laboratory concentrating on the development of MMAM processes. They have developed different multi-material AM systems based on SL and FDM techniques. They have presented a multiple vat carousel design and alternative machine designs to create 3D multiple material objects using a scanning SL system (Wicker *et al*. 2004). Figure 1 depicts a schematic of their multiple material SL system with some fabricated parts. Firstly, the platform is moved below the surface of a liquid polymer in one of the build vats. Then the platform is raised out of the current vat and the vat underneath the platform is rotated to provide access to a different material (Inamdar *et al*. 2006). To reduce contamination, the process offers a cleaning step where the platform is submerged and cleaned in a cleaning vat before being submerged in a different material vat (Choi *et al*. 2011). To improve the processing time, Kim *et al*. (2010) developed a process-planning algorithm to reduce the number of material changeovers by using low viscosity polymers without a sweeping process. The capabilities of scanning SL for fabricating multi-material spatially controlled poly(ethylene glycol) bioactive scaffolds were explored by researchers at the W. M. Keck Centre for 3D Innovation (Arcaute *et al*. 2010). They used two photocrosslinkable hydrogel biopolymers as the primary scaffold materials, poly(ethylene glycol) dimethacrylate (PEG-dma, MW 1000) and poly(ethylene glycol) diacrylate (PEG-da, MW 3400).

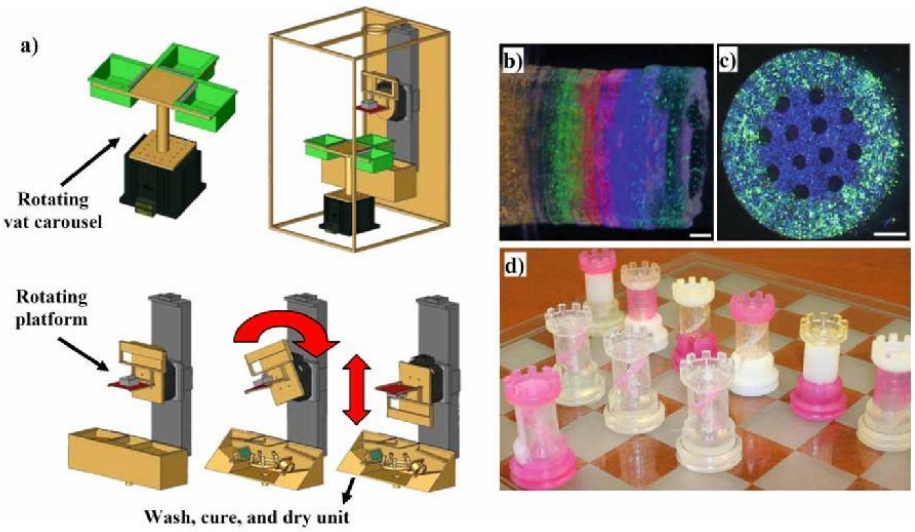

Figure 1. a) Multiple vat carousel including intermediate wash, cure and dry unit (Wicker *et al*. 2004); b, c) Side and top view of nerve guidance conduit fabricated using SL process from different materials. Precise placement of different materials both within and across layers can be seen. In (c) the outer portion of the conduit contains 15μm fluorescent green particles while the inner portion contains 10μm fluorescent blue particles, scale bars are 1 mm (Arcaute *et al*. 2006); d) Various multiple material chess parts (Choi *et al*. 2011).

The key benefits of the multiple material scanning SL technique are high quality of surface finish and dimensional accuracy. Moreover, it offers a wide range of polymers to embed different colours in medical models and to tailor bioactive and mechanical properties in tissue engineering applications. The system can fabricate multiple material objects with horizontally and vertically oriented interfaces. However, contamination is difficult to eliminate with this technique. A multiple vat system requires a large area to operate the process and consumes time in pumping processes. Additionally draining and cleaning the previous material before changing to another resin vat takes a long time and leads to considerable material waste (Kim *et al.* 2010). In addition, there are some problems that affect the shape of the desired object such as shadowing obstruction of the previously built part, trapped volumes when creating one material inside another, surface tension between two materials, and surface tension with the previous layer (Choi *et al.* 2011).

In projection SL, build time is significantly less when compared with scanning SL as a whole layer of the photopolymer is cured once via exposure through a mask. However, the first generation of projection SL systems were slow and costly as a lot of projection masks had to be produced. In 1997, Bertsch *et al.* (1997) proposed that a liquid crystal display (LCD) could be applied as the dynamic mask to generate the pattern expected in each layer in the projection SL process. Later in 1999, they proposed that the Digital Micromirror Device (DMD^2) which is embedded in digital light processing (DLP) projectors could be applied more efficiently as the dynamic mask in the SL process (Beluze *et al.* 1999). In 2004, Stampfl *et al.* (2004) used DMD^2-based SL, in which visible light is projected from below the resin vat to produce high quality 3D micro-parts. Furthermore, UV light was used by Hadipoespito *et al.* (2003) and Cheng *et al.* (2005) instead of visible light, to cure the resin.

Several advantages would potentially be derived by setting up a multiple material DMD^2-based SL system. In 2010, researchers at the W. M. Keck Centre for 3D Innovation developed a DMD^2-based multi-material SL using a syringe pump system to add a material to a small, and removable vat designed specifically for the multi-material SL system (Choi *et al.* 2010). Multi-material fabrication was accomplished using a material changeover process that included manually removing the vat, draining the current material, rinsing the vat, returning the vat to the system, and finally dispensing a prescribed volume in the vat using the syringe pump. Han *et al.* (2010) also presented an automatic material switching approach by dispensing the solution using a pipette into a custom-made small vat, and subsequently washing out the current solution before changing to the next solution. Based on the technique, they fabricated 3D hybrid scaffolds for heterogeneous tissue engineering. Both the DMD^2-based systems mentioned were based on top-down projection. Due to the need to drain and clean the first resin from the deep vat before changing to another resin, it took a long time and led to significant material waste. To overcome this problem, researchers at the University of Southern California developed a DMD^2-based SL system called Multi-material Mask-Image-Projection-based Stereolithography (MIP-SL) which uses bottom-up projection to fabricate 3D multi-material objects faster (Zhou *et al.* 2011). Using bottom-up projection the portion of built up material to be cleaned when switching to new material vats was reduced. A prototype of the system is shown in Figure 2. As seen in the figure, the next step after polymerisation and before changing to the new material is to remove excessive material on the part surface by a soft brush in rough cleaning and by immersion in an ultrasonic cleaner for final cleaning. After cleaning, the part is dried before putting it into the new material and repeating the processes until the complete object is obtained.

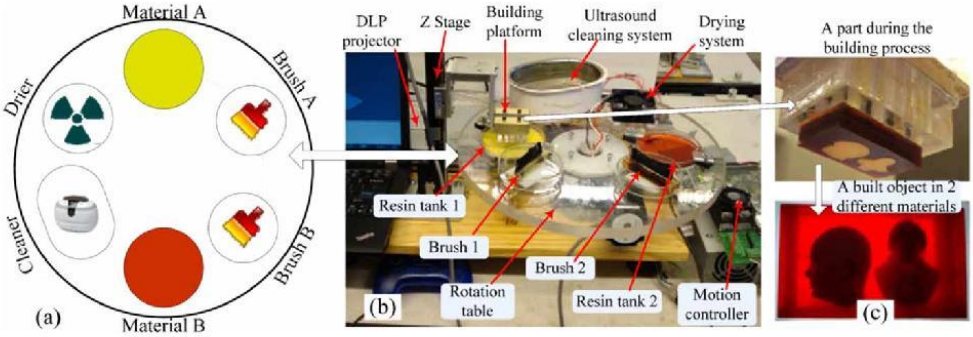

Figure 2. Multiple materials DMD^2-based SL system developed at the University of Southern California (Zhou *et al.* 2011).

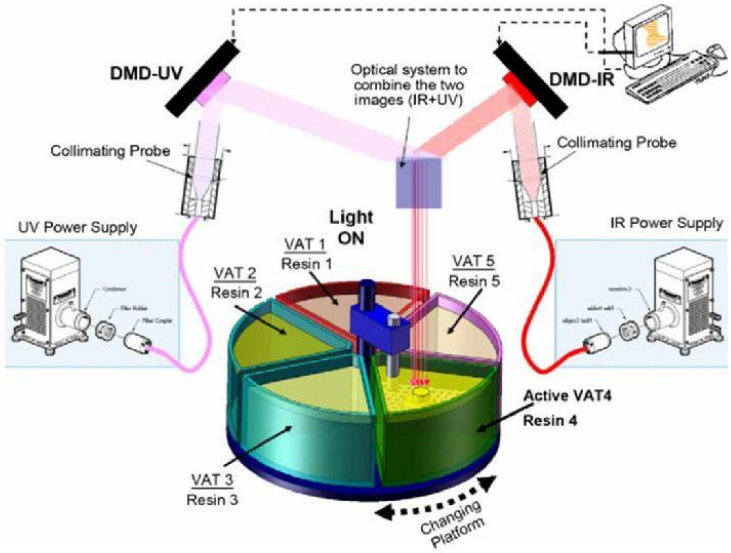

Figure 3. The micro stereo-thermal-lithographic process: multi-vat system (Bartolo 2011).

To produce multi-material functionally graded scaffolds, researchers from the Centre for Rapid and Sustainable Product Development of the Polytechnic Institute of Leiria (Portugal) are developing a new stereolithographic fabrication process called Stereo-Thermal-Lithography (STLG) (Bartolo and Mitchell 2003, Bartolo 2011, Melchels *et al.* 2012). This process uses ultraviolet radiation and thermal energy (produced by infrared (IR) radiation) to initiate the polymerisation reaction in a medium containing both photo- and thermal-initiators. The system also contains a rotating multi-vat that enables the fabrication of multi-material structures (Figure 3).

2.2 *Material jetting processes*

Material jetting is the use of inkjet printing or other similar techniques to deposit droplets of build material that are selectively dispensed through a nozzle or orifice to build up a 3D structure (Stucker 2011). In recent years there has been a propensity to mutate inkjet printing technology into a tool that can be used in different manufacturing processes such as soldering microelectronics or fabrication of micro-optical components using photocurable resins. Furthermore, inkjet printing technology has been used as a robust material jetting technique to fabricate complex 3D structures through a layer-by-layer process. In material jetting processes, liquid material (in the form of a droplet) is jetted and often turns into solid after deposition via cooling (e.g. by crystallisation or vitrification), chemical changes (e.g. through the cross-linking of a polymer) or solvent evaporation (Hon *et al.* 2008). Two different modes are predominantly used for material droplet creation, namely Drop on Demand (DoD) and continuous inkjet (CIJ). Generally, CIJ systems use fluids with lower viscosity at higher drop velocity than DoD and are mostly used where printing speed is an important matter. In contrast, DoD is used where smaller drop size, and higher accuracy is required and it has fewer limitations on ink properties as compared with CIJ (Vaezi *et al.* 2012).

In DoD printing, droplets are formed only when individual pressure pulses in the nozzle cause the fluid to be expelled; these pressure pulses are created at specific times by thermal, electrostatic, piezoelectric, acoustic, or other actuators (Gibson *et al.* 2010). In the current DoD printing industry, thermal and piezoelectric actuator technologies dominate. Thermal actuators rely on a resistor to heat the liquid within a reservoir until a bubble expands in it, forcing a droplet out of the nozzle. Thermal DoD is restricted to water as a solvent and thus places strict limitations on the number of polymers that can be processed (de Gans and Schubert 2003). Piezoelectric actuators rely on the deformation of a piezoelectric element to reduce the volume of the liquid reservoir, which causes a droplet to be ejected. Piezoelectric DoD is an appropriate technique for a variety of solvents, and thus suited for different nanobiotechnology applications. The Jetlab® printing platform by

MicroFab Technologies Inc. (www.microfab.com) is a good commercial example of a material jetting system based on piezoelectric DoD in which droplets are ejected through voltage waveform changes.

There are several significant phenomena which affect the quality of the material jetting processes. The shape of the deposited droplet is critical in forming 3D structures as it affects resolution, precision, and accuracy. Droplet splash must be avoided and jetting frequency must be coordinated with the print-head sweep velocity. The application of fluid mechanics theory has demonstrated that there is an important relationship between the Reynolds number ($\rho_g vd/\mu$) and Weber number ($\rho_l v^2 d/\sigma$) where ρ_g and ρ_l are the densities of the process gas and liquid drop, respectively. The variables v, d, μ and σ are the droplet velocity, droplet diameter, liquid dynamic viscosity and liquid surface tension, respectively. It has been observed that these characteristics should satisfy $1 < \mathrm{Re}/\sqrt{\mathrm{We}} < 10$, which is the normal regime for Drop on Demand (DoD) printing (Beaman *et al.* 2004, Vaezi *et al.* 2012). Researchers from the University of Manchester Institute of Science and Technology (UMIST) reported that droplets should not be smaller than 10 μm in diameter as air resistance then becomes a problem. If printing in a vacuum, to eliminate air resistance, the droplets tend to evaporate (Beaman *et al.* 2004). In short, the basic requirement conditions for successful 3D inkjet printing are: ink properties (viscosity, surface tension); jetting parameters (signal width, voltage magnitude, jetting frequency); and environment (pressure, environment and substrate temperature, humidity) (Ko *et al.* 2010). Material jetting processes are capable of printing multi-material and gradient-material structures. Applications of multi-material parts range from parts with controlled hardness and flexibility to parts with differing electrical properties in various regions to tissue-engineered structures with different biological properties in different regions of the part (Stucker 2011). For multi-material printing, print heads usually include several separate nozzles which are fed with different materials and are separately controllable. MicroFab Technologies Inc. provides a four-channel piezoelectric nozzle set with other components including drive electronics; pressure control; and optics for drop and substrate observation.

There are several reports on the printing of multi-material and functionally gradient materials (FGMs). A thin, zirconia-alumina, one-dimensional FGM was fabricated by Mott and Evans (1999) and Wang and Shaw (2006) which used a drop-on-demand jet printer and an ink mixing protocol. Ibrahim *et al.* (2006) modified a commercial inkjet printer to fabricate 3D multi-material patterns layer by layer. The design, fabrication and performance of a multi-material DoD inkjet system based on a pneumatic diaphragm actuator was described by Xie *et al.* (2010).

These systems could dispense multiple materials but are limited to the use of one type of actuating mode. Researchers at the National University of Singapore (NUS) conducted a comprehensive study on applying inkjet printing for multiple material printing with a multiple actuating system (Li *et al.* 2008, Li *et al.* 2009, Sun *et al.* 2010). They used two micro dispensing units including a solenoid actuating micro-valve and a piezoelectric print head for printing multi-materials.

Conversion of the fine droplets into solid (phase transition) can be accomplished by different methods. Material cooling and curing of a photopolymer ink using UV light are the two most common phase transition methods in multi-material inkjet printing. Molten materials can be jetted through a multi-nozzle piezoelectric head and are cooled upon deposition to make high resolution multi-material parts. Solidscape's 3D printers (www.solid-scape.com) are commercial printers for multiple type polymer printing based on the droplet cooling technique. In these printers, a wax material is deposited by a single jet piezoelectric head and a second wax material with a lower melting temperature is deposited via another piezoelectric head.

UV curable photopolymers can also be jetted through a multi-nozzle head and each photopolymer layer is cured by UV light immediately as it is printed, producing fully cured 3D multi-material parts. Two MMAM systems, namely: Connex™ printers by Objet Geometries Ltd. (www.objet.com) and ProJet printers (formerly InVision™) by 3D Systems Inc. (www.3dsystems.com) based on this principle have been commercialised. In ProJet printers, a print head jets two separate materials, an acrylic UV-curable photopolymer-based model material and a wax-like material to produce support structures for the model. Objet's Connex series use PolyJet™ technology containing a special print head with many individual nozzles to deposit and cure a number of different acrylic-based photopolymer materials simultaneously in 16-μm layers. ProJet HD series have shown better dimensional stability and surface quality than Objet's 3D printer due to their higher resolution (Vaezi *et al.* 2012). In contrast, Connex printers have been much more successful in producing true multi-material parts. With Objet's Connex series, it is possible to print many different photopolymer materials (over 60 materials) into a single part which have properties ranging from rigid to rubber-like, transparent to opaque and standard to Acrylonitrile butadiene styrene (ABS)-grade engineering plastics, with a large number of in-between Shore grades and shades. As materials mixing in each layer is on a droplet scale (e.g. materials resolution is high), the system is able to create advanced composite materials featuring unique mechanical and thermal properties. Such fabrication capability also opens up exciting new options that were impossible before. Figure 4 shows some example of multi-material parts produced by experimental and commercial material jetting systems.

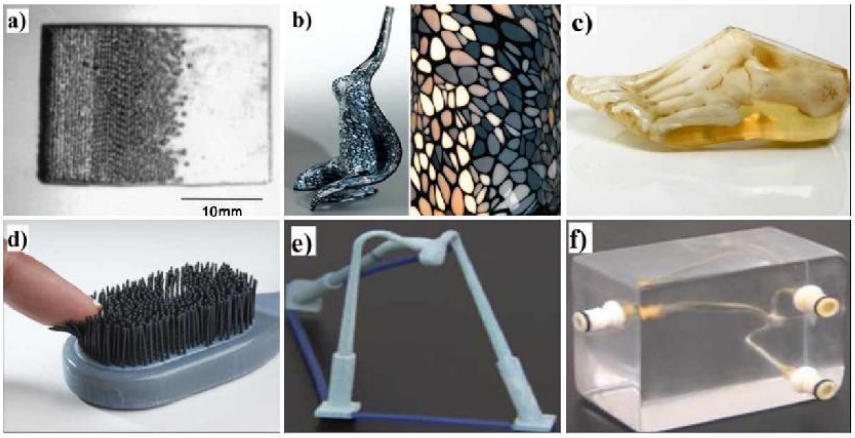

Figure 4. a) Functional gradient structure build from metal which has very low melting temperature (Bi-Pb-Sn-Cd-In alloy, T_m = 47°C) and resin (Yamaguchi *et al.* 2000); b) Chaise longue manufactured using Objet's Connex 3D printer which combines structural, environmental, and corporeal performance by adapting its thickness, pattern density, stiffness, flexibility, and translucency to load, curvature, and skin-pressured areas respectively. Stiffer materials are positioned in surface areas under compression and softer, more flexible materials are placed in surface areas under tension (Oxman 2011); c) 3D printed foot model in transparent and white materials created on the Objet's printer (www.objet.com); d) 3D printed hair brush prototype in rigid and rubber-like materials created on the Objet Connex (www.objet.com) e) core blood vessel multi type wax model produced by solidscape's 3D printer and f) Wax model translated into a transparent polyurethane flow models for fluid dynamics testing (customer case study, Solidscape Inc., www.solid-scape.com).

2.3 Binder jetting processes

Binder-jetting techniques also use nozzles to print material, but instead of printing with the build material, the printed material is 'glue', which holds powder together in the desired shape (Stucker 2011). The 3D printing (3DP) process is the main binder-jetting technique based on inkjet technology and was developed at the Massachusetts Institute of Technology. In this process, droplets of a binder material are deposited over the surface of a powder bed, sticking the powder particles together where the part is to be shaped. The process is followed by lowering the powder bed via a piston and a fresh layer of powder is spread over the previous layer and again binder is deposited over the surface of the new layer. This procedure is repeated to build the whole part. 3DP has demonstrated the capability of fabricating parts of a variety of materials, including ceramics, metals, shape-memory alloys (SMA) and polymers with an array of unique geometries (Cawley 1999, Seitz *et al.* 2005, Lu and Reynolds 2008, Vorndran *et al.* 2009). For multiple-material 3D printing, either the print heads need to deliver different binder materials or different powders need to be applied. However, due to the very limited types of binder delivered from the nozzles, the capacity of MMAM using this method is poor, unless the powder bed materials can be changed by another dry powder dispensing technology.

Several research groups have made contributions in multi-material 3DP and this area has been explored by several tissue engineering groups for more than a decade. Researchers at the Fraunhofer Institute for Manufacturing and Advanced Materials (IFAM) in Bremen, Germany (Beaman *et al.* 2004) developed a two-binder system for 3D Printing technology, where one binder is traditional and one is carbon laden. Their goal was to produce gradient strength steel parts by depositing the carbon according to a desired distribution of hardness.

A heterogeneous osteochondral scaffold was developed by Sherwood *et al.* (2002) using the TheriForm™ 3D printing process. The material composition, porosity, macroarchitecture, and mechanical properties varied throughout the scaffold structure. The upper, cartilage region was 90% porous and composed of $_{D,L}$-poly(L-lactide-co-glycolide)(PLGA)/$_{L}$-polylactic acid (PLA), with macroscopic staggered channels to facilitate homogenous cell seeding. The lower, cloverleaf-shaped bone portion was 55% porous and consisted of a $_{L}$-PLGA/tricalcium phosphate (TCP) composite, designed to maximise bone ingrowth while maintaining critical mechanical properties. The transition region between these two sections contained a gradient of materials and porosity to prevent delamination.

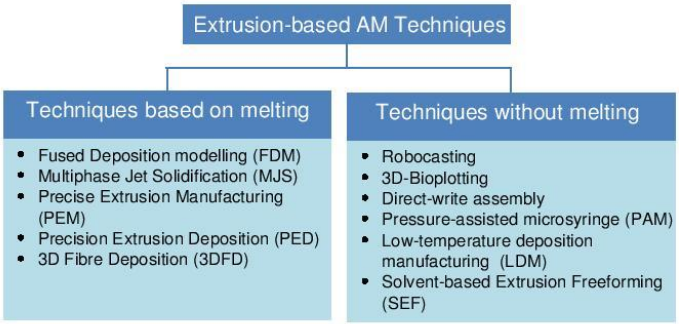

Figure 5. Different extrusion-based AM techniques.

2.4 Extrusion-based systems

Extrusion-based systems deposit material in the form of a continuous flow, layer by layer to make objects. They are very diverse in concept but can be classified into two main sub-groups as shown in Figure 5: processes based on material melting and processes without material melting.

Fused deposition modelling (FDM), multiphase jet solidification (MJS) (Greulich *et al.* 1995), precise extrusion manufacturing (PEM) (Xiong *et al.* 2001), precision extrusion deposition (PED) (Wang *et al.* 2004) and 3D fibre deposition (Woodfield *et al.* 2004) are AM techniques based on the melting process. Robocasting (Cesarano 1999), 3D-Bioplotting (Landers and Mulhaupt 2000), direct-write assembly (Smay *et al.* 2002) (pH-controlled gelled ceramic colloid or polymers freeforming), Pressure-assisted microsyringe (PAM) (Vozzi *et al.* 2002), low-temperature deposition manufacturing (LDM) (Zhuo *et al.* 2002), and solvent-based extrusion freeforming (Grida and Evans 2003) are the most commonly used AM techniques without material melting. Four major nozzle designs have been exploited in non-heating processes: pressure-actuated, volume-driven injection nozzles (normally using a stepper-motor), solenoid and piezoelectric-actuated, whereas two main nozzle designs including filament driving wheels, and mini-screw extruder have been used in processes with material melting.

Two or more extrusion nozzles are often incorporated in extrusion-based AM systems to fabricate multiple material structures. For example, two discrete materials are usually used in the FDM process so that one material may serve as a support structure and can be easily removed once the build has been completed. Apart from hardware, an efficient pre-processing tool needs to be applied. Qiu and Langrana (2002) developed a CAD system which generates high quality tool paths for multi-material part fabrication using extrusion-based systems.

Fused Deposition of Multi-Materials (FDMM) is a FDM method developed at Rutgers University, to produce a variety of ceramic components composed of up to four materials (Hsieh and Langrana 2001, Brennan *et al.* 2003). Safari's group at Rutgers University (Allahverdi *et al.* 2001, Pilleux *et al.* 2002) produced 3D photonic band gap (PBG) structures from alumina and wax (as support structure) directly using FDMM. The co-firing of multiple-materials ceramics parts is made difficult by different ceramics having different sintering temperatures and shrinkage.

Solvent-based extrusion freeforming is another technique developed to produce bioceramic scaffolds (Grida and Evans 2003). A range of bioceramic scaffolds has been fabricated with different compositions of hydroxyapatite (HA) and β-TCP and sintered from 1100 to 1300°C in steps of 50°C. Composite scaffolds with different porosities and pore sizes were produced with raster width down to 60 μm and interconnected pores with interstices from 50 to 500 μm (Yang *et al.* 2008a, Yang *et al.* 2008b, Yang *et al.* 2008c). Other composite ceramic pastes such as alumina/silica, and alumina/graphite have been used successfully for the fabrication of 3D lattice structures with fine filaments (Xuesong *et al.* 2009, Xuesong *et al.* 2010).

The LDM process proposed by Xiong *et al.* (2002) has as its key feature the non-heating liquefying processing of materials. Incorporating multiple nozzles with different designs into the LDM technique gave multi-nozzle low-temperature deposition and manufacturing (M-LDM) and multi-nozzle deposition manufacturing (MDM) (Liu *et al.* 2008, Liu *et al.* 2009). This M-LDM system is proposed as a fabrication route for scaffolds with heterogeneous materials and gradient hierarchical porous structures by the incorporation of more jetting nozzles into the system. The M-LDM process has been used to build PLGA/collagen multi-material scaffolds (Liu *et al.* 2008).

Researchers at Cornell University, USA have enhanced multi-material freeform fabrication of active systems by

combining FDM using molten-extrusion and a Robocasting process using a robotically controlled syringe in the same machine (Malone *et al.* 2004, Malone and Lipson 2008). Moreover, they have developed a system that can print embedded circuits by combining FDM to fabricate a structural part and direct writing (DW) to print conductive circuits on the part (Daniel *et al.* 2007).

In recent years, much attention has been paid to extrusion-based systems in the field of biomedical engineering as they are mechanically simple processes in comparison to other AM techniques and a wide range of multiple biomaterials can be processed effectively. Three or more nozzles are sometimes used in machines designed for tissue-engineering research, so that scaffolds and other biologically compatible materials can be deposited in specific regions of the implant (Stucker 2011).

Ang *et al.* (2002) set up a special robotic bioplotting device called rapid prototyping robot dispensing (RPBOD) for the design and fabrication of chitosan-HA scaffolds. The RPBOD system was further improved to include a new manufacturing method, a dual dispensing system. Besides the pneumatic dispenser, a mechanical dispenser which was driven by a stepper motor was set up to deposit the curing medium (NAOH) (Li *et al.* 2005).

The Polytechnic Institute of Leiria developed a variation of FDM called the BioExtruder with the aim of multiple material TE scaffold fabrication (Domingos *et al.* 2009, Domingos *et al.* 2012). It comprises two different deposition systems: one rotational system for multi-material deposition actuated by a pneumatic mechanism and another one for single material deposition that uses a screw to assist the deposition process. Highly uniform poly(ε-caprolactone) (PCL) scaffolds have been made using the BioExtruder but no multiple-materials scaffold has been reported.

3D bioplotting is a technique that was first developed by Landers and Mulhaupt (2000) at the Freiburger group to produce scaffolds for soft tissue engineering purposes, and to simplify hydrogel manufacturing. Either a filtered air pressure (pneumatic nozzle) or a stepper-motor (volume-driven injection nozzle) is used to plot a viscous material into a liquid (aqueous) plotting medium with a matching density. It is possible to perform either a discontinuous dispensing of micro dots or a continuous dispensing of fine filaments. Khalil *et al.* (2005) developed a special multi-nozzle bioplotting system which was capable of extruding biopolymer solutions and living cells for freeform construction of 3D tissue scaffolds, although multiple materials is still to be reported. The deposition occurs at room temperature and low pressures to reduce damage to cells. The system was capable of depositing controlled amount of cells, growth factors, or other bioactive compounds simultaneously with scaffold construction to form complex cell-seeded tissue constructs with precise spatial position.

Recently, Schuurman *et al.* (2011) used a hybrid bioplotting approach for the fabrication of solid biodegradable materials (polymers, ceramics) with cell-laden hydrogels that could combine favourable mechanical properties with cells positioned at defined locations at high densities. This approach allows the use of multiple hydrogels, and can thus build constructs containing multiple cell types or bioactive factors. Furthermore, since the hydrogel is supported by the thermoplastic material, a broader range of hydrogel types, concentrations and cross-link densities can be used compared to the deposition of hydrogels alone, thereby improving the conditions for encapsulated cells to proliferate and deposit new matrix (Melchels *et al.* 2012).

Inkjet printing and extrusion-based systems can serve in a rather similar way for direct bioprinting. Beads or continuous flows of bioinks are deposited in well-defined topological patterns into biopaper layers. The bioink building blocks typically have a spherical or cylindrical shape and consist of single or multiple cell types. In a post-processing step, the construct is transferred to a bioreactor and the bioink spheres are fused. The biopaper, an inert and biocompatible hydrogel (i.e. agarose), can be removed after construction in a post-processing step (Billiet *et al.* 2012). Norotte *et al.* (2009) reported a fully biological self-assembly approach, which they implemented through a multi-material bioprinting method for scaffold-free small diameter vascular reconstruction. Figure 6 illustrates some examples of multiple material components for different applications produced by commercial and experimental extrusion-based systems.

2.5 Powder bed fusion processes

Powder-bed-fusion machines work in a manner similar to binder jetting; however, instead of printing glue onto a layer of powder, thermal energy is used to melt the powder into the desired pattern (Stucker 2011). Most systems use laser power to melt polymer, metal or ceramic material. For partial melting, the system is called Selective Laser Sintering (SLS). For full melting, the system is named Selective Laser Melting (SLM). Another system that uses an electron beam to melt metal powder is known as Electron Beam Melting (EBM). Also, Selective Mask Sintering (SMS) is a slightly different system that uses IR-light through a digitally printed optical mask to melt a thin layer of plastic powder. The process is governed by powder characteristics (e.g. particle shape, particle size, particle distribution) and processing parameters such as energy source, energy power, spot size, scan speed, spacing distance and layer thickness (Das 2003, Kumar 2003, Kruth *et al.* 2007, Gu and Shen 2009, Chua *et al.* 2010b, Averyanova *et al.* 2012, Leu *et al.* 2012). Tolochko *et al.* (2000) studied the effect of laser wave length on its absorption by powder materials. It was shown that for metal powders laser absorption decreases with

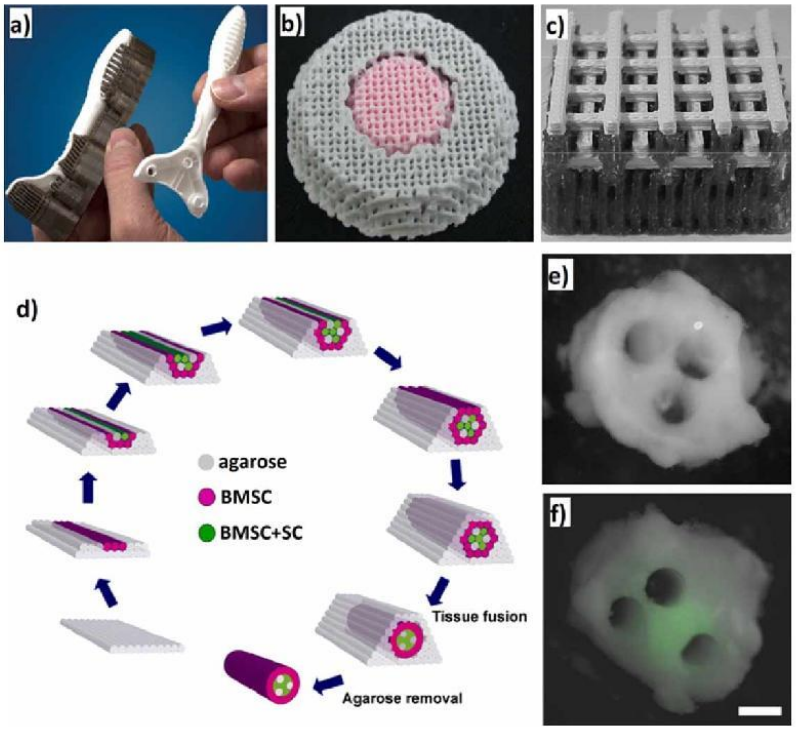

Figure 6. a) A shaver prototype containing two build and support materials produced by the Stratasys FDM system, support material (black) is water soluble and can be easily removed (photo: Stratasys Inc.); b) Multi-material PLGA/collagen scaffold fabricated via M-LDM system (Liu *et al.* 2008); c) FDMM fabrication of the 3D photonic bandgap (PBG) structure made by FDMM process with multi-material deposition of alumina-loaded and wax filaments as feedstock materials (Pilleux *et al.* 2002); d) Possible scheme for bioprinting of multiple cellular and agarose cylinders to build a 3-lumen tube using an extrusion-based bioprinter (red: bone marrow stem cell (BMSC), green: 90% BMSC + 10% Schwann cells (SC), grey: agarose); e) Cross-section of a bioprinted nerve graft, constructed according to the scheme in (d), with three acellular channels after agarose removal; f) Fluorescently labelled SC (green) concentrated at the central region of the graft. Scale bar: 500 μm (Marga *et al.* 2012).

increasing wavelength, while for ceramic and polymer powders it increases with increasing wavelength. The laser wavelength should be adapted to the powder material because laser absorption greatly changes with the type of material. CO_2 lasers are well-matched for polymer powders and oxide ceramic powders, whereas, Nd:YAG lasers are suited for metallic powders (Glardon *et al.* 2001, Savalani *et al.* 2006).

Multiple material powder bed fusion has been investigated in the University of Texas at Austin, USA. They have focused on discrete multiple-materials processing that is performed by two different deposition methods; (1) depositing a complete layer followed by iterative selective removal and blind deposition of a secondary material by a counter-rotating roller as in traditional SLS, and (2) deposition of a primary layer by a roller and depositing a secondary material in the desired location by a nozzle (Lappo *et al.* 2003a). In this process, a cross-section layer is built by the movement of a laser beam which melts the powder in the working area and the excess materials are selectively removed by electrostatic attraction (Lappo *et al.* 2003b). This process can produce objects with nearly full density in a single processing step.

Another system has been developed by researchers from the Laser Insitut Mittelsachsen e.V., Germany (Figure 7). The sintering platform has two cylindrical bores for the copper and silver powder supply and one for the building part piston. Two special rakes serve as a blade and a powder reservoir sweeps the powder material in a circular motion onto the platform. The bonding layers are generated by

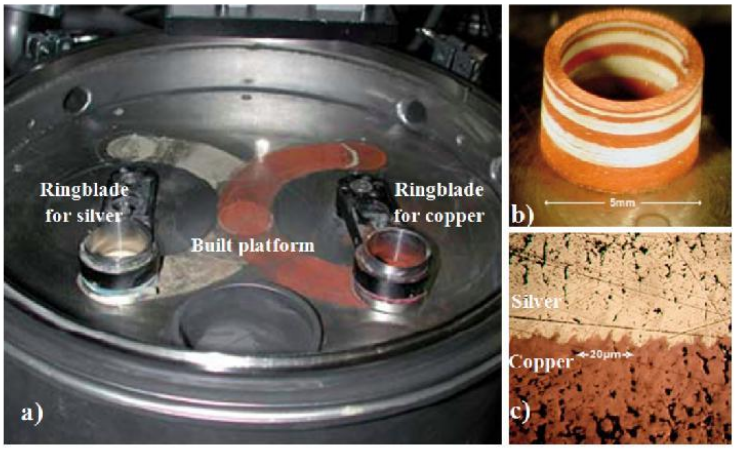

Figure 7. a) Two different materials in ringblades served as rake and powder storage; b) Sintered part from copper and silver; c) The interface between a copper and a silver section (Regenfuss *et al*. 2007).

q-switched laser pulses (Regenfuß *et al*. 2007). This technique is limited to vertical gradients of material. In addition, accurate material feeding systems to recoat multiple materials are difficult to design (Zhou *et al*. 2011). After fabrication, it is difficult to recycle the loose powders due to uncontrolled powder dispensing in layers.

Powder bed fusion processes are fit for functional MMAM parts that require a wider range of materials and material properties than that available from traditional manufacturing methods. They can be used in automotive, medical (Liew *et al*. 2001, Liew *et al*. 2002) and aerospace (Hopkinson *et al*. 2006) applications that require multi-functional capabilities which other manufacturing methods cannot produce. The process can be speeded up via applying optical mask printing techniques as used in the Selective Mask Sintering (SMS) process. The re-use of materials also presents a significant problem because the current recoating system has a contamination problem when changing between materials. Clever design of the material recoating system is still required to solve this problem, which will be further discussed in part 2 of our paper.

2.6 Directed energy deposition processes

Directed energy deposition uses a laser beam to melt and fuse particles of the powder material delivered from the material deposition head. The X-Y table is moved to shape the cross-section of each desired layer. This process is repeated until all the desired cross-sectional layers of the part are created (Figure 8). There are various types of this technology such as Laser Engineering Net Shape (LENS),

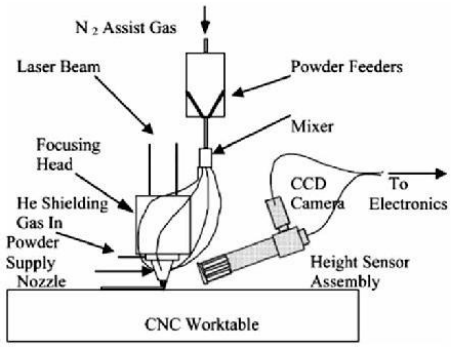

Figure 8. Schematic illustration of directed energy deposition system (Shin *et al.* 2003). *CCD- Charge-Coupled Device.*

Laser Cladding (LC), and Direct Metal Deposition (DMD[1]).

Multiple-material directed energy deposition employs a nozzle to feed multiple powders and these are melted on a substrate by a laser beam to form fully dense objects. The key feature of this process is the powder feeding mechanism that can change or mix materials when fabricating multi-material structures. A wide range of different metals and alloys such as tool steel, stainless, nickel base superalloys, Co–Cr–Mo alloy and titanium have been deposited using this method (Schwendner *et al.* 2001, Vamsi Krishna *et al.* 2008). For FGMs, the powder feeders are used to deposit different powders separately and their feed rates are controlled individually to regulate the material composition (Liu and DuPont 2003, Shin *et al*. 2003). Independently

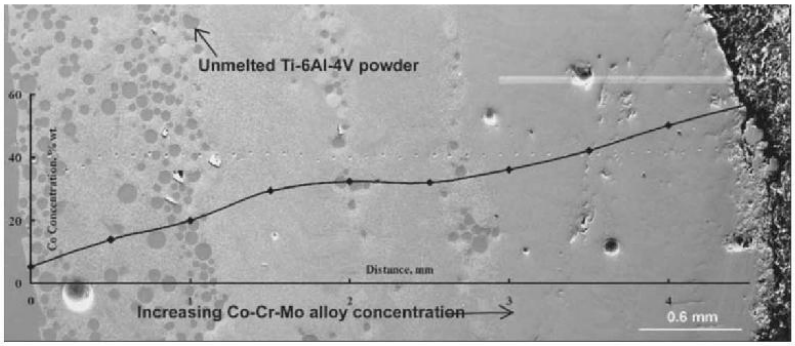

Figure 9. Typical microstructure and Co distribution of laser processed 86% Co–Cr–Mo graded coatings on a porous Ti–6Al–4V alloy (Bandyopadhyay *et al.* 2009).

controllable multiple powder feeders in the LENS process enable variations of composition and porosity simultaneously in one operation and enable the manufacture of novel implant structures. Functionally graded structures with a hard and wear resistant Co–Cr–Mo alloy coating on a porous Ti6Al4V alloy with a metallurgically sound interface have been produced using LENS by Bandyopadhyay *et al.* (2009). The graded structures exhibited good bonding between the individual layers without any gross porosity, cracks or lack of fusion defects as shown in Figure 9. For electronic components and conductive lines, Zeng *et al.* presented a laser micro-cladding method to fabricate electronic pastes on insulated boards that will be useful in the electronic manufacturing industry and other fields such as Microelectromechanical Systems (MEMS) (Zeng *et al.* 2006). The main advantage of this process is its ability to produce a highly controllable microstructure in built parts, because it can exhibit deep structured-phase transformations to fabricate a fully-dense part. The primary restriction of this process is poor resolution and surface roughness. Part geometries of these processes are limited because they cannot build free-hanging features or internal overhang features which require rigid support, since there are no support materials in these processes. Additionally, build times of these processes can be very long (Cooper 2001, Gibson *et al.* 2010).

The key benefit of directed energy deposition is that the system can perform material composition changes during deposition and achieve full density. The system is also suitable for repair applications. With this technology, it is possible to create three-dimensional structures that encapsulate actuators and arrays of sensors without fasteners or connectors (Bailey *et al.* 2000, Dollar *et al.* 2006).

To obtain reliable process, the effects of process parameters need to be carefully understood. The important parameters include types of materials, powder flow rate, powder feed method, laser mode, laser power, laser beam diameter and scanning rate (J. Laeng *et al.* 2000).

2.7 Sheet lamination processes

Sheet lamination techniques work by cutting and bonding sheets of material to form an object. The original system used glue or binder to bond paper or plastic sheets and is called Laminated Object Manufacturing, whereas ultrasonic welding of metal sheets is named Ultrasonic Consolidation (UC).

2.7.1 Laminated object manufacture (LOM)

This technique involves the lamination of sheet material with each sheet representing a cross-sectional layer of the part. The sheets can be cut by either a knife or a laser and then the layers bonded by gluing or adhesive bonding (Figure 10). For a multiple material LOM process, the material supply either comes from two different materials or comes from blended multiple materials. LOM of silicon carbide (SiC) and SiC/SiC composites has been demonstrated to produce high performance ceramic parts by (Klosterman *et al.* 1998). Also, they have developed the Curved-LOM technology which deposits ceramic fibre-reinforced composite green tapes to create a smooth surface with more uniform mechanical properties (Klosterman *et al.* 1999). Also, many researchers have presented preform tapes made from ZrO_2 (Griffin *et al.* 1996), Si_3N_4 (Rodrigues *et al.* 2000), Al_2O_3 (Travitzky *et al.* 2008), TiC/Ni (Zhang *et al.* 2001) and Si-SiC (Windsheimer *et al.* 2007) to fabricate functional and structural parts. Gomes *et al.* have developed water based green tapes of $Li_2O - ZrO_2 - SiO_2 - Al_2O_3$ (LZSA) with high tensile strength, which are able to produce complex geometry, defect-free, laminate glass-ceramic materials (Gomes *et al.* 2009).

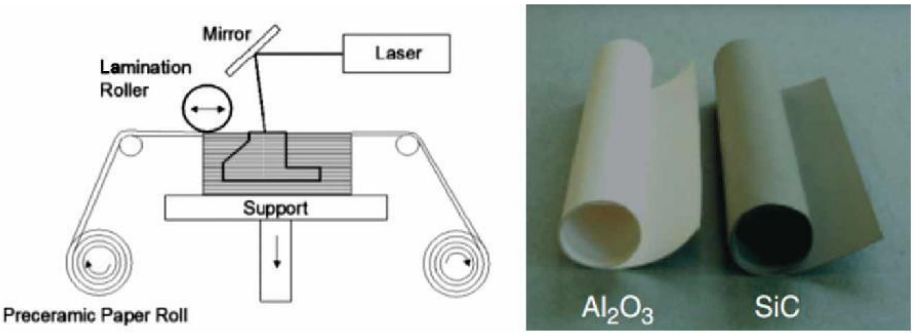

Figure 10. Schematic system of LOM (left) and Al_2O_3 and SiC preceramic papers (right) (Travitzky *et al*. 2008).

The process requires well-prepared material tapes to reduce variations in layer thickness and material content. The laser power has to be carefully controlled to avoid damage to a tape layer below from excessive energy. Additionally, post processing for the reaction bonding process in a pyrolysis cycle is necessary. The separation of the material layers is a major issue of the process.

This technique can process ceramic materials that have mechanical, thermal and chemical stability that is suitable for high-performance shielding. The challenge lies in the bonding process to prevent delamination. Controlling sintering parameters is critical and requires more understanding. Although varying materials between layers can be achieved, the production of a high resolution multiple materials in individual layers is very difficult.

2.7.2 Ultrasonic consolidation (UC)

Ultrasonic Consolidation (UC) is a hybrid fabrication method combining an additive process and a subtractive process. It uses low amplitude ultrasonic frequency energy to bond thin sheet materials to form the objects by means of a rotating sonotrode. Subsequent layers are deposited over the previous layer. The part is finished by a subtractive process such as milling to produce the desired geometry (Figure 11). This process combines additive ultrasonic welding and subtractive contour milling to produce three-dimensional objects (White 2003). The design of multiple material UC is currently under investigation at the Department of Mechanical and Aerospace Engineering in Utah State University, USA. This machine consists of a welding horn (sonotrode) and an automatic

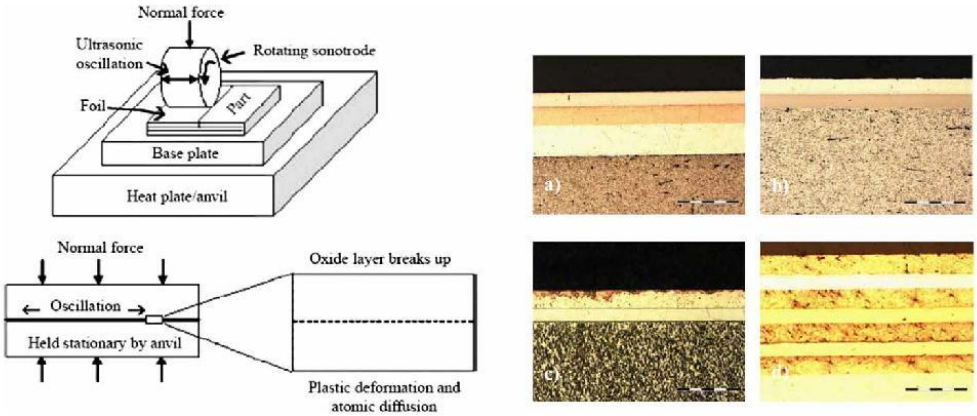

Figure 11. Schematic system of UC (left) and samples of material bonding (right) a) Ni/Ag foils on Al 3003 -H14 substrate; b) 2Ag/Cu/Ni on Al 3003-H14 substrate; c) Ni/Cu foils welded on Al 3003-H14 substrate; and d) Al 6061/Ni/Al 6061/Cu/Al 6061/Ag/Al 6061 on Al 6061-T6 substrate (Obielodan *et al*. 2010a).

foil (sheet) material feeding system (Ram *et al.* 2006). To create 3D multiple material objects, firstly materials are fed by the automatic foil material feeding system and then the process uses ultrasonic vibration at low amplitudes to create solid-state bonding layers of foil materials and build up a 3D cubic object which is machined to a completely 3D object by a milling machine. This technique can process weldable metal materials such as Al, Fe, Ni, Cu and dissimilar combinations such as Al/brass, Al/stainless steel and Al/Ni (Ram *et al.* 2007). Additionally, Siggard *et al.* (2007) have applied this technique to embed Universal Serial Bus (USB) based sensors into aluminium sheets to demonstrate the ability to use UC in embedding mechanical and electrical systems. The process controls several important process parameters such as substrate temperature, vibration amplitude, welding speed, and normal force to achieve adequate bonding (Swank and Stucker 2009). Researchers at Loughborough University reported the use of a UC process to make smart material structures by embedding fibres such as conductor, dielectric, and nano-meter NiTi shape memory alloy fibres into a metal matrix (Friel and Harris 2010).

The strength of this technique lies in the ability of the process to produce metallic parts at high fabrication speeds with accurate dimensions because solid-state welding and no liquid to metal transition process is involved, so it is easy to control accuracy during the building of the part. When compared to other AM methods, this process can be performed at lower temperature, temperatures ranging from 22°C to 204°C are possible; the temperature is normally 150°C (Yang *et al.* 2006). Moreover, it uses a machining process to shape the contour of the final object precisely (Liou 2007). The main problem of this technique is voids that occur along the interfaces between layers because of foil surface roughness, insufficient or excessive welding energy, and positioning inaccuracies of foil placement (Obielodan *et al.* 2010b). This defect affects the strength of built parts (Gibson *et al.* 2010). Also, this technique can use only metal materials and it is inefficient in material usage due to the subtractive process. Furthermore, the system can fabricate multiple material objects but with only vertically oriented interfaces (Obielodan *et al.* 2010a).

The sheet lamination processes use a relative low processing temperature that is suitable for electronic encapsulation and embedded electronic system applications because it does not provide the protection of the embedded components. The challenge is the process parameter that can achieve a defect-free bonding layer at low temperature. Delamination between bonded layer is a critical problem of this technique. If this problem is overcome this technique will offer benefits for embedded applications.

2.8 Hybrid and direct writing processes

2.8.1 Laser chemical vapour deposition (LCVD)

LCVD is a 3D direct writing (DW) process that employs a laser beam to convert gaseous reactants into thin solid layers in a selective manner. In the LCVD process, a laser beam is focused to a spot (1 μm in diameter) via an optical microscope lens and a gaseous reactant comprising the materials to be laid down is fed into a build chamber. The substrate is heated selectively by scanning the laser beam over it at usually 0.5–5 mm/s to dissociate the reactant gas selectively; consequently, a thin layer of the material is set down onto the substrate. In this way, by repeating the laser scan, microcomponents can be made layer by layer. There is a possibility to fabricate multi-material and gradient 3D microstructures by feeding different gases into the build chamber at different times or using a blend of gases with desirable concentrations. A number of factors such as laser beam diameter, energy density, and wavelength as well as substrate thermal properties influence the resolution of this process (Gibson *et al.* 2010). Deposition thickness can be estimated by the equation offered by (Williams *et al.* 1999), for a Gaussian beam profile:

$$h(v_s, t) = \frac{R_0 rt\sqrt{\pi}}{\sqrt{\pi}r + 2(v_s t)} \quad (1)$$

In this equation, r is the laser spot radius, $h(v_s, t)$ is the deposition layer thickness, R_0 is the diffusion-limited axial growth rate, v_s is the scanning speed, and t is process time (Vaezi *et al.* 2012).

Instead of feeding gaseous precursor materials into the build chamber jets of gas can be used to provide a local gaseous atmosphere (Gibson *et al.* 2010). Various microparts from a variety of ceramics and metals can be produced by the LCVD process using different reactant gases. Furthermore, a LCVD process can be used to build carbon fibres and multi-layered carbon structures. (Duty *et al.* 2001) deposited various materials including carbon, silicon carbide, boron, boron nitride, and molybdenum (Mo) on a range of substrates namely graphite, grafoil, zirconia, alumina, tungsten, and silicon using the Georgia Tech's LCVD system.

There are two extensions to LCVD known as Selective Area Laser Deposition (SALD) and Selective Area Layer Deposition Vapour Infiltration (SALDVI) (Figure 12). They can deposit multiple material directly to build objects at low processing temperatures without the use of any secondary low-melting temperature phases (Crocker *et al.* 1998). SALD utilises a laser beam to create a locally heated zone on a substrate enclosed by a reactant gas and SALDVI uses gas precursors and solids in powder form as starting raw materials (Jakubenas *et al.* 1998).

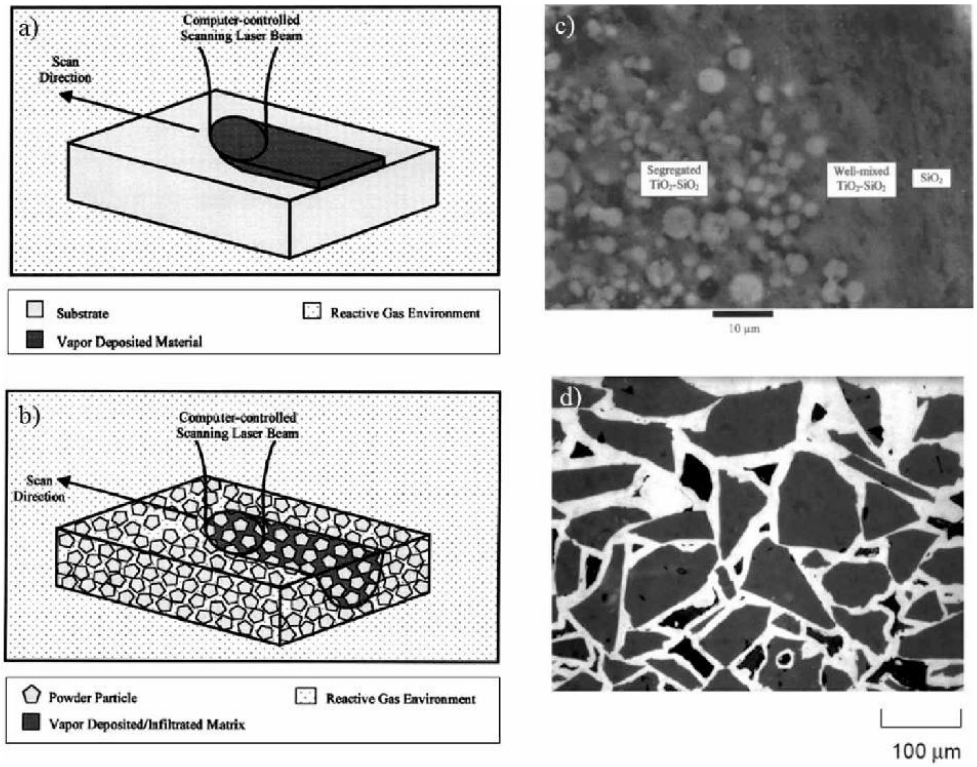

Figure 12. a) schematic of SALD process (Crocker *et al.* 1998); b) schematic of SALDVI process (Crocker *et al.* 1998); c) the three distinct microstructures observed in TiO_2-SiO_2 deposits made by SALD (Jakubenas *et al.* 1998); and d) the cross-section of an Al_2O_3/SiC composite made by SALDVI (Crocker *et al.* 1998).

The deposition speed of this process is naturally low, usually in term of μm/s (Westberg *et al.* 1993), so LCVD might be suitable for micro-scale component applications. To obtain a high deposition rate, the surface reaction mechanisms must be understood so that the process parameters can be adjusted accordingly (Vargas Garcia and Goto 2003). Furthermore, when using multi-source precursors it is difficult to control the deposition of multi-component materials because different precursors have different vaporisation rates, and most precursor gases are toxic, corrosive, flammable and/or explosive (Choy 2003).

2.8.2 *Aerosol jet*

The aerosol jet process is a type of direct writing method which uses a focused aerosol stream instead of liquid ink droplets (as is used in inkjet printing) to deposit a wide range of materials. The process was developed and commercialised by OPTOMEC® under the trademark of M^3D which represents Maskless Mesoscale Material Deposition. Figure 13 depicts a schematic of the aerosol jet printing process and two multiple material printed components. First, a composite suspension is aerosolised in an atomiser to make a dense aerosol of tiny droplets (normally 1 to 5 μm in diameter but droplets as fine as 20 nm have been obtained). Next, the aerosol is transported to the deposition head via a carrier gas flow (usually N_2 gas flow), and within the aerosol head, the aerosol is focused using a flow guidance deposition head, which creates an annular flow of sheath gas to collimate the aerosol. The high velocity co-axial aerosol stream is sprayed onto a substrate layer by layer (minimum layer thickness of 100 nm) to create 3D parts (Hon *et al.* 2008). The high exit velocity of the aerosol stream enables a relatively large separation between the print head and the substrate, typically 2–5 mm. The aerosol stream remains tightly focused over this distance, resulting in the ability to print conformal patterns on 3D substrates.

The aerosol jet can deposit a wide variety of materials, including any materials that can be suspended in liquids

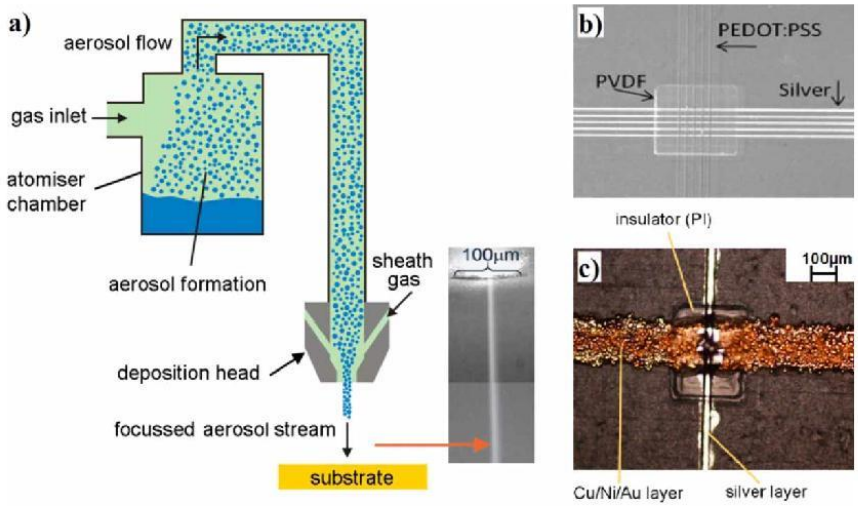

Figure 13. Schematic illustration of aerosol jet process and two multi-layered components fabricated by aerosol jet process (Obliers-Hommrich *et al.* 2008).

(such as metals, ceramics, polymers, composites and biological materials), on virtually any 2D planar surfaces or 3D non-planar substrates. Since aerosol jet is a low temperature process and the droplet size is of the order of a few femtolitres, it is a good candidate for biomanufacturing. The kinetic energy of the droplets is so small due to their tiny mass that it will not demolish living cells. Aerosol jet inks can include polymers, ceramics, metals and biomaterials in the form of solutions, nanoparticle suspensions, etc. Materials including metals (bio-nanoinks containing Ag, Au and Pt nanoparticles, Pd and Cu inks), resistors (carbon polymer thick film (PTF), Ruthenium Oxide), dielectrics (polyimide, polyester, Polytetrafluoroethylene (PTFE), etc.) and biomaterials such as protein and antibody solutions, DNA and biocompatible polymers like PLGA have been employed successfully in the aerosol jet process (Hon *et al.* 2008).

The aerosol jet process was first developed for 2 and 2.5D direct writing purposes but with recent process developments there is the possibility to use this process efficiently for true 3D nano-biomaterials manufacturing.

It has been used successfully to produce bioceramic/polymer nanocomposite scaffolds for bone tissue engineering applications. Liu and Webster (2011) reported its use for the fabrication of 3D nanostructured titania/PLGA nanocomposite scaffolds for orthopaedic applications. In vitro cytocompatibility tests were conducted and the results demonstrated that the 3D nanocomposite scaffold produced enhanced osteoblast infiltration into porous 3D structures in comparison to prior nanostructured surfaces.

2.8.3 Dry powder printing

The dry powder printing technique is one among several techniques that has potential for use as the material delivery system in MMAM. The origin of powder dispensing dates from the sand paintings or manual deposition of the Navajo Indians and has been proposed as a material delivery technique for powder materials. Joseph Pegna is a pioneer in the line printing of dry powders. His experiments studied the feasibility of multi-material deposition by generating a single layer of Portland cement (Pegna 1995) and 220-µm spherical glass beads (Pegna *et al.* 1999). James Santosa *et al.* presented experiments on the delivery of powder under 100 µm through a hopper-nozzle to show the influence of orifice diameters and particle sizes on flow behaviour under gravity (James Santosa 2002). In 2004, Kumar *et al.* proved the concept of multiple dry powder deposition under gravity alone by using low gas pressure-assisted flow and vibration-assisted flow conditions on an X-Y table (Kumar *et al.* 2004). Moreover, they predicted the flow rate under gravity of the experimental powders by Beverloo's correlation. In the meantime there have been many attempts to use ultrasonic vibration to dispense dry powder for MMAM. Matsusaka *et al.* (1995) used a capillary tube vibrated by 20 kHz ultrasound to control the micro-feeding of fine powders. Takehiro and Yoshiro (1998) created a powder feeding device based on an ultrasonic progressive wave. Yang and Evan studied the dispensing mechanism, drop uniformity and dispensing nozzles in ultrasonic micro-dispensing (Yang and Evans 2004a, Yang and Evans 2004b, Evans and Yang 2005, Lu *et al.* 2009). The technique

adopted for powder deposition was acoustic flow rate control of powders in which vibration is used to switch powder flow on and off and to control flow rate by changing amplitude (Yang and Evans 2004a). The static valve is closed by the formation of a powder dome at the end of the orifice tube following conventional architectural principles while flow initiation results from the breakage of domes under vibration force (Lu *et al*. 2009).

There are several different methods for powder delivery in additive manufacturing: pneumatic and screw methods, volumetric methods, electrostatic methods, and vibratory methods (Yang and Evans 2007). Among dry powder dispensing systems, the ultrasonic technique of all the vibratory methods has demonstrated more acceptable results as a material delivery system compared with other systems discussed (Lu *et al*. 2006a). Many experimental results show that the dispensing system can use a variety of materials such as H13 tool steel (Lu *et al*. 2006b), copper (Yang and Li 2003), glass bead (Kumar *et al*. 2004) and silver (Yashchuk *et al*. 2002). Therefore, the powder dispensing nozzles can be integrated onto the building platform of the material delivery system to feed different types of material.

Although many studies have demonstrated the success of this method, more work is required to investigate and improve it. The material flow rate in dry powder dispensing is not so high which is ideal for high resolution patterning but makes the process slow. Multiple nozzles have been proposed to increase the speed of dispensing (Das *et al*. 2009). In addition, powder flow is difficult to calculate theoretically and the stability of the process is poor (Jiang *et al*. 2009). To meet the requirements in terms of processing time and dispensing repeatability and powder compaction, developments should be carried out. (Yang and Evans 2007) have provided a comprehensive review on dry powder dispensing. More details of recent research will be reported in part 2 of our paper.

2.8.4 Shape deposition manufacturing (SDM)

Shape Deposition Manufacturing (SDM) is a hybrid layer-by-layer process that sprays molten material in near net shape onto the substrate, then uses subtractive processes to remove unwanted material (Pham and Dimov 2001). This process was introduced by researchers at Carnegie Mellon University for creating multi-material metal parts (e.g. copper and stainless steel) (Weiss *et al*. 1997) and was subsequently extended at Stanford university for polymer and ceramic parts (Cooper *et al*. 1999). The technology can fabricate multi-material parts by stacking different material layers but there are no multiple materials in the same layer. In SDM, parts or assemblies are built up through a cycle of alternating layers of structural and support material. Unlike most other MMAM processes, SDM shapes each layer of material on a computer-controlled milling machine

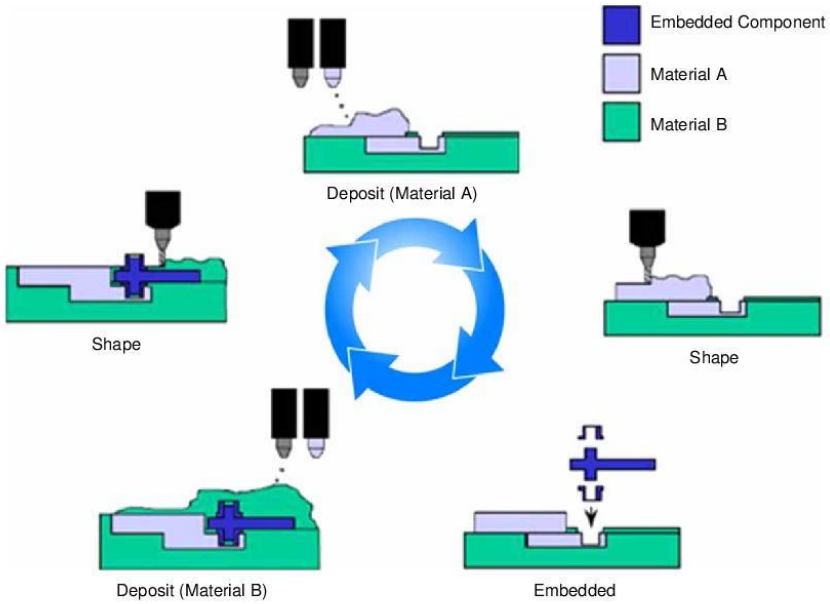

Figure 14. Shape Deposition Manufacturing diagram (modified (Cham *et al*. 1999)).

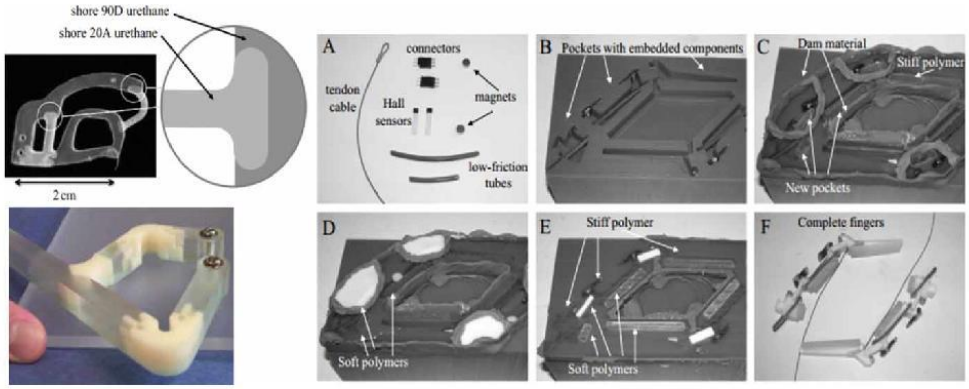

Figure 15. Left is a robot part combining soft and hard materials (Bailey *et al.* 2000, Cutkosky and Kim 2009); Right are the steps of SDM integrating different polymer materials for various functions according to each component: a) The components; b) The pockets corresponding to the shape of the stiff links are machined into a support material; c) The components are put into place in the pockets and the dam material is used to block the resin; d) The soft polymer resin is poured to cover the first group components; e) After the layer cures, the block is faced off to level the surface; f) the complete multi-material parts are removed from the support material (Dollar *et al.*, 2006).

after it is deposited (Figure 14). This approach allows for tolerances of $\pm$ 0.01 mm and avoids the stair-stepping effect of additive processes. The intermittent addition of sacrificial support material allows for the construction of nearly arbitrary geometries and facilitates the inclusion of embedded components (Cutkosky and Kim 2009). Interesting capabilities of SDM include the fabrication of parts with embedded electronic and mechanical components and of complete mechanisms in a preassembled configuration as shown in Figure 15. Some researchers use this technique to fabricate multiple material structures that combine rigid materials, compliant materials and integrate sensors and other discrete components (Dollar and Howe 2006, Cutkosky and Kim 2009) that allow components to be embedded, decreasing the damage to sensor components by encasing them within the part structure and removing the need for assembly (Weiss *et al.* 1996, Dollar *et al.* 2006). However, SDM has not been widely adopted as there are several major obstacles such as the experimental nature of the process, and lack of knowledge about SDM in the design community that must be overcome. The challenge of educating designers about these techniques, however, is not being sufficiently addressed (Binnard and Cutkosky 2000).

3. Impacts and applications

AM has been identified by many national agencies as one of the strategic technologies which will play an important role in the high-value manufacturing economy. In the same way, MMAM can offer more advantages and open more opportunities to meet future challenges, and enable business competency to respond to changing global trends and new market drivers. Single material AM systems cannot fulfil the requirements of some applications that require multiple material objects from one machine, such as compliant mechanisms, embedded components, 3D circuits, human tissues, medical compatible implants etc. The novel MMAM technology has the potential to offer these merits:

- *Design freedom:* The powerful benefit of this technology is in offering freedom of design and creation. With MMAM, it is possible to define specific material properties in the design. The freedom to design without constraints allows designers to create varieties of shape and functions in a single part that would be impossible to produce by any traditional manufacturing processes. Moreover, it can make design compact. The system can reduce the size of electronic systems by producing fine feature circuitry, embedded components and miniaturised devices, a reduction of excess space can have a significant effect by producing smaller parts and requiring minimum space.
- *Design protection:* MMAM can easily create the protection of products. This technique is suitable for products that require high security or need protection for commercial purpose because every component is attached in a single object and is hard to disclose. Multiple materials can provide a unique 'finger print' in each part to protect new products from reverse engineering by using large numbers of material combinations.

- *Increased functionality:* Direct Digital Manufacturing (DDM) is currently a major goal of many AM vendors and application researchers. A problem that has always faced manufacturers looking at DDM is that AM produced parts are generally inferior in performance compared with similar parts made using conventional manufacturing technologies. DDM benefits are mainly in terms of geometry, speed and cost. Using multiple materials with the possibility of functional gradients provides a means to create parts that are not directly competitive but in fact provide additional functionality to components. MMAM allows designers to create parts with complex functions and high capabilities. Material integration and material property tailoring can enable the creation of new products, through the design and integration of innovative material. Furthermore, it can embed electronic components to create new functional parts and superior value systems. For example, moulds and dies can integrate conformal cooling channels that have high heat transfer properties and high strength properties in the external structure. This method can embed sensors for structural health or other monitoring purposes.
- *Elimination of assembly:* A product comprised of various components can be fabricated in one build, eliminating fasteners and assembly labour, especially for the electronic industry. The cost-related processes such as fabrication, inspection and paperwork are eliminated. Also, the costs of material and associated fastening components can be greatly diminished. Consequently, the process is more streamlined and highly productive.
- *Efficient manufacturing system:* The new manufacturing process enables the fabrication of 3D functionally complex structures within a single integrated manufacturing environment. That can reduce some of the procedures or change the time between processes that are required in conventional processes. Besides, traditional manufacturing processes require more energy consumption. MMAM technology reduces material usage, produces minimal waste and utilises less energy. That provides more cost-effective manufacturing enabling green manufacturing.

The use of discrete multi-materials within single components may be viewed as a technically challenging and economically favourable manufacturing method that can enable unprecedented levels of functionality and adaptability. By using multi-material components, economic and lightweight designs may be achieved via the reduction of assembly processes and parts required. The automotive industry has already begun taking advantage of multi-material designs in numerous applications (e.g., multi-coloured tail-lights, components with compliant hinges) (Espalin *et al.* 2012).

The aerospace industry shows interest in the development of multiple material objects because the cost of launching depends on the weight lifted into space. Also, an optimal design for weight and performance can decrease costs. Moreover, a safety perspective is always a concern in the mission. The heat shield of space shuttles could be designed to increase reliability by using multiple material components (Gibson *et al.* 2010, Zhou *et al.* 2011).

In the medical sector, implants make use of the mechanical properties of alloys or ceramics and composites and would benefit from grading with biocompatible materials. Thus an implant can benefit from a strong and tough material in the core, material compatible with bone tissue around the surface and material with low friction around the joint area. In tissue engineering, the possibility of creating multiple cellular structures using printing technology could eventually lead to the creation of artificial replacement organs. The challenges are immense, but the possible benefits are also huge and the knowledge gained along the way may also spill into other areas (Gibson *et al.* 2010, Zhou *et al.* 2011). Cell-based printing techniques have been intensively investigated in recent years and many innovative approaches such as organ bioprinting (Mironov *et al.* 2007), laser writing of cells (Schiele *et al.* 2009), bio-electrospraying (Jayasinghe 2007), and Biological Laser Printing (BioLP) (Barron *et al.* 2004) have surfaced to complement limitations in scaffold-based tissue engineering.

Several inkjet and extrusion-based systems such as the 3D bioplotter described earlier can serve as a bioprinter, if sterile conditions can be acquired. Current inkjet printing systems suffer from loss of cell viability and clogging. To overcome these limitations, Moon *et al.* (2010) developed a bioprinter based on inkjet technology that uses mechanical valves to print 3D high viscosity hydrogel precursors containing smooth muscle cells. Their bioprinting platform enabled printing of multi-layered 3D cell-laden hydrogel structures as well. Nakamura *et al.* (2011) developed a custom-made 3D bioprinter using inkjet technology for printing living cells and hydrogel. In a rather similar way, Xu *et al.* (2013) developed a versatile method for fabricating complex and heterogeneous 3D tissue constructs using simultaneous ink-jetting of multiple cell types. The biological functions of the 3D printed constructs were evaluated in vitro and in vivo. Each of the printed cell types maintained their viability and normal proliferation rates, phenotypic expression, and physiological functions within the heterogeneous constructs.

Extrusion-based systems are also being used efficiently for multi-material bioprinting. Lee *et al.* (2009) present a method to create multi-layered engineered tissue composites consisting of human skin fibroblasts and keratinocytes which mimic skin layers. The production of 3D cell-laden structures using various scaffold-free cell printing technologies has opened up new possibilities. However, ideal 3D

complex tissues or organs have not yet been printed because gel-state hydrogels have been used as the principal material and are unable to maintain the desired 3D structure due to their poor mechanical strength. A new hybrid scaffold consisting of poly(ε-caprolactone) (PCL) and cell-embedded alginate struts has been designed by (Lee *et al.* 2013). The PCL and alginate struts are stacked in an interdigitated pattern in successive layers to acquire a 3D shape. The hybrid scaffold exhibits a two-phase structure consisting of cell (MC3T3-E1)-laden alginate struts able to support biological activity and PCL struts able to provide controllable mechanical support of the cell-laden alginate struts.

Figure 16 shows an example of hybrid scaffolds produced by Shim *et al.* (2012) using PCL which shows relatively high mechanical properties as compared with hydrogel, as a framework for enhancing the mechanical stability of the bioprinted construct. Two different alginate solutions were then infused into the previously prepared framework consisting of PCL to create the 3D construct for osteochondral

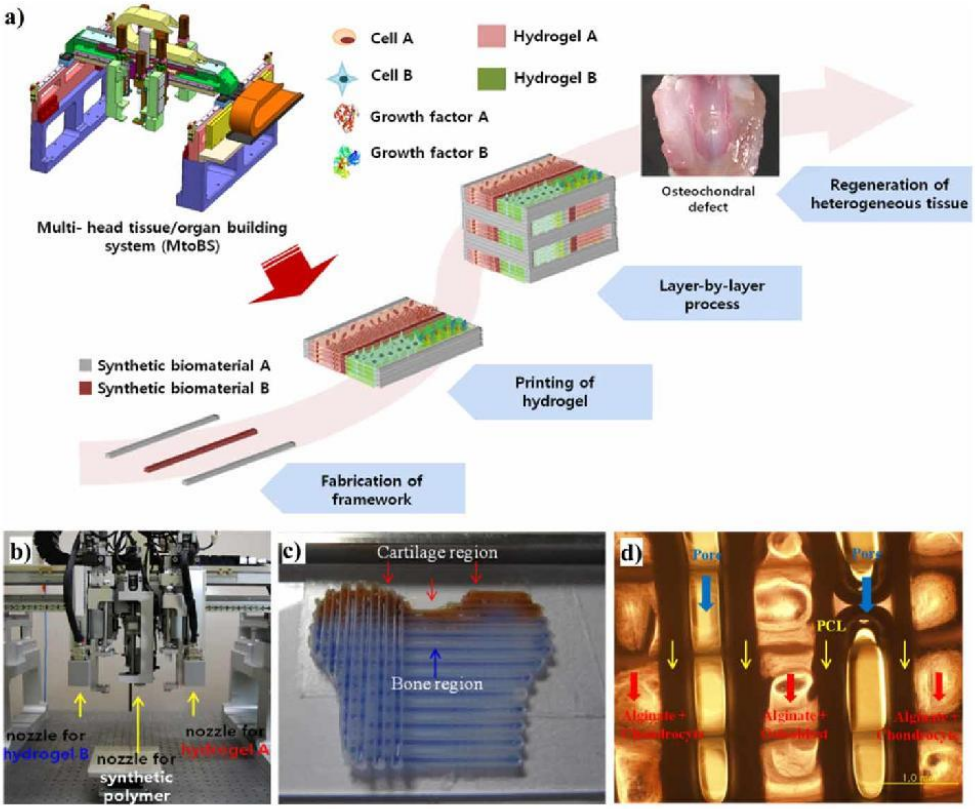

Figure 16. a) Schematic diagram of the bioprinting process using MtoBS. First, a framework made up of synthetic biomaterials such as PCL and PLGA is fabricated to support the entire mechanical stability of 3D tissue or organ. Second, the hydrogel which is able to encapsulate cells and growth factors is dispensed into the pores. The sequential dispensing of synthetic biomaterials and hydrogel is repeated and stacked to build a 3D tissue or an organ; b) MtoBS dispensing parts: Six dispensing heads are equipped for dispensing of relevant biomaterials in the MtoBS. Three heads, where one is for synthetic biomaterials and the remaining two are for hydrogel, are symmetrically installed at each side (front and rear sides) to make up the six heads of the MtoBS; c) A conceptual 3D osteochondral structure made up of PCL and two different alginates. Cartilage and bone regions are filled with red stained alginate and blue stained alginate, respectively; d) Image of the bioprinted structure using chondrocyte and osteoblast encapsulated in the alginate. Every second pore is filled with alginate. The others are empty for oxygen and nutrient transportation (Shim *et al.* 2012).

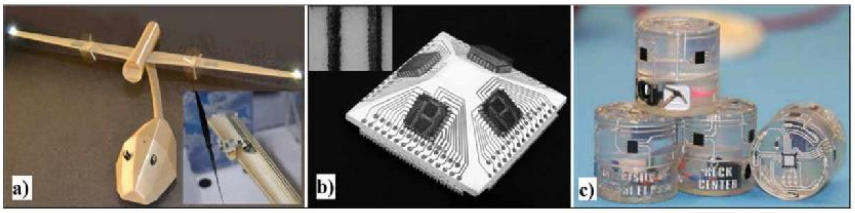

Figure 17. a) Circuits, sensor, and antenna printed with Aerosol Jet on unmanned aerial vehicle (UAV) structure which was printed with Stratasys FDM (Paulsen *et al.* 2012); b) Ceramic Inertial Measurement Unit with four gyroscopes and circuit patterns. 3DP was used for the ceramic layer manufacturing process, and inkjet printing was used for the printing of silver ink for circuit patterns (silver line, 300 μm) (Johander *et al.* 2007); c) 3D component placement and routing for electronic integration using a SLA technique to create a dielectric substrate and using a DW technique to dispense conductive inks onto the substrate (Lopes *et al.* 2012).

printing. For this work, a multi-head tissue/organ building system (MtoBS), which was particularly designed to dispense thermoplastic biomaterial and hydrogel having completely different rheology properties, was developed and used to bioprint osteochondral tissue.

Fabricating biohybrid cantilevers and actuators with hydrogels and cardiac cells using a multi-material SL process has also been reported (Chan *et al.* 2012). The multi-material capability of the SL system can be used to change the synthetic material composition or insert cells and proteins at precise locations on the structure. Cell-encapsulated hydrogels with complex (3D) structures were fabricated from photopolymerisable poly(ethylene glycol) diacrylate (PEG-da) using modified 'top-down' and 'bottoms-up' versions of a commercially available SL system (Chan *et al.* 2010).

There is also the possibility to integrate two or more AM processes to make multiple materials or embed components. Printing of tailor made inks using inkjet printing or aerosol jet processes on the 3D surface produced previously by other AM techniques is a typical approach which has opened up new opportunities. Inks from a variety of materials including semiconductors, dielectric polymers, conductive metals, resistive materials, piezoelectric, battery elements, capacitors, and biological materials can be used for direct writing on 3D surfaces. Figure 17 shows some examples of the combination of AM and DW technologies to produce a final products with embedded components. In fact, many multiple-material systems are likely to be hybrid rather than using a single category of material or process.

Using a multiple material SL process, the optical, electrical and mechanical properties of photocurable polymers can be combined. This would advance polymer Microelectromechanical Systems (MEMS) technology and make a substantial contribution to microoptics and microchemical devices for BioMEMS (Maruo *et al.* 2001). microTEC is a company moving towards rapid micromanufacturing using the micro SL process and has demonstrated interesting results along the way. microTEC's unique 3D Chip Size Packaging (3D-CSP) technology is used to integrate, interconnect, and protect bare dies or other microelectronic elements to get a complete multifunctional system. No wire bonding is needed; interconnection is realised by microstructured metal layers; 3D ultrahigh-density integration is possible; and cooling channels can be integrated to cool hot spots. 3D-CSP technology in combination with Rapid microproduct development (RMPD) makes an efficient rapid micromanufacturing approach which is applied to many applications, such as life science (e.g., lab on a chip microfluidics), sensor technology (e.g., food control solutions), consumer electronics (e.g., very slim connectors for smart cards), micromechanical parts for metrology tools, etc. RMPD technology is a projection SL

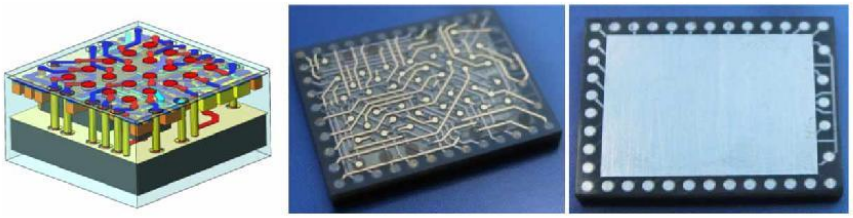

Figure 18. A complete 3D transceiver module in smallest space ($5.2 \times 5.2 \times 2.2$ mm^3) for wireless solutions fabricated using integrated SL and 3D-CSP process (www.microtec-d.com).

which has been invented by microTEC GmbH and the technologies are not based on US-patented DMD^2. Figure 18 shows an example of microTEC's integrated RMPD and 3D-CSP applications in rapid micromanufacturing of multiple material/embedded microsystems.

Material jetting systems seem currently to be the most successful MMAM process among AM technologies. To date, fabrication of true 3D multiple material polymeric components using material jetting processes has been demonstrated. 3D parts by commercially available MMAM systems such as Objet's Connex prove that. Moreover, the ability of inkjet printing technology to produce micro-parts from a wide range of materials including optical polymers, solders, thermoplastics, light-emitting polymers, organic transistor, biologically active fluids, and precursors for chemical synthesis has been demonstrated. Inkjet printing can be used for 3D metal-insulator-metal crossovers (Sanchez-Romaguera *et al.* 2008) and in combination with the printed electronics technology makes it possible to manufacture multi-material Microelectromechanical Systems (MEMS) components (Subramanian *et al.* 2005, Ko *et al.* 2007). Ahn's group investigated the design and manufacture of printed circuits using extrusion freeforming of lead-based alloy having low melting temperature and insulating polymer (Kim *et al.* 2009).

4. Challenges and future trends

As a consequence of what has been discussed above, MMAM processes enable new types of design and manufacturing previously impossible while offering cost reduction on specific types of products. Conventional manufacturing technologies have still a justification for their existence and are often a preferable approach in many cases in terms of cost, time, functionality, and reliability. But MMAM technologies can be an effective tool when there is complexity in terms of both shape and material. Choosing the right MMAM process to be used needs a comprehensive knowledge on capabilities and limitations of each process. A comparison of MMAM systems is presented in Table 2.

Several research centres and institutes have been developing MMAM technologies to allow more materials to be used in a single process. Most of the MMAM systems discussed in this paper are still being investigated as research projects. There is still much effort to be made to incorporate multiple materials into AM commercially. In this section, some of the challenges that need to be faced so that MMAM becomes more widespread will be discussed. The general improvements and technological barriers that need to be considered in MMAM processes are as follows:

- *Contamination:* Contamination in the material feeding system when changing to a different material is an important issue in most MMAM systems. This makes the processes imperfect and the reuse of materials difficult.
- *Bonding:* Bonding of dissimilar materials has often been a challenging issue even in conventional manufacturing techniques. In the same way, achieving a good bond between dissimilar layers in MMAM is a matter that needs to be taken into consideration.
- *Data processing:* Most AM systems currently take STL files as standard input which is a surface approximation only and there is no information of the material content. A demand for a powerful Computer-Aided Design (CAD) system for multiple material pre-processing has appeared so that the operator is able to identify the type of materials from region to region in a part.
- *Process interruption:* Using multiple materials in a single process may cause some interruption and loss of time in some MMAM or hybrid processes (e.g. SL process or embedded component) due to material/component changeover during the build process. The challenge is to ensure that applying multiple materials or extra components causes the least interruption in the process.
- *Hybrid and multi-axis systems:* Some AM processes do not have high potential for multiple materials processing but they possess good capability to be integrated with other AM or conventional techniques to create an efficient hybrid system. For example, dry powder printing can be integrated with a laser sintering process to make multi-materials. Moreover, processes such as LENS, FDM, and LOM have all been shown to benefit from the additional complexity of motion. Integrating different processes is a challenge.
- *Materials development:* In addition to the creation of a wider range of blended composites, other forms of multiple material systems will possibly come into use. This indeed could be the most interesting development as electrically or thermally conductive, semiconductor, liquid crystal, carbon nanotubes, functional ceramics, etc., come into use. In addition to the further development of embedded technologies, sensors can even be created from their fundamental material components within the part itself using direct write (Gibson *et al.* 2010).

A MMAM system should consist of at least two main subsystems: multi-material delivery and layer bonding systems (Figure 19a). In some processes, such as materials jetting, both of these two steps are accomplished simultaneously; while in some others such as SLS or 3DP, the two steps need to be implemented one by one. Although most of the single material AM systems also consist of materials delivery and layer bonding systems, in MMAM, these two subsystems could be very different.

Table 2. Comparison of different MMAM systems.

Category	Techniques	Advantages	Disadvantages	Bonding Interface	Materials resolution	Capability of multiple materials printing	Material solidification and bonding in layer
Photopolymer Vat	Scanning SL	High dimensional accuracy, offering transparent materials, living cells can be incorporated	Only photopolymers, time consuming materials changing, material contamination and waste in process	Between and within layers	Low	Good	Point by point
	DMD[2]-based SL	Same as scanning SL	Same as scanning SL	Between and within layers	Low	Good	Whole layer once
Material extrusion	Material extrusion with melting	Fast, no toxic materials, good material properties	Low dimensional accuracy, delamination, weak bonding between dissimilar polymers	Between and within layers	Medium	Good	Line by line
	Material extrusion without melting	Easy and cheap mechanism, no trapped materials, low material waste, fair fabrication speed, living cells can be incorporated	Relatively low dimensional accuracy and mechanical strength	Between and within layers	Medium	Good	Line by line
Powder bed fusion	SLS	Wide range of materials, great material properties, high materials strength	Thermal stress, degradation, accuracy limited by the particle size of materials, material contamination when changing to other materials, require atmosphere control for metals	Between layers	Low	Fair	Point by point
Directed energy deposition	LENS DMD[1] LC	Wide range of materials, great material properties	Low dimensional accuracy, thermal stress, require atmosphere control, require machining process for finishing the part	Between and within layers	High	Fair	Point by point
Sheet lamination	LOM	Fast process, accuracy in Z-axis is lower than SL and SLS	Shrinkage, great amount of scrap, delamination, require changeover when changing other materials, require pyrolysis process	Between layers	Low	Fair	Plane
	UC	High dimensional accuracy, Fast process, Low temperature effects	Wastage of material in the machining process, delamination, only metals, require changeover when changing other materials	Between layers	Low	Good	Plane
Material jetting	Inkjet Printing	Fast process, wide range of materials, materials mixing on droplet scale	Limited to jettable materials, clogging problem, low viscosity prevents build-up in 3D	Between and within layers	High	Very Good	Point by point
	PJT	Fast process, wide range of materials, materials mixing in droplet scale	Limited to jettable photopolymers, clogging problem	Between and within layers	High	Excellent	Multi-Point
Binder jetting	3DP	Low temperature process, fast process	High porosity, low surface quality, accuracy limited by the particle size of materials, difficult to remove trapped materials	Between and within layers	Medium	Poor	Point by point
Hybrid & DW	LCVD	high-resolution process, metals and semiconductors	Low-deposition rate, toxic/explosive gas might be involved	Between and within layers	Medium	Poor	Point by point
	Aerosol Jet Printing	High resolution, wide range of materials, ability of writing in 3D space, ideal for deposition of biological inks, noncontact, easy material handling	Solvent involved, Shield gas may blow off powders when integrated with powder bed systems	Between and within layers	High	Good	Line by line
	SDM	Wide range of materials	Require machining process during fabrication, feature size is limited by cutting tool	Between and within layers	Low	Fair	Line by line
	DPP + binder printing or laser sintering	Wide range of materials, possible complex materials and geometry control	Limited to good flowability powders, overflow problem, low compaction density of discharged powders	Between and within layers	High	Good	Point by point

The first step is to deliver multiple materials. Some MMAM systems can vary materials between layers and some have the ability to deposit and bond several materials within a layer. Figure 19b shows the typical configurations of different ways to make a multiple-materials parts using MMAM systems. The most promising MMAM system should be able to vary materials between and within layers to make multi-oriented interfaces.

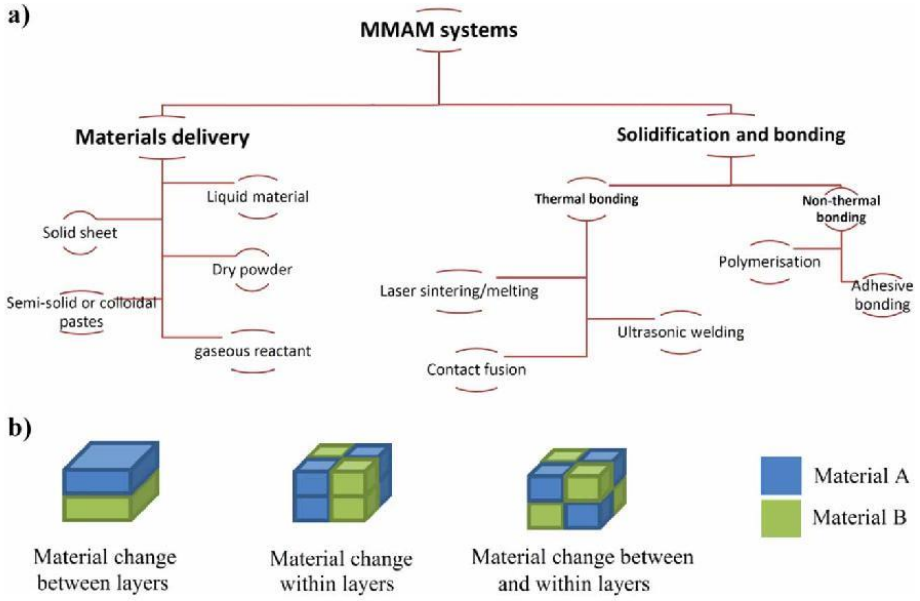

Figure 19. a) MMAM main subsystems and b) different kinds of multiple-materials parts.

Materials can be delivered in different forms: dry powder (SLS, LENS, SLM, and 3DP), semi-solid or colloidal pastes (FDM and other extrusion-based systems), liquid material (SL and ink jet printing), solid sheet (LOM, ultrasonic consolidation), and gaseous reactant containing build material (LCVD). Material state and delivery mechanism bring some limitations to each process for multiple material fabrication. For example in Objet only blends of similar monomers with good mixing capacity in the liquid state can be used. In FDM it is very difficult to get such high viscous semi-solid mixes (probably achievable using a static mixer but the mixing range is limited and materials are wasted during purging when changing composition). Solid sheets cannot mix between layers but a change of materials can be achieved by changing sheets, although atomic level of diffusion and mixing can occur at the layer interface. Chemical vapor deposition (CVD) is good for different materials but in order to change materials the majority of the gas in the chamber needs to be changed. Although localized supplying of gas has been used to supply mixtures without changing the whole chamber of gas, it is difficult and expensive to recycle and reuse the gas. A liquid vat has very limited capacity to manufacture complex discrete MMAM and almost no capacity for mixing. Powder-based systems such as SLS, SLM, and 3DP have limited capacity to change materials unless the powder dispensing method is changed as was discussed. Moreover, 3DP does not seem to be successful in changing material composition by just changing inks. A key factor in the material delivery system is to deliver material fast, accurately, and with the ability to change materials both between and within layers. Another issue in MMAM could be to level layers after the deposition of different materials, if the materials delivery system is not accurate enough.

In MMAM, the bonding between different materials could be a very challenging issue compared with single materials AM. The bonding methods can be thermal bonding (sintering/melting, ultrasonic welding or contact fusion) and non-thermal bonding (polymerisation or adhesive bonding). A key factor in a layer bonding system is to ensure enough bonding between different layers and different materials. However, differences in the physical properties of materials (for example thermal expansion rate, melting or sintering temperature), chemical properties (for example chemical bond, Van der Waals forces) and bonding methods (for example polymerisation, laser sintering/melting) are the main reasons that make it difficult to bond dissimilar materials in MMAM. For example, in the ultrasonic consolidation of solid sheet method, it is very difficult to bond polymers and metals but it's possible to bond different metals with different melting temperatures. In the materials jetting method it is difficult to jet and bond polymers and metals (except metals with very low melting points).

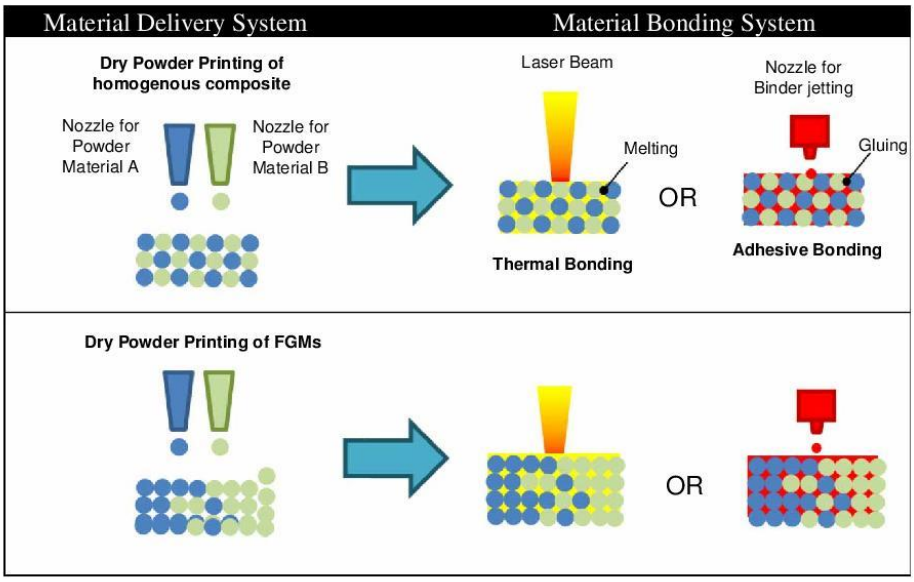

Figure 20. Incorporating dry powder printing with laser sintering and binder jetting systems.

Potential challenges that need to be addressed in future work on the SL process can be identified as material contamination, build speed, material waste, material bonding, trapped air and bubbles, accuracy and resolution. For multi-material fabrication, process planning plays an important role in the SL process. In particular, bond strength between different types of resins (e.g. acrylic resins and conductive polymers) may be an issue for future development of the multi-material MIP-SL process.

There have also been attempts at using powder-based AM systems such as SLS and 3DP for multi-material fabrication. However, the accurate material feeding and recoating required by digital material fabrication is difficult to design into the powder-based processes. Using dry powder dispensing techniques instead of conventional powder recoating can be a good solution to overcome the problem of handling fine powder. Dry powder dispensing systems (especially ultrasonic nozzle dispensing systems) have demonstrated their great ability to precisely place fine powders. It is believed that employing a selective dry powder dispensing mechanism incorporated with current powder-based systems, including SLS and binder jetting systems, would be an efficient measure to solve the problem of fine powder handling as well as increasing their capability of producing multi-material parts with lateral material change (Figure 20). In this way, a higher level of material deposition control could be obtained which is very attractive and is an issue in much demand for TE scaffold fabrication. Moreover, it is possible to incorporate growth-factors and fabricate controlled-release scaffolds, using subsequent bonding methods in which temperature is carefully controlled to avoid inactivation of proteins and degradation of polymers. On-going work in our laboratory is focused on incorporating dry powder printing with the SLS process so as to extend the approach to multi-material micromanufacturing areas. A challenge in this method is heat management in which laser power needs to be carefully controlled to avoid degradation and remelting of a low melting point component. The feasibility of bonding metal on polymers has been demonstrated by laser microcladding of silver paste on resin board (Zeng *et al.* 2006).

Material jetting systems are currently being used mostly for polymer jetting so that there is a limitation on the number of materials since only jettable polymers that have good flowability at restricted temperatures can be used. In particular, processes such as Objet's PolyJet technology have inherent limitations on the selection of base materials since the jetted liquid needs to have certain properties of viscosity and curing temperatures in order to be jetted. However, the resolution of the process should be improved to expand its range of applications. More emphasis should be placed on the development of inkjet printing systems which are able to produce high-quality true 3D multiple-material components from functional materials, such as

Table 3. Summary of research work that has been performed on MMAM using hybrid systems.

Technology	Material	Institution	Reference
SLA + DW	Photopolymer, silver-based ink	University of Texas, USA	(Lopes *et al.* 2012)
FDM + DW	Thermoplastic, silver-based ink	Stratasys and Optimec Inc., USA	(Paulsen *et al.* 2012)
UC + DW	Polymer, silver-based ink	Utah State University and University of Texas and Sandia National Laboratories, USA	(Robinson *et al.* 2006)
FDM + UC	Thermoplastic, silver-based ink	Utah State University, USA	(Swank *et al.*, 2009)
FDM + Robocasting	Thermoplastic, low-melting-point alloys and a variety of gels and slurries	Cornell University, USA	(Malone and Lipson, 2004, Periard *et al.* 2007, Malone and Lipson 2008)
DW + Electrophoretic Deposition	Aluminium, copper oxide	Lawrence Livermore National Laboratory, USA	(Meissner 2012)

metals, ceramics, and smart materials so as to be able to achieve the required thermal, mechanical, and electrical properties for the MEMS/Micro-Opto-Electro-Mechanical Systems (MOEMS) industry. The applications of inkjet printing in multiple materials fabrication will expand with the emergence of new jetting techniques such as electrostatic and with better understanding of the process and the utilisation of efficient modelling techniques. Future work may focus on the fabrication of true 3D parts with high accuracy and improved surface finish by using multi-material printing processes based on tailor made inks. As for ceramics printing, future work can concentrate on the utilisation of inkjet printing in an innovative way for manufacturing various components, such as: multi-layered ceramics (capacitors, sensors, and actuators), 3D electronic ceramic components (high-temperature cofired ceramic and low-temperature cofired ceramic), and conductive layers on ceramic (photovoltaic components and thick film electronics) (Vaezi *et al.* 2012).

Regarding the extrusion-based systems, precise control of extrusion in melt-based extrusion freeforming systems would be an asset for multiple materials printing. Assembling multi type cells and biomimic extracellular matrix materials in a single construct is a promising method to regenerate complex tissues/organs in vitro. As described earlier, future work could focus on effective utilisation of multi-nozzle extrusion-based AM systems to produce living macro/microstructures with controlled compositions and improved accuracy. However, it should be noted that, technologically, bioprinting using AM techniques is still in its infancy. Different living structures have been produced using hydrogel structures containing viable cells, but the designs have been simple and isotropic, and mechanical properties were not satisfactory (Melchels *et al.* 2012).

Directed energy deposition and sheet lamination processes have demonstrated their potential for manufacturing both discrete multi-material and FGMs. However, there have been fewer reports on the utilisation of these classes of MMAM systems compared with other methods. Moreover, according to the statistics fewer research centres are dealing with these MMAM technologies than others (Wohlers 2011). This might indicate that they need much more improvement and are a longer way from becoming efficient approaches for multiple material manufacturing. Perhaps, hybrid and DW technologies such as aerosol jet process have been more successful in the field of multiple materials. A wide range of materials and complexity of parts are the most significant advantages of DW processes which make them a viable technology for further developments in the MMAM area. In particular, hybrid systems are being developed and becoming more widespread these days as they provide new possibilities. Table 3 presents research work that has been conducted on multiple material manufacturing using hybrid systems.

The next generation of MMAM technology should provide full functionality, offer changeable material systems, and provide the entire bonding system at an affordable price. Even if multi-layer or multiple materials can be made, there is still the need to be able to fabricate digital material in which different materials are interlocked with each other. For instance, the FDM process can naturally be extended to fabricate parts out of multi-materials since FDM has separate extrusion nozzles for the build and support materials. But the FDM process is not suitable currently for digital material fabrication. It is believed that future work will be mainly concentrated on making MMAM processes more favourable for rapid manufacturing of high performance products through improving MMAM processes with the aim of digital materials fabrication and integration of multiple AM processes to provide new possibilities.

5. Conclusion

Some products may require specific materials in a component structure to achieve different functional properties. MMAM technologies have the potential to become an important resource for the next generation of manufacturing technologies. Processes such as material jetting and extrusion freeforming techniques have shown very good compatibility with multiple material manufacturing. Material jetting systems are able to fabricate complex multi-material and FGMs with variable properties which have permitted a great advance in product design and manufacturing. Moreover, extrusion-based systems are being

employed widely in both scaffold-based and scaffold-free tissue engineering due to their unique capability to deposit a wide range of advanced biomaterials simultaneously. Some of the other MMAM techniques described in this paper still suffer from some inherent limitations for multiple material printing and need to be improved. On the other hand, hybrid and DW systems have demonstrated some promising results and it can be expected that their use will spread more in the near future.

Acknowledgments

The authors are grateful to Engineering Sciences, Faculty of Engineering and the Environment, University of Southampton, Invibio Ltd and The Royal Thai Government for supporting this work by providing research studentship to Mr. Mohammad Vaezi and Mr. Srisit Chianrabutra.

References

Allahverdi, M., *et al.*, 2001. Processing of advanced electroceramic components by fused deposition technique. *Journal of the European Ceramic Society*, **21**, 1485–1490.

Ang, T.H., *et al.*, 2002. Fabrication of 3D chitosan-hydroxyapatite scaffolds using a robotic dispensing system. *Materials Science and Engineering C-Biomimetic and Supramolecular Systems*, **20**, 35–42.

Arcaute, K., Mann, B., and Wicker, R., 2006. Stereolithography of three-dimensional bioactive poly(ethylene glycol) constructs with encapsulated cells. *Annals of Biomedical Engineering*, **34**, 1429–1441.

Arcaute, K., Mann, B., and Wicker, R., 2010. Stereolithography of spatially controlled multi-material bioactive poly(ethylene glycol) scaffolds. *Acta Biomaterialia*, **6**, 1047–1054.

Averyanova, M., Bertrand, P.H., and Verquin, B., 2012. Studying the influence of initial powder characteristics on the properties of final parts manufactured by the selective laser melting technology. *Virtual and Physical Prototyping*, **6** (4), 215–223.

Bailey, S.A., *et al.*, 2000. *Biomimetic robotic mechanisms via shape deposition manufacturing*. Godalming: Springer-Verlag London Ltd.

Bandyopadhyay, A., *et al.*, 2009. Application of laser engineered net shaping (LENS) to manufacture porous and functionally graded structures for load bearing implants. *Journal of Materials Science: Materials in Medicine*, **20**, 29–34.

Barron, J.A., *et al.*, 2004. Biological laser printing: a novel technique for creating heterogeneous 3-dimensional cell patterns. *Biomedical Microdevices*, **6**, 139–147.

Bartolo, P. and Bidanda, B., 2008. *Bio-materials and prototyping applications in medicine*. New York, NY: Springer.

Bartolo, P., *et al.*, 2012. Biomedical production of implants by additive electro-chemical and physical processes. *CIRP Annals - Manufacturing Technology*, **61**, 635–655.

Bartolo, P.J., 2011. *Stereolithography: Materials, processes and applications*. New York, NY: Springer.

Bartolo, P.J. and Mitchell, G., 2003. Stereo-thermal-lithography. *Rapid Prototyping Journal*, **9**, 150–156.

Beaman, J., *et al.*, 2004. *Assessment of European research and development in additive/subtractive manufacturing*. Final report from WTEC panel.

Beluze, L., Bertsch, A., and Renaud, P., 1999. Microstereolithography: a new process to build complex 3D objects. *Proceedings of the Society of Photo-Optical Instrumentation Engineers (SPIE)*, 808–817.

Bertsch, A., *et al.*, 1997. Microstereophotolithography using a liquid crystal display as dynamic mask-generator. *Microsystem Technologies*, **3**, 42–47.

Bidanda, B. and Bartolo, P., 2008. *Virtual Prototyping & Bio Manufacturing in Medical Applications*. New York, NY: Springer.

Billiet, T., *et al.*, 2012. A review of trends and limitations in hydrogel-rapid prototyping for tissue engineering. *Biomaterials*, **33**, 6020–6041.

Binnard, M. and Cutkosky, M.R., 2000. Design by composition for layered manufacturing. *Journal of Mechanical Design*, **122**, 91–101.

Brennan, R.E., *et al.*, 2003. Fabrication of electroceramic components by layered manufacturing (LM). *Ferroelectrics*, **293**, 3–17.

Cawley, J.D., 1999. Solid freeform fabrication of ceramics. *Current Opinion in Solid State and Materials Science*, **4**, 483–489.

Cesarano, J., 1999. A review of robocasting technology. *In*: D. Dimos, S.C. Danforth, and M.J. Cima, eds. *Solid freeform and additive fabrication*. Warrendale: Materials Research Society, 133–139.

Cham, J., *et al.*, 1999. Layered manufacturing with embedded components: process planning considerations. *DETC99: 1999 ASME Design Engineering Technical Conference*.

Chan, V., *et al.*, 2010. Three-dimensional photopatterning of hydrogels using stereolithography for long-term cell encapsulation. *Lab on a Chip*, **10**, 2062–2070.

Chan, V., *et al.*, 2012. Multi-material bio-fabrication of hydrogel cantilevers and actuators with stereolithography. *Lab on a Chip*, **12**, 88–98.

Cheng, Y., *et al.*, 2005. Development of dynamic mask photolithography system. *Proceedings of the 2005 IEEE International Conference on Mechatronics*, 2005 Taipei, Taiwan. 467–471.

Choi, J.-W., Kim, H.-C., and Wicker, R., 2011. Multi-material stereolithography. *Journal of Materials Processing Technology*, **211**, 318–328.

Choi, J.-W., Macdonald, E., and Wicker, R., 2010. Multi-material microstereolithography. *The International Journal of Advanced Manufacturing Technology*, **49**, 543–551.

Choy, K.L., 2003. Chemical vapour deposition of coatings. *Progress in Materials Science*, **48**, 57–170.

Chua, C.K., Leong, K.F., and Lim, C.S., 2010a. *Rapid prototyping: principles and applications*. Singapore: World Scientific.

Chua, C.K., Liu, A., and Leong, K.F., 2010b. A practical approach on temperature variation in selective laser melting with a novel heat transfer model. *In*: *Innovative Developments in design and manufacturing - Advanced research in virtual and rapid prototyping*. The Netherlands: CRC Press, 363–367.

Cooper, A.G., *et al.*, 1999. Automated fabrication of complex molded parts using mold shape deposition manufacturing. *Materials and Design*, **20**, 83–89.

Cooper, K.G., 2001. *Rapid prototyping technology: Selection and application*. New York: Marcel Dekker.

Crocker, J., *et al.*, 1998. Using SALDVI and SALD with multi-material structures. *JOM*, **50**, 21–23.

Cutkosky, M.R. and Kim, S., 2009a. Design and fabrication of multi-material structures for bioinspired robots. *Philosophical Transactions of the Royal Society a-Mathematical Physical and Engineering Sciences*, **367**, 1799–1813.

Daniel, P., Evan, M., and Hod, L., 2007. Printing embedded circuits. *Solid Freeform Fabrication Symposium*. Austin, Texas, USA.

Das, S., 2003. Physical aspects of process control in selective laser sintering of metals. *Advanced Engineering Materials*, **5**, 701–711.

Das, S., *et al.*, 2009. *Solid freeform fabrication of structurally engineered multifunctional devices*. (US 7,509,240 B2) United States patent application.

De Gans, B.J. and Schubert, U.S., 2003. Inkjet printing of polymer microarrays and libraries: instrumentation, requirements, and perspectives. *Macromolecular Rapid Communications*, **24**, 659–666.

Dollar, A.M. and Howe, R.D., 2006. A robust compliant grasper via shape deposition manufacturing. *IEEE-ASME Transactions on Mechatronics*, **11**, 154–161.

Dollar, A.M., Wagner, C.R., and Howe, R.D., 2006a. Embedded sensors for biomimetic robotics via shape deposition manufacturing. *2006 1st IEEE RAS & EMBS International Conference on Biomedical Robotics and Biomechatronics*, 763–768.

Domingos, M., *et al*., 2009. Polycaprolactone scaffolds fabricated via bioextrusion for tissue engineering applications. *International Journal of Biomaterials*, **2009**, 239643.

Domingos, M., *et al*., 2012. Effect of process parameters on the morphological and mechanical properties of 3D Bioextruded poly(epsilon-caprolactone) scaffolds. *Rapid Prototyping Journal*, **18**, 56–67.

Duty, C., Jean, D. and Lackey, W.J., 2001. Laser chemical vapour deposition: materials, modelling, and process control. *International Materials Reviews*, **46**, 271–287.

Espalin, D., *et al*., 2012. Multi-material, multi-technology FDM system. *SFF Symposium*, 2012, Austin, TX, USA.

Evans, J.R.G. and Yang, S., 2005. Flow rate of metal powders at reduced and elevated air pressure. *Powder Technology*, **154**, 95–98.

Friel, R.J. and Harris, R.A., 2010. A nanometre-scale fibre-to-matrix interface characterization of an ultrasonically consolidated metal matrix composite. *Proceedings of the Institution of Mechanical Engineers, Part L: Journal of Materials Design and Applications*, **224**, 31–40.

Gebhardt, A., 2003. *Rapid prototyping*. Munich, Germany: Hanser Gardner.

Gibson, I., 2006. *Advanced manufacturing technology for medical applications: Reverse engineering, software conversion and rapid prototyping*. West Sussex, England: Wiley.

Gibson, I., Rosen, D.W., and Stucker, B., 2010. *Additive manufacturing technologies*. New York, NY, USA: Springer.

Glardon, R., *et al*., 2001. Influence of Nd:YAG parameters on the selective laser sintering of metallic powders. *CIRP Annals - Manufacturing Technology*, **50**, 133–136.

Gomes, C.M., *et al*., 2009. Colloidal processing of glass–ceramics for laminated object manufacturing. *Journal of the American Ceramic Society*, **92**, 1186–1191.

Greulich, M., Greul, M., and Pintat, T., 1995. Fast, functional prototypes via multiphase jet solidification. *Rapid Prototyping Journal*, **1**, 20–25.

Grida, I. and Evans, J.R.G., 2003. Extrusion freeforming of ceramics through fine nozzles. *Journal of the European Ceramic Society*, **23**, 629–635.

Griffin, E.A., Mumm, D.R., and Marshall, D.B., 1996. Rapid prototyping of functional ceramic composites. *American Ceramic Society Bulletin*, **75**, 65–68.

Gu, D. and Shen, Y., 2009. Balling phenomena in direct laser sintering of stainless steel powder: metallurgical mechanisms and control methods. *Materials and Design*, **30**, 2903–2910.

Hadipoespito, G., *et al*., 2003. Digital micromirror device based microstereolithography for micro structures of transparent photopolymer and nanocomposites. *Proceedings of the 14th Solid Freeform Fabrication Symposium*, 2003, Austin, TX, USA, 13–24.

Han, L.-H., *et al*., 2010. Fabrication of three-dimensional scaffolds for heterogeneous tissue engineering. *Biomedical Microdevices*, **12**, 721–725.

Hon, K.K.B., Li, L., and Hutchings, I.M., 2008. Direct writing technology-Advances and developments. *CIRP Annals-Manufacturing Technology*, **57**, 601–620.

Hopkinson, N., Hague, R., and Dickens, P., 2006. *Rapid manufacturing: An industrial revolution for the digital age*. West Sussex, England: John Wiley & Sons.

Hsieh, C.-T. and Langrana, N.A., 2001. A System approach in extrusion-based multi-material CAD. *SFF Symposium*, 2001, Austin, TX, USA.

Ibrahim, M., *et al*., 2006. Inkjet printing resolution study for multi-material rapid prototyping. *JSME International Journal Series C Special Issue on Advanced Manufacturing Technology*, **49**, 353–360.

Inamdar, A., *et al*., 2006. Development of an automated multiple material stereolithography machine. *SFF Symposium*, 2006, Austin, TX, USA.

Jakubenas, K.J., Sanchez, J.M., and Marcus, H.L., 1998. Multiple material solid free-form fabrication by selective area laser deposition. *Materials and Design*, **19**, 11–18.

James Santosa, D.J.A.S.D., 2002. Experimental and numerical study on the flow of fine powders from small-scale hoppers applied to SLS multi-material deposition-Part I. *SFF Symposium*, 2002 Austin, TX, USA.

Jayasinghe, S.N., 2007. Bio-electrosprays: the development of a promising tool for regenerative and therapeutic medicine. *Biotechnology Journal*, **2**, 934–937.

Jiang, Y., *et al*., 2009. Development of measurement system for powder flowability based on vibrating capillary method. *Powder Technology*, **188**, 242–247.

Johander, P., *et al*., 2007. Layer manufacturing as a generic tool for microsystem integration. *4M2007 Conference Proceedings*, 2007 Borovets, Bulgaria.

Khalil, S., Nam, J., and Sun, W., 2005. Multi-nozzle deposition for construction of 3D biopolymer tissue scaffolds. *Rapid Prototyping Journal*, **11**, 9–17.

Kim, H., Choi, J.-W., and Wicker, R., 2010. Scheduling and process planning for multiple material stereolithography. *Rapid Prototyping Journal*, **16**, 232–240.

Kim, M.-S., *et al*., 2009. Direct metal printing of 3D electrical circuit using rapid prototyping. *International Journal of Precision Engineering and Manufacturing*, **10**, 147–150.

Klosterman, D., *et al*., 1998. Interfacial characteristics of composites fabricated by laminated object manufacturing. *Composites Part A: Applied Science and Manufacturing*, **29**, 1165–1174.

Klosterman, D.A., *et al*., 1999. Development of a curved layer LOM process for monolithic ceramics and ceramic matrix composites. *Rapid Prototyping Journal*, **5**, 61–71.

Ko, S.H., *et al*., 2007. All-inkjet-printed flexible electronics fabrication on a polymer substrate by low-temperature high-resolution selective laser sintering of metal nanoparticles. *Nanotechnology*, **18**, 345202.

Ko, S.H., *et al*., 2010. Metal nanoparticle direct inkjet printing for low-temperature 3D micro metal structure fabrication. *Journal of Micromechanics and Microengineering*, **20**.

Kruth, J.P., *et al*., 2007. Consolidation phenomena in laser and powder-bed based layered manufacturing. *CIRP Annals - Manufacturing Technology*, **56**, 730–759.

Kumar, P., *et al*., 2004. Direct-write deposition of fine powders through miniature hopper-nozzles for multi-material solid freeform fabrication. *Rapid Prototyping Journal*, **10**, 14–23.

Kumar, S., 2003. Selective laser sintering: a qualitative and objective approach. *JOM*, **55**, 43–47.

Kumar, S. and Kruth, J.P., 2010. Composites by rapid prototyping technology. *Materials and Design*, **31**, 850–856.

Laeng, J., Stewart, J. G. and Liou, F. W., 2000. Laser metal forming processes for rapid prototyping - A review. *International Journal of Production Research*, **38**, 3973–3996.

Landers, R. and Mulhaupt, R., 2000. Desktop manufacturing of complex objects, prototypes and biomedical scaffolds by means of computer-assisted design combined with computer-guided 3D plotting of polymers and reactive oligomers. *Macromolecular Materials and Engineering*, **282**, 17–21.

Lappo, K., Jackson, B., and Wood, K., 2003a. Discrete multiple material selective laser sintering (M^2SLS): experimental study of part processing. *SFF Symposium*, 2003, Austin, TX, USA.

Lappo, K., *et al*., 2003b. Discrete multiple material selective laser sintering (M^2SLS): nozzle design for powder delivery. *SFF Symposium*, 2003, Austin, TX, USA.

Lee, H., *et al.*, 2013. Cell(MC3T3-E1)-printed poly(∈-caprolactone)/alginate hybrid scaffolds for tissue regeneration. *Macromolecular Rapid Communications*, **34**, 142–149.

Lee, W., *et al.*, 2009. Multi-layered culture of human skin fibroblasts and keratinocytes through three-dimensional freeform fabrication. *Biomaterials*, **30**, 1587–1595.

Leu, M.C., Pattnaik, S. and Hilmas, G.E., 2012. Investigation of laser sintering for freeform fabrication of zirconium diboride parts. *Virtual and Physical Prototyping*, **7** (1), 25–36.

Li, G., *et al.*, 2005. Direct writing of chitosan scaffolds using a robotic system. *Rapid Prototyping Journal*, **11**, 90–97.

Li, L., *et al.*, 2008. Development of a drop-on-demand system for multiple material dispensing. *Automation and Logistics, 2008. ICAL 2008. IEEE International Conference*, 1–3 September 2008, 61–66.

Li, L., *et al.*, 2009. Development of a multi-nozzle drop-on-demand system for multi-material dispensing. *Journal of Materials Processing Technology*, **209**, 4444–4448.

Liew, C.L., *et al.*, 2001. Dual material rapid prototyping techniques for the development of biomedical devices. Part 1: Space creation. *The International Journal of Advanced Manufacturing Technology*, **18**, 717–723.

Liew, C.L., *et al.*, 2002. Dual material rapid prototyping techniques for the development of biomedical devices. Part 2: Secondary powder deposition. *The International Journal of Advanced Manufacturing Technology*, **19**, 679–687.

Liou, F.W., 2007. *Rapid prototyping and engineering applications: a toolbox for prototype development*. Boca Raton, US: CRC Press.

Liu, H.N. and Webster, T.J., 2011. Enhanced biological and mechanical properties of well-dispersed nanophase ceramics in polymer composites: from 2D to 3D printed structures. *Materials Science and Engineering C-Materials for Biological Applications*, **31**, 77–89.

Liu, L., *et al.*, 2008. Multinozzle low-temperature deposition system for construction of gradient tissue engineering scaffolds. *Journal of Biomedical Materials Research Part B-Applied Biomaterials*, **88B**, 254–263.

Liu, L., *et al.*, 2009. A novel osteochondral scaffold fabricated via multi-nozzle low-temperature deposition manufacturing. *Journal of Bioactive and Compatible Polymers*, **24**, 18–30.

Liu, V. and Bhatia, S., 2002. Three-dimensional photopatterning of hydrogels containing living cells. *Biomedical Microdevices*, **4**, 257–266.

Liu, W. and Dupont, J.N., 2003. Fabrication of functionally graded TiC/Ti composites by laser engineered net shaping. *Scripta Materialia*, **48**, 1337–1342.

Lopes, A.J., Macdonald, E., and Wicker, R.B., 2012. Integrating stereolithography and direct print technologies for 3D structural electronics fabrication. *Rapid Prototyping Journal*, **18**, 129–143.

Lu, K. and Reynolds, W.T., 2008. 3DP process for fine mesh structure printing. *Powder Technology*, **187**, 11–18.

Lu, X., *et al.*, 2006a. Dry powder microfeeding system for solid freeform fabrication. *SFF Symposium*, 2006, Austin, TX, USA.

Lu, X., Yang, S. and Evans, J.R.G., 2006b. Studies on ultrasonic microfeeding of fine powders. *Journal of Physics D: Applied Physics*, **39**, 2444–2453.

Lu, X., Yang, S., and Evans, J.R.G., 2009. Microfeeding with different ultrasonic nozzle designs. *Ultrasonics*, **49**, 514–521.

Malone, E. and Lipson, H., 2004. Solid freeform fabrication for autonomous manufacturing of complete mobile robots. *SFF Symposium*, 2004, Austin, TX, USA.

Malone, E. and Lipson, H., 2008. Multi-material freeform fabrication of active systems. *Proceedings of the 9th Biennial ASME Conference on Engineering Systems Design and Analysis ESDA08*, 2008, Haifa, Israel.

Malone, E., *et al.*, 2004. Freeform fabrication of zinc-air batteries and electromechanical assemblies. *Rapid Prototyping Journal*, **10**, 58–69.

Marga, F., *et al.*, 2012. Toward engineering functional organ modules by additive manufacturing. *Biofabrication*, **4**, 022001.

Maruo, S., Ikuta, K., and Ninagawa, T., 2001. Multi-polymer microstereolithography for hybrid opto-MEMS.*MEMS 2001, The 14th IEEE International Conference on Micro Electro Mechanical Systems*, 2001.

Matsusaka, S., Urakawa, M., and Masuda, H., 1995. Micro-feeding of fine powders using a capillary tube with ultrasonic vibration. *Advanced Powder Technology*, **6**, 283–293.

Meissner, C., 2012. *Materials by design: Science & technology review*. Lawrence Livermore National Laboratory: U.S. Department of Energy's National Nuclear Security Administration, USA.

Melchels, F.P.W., *et al.*, 2012. Additive manufacturing of tissues and organs. *Progress in Polymer Science*, **37**, 1079–1104.

Mironov, V., Prestwich, G., and Forgacs, G., 2007. Bioprinting living structures. *Journal of Materials Chemistry*, **17**, 2054–2060.

Moon, S., *et al.*, 2010. Layer by layer three-dimensional tissue epitaxy by cell-laden hydrogel droplets. *Tissue Engineering Part C: Methods*, **16**, 157–166.

Mott, M. and Evans, J.R.G., 1999. Zirconia/alumina functionally graded material made by ceramic ink jet printing. *Materials Science and Engineering: A*, **271**, 344–352.

Nakamura, M., *et al.*, 2011. Computer-assisted biofabrication: the challenges on manufacturing 3-D biological tissues for tissue and organ engineering. *VLSI Technology (VLSIT), 2011 Symposium*, 14–16 June 2011, 2–5.

Norotte, C., *et al.*, 2009. Scaffold-free vascular tissue engineering using bioprinting. *Biomaterials*, **30**, 5910–5917.

Obielodan, J.O., *et al.*, 2010a. Multi-material bonding in ultrasonic consolidation. *Rapid Prototyping Journal*, **16**, 180–188.

Obielodan, J.O., *et al.*, 2010b. Minimizing defects between adjacent foils in ultrasonically consolidated parts. *Journal of Engineering Materials and Technology*, **132**, 011006–8.

Obliers-Hommrich, B., *et al.*, 2008. Single- and multi-layer conductive patterns fabricated using M3D technology. *In*: S. Dimov and W. Menz, eds. *Multi-material micro manufacture, 2008 Cardiff University*. Scotland, UK: Whittles Publishing Ltd., 1–4.

Oxman, N., 2011. Variable property rapid prototyping. *Virtual and Physical Prototyping*, **6**, 3–31.

Paulsen, J.A., *et al.*, 2012. Printing conformal electronics on 3D structures with aerosol jet technology. *Future of Instrumentation International Workshop (FIIW)*, 8–9 October 2012, 1–4.

Pegna, J., 1995. Application of cementitious bulk materials to site processed solid freeform construction. *SFF Symposium*, 1995, Austin, TX, USA.

Pegna, J., *et al.*, 1999. The sand-painter: Two-dimensional powder deposition. *SFF Symposium*, 1999, Austin, TX, USA.

Periard, D., Malone, E., and Lipson, H., 2007. Printing embedded circuits. *SFF Symposium*, 2007, Austin, TX, USA.

Pham, D.T. and Dimov, S.S., 2000. *Rapid manufacturing - Technologies for rapid prototyping and tooling*. London: Springer-Verlag.

Pham, D.T. and Dimov, S.S., 2001. *Rapid manufacturing: The technologies and applications of rapid prototyping and rapid tooling*. London, UK: Springer-Verlag.

Pilleux, M.E., *et al.*, 2002. 3-D photonic bandgap structures in the microwave regime by fused deposition of multimaterials. *Rapid Prototyping Journal*, **8**, 46–52.

Qiu, D. and Langrana, N.A., 2002. Void eliminating toolpath for extrusion-based multi-material layered manufacturing. *Rapid Prototyping Journal*, **8**, 38–45.

Ram, G.D.J., *et al.*, 2007. Use of ultrasonic consolidation for fabrication of multi-material structures. *Rapid Prototyping Journal*, **13**, 226–235.

Ram, G.D.J., Robinson, C., and Stucker, B.E., 2006. Multi-material ultrasonic consolidation. *SFF Symposium*, 2006, Austin, TX, USA.

Regenfuss, P., Ebert, R., and Exner, H., 2007. Laser micro sintering, a versatile instrument for the generation of microparts. In: *Laser micro machining*. Weinheim: Wiley-VCH Verlag GmbH & Co. KGaA.

Regenfuß, P., *et al*., 2007. Principles of laser micro sintering. *Rapid Prototyping Journal*, **13**, 204–212.

Robinson, C.J., *et al*., 2006. Integration of direct-write (DW) and ultrasonic consolidation (UC) technologies to create advanced structures with embedded electrical circuitry. *SFF Symposium*, 2006, Austin, TX, USA.

Rodrigues, S.J., *et al*., 2000. Solid freeform fabrication of functional silicon nitride ceramics by laminated object manufacturing. *SFF Symposium*, 2000, Austin, TX, USA.

Sanchez-Romaguera, V., Madec, M.-B. and Yeates, S.G., 2008. Inkjet printing of 3D metal–insulator–metal crossovers. *Reactive and Functional Polymers*, **68**, 1052–1058.

Savalani, M.M., Hao, L., and Harris, R.A., 2006. Evaluation of CO2 and Nd:YAG lasers for the selective laser sintering of HAPEX®. *Proceedings of the Institution of Mechanical Engineers. Part B: Journal of Engineering Manufacture*, **220**, 171–182.

Schiele, N.R., *et al*., 2009. Laser direct writing of combinatorial libraries of idealized cellular constructs: biomedical applications. *Applied Surface Science*, **255**, 5444–5447.

Schuurman, W., *et al*., 2011. Bioprinting of hybrid tissue constructs with tailorable mechanical properties. *Biofabrication*, **3**, 021001.

Schwendner, K.I., *et al*., 2001. Direct laser deposition of alloys from elemental powder blends. *Scripta Materialia*, **45**, 1123–1129.

Seitz, H., *et al*., 2005. Three-dimensional printing of porous ceramic scaffolds for bone tissue engineering. *Journal of Biomedical Materials Research Part B: Applied Biomaterials*, **74B**, 782–788.

Sherwood, J.K., *et al*., 2002. A three-dimensional osteochondral composite scaffold for articular cartilage repair. *Biomaterials*, **23**, 4739–4751.

Shim, J.-H., *et al*., 2012. Bioprinting of a mechanically enhanced three-dimensional dual cell-laden construct for osteochondral tissue engineering using a multi-head tissue/organ building system. *Journal of Micromechanics and Microengineering*, **22**, 085014.

Shin, K.-H., *et al*., 2003. A method for the design and fabrication of heterogeneous objects. *Materials and Design*, **24**, 339–353.

Siggard, E.J., *et al*., 2007. Structurally embedded electrical systems using ultrasonic consolidation (UC). *SFF Symposium*, 2007, Austin, TX, USA.

Smay, J.E., *et al*., 2002. Directed colloidal assembly of 3D periodic structures. *Advanced Materials*, **14**, 1279–1283.

Stampfl, J., *et al*., 2004. Fabrication and moulding of cellular materials by rapid prototyping. *International Journal of Materials and Product Technology*, **21**, 285–296.

Stucker, B., 2011. Additive manufacturing technologies: technology introduction and business implications. *In*: *Frontiers of Engineering: Reports on Leading-Edge Engineering from the 2011 Symposium* The National Academies press, US, pp. 5–14.

Subramanian, V., *et al*., 2005. Progress toward development of all-printed RFID tags: materials, processes, and devices. *Proceedings of the IEEE*, **93**, 1330–1338.

Sun, J., *et al*., 2010. Performance characterization of drop-on-demand micro-dispensing system with multi-printheads. *Microsystem Technologies*, **16**, 2087–2097.

Swank, M.L. and Stucker, B.E., 2009. Investigation of support materials for use in ultrasonic consolidation. *SFF Symposium*, 2009, Austin, TX, USA.

Swank, M.L., *et al*., 2009. Integrating UC and FDM to create a support materials deposition system. *SFF Symposium*, 2009, Austin, TX, USA.

Takehiro, T. and Yoshiro, T., 1998. Excitation of a progressive wave in a lossy ultrasonic transmission line and an application to a powder-feeding device. *Smart Materials and Structures*, **7**, 417.

Tay, B.Y., Evans, J.R.G., and Edirisinghe, M.J., 2003. Solid freeform fabrication of ceramics. *International Materials Reviews*, **48**, 341–370.

Tolochko, N.K., *et al*., 2000. Absorptance of powder materials suitable for laser sintering. *Rapid Prototyping Journal*, **6**, 155–161.

Travitzky, N., *et al*., 2008. Preceramic paper-derived ceramics. *Journal of the American Ceramic Society*, **91**, 3477–3492.

Vaezi, M., Seitz, H., and Yang, S., 2012. A review on 3D micro-additive manufacturing technologies. *The International Journal of Advanced Manufacturing Technology*, 1–34.

Vamsi Krishna, B., *et al*., 2008. Functionally graded Co–Cr–Mo coating on Ti–6Al–4V alloy structures. *Acta Biomaterialia*, **4**, 697–706.

Vargas Garcia, J.R. and Goto, T., 2003. Chemical vapor deposition of iridium, platinum, rhodium and palladium. *Materials Transactions*, **44**, 1717–1728.

Vorndran, E., *et al*., 2009. 3D printing of β-tricalcium phosphate ceramics. *Dental Materials*, **25**, e18–e19.

Vozzi, G., *et al*., 2002. Microfabricated PLGA scaffolds: a comparative study for application to tissue engineering. *Materials Science and Engineering C-Biomimetic and Supramolecular Systems*, **20**, 43–47.

Wang, F., *et al*., 2004. Precision extruding deposition and characterization of cellular poly-epsilon-caprolactone tissue scaffolds. *Rapid Prototyping Journal*, **10**, 42–49.

Wang, J. and Shaw, L.L., 2006. Fabrication of functionally graded materials via inkjet color printing. *Journal of the American Ceramic Society*, **89**, 3285–3289.

Weiss, L., *et al*., 1996. Shape deposition manufacturing of wearable computers. *In*: D.L. Bourell, J.J. *et al*., eds., *Solid freeform fabrication proceedings, September 1996*. University of Texas, Austin, 31–38.

Weiss, L.E., *et al*., 1997. Shape deposition manufacturing of heterogeneous structures. *Journal of Manufacturing Systems*, **16**, 239–248.

Westberg, H., *et al*., 1993. Free-standing silicon microstructures fabricated by laser chemical processing. *Journal of Applied Physics*, **73**, 7864–7871.

White, D.R., 2003. Ultrasonic consolidation of aluminum tooling. *Advanced Materials and Processes*, **161**, 64–65.

Wicker, R., Medina, F., and Elkins, C., 2004. Multiple material microfabrication: extending stereolithography to tissue engineering and other novel applications. *SFF Symposium*, 2004, Austin, TX, USA.

Williams, K., *et al*., 1999. Freeform fabrication of functional microsolenoids, electromagnets and helical springs using high-pressure laser chemical vapor deposition. *Micro Electro Mechanical Systems, 1999. MEMS '99. Twelfth IEEE International Conference*, 17–21 January 1999, 232–237.

Windsheimer, H., *et al*., 2007. Laminated object manufacturing of preceramic-paper-derived Si-SiC composites. *Advanced Materials*, **19**, 4515–4519.

Wohlers, T., 2011. *Wohlers report 2011: Additive manufacturing and 3D printing, state of the industry*. Colorado, USA: Wohlers Associates.

Wohlers, T. 2012. *Wohlers report 2012: Additive manufacturing and 3D printing, state of the industry*. Colorado, USA: Wohlers Associates.

Woodfield, T.B.F., *et al*., 2004. Design of porous scaffolds for cartilage tissue engineering using a three-dimensional fiber-deposition technique. *Biomaterials*, **25**, 4149–4161.

Xie, D., *et al*., 2010. Multi-materials drop-on-demand inkjet technology based on pneumatic diaphragm actuator. *Science China Technological Sciences*, **53**, 1605–1611.

Xiong, Z., *et al*., 2001. Fabrication of porous poly(L-lactic acid) scaffolds for bone tissue engineering via precise extrusion. *Scripta Materialia*, **45**, 773–779.

Xiong, Z., *et al*., 2002. Fabrication of porous scaffolds for bone tissue engineering via low-temperature deposition. *Scripta Materialia*, **46**, 771–776.

Xu, T., *et al*., 2013. Complex heterogeneous tissue constructs containing multiple cell types prepared by inkjet printing technology. *Biomaterials*, **34**, 130–139.

Xuesong, L., *et al*., 2009. Fine lattice structures fabricated by extrusion freeforming: process variables. *Journal of Materials Processing Technology*, **209**, 4654–4661.

Xuesong, L., *et al*., 2010. Solvent-based paste extrusion solid freeforming. *Journal of the European Ceramic Society*, **30**, 1–10.

Yamaguchi, K., *et al*., 2000. Generation of three-dimensional micro structure using metal jet. *Precision Engineering*, **24**, 2–8.

Yang, H.Y., *et al*., 2008a. Dissolution characteristics of extrusion free-formed hydroxyapatite-tricalcium phosphate scaffolds. *Journal of Materials Science-Materials in Medicine*, **19**, 3345–3353.

Yang, H.Y., *et al*., 2008b. Sintering behaviour of calcium phosphate filaments for use as hard tissue scaffolds. *Journal of the European Ceramic Society*, **28**, 159–167.

Yang, S. and Evans, J.R.G., 2004a. Acoustic control of powder dispensing in open tubes. *Powder Technology*, **139**, 55–60.

Yang, S. and Evans, J.R.G., 2004b. A multi-component powder dispensing system for three dimensional functional gradients. *Materials Science and Engineering A (Structural Materials: Properties, Microstructure and Processing)*, **A379**, 351–359.

Yang, S. and Evans, J.R.G., 2007. Metering and dispensing of powder; the quest for new solid freeforming techniques. *Powder Technology*, **178**, 56–72.

Yang, S.F., *et al*., 2008c. Rapid prototyping of ceramic lattices for hard tissue scaffolds. *Materials and Design*, **29**, 1802–1809.

Yang, Y. and Li, X., 2003. Experimental and analytical study of ultrasonic micro powder feeding. *Journal of Physics D: Applied Physics*, **36**, 1349.

Yang, Y., Ram, G.D.J., and Stucker, B.E., 2006. Process parameters optimization for ultrasonically consolidated fiber-reinforced metal matrix composites. *SFF Symposium*, 2006, Austin, TX, USA.

Yashchuk, V.V., *et al*., 2002. Production of dry powder clots using a piezoelectric drop generator. *Review of Scientific Instruments*, **73**, 2331–2335.

Zeng, X., *et al*., 2006. Direct fabrication of electric components on insulated boards by laser microcladding electronic pastes. *IEEE Transactions on Advanced Packaging*, **29**, 291–294.

Zhang, Y., *et al*., 2001. Al2O3 ceramics preparation by LOM (laminated object manufacturing). *The International Journal of Advanced Manufacturing Technology*, **17**, 531–534.

Zhou, C., *et al*., 2011. Development of a multi-material mask-image-projection-based stereolithography for the fabrication of digital materials. *SFF Symposium*, 2011, Austin, TX, USA.

Zhuo, X., *et al*., 2002. Fabrication of porous scaffolds for bone tissue engineering via low-temperature deposition. *Scripta Materialia*, **46**, 771–776.

A Dry Powder Material Delivery Device for Multiple Material Additive Manufacturing

S. Chianrabutra, B.G. Mellor, S. Yang

Engineering Sciences Unit, Faculty of Engineering and the Environment,
University of Southampton, Southampton SO17 1BJ, United Kingdom

Abstract

This research is to develop a novel material delivery device for a next generation additive manufacturing system which is capable of directly manufacturing objects by depositing several materials layer by layer. The successful deposition of multiple material layers by using this novel dry powder printing technique reveals its great potential as a means of incorporating multiple materials in the traditional additive manufacturing process since this technology is suitable for a wide range of materials and it has the capability to manufacture 2D layers composed of multiple materials. This paper will outline the basics of the dry powder printing technology and present and discuss selected experimental studies from our research.

Introduction

Currently, most commercial additive manufacturing systems are designed to produce parts from a single material [1]. Multiple Materials Additive Manufacturing (MMAM) using direct inkjet printing technology was pioneered by Evans and co-workers nearly 20 years ago [2] and is now researched by various groups. Objet has commercialized direct inkjet 3D printers and claim that they represent the only MMAM system. However, Objet can only print photopolymer materials, which have limited mechanical properties and other functionalities, compared to direct metal and/or ceramic printing. MMAM is a new technology that can fabricate three-dimensional multiple material (heterogeneous) objects. This technology can create multiple material objects and can vary material compositions within the layer [3]. The ability to print multiple materials from an additive manufacturing system can improve either the mechanical properties of the parts or provide additional functions to the 3D printed parts [4]. MMAM technology has the potential to become an important manufacturing resource for the next generation of AM technology. This is because single material AM systems cannot fulfil the requirements of some applications that require multiple material objects from one machine, such as compliant mechanisms, embedded components, 3D circuits, human tissues, medical compatible implants etc. Moreover, the next generation of AM technology should provide full functionality, offer changeable material systems, and give the entire bonding system at an affordable price [5-7].

Multiple material objects are more interesting and will be highly important in many industrial applications. Many research institutes and companies have been developing AM technologies to allow more materials to be used in single material AM technology, and to improve the properties of the AM part and to enhance the capability of the basic process [4]. Powder based materials are very important as they can provide a wide variety of material options. The Dry Powder Printing (DPP) technique is one of the promising techniques

available to dispense fine powders [8]. Among the DPP techniques, the ultrasonic dispensing method has many significant advantages for depositing fine powders uniformly and controllability and has the ability to handle a wide variety of powder materials. In most of the current powder based AM systems, powders are spread using a roller onto a powder bed which made it impossible to fill multiple materials without cross-contamination [9, 10]. Therefore, it is essential to develop processing technologies that can handle fine powder particles for use in material delivery devices for the next generation of AM systems. However, processing and handling powder materials is very challenging due to their unique properties. To deposit such materials it is necessary to understand thoroughly the powder flow in the dispensing nozzle.

Dry Powder Printing (DPP) or dry powder micro-feeding or fine powder dispensing is based on vibration, resulting from the ultrasonic vibration of a piezoelectric transducer, being used to assist flow. Over the recent past this DPP method has proved capable of handling fine powders. Pegna, who is a pioneer in this field, studied the possibility of multiple material deposition by creating a single layer of Portland cement [11] and spherical glass beads [12]. Santosa et al. demonstrated the influence of orifice diameters and under 100 μm particle sizes on flow behaviour under gravity through a hopper-nozzle [13]. Matsusaka et al. [14] investigated the microfeeding of fine powders in a capillary tube vibrated by a 20 kHz piezoelectric transducer. Takano and Tomikawa [15] developed feeding devices based on the excitation of a progressive wave in an ultrasonic transmission line. Li et al. [16] used an ultrasonic-based micropowder-feeding mechanism to form thin patterns of dry powders on a substrate which were subsequently sintered by a laser beam. Kumar et al. examined the concept of multiple dry powder deposition under gravity flow including low gas pressure-assisted flow and vibration-assisted flow and developed a model to predict the flow rate under gravity of the experimental powders [17]. Jiang et al. evaluated the flowability of nanoparticle powders [18] and developed a measurement system of powder flowability based on a vibrating capillary [19]. Yang and Evans [20, 21] presented the factors and mechanisms that were responsible for the initiation and cessation of flow in a vibration controlled dispensing system. Additionally, they identified the powder characteristics controlling powder handling so as to find effective metering and dispensing methods for shape and composition control for solid freeform fabrication [22]. Furthermore, they investigated the effects of acoustic frequency, amplitude, tube diameter, mechanical damping and particle size distribution on particle deposition from open capillaries subject to acoustic vibration [23]. They invented a discontinuous dispensing device using short pulses of ultrasonic vibration to dispense the dry powders in a drop on demand format [24]. Lu et al.[8, 25-27] studied dispensing mechanisms, drop size control, dose uniformity and different design of dispensing nozzles.

However, only a few studies have been carried out using ultrasonic vibration to dispense dry powders for MMAM [4]. The detailed mechanism of DPP has not been fully clarified and is needed for the technique to be a commercial success. The processing of fine powder in the micrometre size range has proved difficult [28, 29]. This is due to the feature size being driven by the size of the dispenser orifice, a smaller feature size resulting from a

smaller diameter orifice. For the production of drops from sub-micrometre diameter size fine powders, the process is difficult to control reliably or sometimes powders cannot be dispensed because of their poor flowability. In this work, we have systematically investigated the effects of printing parameters on printing results which reveals the basic characteristics of our powder printing device. Furthermore, our study shows that dry powder printing, driven by ultrasonic vibration, can be exploited for fine powder printing of many types of powder materials.

Materials and methods

Materials

In this study, the selected powder materials were copper (Osprey Metals, Neath, Wales), solder (Sn63Pb37, IPS (Suzhou) New Materials Co. Ltd., China), 316L stainless steel (Osprey Metals, Neath, Wales), tungsten carbide (Sandvik, Conventry, UK), alumina (Al_2O_3, BA Chemicals Ltd., Buckinghamshire, UK), CoCr (Concept Laser GmbH, Lichtenfels, Germany), 420S45 stainless steel (Osprey Metals, Neath, Wales), glass bead (Whitehouse Scientific Ltd., UK), and Glass-filled Nylon (DuraForm® GF, 3D Systems Corp., USA) in the size range 14-72 µm and their details are shown in Figure 1 and Table 1. These materials were selected to cover metals, polymers and ceramics with different densities, particle sizes and particle shapes used in AM systems.

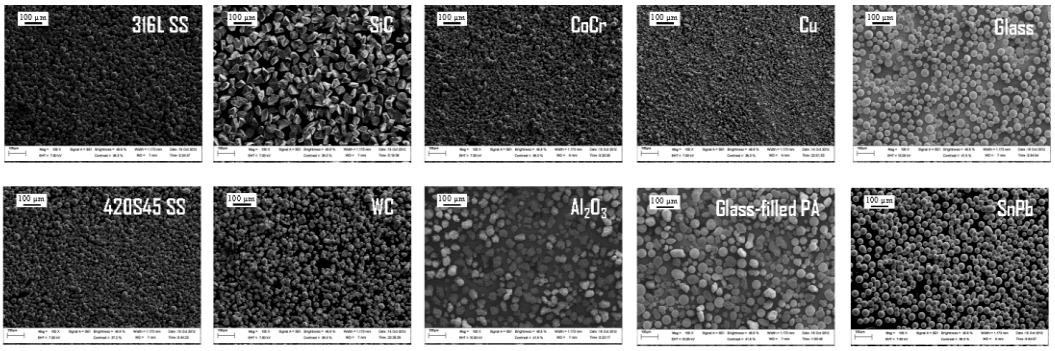

Figure 1 Scanning Electron Micrographs of the experimental powders.

The powders were analyzed to confirm that the size range was within specification by using a Malvern Mastersizer 2000 particle size analyzer. The particles were also characterized by a LEO 1455 VP Scanning Electron Microscope (SEM).

Table 1 Physical characteristics of the experimental materials.

Powder	Cu	SiC	Al2O3	Glass	CoCr	SnPb	316L SS	420S45 SS	WC	Glass-filled PA
D_{50} (µm)	14	54	52	41	18	35	32	20	35	72
Particle density(kg/m3)	8940	3220	3970	2300	8290	8400	7890	7740	15500	1490

Experimental setup

The experimental setup consists of a computer, an analogue waveform generator (NI 6733 DAQmx card, National Instruments Corporation Ltd. Berkshire, UK), a power amplifier (50w, Sonic Systems Ltd, Somerset, UK), a glass nozzle (Pasteur glass pipette) attached to a piezoelectric ceramic ring (SPZT8-100-50x20, MPI Co., Switzerland) by an adhesive epoxy (Araldite Rapid Syringe-Epoxy Extra Strong, Huntsman Corp., USA), Z column and X-Y table (Parker Hannifin, supplied by Micromech, Braintree, UK). The experimental setup is as shown schematically in Figure 2.

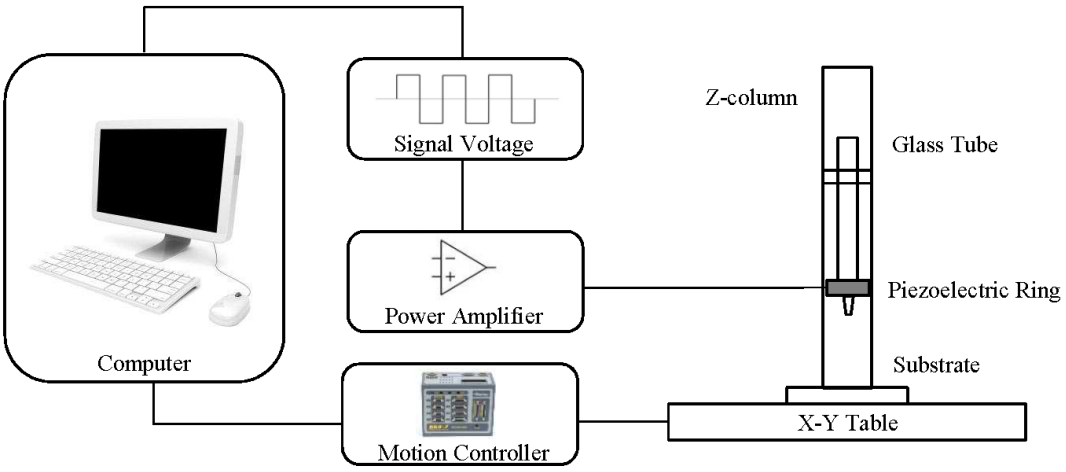

Figure 2 Schematic diagram of the dry powder printing system.

To capture images of the powder as it discharges in the experiment, a high- speed Photron Fastcam SA-1 (Photron Limited, Japan) camera attached to a c-mount adapter on a Leica Monozoom 7 (Leica Microsystem Inc., USA) macro lens was installed close to the dispenser.

Experimental conditions

The experiments were carried out under room conditions (23-28 °C and 36-45 % RH). As contaminants in the powder can reduce their mass flow rate from the dispenser and even clog the orifice a clean environment and sieving the powder before testing are essential. In this study, powders, which were kept in air tight packages, were sieved through a 100-micrometre sieve size before filling the dispenser, i.e. all particles dispensed passed through a 100-micrometre sieve size.

Results and discussions

Dispensing behaviour

The powder is dispensed by a vibration-assisted system using a glass nozzle as a funnel and a computer control system. Powder drops are discharged directly from the dispenser. Initially, particles form a stable dome structure across the orifice as shown in Figure 3. Powders are dispensed through the orifice by breaking the dome structure by activating a voltage signal pulse to the piezoelectric transducer attached to the dispenser.

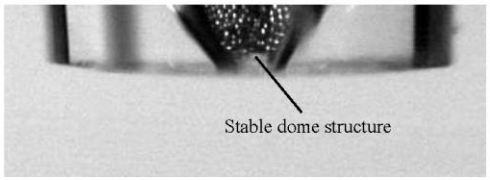

Figure 3 Dome structure of a fine powder inside the glass nozzle.

During dispensing, the vibration from the piezoelectric transducer transmits energy through the glass tube to particles around the dome structure and the result is to break the dome structure and so achieve flow of the powders. On switching off the vibrations, particle-particle and particle-wall friction lead to the formation of domes causing powder flow to arrest in the nozzle. Figure 4 shows the sequential images captured by a high speed camera at 0.01 second increments from the start of dispensing (B) to the cessation of dispensing (G) when the powder forms a new stable dome structure (H-J) inside the glass nozzle.

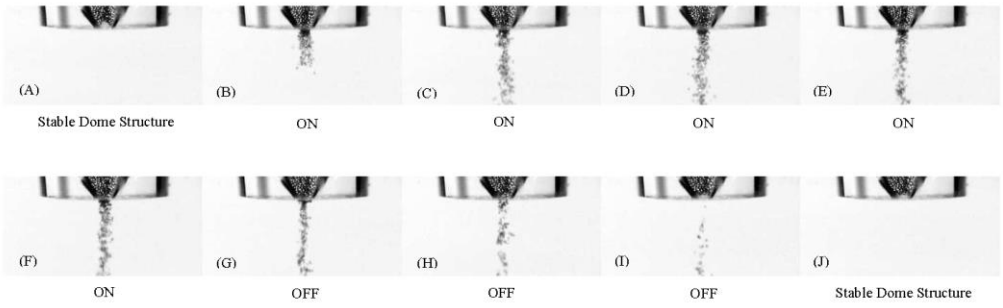

Figure 4 Sequence of images captured from the start of dispensing to the cessation of dispensing of a fine powder from the glass nozzle.

Printable materials

The ten experimental powders detailed in Table 1 were successfully discharged as can be seen in Figure 5. All of these results came from the same dispenser geometry, i.e. a 250 µm nozzle diameter with a nozzle angle of 75°. Throughout this study, the experiments were carried out at an applied signal voltage of 2 Volts, standoff distance of 200 µm and moving

speed of 10 mm/s. Notably, the appropriate control of parameters for each experimental powder can improve markedly the deposited powder patterns.

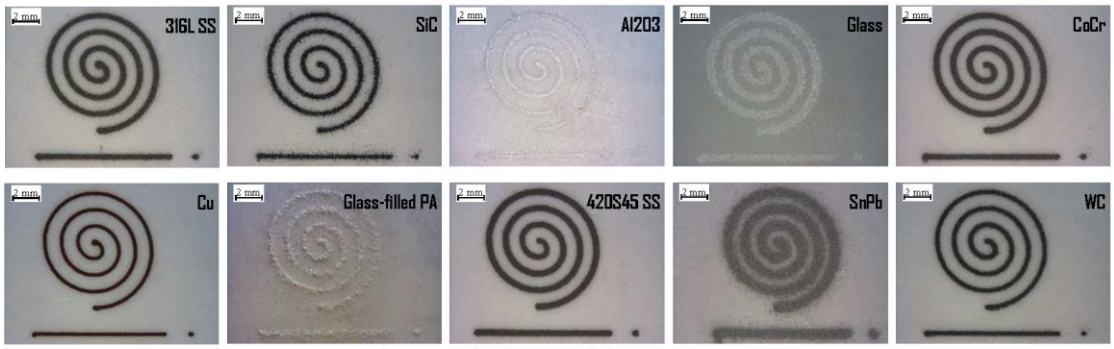

Figure 5 Single material patterns.

The quality of the patterns, which is characterised in term of continuity, consistency and fineness of the edge of the printing line produced mainly depends on the powder's flowability and the orifice size. Based on the particle's density and mean particle diameter all the experimental powders, except for copper and glass-filled nylon, fit into groups A and B of Geldart's classification presented in Figure 6, The copper powder and the glass-filled nylon are located in group C. Group A powders are ideal for conveying in sliding bed flow, Group B powders are easy to fluidize and they rapidly de-aerate while Group C powders are difficult to fluidize and are cohesive [30, 31]. Moreover, all of the experimental powders in Figure 1 do not agglomerate and have discrete particles. It may be concluded that in all cases, the powders used in this study are free-flowing materials or not extremely cohesive.

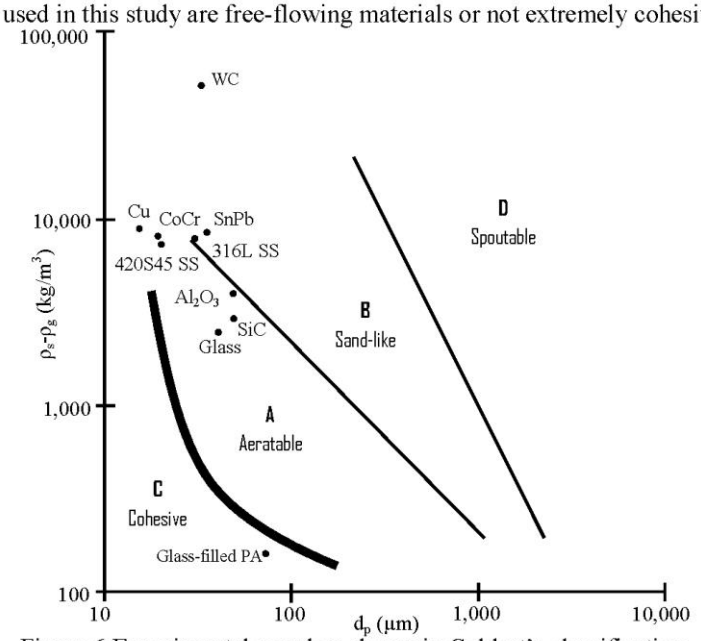

Figure 6 Experimental powders shown in Geldart's classification (ρ_s-solid density, ρ_g-gas density, d_p- mean particle diameter)

Printing of fine track width

The printing patterns are produced by CAD programs such as SolidWorks. The printing parameters of signal voltage, standoff distance and moving speed are programmable input via software. High precision stages are used to achieve x, y and z movement. The experimental studies found that high resolution depends on powder flowability, nozzle orifice geometry (nozzle diameter and nozzle angle), standoff distance and moving speed (the relative velocity between the substrate and the nozzle) as well as the signal voltage used to activate the piezoelectric transducer. Different parameters in the dispenser system need to be carefully adjusted for optimum results as the different powders have their own flow properties. A different adjustment of parameters can result in the feature sizes shown in Figure 7.

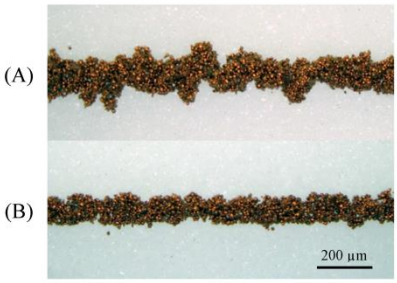

Figure 7 Patterns obtained from two printing conditions with the same nozzle diameter (70 µm) and the same signal voltage (2 Volts): (A) the standoff distance is 475µm, and the moving speed is 10 mm/s, (B) the standoff distance is 125 µm and the moving speed is 15 mm/s.

At present, the DPP printing device using an orifice diameter of 60 µm can realize a feature size down to 85 µm as shown in Figure 8. During the printing process the standoff distance of the deposition nozzle from the substrate was 150 µm, the moving speed was 5 mm/s and the signal voltage was 2 Volts.

Figure 8 Samples with a track width of less than 100 µm.

Nozzle diameter

Mass flow rate as a function of dispensing nozzle diameter was determined for the copper powder and solder powder of 14 µm and 35 µm mean particle size respectively. The nozzle diameters used were 110, 200, 250, 280, 320, 375 and 400 µm. The signal voltage was fixed at 2 Volts and the nozzle angle was 66°. Figure 9 shows the results of the mass flow rate for the two selected powders tested with this range of nozzle diameters. The mass flow rates increase with nozzle diameter. The results show that with the smallest nozzle diameters, the mass flow rates of the experimental powders are similar but they rapidly increase with increasing nozzle diameter. Throughout the range of these nozzle diameters, the solder powder has a higher flow rate (higher power law exponent) than the copper. This reflects the fact that a free-flowing powder such as the solder powder has higher flowability and thus greater mass flow rate than a cohesive powder such as the copper powder.

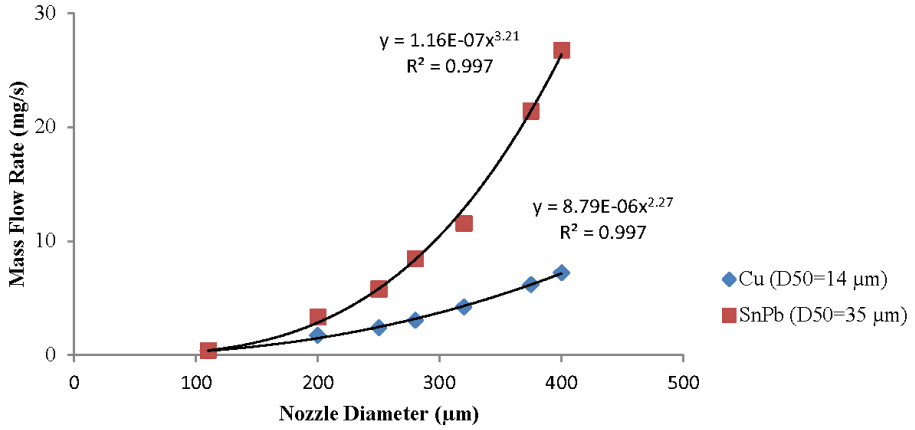

Figure 9 Mass flow rate as a function of nozzle diameter for copper and solder powder.

Signal voltage

The piezoelectric vibration enables powder printing to be achieved. The mass flow rate can be regulated by the vibration energy generated by the signal voltage, which controls the deformation amplitude of the piezoelectric transducer. Generally, when a greater voltage is applied the vibration amplitude increases. In our study a free-flowing powder, such as the solder powder, discharged as a spray of particles as shown in Figure 10 and the spray angle increased with increasing signal voltage. For a signal voltage of 0.15 Volts, the spray angle was less than 10° while for the signal voltage of 0.5 Volts and 2.0 Volts, the spray angle was around 30° and 90° respectively. The reason might be that the high vibration energy transmitted to the powder particles results in greater vibration of powder particles around the nozzle wall. As the particles exit the nozzle they hit the edge of the orifice and thus spread out. This effect is less when using a larger nozzle diameter or using a cohesive powder such as copper. Thus it can be seen that by choosing a suitable signal more uniform and consistent powder dispensing can be achieved and therefore more precise patterns produced.

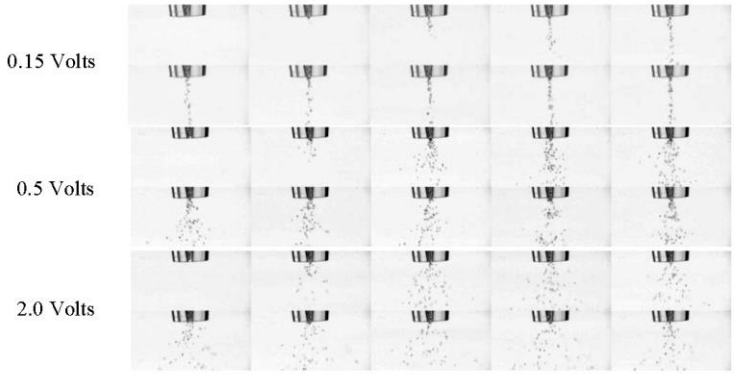

Figure 10 Sequence of images obtained from a high speed camera at 0.05 second increments showing the successive stages of discharge of solder powders. The nozzle diameter is 250 μm.

Standoff distance

Standoff distance is the distance of the tip of the nozzle to the top of the substrate. From the previous discussion, it can be seen that powders normally spread out, the spray angle depending on the signal voltage. Therefore, the standoff distance should be as small as possible. However, the lower limit to standoff distance depends on the moving speed as the standoff distance must be sufficient to avoid powder blocking flow between the tip of the nozzle and the top of the substrate. Figure 11 shows the results of printing at different standoff distances. The track line at the 125-μm standoff distance results in the tip of the nozzle coming into contact with the powder resulting in compressing the printed line and might interrupt the powder flow at the outlet.

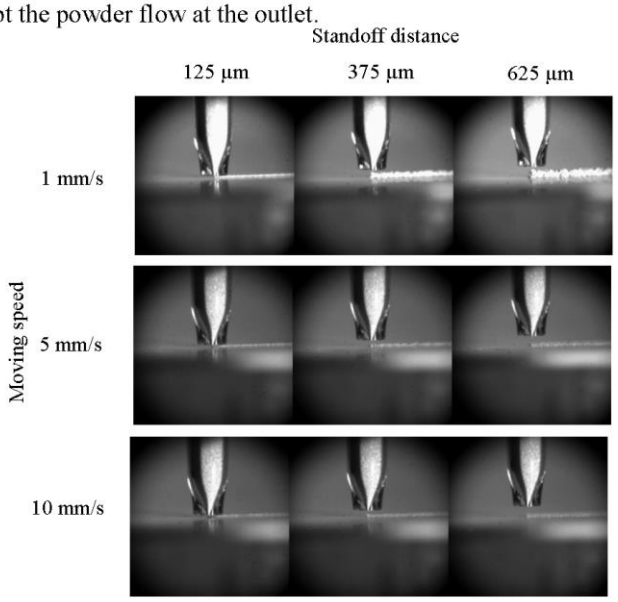

Figure 11 Sequence of images obtained from a high speed camera for copper powder dispensing with different moving speeds and standoff distances. The nozzle diameter is 250 μm.

Moving speed

Moving speed is the relative speed between the nozzle and the substrate. A fast moving speed can increase the printing speed of the process. However, the moving speed must not be so fast as to produce a discontinuity in the printed line. Figure 12 shows that copper printing with moving speeds of 20 mm/s and 25 mm/s cannot create complete printed lines. It indicates that the maximum moving speed in this test should be less than 20 mm/s.

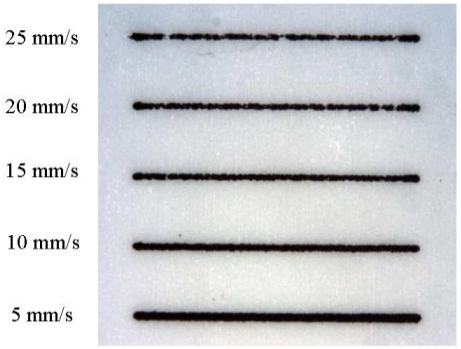

Figure 12 Printing results for copper powder obtained from different moving speeds. The nozzle diameter is 250 µm, the signal voltage is 2 Volts and the standoff distant is 200 µm.

Multiple material patterns

Figure 13 demonstrates the capability of printing multiple powder materials. Three sets of optimal parameter were used to produce a fine pattern. The pattern combines stainless steel, tungsten carbide and copper powder. A system consisting of three dispensers was installed on the z column and the x-y table was synchronised by the motor controller.

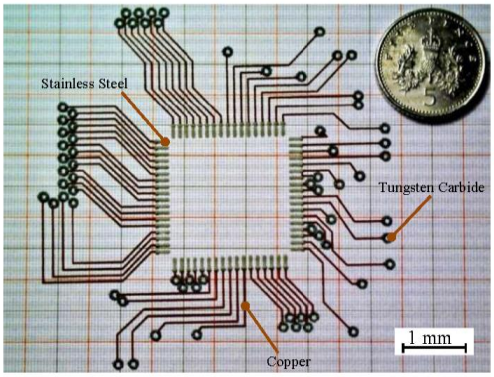

Figure 13 Multiple material pattern.

Advantages

This DPP technique can print various materials and little material preparation needs to be carried out. Using separate nozzles to deposit powder material in selective areas is an accurate, efficient and easy method which avoids contamination between materials. The device has few components resulting in less maintenance and an economical cost. Different materials can be printed simply by adding a new dispenser to the system. Utilising a nozzle based method, powder materials can be delivered between and within layers to make multi-oriented interfaces in a final part. It is believed that using a dry powder dispensing system integrated with current powder-based additive manufacturing systems, such as laser sintering, laser melting or binder jetting, would increase their ability to produce multiple material parts.

Limitations

A limitation of this device is that the process requires a small standoff distance to provide high resolution and to avoid spreading due to the spray effect. Additionally, accidental vibration from the environment, e.g. movement of the x-y table, can affect the controllability of powder dispensing. However, this can be overcome by mounting the device in a system with smooth movement and adequate damping. Furthermore, the dispenser must be installed vertically because the device combines vibration and gravitational force to discharge material.

Conclusions

In this paper, a novel Dry Powder Printing (DPP), based on an ultrasonic dispensing device where powder flow can be regulated by controlling input to the piezoelectric transducer, is introduced. The development of this novel DPP method would allow the layering of high quality multiple material patterns. By programming the print heads, this powder printing technique can achieved selective area deposition of different dry powder materials using ultrasonic activation without sophisticated material preparation. The novel device allows the deposition of a wide range of powder materials. This device represents a step forward in realizing multiple material objects in MMAM systems.

Acknowledgement

The authors thank the Royal Thai Government for supporting a scholarship of Mr. Srisit Chianrabutra and the EPSRC Engineering Instrument Pool for providing the loan of a Photron FASTCAM high speed camera.

References

1. Wohlers, T., *Wohlers Report 2011: Additive Manufacturing and 3D Printing, State of the Industry*. 2011: Wohlers Associates, Inc.
2. Blazdell, P., et al., *The computer aided manufacture of ceramics using multilayer jet printing.* Journal of Materials Science Letters, 1995. **14**(22): p. 1562-1565.
3. Gibson, I., D.W. Rosen, and B. Stucker, *Additive Manufacturing Technologies: Rapid Prototyping to Direct Digital Manufacturing*2009: Springer.
4. Vaezi, M., et al., *Multiple material additive manufacturing–Part 1: a review: This review paper covers a decade of research on multiple material additive manufacturing technologies which can produce complex geometry parts with different materials.* Virtual and Physical Prototyping, 2013. **8**(1): p. 19-50.
5. N. Hopkinson, R.J.M.H., P.M. Dickens, *Rapid Manufacturing: An Industrial Revolution for the Digital Age*2006: John Wiley & Sons, Ltd.
6. Malone, E., M. Berry, and H. Lipson, *Freeform fabrication and characterization of Zn-air batteries.* Rapid Prototyping Journal, 2008. **14**(3): p. 128-140.
7. Malone, E. and H. Lipson. *Multi-material freeform fabrication of active systems.* in *ASME 2008 9th Biennial Conference on Engineering Systems Design and Analysis*. 2008. American Society of Mechanical Engineers.
8. Lu, X., S. Yang, and J.R. Evans, *Studies on ultrasonic microfeeding of fine powders.* Journal of Physics D: Applied Physics, 2006. **39**(11): p. 2444.
9. Lappo, K., et al. *Discrete multiple material selective laser sintering (M2SLS): experimental study of part processing.* in *Solid Freeform Fabrication Symposium, Austin, Texas, The University of Texas*. 2003.
10. Lappo, K., et al., *Discrete multiple material selective laser sintering (M2SLS): nozzle design for powder delivery.* Proceedings of the Solid Freeform Fabrication. Austin, TX, 2003: p. 93-108.
11. Pegna, J. *Application of Cementitious Bulk Materials to Site Processed Solid Freeform Construction.* in *SFF Symposium*. 1995. Austin, Texas, USA.
12. Pegna, J., et al., *THE SAND-PAINTER: Two-dimensional powder deposition*, in *SFF Symposium*1999: Austin, Texas, USA.
13. James Santosa, D.J.a.S.D. *Experimental and numerical study on the flow of fine powders from small-scale hoppers applied to SLS multi-material deposition-Part I.* . in *SFF Symposium*. 2002 Austin, Texas, USA.
14. Matsusaka, S., K. Yamamoto, and H. Masuda. *Micro-feeding of a fine powder using a vibrating capillary tube.* Advanced Powder Technology, 1996. **7**(2): p. 141-151.
15. Takano, T. and Y. Tomikawa, *Excitation of a progressive wave in a lossy ultrasonic transmission line and an application to a powder-feeding device.* Smart Materials and Structures, 1998. **7**(3): p. 417.
16. Li, X., H. Choi, and Y. Yang, *Micro rapid prototyping system for micro components.* Thin Solid Films, 2002. **420**: p. 515-523.
17. Kumar, P., et al., *Direct-write deposition of fine powders through miniature hopper-nozzles for multi-material solid freeform fabrication.* Rapid Prototyping Journal, 2004. **10**(1): p. 14-23.
18. Jiang, Y., et al., *Evaluation of flowability of composite particles and powder mixtures by a vibrating capillary method.* Journal of chemical engineering of Japan, 2006. **39**(1): p. 14-21.
19. Jiang, Y., et al., *Development of measurement system for powder flowability based on vibrating capillary method.* Powder Technology, 2009. **188**(3): p. 242-247.
20. Yang, S. and J.R. Evans, *Acoustic initiation of powder flow in capillaries.* Chemical Engineering Science, 2005. **60**(2): p. 413-421.
21. Yang, S. and J.R. Evans, *Acoustic control of powder dispensing in open tubes.* Powder Technology, 2004. **139**(1): p. 55-60.
22. Yang, S. and J. Evans, *Metering and dispensing of powder: the quest for new solid freeforming techniques.* Powder Technology, 2007. **178**(1): p. 56-72.

23. Yang, S. and J.R. Evans, *A multi-component powder dispensing system for three dimensional functional gradients.* Materials Science and Engineering: A, 2004. **379**(1): p. 351-359.
24. Yang, S. and J.R. Evans, *A dry powder jet printer for dispensing and combinatorial research.* Powder Technology, 2004. **142**(2): p. 219-222.
25. Lu, X., et al. *Dry powder microfeeding system for solid freeform fabrication.* in *International Solid Freeform Fabrication Symposium, Austin, TX.* 2006.
26. Lu, X., S. Yang, and J.R. Evans, *Dose uniformity of fine powders in ultrasonic microfeeding.* Powder Technology, 2007. **175**(2): p. 63-72.
27. Lu, X., S. Yang, and J.R. Evans, *Microfeeding with different ultrasonic nozzle designs.* Ultrasonics, 2009. **49**(6): p. 514-521.
28. Li, Z. and S. Yang, *Nanobiomaterials library synthesis for high-throughput screening using a dry powder printing method* Nano LIFE, 2012. **02**(01): p. 1250006.
29. Yang, Y. and X. Li, *Experimental and analytical study of ultrasonic micro powder feeding.* Journal of Physics D: Applied Physics, 2003. **36**(11): p. 1349.
30. McGlinchey, D., *Bulk solids handling: equipment selection and operation*2008: Blackwell Pub.
31. Mills, D., *Pneumatic Conveying Design Guide*2003: Elsevier Science.

UNIVERSITY OF Southampton
School of Engineering Sciences

Multiple material patterns fabricated by 3D printing using a dry powder direct-write technology

S. Chianrabutra, B. G. Mellor, S. Yang

Engineering Materials Group, Faculty of Engineering and the Environment, University of Southampton, UK

Introduction

Interest in multifunctional structures made by automatically fabricating the completed part from multiple materials poses a challenge for today's 3D printing/additive manufacturing technology. Currently, most commercial additive manufacturing systems are designed to produce parts from a single material. However, the capability to print multiple materials can improve the process, either by optimizing the mechanical properties of the parts or by providing additional functions to the final parts.

The application addressed in this project is the development of a next generation additive manufacturing system which is capable of directly manufacturing objects by depositing several materials layer by layer. This paper will report our latest results of the direct writing of various powder materials onto substrates as well as in producing additive manufactured parts. Furthermore it will present multiple material patterns fabricated using this technology.

METHODOLOGY

A schematic diagram of the ultrasonic dispensing system used for the fabrication of multiple material patterns is shown in Figure 1. The experiments were carried out in a semi-continuous mode. The experimental apparatus consists of a computer, an analogue waveform generator (NI 6733 DAQmx card, National Instruments Corporation Ltd. Berkshire, UK), a power amplifier (50w, Sonic Systems Ltd, Somerset, UK), a glass nozzle (Pasteur glass pipette) placed in plastic case with a piezoelectric ceramic disc (SPZT-8 3053W-W, MPI Co., Switzerland) installed at the bottom by an adhesive epoxy (9340 GRAY Hysol Epoxi-Patch Structural Adhesive, DEXTER Co., Seabrook, USA) and a platform driven by an X-Y table (Parker Hannifin, supplied by Micromech, Braintree, UK).

The powders in the study were 316L stainless steel (Osprey Metals, Neath, Wales), copper (Osprey Metals, Neath, Wales) and tungsten carbide (Sandvik, Coventry, UK) in the size range 20-60 µm.

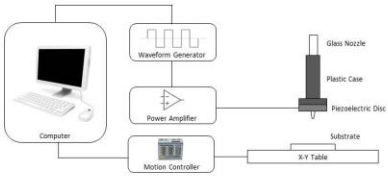

Figure 1: Schematic diagram of the micro powder ultrasonic dispensing system.

The powders were sieved to screen contaminants before dispensing. The powder was contained in a glass tube with 5 mm internal diameter and an orifice size of 70-240 µm. The experimental powders are discharged from the dispenser to create layer patterns on a substrate placed on an x-y table.

RESULTS AND DISCUSSION

At present, a feature size down to 125 µm can be realized. During the printing process the standoff distance of the deposition nozzle from the substrate is between 125 and 250 µm. At the moment the printing velocity of the micro powder ultrasonic dispensing system for good printing results is in the range 1.25 mm/s to 50 mm/s. Figure 2 and Figure 3 show the printing results for a single material layer and multiple material layer s respectively.

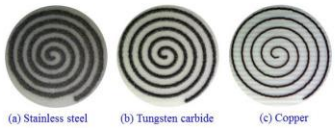

Figure 3: Single material layer.

This novel micro powder dispensing technology thus offers the potential for printing fine layers of multiple materials. Therefore it could be an interesting technology to meet the requirements of additive manufacturing systems.

High resolution quality from this powder dispensing process depends on powder flowability, nozzle orifice geometry, the standoff distance of the nozzle and the velocity of the substrate table. Since this technology is suitable for a wide range of materials and there is no need to prepare raw materials with a solvent, it has the capability to manufacture 3D objects composed of multiple materials.

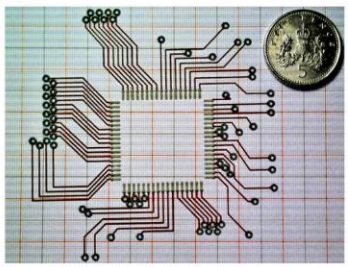

Figure 3 : Multiple material layer.

CONCLUSIONS

The successful printing of multiple material layers by using this novel micro powder dispensing technique shows great potential as a means of incorporating multiple materials in the traditional SLS process and proposes a new material delivery method.

Future work includes the development of a numerical model of the ultrasonic dispensing process and a model to predict the line width and line thickness. Further experiments will be performed to test and validate the feasibility of the completed system.

REFERENCES

1. S. Yang, J.R.G. Evans, Materials Science and Engineering, 2004, 351-359.
2. S. Yang, M.M. Mohebi, J.R.G. Evans, Rapid Prototyping Journal, 2008, 35-43.
3. P. Kumar, J.K. Santosa, E. Beck, S. Das, Rapid Prototyping Journal, 2004, 14-23.
4. X. Lu, S. Yang, J.R.G. Evans, Ultrasonics, 2009, 514-521.
5. Y. Yang, X. Li, Journal of Physics D:Applied Physics, 2003, 514-521.

www.soton.ac.uk/engineering | email: sc9e10@soton.ac.uk
Engineering Materials Group, Faculty of Engineering and the Environment, University of Southampton, SO17 1BJ, UK

UNIVERSITY OF Southampton
School of Engineering Sciences

Material delivery device for Multiple Material Additive Manufacturing using a Dry Powder Printing technology

S. Chianrabutra, B. G. Mellor, S. Yang

Engineering Materials Group, Faculty of Engineering and the Environment, University of Southampton, UK

Background

Currently, most commercial additive manufacturing systems are designed to produce parts from a single material. However, the capability to print multiple materials can improve the process, either by optimizing the mechanical properties of the parts or by providing additional functions to the final parts.

Objective

This research is to develop a novel material delivery device for a next generation additive manufacturing system which is capable of directly manufacturing objects by depositing several materials layer by layer.

Method

A schematic diagram of the dry powder printing system used for the deposition of multiple material powders is shown in Figure 1.

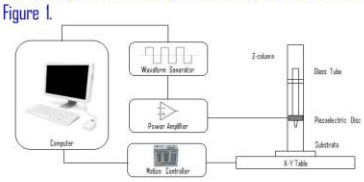

Figure 1: Schematic diagram of the dry powder printing system.

Experimental materials

The ten selected powders in the study are shown in Table 1 and Figure 2. They are in the size range of 14-72 μm and their angle of repose in between 30 and 62° .

Table 1: Physical characteristics of the experimental powders.

Powder	Apparent Density (g/cm³)	Angle of Repose (degree)	D(0.5) (μm)	Shape
Cu	4.7	43-50	14	Spherical
SiC	1.5	48-52	54	Irregular
Al2O3	1.4	46-62	52	Spherical
Glass	1.3	30-35	41	Spherical
CoCr	4.5	45-52	18	Spherical
SnPb	4.8	37-41	35	Spherical
316L SS	4.2	45-49	32	Spherical
420S45 SS	3.9	49-56	20	Spherical
WC	7.8	41-49	35	Irregular
Glass-filled PA	0.8	40-44	72	Mixed

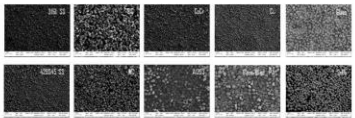

Figure 2: Scanning Electron Micrograph of the experimental powders.

Results

The dry powders detailed in Table 1 can be successfully be delivered in a continuous manner under gravity by using ultrasonic vibration assistance. By changing the nozzle geometry, the printing track can be varied from micrometer scale to millimeter scale (Figure 3). At present, a feature size down to 85 μm can be realized as shown in Figure 4. During the printing process the standoff distance of the deposition nozzle from the substrate is between 125 and 250 μm.

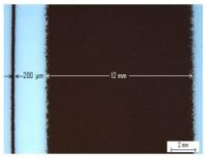

Figure 3 : From micrometre-scale to millimetre scale track width.

Figure 4 : Samples with a track width less than 100 μm.

At the moment the printing velocity of the dry powder ultrasonic dispensing system for good printing results is in the range 1.25 mm/s to 50 mm/s. Figure 5 and Figure 6 show the printing results for a single material layer and multiple material layers respectively.

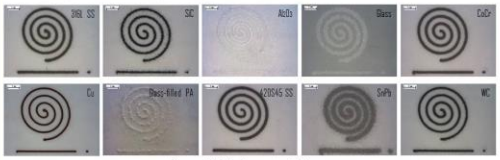

Figure 5: Single material layers.

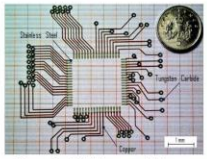

Figure 6 : Multiple material layer.

Conclusions

The successful deposition of multiple material layers by using this novel dry powder printing technique shows great potential as a means of incorporating multiple materials in the traditional additive manufacturing process and proposes a new material delivery method.

High resolution from this powder printing process depends on powder flowability, nozzle orifice geometry, the standoff distance of the nozzle and the velocity of the substrate table. Since this technology is suitable for a wide range of materials and there is no need to prepare raw materials with a solvent, it has the capability to manufacture 3D objects composed of multiple materials.

Therefore it could be an interesting technology to meet the requirements of Multiple Material Additive Manufacturing (MMAM). With the device, the following advantages are realized.

- **Design freedom:** The powerful benefit of this technology is in offering freedom of design and creation.
- **Design protection:** MMAM can easily create the protection of products.
- **Increased functionality:** Material integration and material property tailoring can enable the creation of new products through the design and integration of innovative material. Furthermore, it can embed electronic components to create new functional parts and superior value systems.
- **Elimination of assembly:** A product comprised of various components can be fabricated in one build, eliminating fasteners and assembly labor, especially for the electronic industry.
- **Efficient manufacturing system:** The new manufacturing process enables the fabrication of 3D functionally complex structures within a single integrated manufacturing environment.

Acknowledgement

The authors are grateful to The Royal Thai Government for supporting this work by providing research studentship to Mr.Srisit Chianrabutra.

Further information

There is much useful information on this technology in our group web site. Scan the QR code for more information.

www.soton.ac.uk/engineering | email: sc9e10@soton.ac.uk

Engineering Materials Group, Faculty of Engineering and the Environment, University of Southampton, SO17 1BJ, UK

List of References

1. N. Hopkinson, R.J.M.H., P.M. Dickens, *Rapid Manufacturing: An Industrial Revolution for the Digital Age*. 2006: John Wiley & Sons, Ltd.
2. Malone, E., M. Berry, and H. Lipson, *Freeform fabrication and characterization of Zn-air batteries*. Rapid Prototyping Journal, 2008. 14(3): p. 128-140.
3. Malone, E. and H. Lipson. *Multi-material freeform fabrication of active systems*. in ASME 2008 9th Biennial Conference on Engineering Systems Design and Analysis. 2008: American Society of Mechanical Engineers.
4. Gibson, I., D.W. Rosen, and B. Stucker, *Additive Manufacturing Technologies: Rapid Prototyping to Direct Digital Manufacturing*. 2009: Springer.
5. Vaezi, M., Chianrabutra, S., Mellor, B., and Yang, S., *Multiple material additive manufacturing–Part 1: a review: This review paper covers a decade of research on multiple material additive manufacturing technologies which can produce complex geometry parts with different materials*. Virtual and Physical Prototyping, 2013. 8(1): p. 19-50.
6. Wohlers, T., *Wohlers Report 2011: Additive Manufacturing and 3D Printing, State of the Industry.* 2011: Wohlers Associates, Inc.
7. Lappo, K., Jackson, B., Wood, K., Bourell, D. L., and Beaman, J. J., *Discrete multiple material selective laser sintering (M2SLS): experimental study of part processing*. Solid Freeform Fabrication Symposium, Austin, Texas, The University of Texas. 2003.
8. Lappo, K., Wood, K., Bourell, D., and Beaman, J. J., *Discrete multiple material selective laser sintering (M2SLS): nozzle design for powder delivery*. Solid Freeform Fabrication Symposium, Austin, Texas, The University of Texas. 2003: p. 93-108.
9. Lu, X., S. Yang, and J.R. Evans, *Studies on ultrasonic microfeeding of fine powders*. Journal of Physics D: Applied Physics, 2006. 39(11): p. 2444.
10. Li, Z. and S. Yang, Nanobiomaterials library synthesis for high-throughput screening using a dry powder printing method Nano LIFE, 2012. 02(01): p. 1250006.
11. Yang, Y. and X. Li, *Experimental and analytical study of ultrasonic micro powder feeding*. Journal of Physics D: Applied Physics, 2003. 36(11): p. 1349.
12. Gibson, I., D.W. Rosen, and B. Stucker, *Additive Manufacturing Technologies*. 2010: Springer
13. Wohlers, T., Wohlers Report 2012: *Additive Manufacturing and 3D Printing*, State of the Industry. 2012.
14. Zhou, C., Chen, Y., Yang, Z. G., and Khoshnevis, B., *Development of a Multi-material Mask-Image-Projection-based Stereolithography for the Fabrication of Digital Materials*., Solid Freeform Fabrication Symposium, Austin, Texas, The University of Texas. 2011.

15. Shin, K. H., Natu, H., Dutta, D., and Mazumder, J., *A method for the design and fabrication of heterogeneous objects*. Materials & Design, 2003. 24(5): p. 339-353.
16. Dutta, D. and M. Shpitalni, *Heterogeneous Solid Modeling for Layered Manufacturing*. CIRP Annals - Manufacturing Technology, 2000. 49(1): p. 109-112.
17. Choi, S. H., and H. H. Cheung., *Digital fabrication of multi-material objects for biomedical applications. INTECH Open Access Publisher, 2011.*
18. K Lappo, B.J., K Wood. *Discrete Multiple Material Selective Laser Sintering (M2SLS): Experimental Study of Part Processing*. Solid Freeform Fabrication Symposium, Austin, Texas, The University of Texas.2003.
19. Igor, S., *Synthesis of functional gradient parts via RP methods*. Rapid Prototyping Journal, 2001. 7(4): p. 207-211.
20. Stucker, B., *Additive Manufacturing Technologies: Technology Introduction and Business Implications*, in Frontiers of Engineering: Reports on Leading-Edge Engineering from the 2011 Symposium, N.A.o. Engineering, Editor. 2011.
21. Gebhardt, A., *Understanding Additive Manufacturing*. 2012, Munich: Carl Hanser Verlag GmbH & Co. KG.
22. Maruo, S., K. Ikuta, and T. Ninagawa, *Multi-polymer microstereolithography for hybrid opto-MEMS*, Micro Electro Mechanical Systems, 2001. MEMS 2001. The 14th IEEE International Conference on. 2001. p. 151-154.
23. Liu, V. and S. Bhatia, *Three-Dimensional Photopatterning of Hydrogels Containing Living Cells*. Biomedical Microdevices, 2002. 4(4): p. 257-266.
24. Wicker, R., F. Medina, and C. Elkins, Multiple Material Micro-fabrication: Extending Stereolithography to Tissue Engineering and Other Novel Applications, Solid Freeform Fabrication Symposium, Austin, Texas, The University of Texas. 2004.
25. Inamdar, A., Magana, M., Medina, F., Grajeda, Y., and Wicker, R.,*Development of an automated multiple material stereolithography machine. Solid Freeform Fabrication Symposium, Austin, Texas, The University of Texas. 2006.*
26. Choi, Jae-Won, Ho-Chan Kim, and Ryan Wicker. "Multi-material stereolithography." Journal of Materials Processing Technology 211.3 (2011): 318-328.
27. Kim, H., J.-W. Choi, and R. Wicker, *Scheduling and process planning for multiple material stereolithography*. Rapid Prototyping Journal, 2010. 16(4): p. 232-240.
28. Arcaute, K., B. Mann, and R. Wicker, *Stereolithography of spatially controlled multi-material bioactive poly(ethylene glycol) scaffolds*. Acta Biomaterialia, 2010. 6(3): p. 1047-1054.
29. Bertsch, A., Zissi, S., Jezequel, J. Y., Corbel, S., and Andre, J. C., *Microstereophotolithography using a liquid crystal display as dynamic mask-generator*. Microsystem Technologies, 1997. 3(2): p. 42-47.

30. Beluze, L., A. Bertsch, and P. Renaud, *Microstereolithography: a new process to build complex 3D objects*. 1999: p. 808-817.
31. Stampfl, J., Fouad, H., Seidler, S., Liska, R., Schwager, F., Woesz, A., and Fratzl, P., *Fabrication and moulding of cellular materials by rapid prototyping*. International Journal of Materials and Product Technology, 2004. 21: p. 285–96.
32. Hadipoespito, G., Yang, Y., Choi, H., Ning, G., and Li, X., *Digital micromirror device based microstereolithography for micro structures of transparent photopolymer and nanocomposites*. Solid Freeform Fabrication Symposium, Austin, Texas, The University of Texas. 2003.
33. Cheng, Y. L., Li, M. L., Lin, J. H., Lai, J. H., Ke, C. T., and Huang, Y. C., *Development of dynamic mask photolithography system*. Proceedings of the 2005 IEEE International Conference on Mechatronics. 2005. Taipei, Taiwan.
34. Choi, J.-W., E. MacDonald, and R. Wicker, *Multi-material microstereolithography*. The International Journal of Advanced Manufacturing Technology, 2010. 49(5-8): p. 543-551.
35. Han, L. H., Suri, S., Schmidt, C. E., and Chen, S., *Fabrication of three-dimensional scaffolds for heterogeneous tissue engineering*. Biomedical Microdevices, 2010. 12(4): p. 721-725.
36. Bartolo, P.J. and G. Mitchell, *Stereo-thermal-lithography*. Rapid prototyping journal, 2003. 9: p. 150–156.
37. Bartolo, P.J., *Stereolithography: Materials, Processes and Applications*. 2011, New York: Springer.
38. Melchels, F. P., Domingos, M. A., Klein, T. J., Malda, J., Bartolo, P. J., and Hutmacher, D. W., *Additive manufacturing of tissues and organs*. Progress in Polymer Science, 2012. 37(8): p. 1079-1104.
39. Hon, K.K.B., L. Li, and I.M. Hutchings, *Direct writing technology-Advances and developments*. Cirp Annals-Manufacturing Technology, 2008. 57(2): p. 601-620.
40. Vaezi, M., H. Seitz, and S. Yang, *A review on 3D micro-additive manufacturing technologies*. The International Journal of Advanced Manufacturing Technology, 2012: p. 1-34.
41. Mott, M. and J.R.G. Evans, *Zirconia/alumina functionally graded material made by ceramic ink jet printing*. Materials Science and Engineering: A, 1999. 271(1–2): p. 344-352.
42. Wang, J. and L.L. Shaw, *Fabrication of Functionally Graded Materials Via Inkjet Color Printing*. Journal of the American Ceramic Society, 2006. 89(10): p. 3285-3289.
43. Ibrahim, M., Otsubo, T., Narahara, H., Koresawa, H., and Suzuki, H., *Inkjet printing resolution study for multi-material rapid prototyping*. JSME International Journal Series C Special Issue on Advanced Manufacturing Technology, 2006. 49: p. 353–360.
44. Xie, D., Zhang, H., Shu, X., Xiao, J., and Cao, S., *Multi-materials drop-on-demand inkjet technology based on pneumatic diaphragm actuator*. Science China Technological Sciences, 2010. 53(6): p. 1605-1611.

45. Sun, J., Yang, R., Tan, K. K., Fuh, J. Y. H., Wong, Y. S., and Ng, J. H., *Performance characterization of drop-on-demand micro-dispensing system with multi-printheads*. Microsystem Technologies, 2010. 16(12): p. 2087-2097.
46. Li, L., J. H. Ng, J. Y. H. Fuh, Y. S. Wong, H. T. Loh, W. Feng, M. Saedan, J. Sun, S. T. Thoroddsen, and L. Lu., *Development of a drop-on-demand system for multiple material dispensing*. Automation and Logistics, 2008. ICAL 2008. IEEE International Conference on. 2008.
47. Li, L., M. Saedan, W. Feng, J. Y. H. Fuh, Y. S. Wong, H. T. Loh, S. C. H. Thian, S. T. Thoroddsen, and L. Lu., *Development of a multi-nozzle drop-on-demand system for multi-material dispensing*. Journal of Materials Processing Technology, 2009. 209(9): p. 4444-4448.
48. Cawley, J.D., *Solid freeform fabrication of ceramics*. Current Opinion in Solid State and Materials Science, 1999. 4(5): p. 483-489.
49. Lu, K. and W.T. Reynolds, *3DP process for fine mesh structure printing*. Powder Technology, 2008. 187(1): p. 11-18.
50. Seitz, H., Rieder, W., Irsen, S., Leukers, B., and Tille, C., *Three-dimensional printing of porous ceramic scaffolds for bone tissue engineering*. Journal of Biomedical Materials Research Part B: Applied Biomaterials, 2005. 74B(2): p. 782-788.
51. Vorndran, E., Klammert, U., Klarner, M., Grover, L. M., Barralet, J. E., and Gbureck, U., *3D printing of β-tricalcium phosphate ceramics*. Dental Materials, 2009. 25(5): p. e18-e19.
52. Beaman, J., Atwood, C., Bergman, T. L., Bourell, D., Hollister, S., and Rosen, D., *Assessment of European Research and Development in Additive/Subtractive Manufacturing*. Final report from WTEC panel. 2004.
53. Sherwood, J. K., Riley, S. L., Palazzolo, R., Brown, S. C., Monkhouse, D. C., Coates, M., Linda G. G., Lee K. L., and Ratcliffe, A., *A three-dimensional osteochondral composite scaffold for articular cartilage repair*. Biomaterials, 2002. 23(24): p. 4739-4751.
54. Greulich, M., M. Greul, and T. Pintat, *Fast, functional prototypes via multiphase jet solidification.* Rapid Prototyping Journal, 1995. 1(1): p. 20-25.
55. Xiong, Z., Yan, Y., Zhang, R., and Sun, L., *Fabrication of porous poly(L-lactic acid) scaffolds for bone tissue engineering via precise extrusion*. Scripta Materialia, 2001. 45(7): p. 773-779.
56. Wang, F., Shor, L., Darling, A., Khalil, S., Sun, W., Güçeri, S., and Lau, A, *Precision extruding deposition and characterization of cellular poly-epsilon-caprolactone tissue scaffolds*. Rapid Prototyping Journal, 2004. 10(1): p. 42-49.
57. Woodfield, T. B., Malda, J., De Wijn, J., Peters, F., Riesle, J., and van Blitterswijk, C. A., *Design of porous scaffolds for cartilage tissue engineering using a three-dimensional fiber-deposition technique*. Biomaterials, 2004. 25(18): p. 4149-4161.

58. Cesarano, J., *A review of robocasting technology, in Solid Freeform and Additive Fabrication*, D. Dimos, S.C. Danforth, and M.J. Cima, Editors. 1999, Materials Research Society: Warrendale. p. 133-139.
59. Landers, R. and R. Mulhaupt, *Desktop manufacturing of complex objects, prototypes and biomedical scaffolds by means of computer-assisted design combined with computer-guided 3D plotting of polymers and reactive oligomers*. Macromolecular Materials and Engineering, 2000. 282(9): p. 17-21.
60. Vozzi, G., Flaim, C. J., Bianchi, F., Ahluwalia, A., and Bhatia, S., *Microfabricated PLGA scaffolds: a comparative study for application to tissue engineering*. Materials Science & Engineering C-Biomimetic and Supramolecular Systems, 2002. 20(1-2): p. 43-47.
61. Xiong, Z., Yan, Y., Wang, S., Zhang, R., and Zhang, C., *Fabrication of porous scaffolds for bone tissue engineering via low-temperature deposition*. Scripta Materialia, 2002. 46(11): p. 771-776.
62. Grida, I. and J.R.G. Evans, *Extrusion freeforming of ceramics through fine nozzles*. Journal of the European Ceramic Society, 2003. 23(5): p. 629-635.
63. Qiu, D. and N. Langrana, A., *Void eliminating toolpath for extrusion-based multi-material layered manufacturing*. Rapid Prototyping Journal, 2002. 8(1): p. 38 - 45.
64. Hsieh, C.-T. and N.A. Langrana, *A System Approach in Extrusion-Based Multi-Material CAD*, Solid Freeform Fabrication Symposium, Austin, Texas, The University of Texas.2001.
65. Brennan, R. E., Turcu, S., Hall, A., Hagh, N. M., and Safari, A., *Fabrication of Electroceramic Components by Layered Manufacturing (LM)*. Ferroelectrics, 2003. 293(1): p. 3-17.
66. Allahverdi, M., Danforth, S. C., Jafari, M., and Safari, A., *Processing of advanced electroceramic components by fused deposition technique.* Journal of the European Ceramic Society, 2001. 21(10–11): p. 1485-1490.
67. Pilleux, M. E., Safari, A., Allahverdi, M., Chen, Y., Lu, Y., and Jafari, M. A., *3-D photonic bandgap structures in the microwave regime by fused deposition of multimaterials*. Rapid Prototyping Journal, 2002. 8(1): p. 46–52.
68. Lu, X., Lee, Y., Yang, S., Hao, Y., Evans, J. R., and Parini, C. G., *Fine lattice structures fabricated by extrusion freeforming: process variables*. Journal of Materials Processing Technology, 2009. 209(10): p. 4654-46614661.
69. Lu, X., Lee, Y., Yang, S., Hao, Y., Evans, J. R., and Parini, C. G., *Solvent-based paste extrusion solid freeforming*. Journal of the European Ceramic Society, 2010. 30(1): p. 1-1010.
70. Xiong, Z., Yan, Y., Wang, S., Zhang, R., and Zhang, C., *Fabrication of porous scaffolds for bone tissue engineering via low-temperature deposition*. Scripta Materialia, 2002. 46(11): p. 771-776.
71. Liu, L., Xiong, Z., Yan, Y., Zhang, R., Wang, X., and Jin, L., *Multinozzle Low-Temperature Deposition System for Construction of Gradient Tissue*

Engineering Scaffolds. Journal of Biomedical Materials Research Part B-Applied Biomaterials, 2008. 88B(1): p. 254-263.
72. Liu, L., Xiong, Z., Zhang, R., Jin, L., and Yan, Y., *A Novel Osteochondral Scaffold Fabricated via Multi-nozzle Low-temperature Deposition Manufacturing*. Journal of Bioactive and Compatible Polymers, 2009. 24: p. 18-30.
73. Malone, E. and H. Lipson. *Multi-Material Freeform Fabrication of Active Systems*. ASME 9th Biennial Conference on Engineering Systems Design and Analysis 2008. Haifa, Israel.
74. Malone, E., Rasa, K., Cohen, D., Isaacson, T., Lashley, H., and Lipson, H., *Freeform fabrication of zinc-air batteries and electromechanical assemblies*. Rapid Prototyping Journal, 2004. 10(1): p. 58-69.
75. Daniel, P., M. Evan, and L. Hod, *Printing Embedded Circuits*, Solid Freeform Fabrication Symposium, Austin, Texas, The University of Texas. 2007.
76. Ang, T. H., Sultana, F. S. A., Hutmacher, D. W., Wong, Y. S., Fuh, J. Y. H., Mo, X. M., Loh, H.T., Burdet, E. and Teoh, S. H., *Fabrication of 3D chitosan-hydroxyapatite scaffolds using a robotic dispensing system*. Materials Science & Engineering C-Biomimetic and Supramolecular Systems, 2002. 20(1-2): p. 35-42.
77. Geng, L., Feng, W., Hutmacher, D. W., San Wong, Y., Tong Loh, H., and Fuh, J. Y., *Direct writing of chitosan scaffolds using a robotic system*. Rapid Prototyping Journal, 2005. 11(2): p. 90-9797.
78. Domingos, M., Chiellini, F., Gloria, A., Ambrosio, L., Bartolo, P., and Chiellini, E., *Effect of process parameters on the morphological and mechanical properties of 3D Bioextruded poly(epsilon-caprolactone) scaffolds*. Rapid Prototyping Journal, 2012. 18(1): p. 56-67.
79. Domingos, M., Dinucci, D., Cometa, S., Alderighi, M., Bártolo, P. J., and Chiellini, F. (, *Polycaprolactone Scaffolds Fabricated via Bioextrusion for Tissue Engineering Applications*. International journal of biomaterials, 2009: p. 239643.
80. Schuurman, W., Khristov, V., Pot, M. W., Van Weeren, P. R., Dhert, W. J. A., and Malda, J., *Bioprinting of hybrid tissue constructs with tailorable mechanical properties*. Biofabrication, 2011. 3(2): p. 021001.
81. Jafari, M. A., Han, W., Mohammadi, F., Safari, A., Danforth, S. C., and Langrana, N., *A novel system for fused deposition of advanced multiple ceramics*. Rapid Prototyping Journal, 2000. 6(3): p. 161-175.
82. Das, S., *Physical Aspects of Process Control in Selective Laser Sintering of Metals*. Advanced Engineering Materials, 2003. 5(10): p. 701-711.
83. Gu, D. and Y. Shen, *Balling phenomena in direct laser sintering of stainless steel powder: Metallurgical mechanisms and control methods*. Materials & Design, 2009. 30(8): p. 2903-2910.
84. Kruth, J. P., Levy, G., Klocke, F., and Childs, T. H. C., *Consolidation phenomena in laser and powder-bed based layered manufacturing*. CIRP Annals - Manufacturing Technology, 2007. 56(2): p. 730-759.
85. Kumar, S., *Selective laser sintering: A qualitative and objective approach*. JOM, 2003. 55(10): p. 43-47.

86. Tolochko, N. K., Khlopkov, Y. V., Mozzharov, S. E., Ignatiev, M. B., Laoui, T., and Titov, V. I., *Absorptance of powder materials suitable for laser sintering*. Rapid Prototyping Journal, 2000. 6(3): p. 155 - 161.
87. Glardon, R., Karapatis, N., Romano, V., and Levy, G. N., *Influence of Nd:YAG Parameters on the Selective Laser Sintering of Metallic Powders*. CIRP Annals - Manufacturing Technology, 2001. 50(1): p. 133-136.
88. Savalani, M.M., L. Hao, and R.A. Harris*, Evaluation of CO_2 and Nd:YAG Lasers for the Selective Laser Sintering of HAPEX®*. Proceedings of the Institution of Mechanical Engineers, Part B: Journal of Engineering Manufacture, 2006. 220(2): p. 171-182.
89. Regenfuss, P., Streek, A., Hartwig, L., Klötzer, S., Brabant, T., Horn, M., Ebert, R., and Exner, H., *Principles of laser micro sintering*. Rapid Prototyping Journal, 2007. 13(4): p. 204-212.
90. Zhou, C., Chen, Y., Yang, Z. G., and Khoshnevis, B., *Development of a Multi-material Mask-Image-Projection-based Stereolithography for the Fabrication of Digital Materials*, Solid Freeform Fabrication Symposium, Austin, Texas, The University of Texas.2011. p. 65-80.
91. Liew, C. L., Leong, K. F., Chua, C. K., and Du, Z., *Dual Material Rapid Prototyping Techniques for the Development of Biomedical Devices*. Part 1: Space Creation. The International Journal of Advanced Manufacturing Technology, 2001. 18(10): p. 717-723.
92. Liew, C. L., Leong, K. F., Chua, C. K., and Du, Z., *Dual Material Rapid Prototyping Techniques for the Development of Biomedical Devices. Part 2: Secondary Powder Deposition*. The International Journal of Advanced Manufacturing Technology, 2002. 19(9): p. 679-687.
93. Hopkinson, N., R. Hague, and P. Dickens, *Rapid Manufacturing: An Industrial Revolution for the Digital Age*. 2006: Wiley.
94. Schwendner, K. I., Banerjee, R., Collins, P. C., Brice, C. A., and Fraser, H. L., *Direct laser deposition of alloys from elemental powder blends*. Scripta Materialia, 2001. 45(10): p. 1123-1129.
95. Krishna, B. V., Xue, W., Bose, S., and Bandyopadhyay, A., *Functionally graded Co–Cr–Mo coating on Ti–6Al–4V alloy structures.* Acta Biomaterialia, 2008. 4(3): p. 697-706.
96. Shin, K. H., Natu, H., Dutta, D., and Mazumder, J., *A method for the design and fabrication of heterogeneous objects*. Materials & Design, 2003. 24(5): p. 339-353.
97. Liu, W. and J.N. DuPont, *Fabrication of functionally graded TiC/Ti composites by Laser Engineered Net Shaping*. Scripta Materialia, 2003. 48(9): p. 1337-1342.
98. Bandyopadhyay, A., Krishna, B., Xue, W., and Bose, S., *Application of Laser Engineered Net Shaping (LENS) to manufacture porous and functionally graded structures for load bearing implants*. Journal of Materials Science: Materials in Medicine, 2009. 20(1): p. 29-34.
99. Zeng, X., Li, X., Liu, J., and Qi, X., *Direct fabrication of electric components on insulated boards by laser microcladding electronic pastes*. Advanced Packaging, IEEE Transactions on, 2006. 29(2): p. 291-294.

100. Bailey, S. A., Cham, J. G., Cutkosky, M. R., and Full, R. J., *Biomimetic robotic mechanisms via shape deposition manufacturing*. Robotics Research, ed. J.M. Hollerbach and D.E. Koditschek. 2000, Godalming: Springer-Verlag London Ltd. 403-410.
101. Dollar, A. M., Wagner, C. R., and Howe, R. D., *Embedded sensors for biomimetic robotics via shape deposition manufacturing*, IEEE Ras-Embs International Conference on Biomedical Robotics and Biomechatronics, New York., Vols 1-3. 2006, p. 43-48.
102. Cooper, K.G., *Rapid Prototyping Technology: Selection and Application*. 2001: Marcel Dekker, Inc.
103. Dai, K. and L. Shaw, *Thermal and stress modeling of multi-material laser processing*. Acta Materialia, 2001. 49(20): p. 4171-4181.
104. Klosterman, D., Chartoff, R., Graves, G., Osborne, N., and Priore, B., *Interfacial characteristics of composites fabricated by laminated object manufacturing*. Composites Part A: Applied Science and Manufacturing, 1998. 29(9–10): p. 1165-1174.
105. Klosterman, D. A., Chartoff, R. P., Osborne, N. R., Graves, G. A., Lightman, A., Han, G., Bezeredi, A. and Rodrigues, S., *Development of a curved layer LOM process for monolithic ceramics and ceramic matrix composites.* Rapid Prototyping Journal, 1999. 5(2): p. 61-71.
106. Griffin, E.A., D.R. Mumm, and D.B. Marshall, *Rapid prototyping of functional ceramic composites*. American Ceramic Society Bulletin, 1996. 75(7): p. 65-68.
107. Rodrigues, S. J., Chartoff, R. P., Klosterman, D. A., Agarwala, M., and Hecht, N., *Solid Freeform Fabrication of Functional Silicon Nitride Ceramics by Laminated Object Manufacturing*. Solid Freeform Fabrication Symposium, Austin, Texas, The University of Texas. 2000.
108. Travitzky, N., Windsheimer, H., Fey, T., and Greil, P., *Preceramic Paper-Derived Ceramics*. Journal of the American Ceramic Society, 2008. 91(11): p. 3477-3492.
109. Zhang, Y., He, X., Du, S., and Zhang, J., *Al_2O_3 Ceramics Preparation by LOM (Laminated Object Manufacturing)*. The International Journal of Advanced Manufacturing Technology, 2001. 17(7): p. 531-534.
110. Windsheimer, H., Travitzky, N., Hofenauer, A., and Greil, P., *Laminated Object Manufacturing of Preceramic-Paper-Derived Si-SiC Composites*. Advanced Materials, 2007. 19(24): p. 4515-4519.
111. Gomes, C. M., Rambo, C. R., De Oliveira, A. P. N., Hotza, D., Gouveˆa, D., Travitzky, N., and Greil, P., *Colloidal Processing of Glass–Ceramics for Laminated Object Manufacturing*. Journal of the American Ceramic Society, 2009. 92(6): p. 1186-1191.
112. White, D.R., *Ultrasonic consolidation of aluminum tooling*. Advanced Materials & Processes, 2003. 161(1): p. 64-65.
113. Ram, G.D.J., C. Robinson, and B.E. Stucker, *Multi-Material Ultrasonic Consolidation.* Solid Freeform Fabrication Symposium, Austin, Texas, The University of Texas. 2006.

114. Janaki Ram, G. D., Robinson, C., Yang, Y., and Stucker, B. E., *Use of ultrasonic consolidation for fabrication of multi-material structures*. Rapid Prototyping Journal, 2007. 13(4): p. 226-235.
115. Siggard, E. J., Madhusoodanan, A. S., Stucker, B., and Eames, B., *Structurally Embedded Electrical Systems Using Ultrasonic Consolidation (UC).* Solid Freeform Fabrication Symposium, Austin, Texas, The University of Texas. 2007.
116. Swank, M.L. and B.E. Stucker, *Investigation of Support Materials for use in Ultrasonic Consolidation.* Solid Freeform Fabrication Symposium, Austin, Texas, The University of Texas. 2009. p. 231-256256.
117. Friel, R.J. and R.A. Harris, *A nanometre-scale fibre-to-matrix interface characterization of an ultrasonically consolidated metal matrix composite*. Proceedings of the Institution of Mechanical Engineers, Part L: Journal of Materials Design and Applications, 2010. 224: p. 31-40.
118. Yang, Y., G.D.J. Ram, and B.E. Stucker, *Process Parameters Optimization for Ultrasonically Consolidated Fiber-Reinforced Metal Matrix Composites.* Solid Freeform Fabrication Symposium, Austin, Texas, The University of Texas. 2006.
119. Liou, F.W., *Rapid prototyping and engineering applications: a toolbox for prototype development*. 2007: CRC Press.
120. Obielodan, J. O., Ram, G. J., Stucker, B. E., and Taggart, D. G., *Minimizing Defects Between Adjacent Foils in Ultrasonically Consolidated Parts*. Journal of Engineering Materials and Technology, 2010. 132(1): p. 011006-8.
121. Obielodan, J. O., Ceylan, A., Murr, L. E., and Stucker, B. E., *Multi-material bonding in ultrasonic consolidation*. Rapid Prototyping Journal, 2010. 16(3): p. 180-188.
122. Lopes, A.J., E. MacDonald, and R.B. Wicker, *Integrating stereolithography and direct print technologies for 3D structural electronics fabrication*. Rapid Prototyping Journal, 2012. Vol. 18 (2): p. 129 - 143.
123. Paulsen, J., Renn, M., Christenson, K., and Plourde, R., *Printing conformal electronics on 3D structures with Aerosol Jet technology*. Future of Instrumentation International Workshop (FIIW), 2012. 2012.
124. Robinson, C. J., Stucker, B., Lopes, A. J., Wicker, R., and Palmer, J., *Integration of Direct-Write (DW) and Ultrasonic Consolidation (UC) Technologies to Create Advanced Structures with Embedded Electrical Circuitry.* Solid Freeform Fabrication Symposium, Austin, Texas, The University of Texas. 2006.
125. Swank, M. L., Stucker, B. E., Medina, F. R., and Wicker, R. B., *Integrating UC and FDM to Create a Support Materials Deposition System.* Solid Freeform Fabrication Symposium, Austin, Texas, The University of Texas. 2009.
126. Periard, D., E. Malone, and H. Lipson. *Printing Embedded Circuits*. Solid Freeform Fabrication Symposium, Austin, Texas, The University of Texas. 2007.

127. Malone, E. and H. Lipson. *MULTI-MATERIAL FREEFORM FABRICATION OF ACTIVE SYSTEMS*. Proceedings of the 9th Biennial ASME Conference on Engineering Systems Design and Analysis ESDA08. 2008. Haifa, Israel.
128. Malone, E. and H. Lipson., *Solid Freeform Fabrication for Autonomous Manufacturing of Complete Mobile Robots*. Solid Freeform Fabrication Symposium, Austin, Texas, The University of Texas. 2004.
129. Duty, C., D. Jean, and W.J. Lackey, *Laser chemical vapour deposition: materials, modelling, and process control*. International Materials Reviews, 2001. 46(6): p. 271-287.
130. Crocker, J. E., Harrison, S., Sun, L., Shaw, L. L., and Marcus, H. L., *Using SALDVI and SALD with multi-material structures*. JOM, 1998. 50(12): p. 21-23.
131. Jakubenas, K.J., J.M. Sanchez, and H.L. Marcus, *Multiple material solid free-form fabrication by selective area laser deposition*. Materials & Design, 1998. 19(1–2): p. 11-18.
132. Westberg, H., Boman, M., Johansson, S., and Schweitz, J. Å., *Free-standing silicon microstructures fabricated by laser chemical processing*. Journal of Applied Physics, 1993. 73(11): p. 7864-7871.
133. Vargas Garcia, J.R. and T. Goto, *Chemical vapor deposition of iridium, platinum, rhodium and palladium*. Materials Transactions, 2003. 44(9): p. 1717-17281728.
134. Choy, K.L., *Chemical vapour deposition of coatings*. Progress in Materials Science, 2003. 48(2): p. 57-170.
135. Pegna, J. *Application of Cementitious Bulk Materials to Site Processed Solid Freeform Construction*. Solid Freeform Fabrication Symposium, Austin, Texas, The University of Texas. 1995.
136. Pegna, J., Pattofatto, S., Berge, R., Bangalan, C., Herring, H., LeSaux, M., and Engler, J., *THE SAND-PAINTER: Two-dimensional powder deposition*, Solid Freeform Fabrication Symposium, Austin, Texas, The University of Texas.1999.
137. James Santosa, D.J.a.S.D. *Experimental and numerical study on the flow of fine powders from small-scale hoppers applied to SLS multi-material deposition-Part I*. Solid Freeform Fabrication Symposium, Austin, Texas, The University of Texas. 2002.
138. Kumar, P., Santosa, J. K., Beck, E., and Das, S., *Direct-write deposition of fine powders through miniature hopper-nozzles for multi-material solid freeform fabrication*. Rapid Prototyping Journal, 2004. 10(1): p. 14-23.
139. Matsusaka, S., M. Urakawa, and H. Masuda, *Micro-feeding of fine powders using a capillary tube with ultrasonic vibration*. Advanced Powder Technology, 1995. 6(4): p. 283-293.
140. Takehiro, T. and T. Yoshiro, *Excitation of a progressive wave in a lossy ultrasonic transmission line and an application to a powder-feeding device*. Smart Materials and Structures, 1998. 7(3): p. 417.
141. Yang, S. and J.R.G. Evans, *A multi-component powder dispensing system for three dimensional functional gradients*. Materials Science & Engineering A (Structural Materials: Properties, Microstructure and Processing), 2004. A379(1-2): p. 351-9.

142. Yang, S. and J.R.G. Evans, *Acoustic control of powder dispensing in open tubes*. Powder Technology, 2004. 139(1): p. 55-60.
143. Evans, J.R.G. and S. Yang, *Flow rate of metal powders at reduced and elevated air pressure*. Powder Technology, 2005. 154(2-3): p. 95-8.
144. Lu, X., S. Yang, and J.R.G. Evans, *Microfeeding with different ultrasonic nozzle designs.* Ultrasonics, 2009. 49(6-7): p. 514-21.
145. Yang, S. and J.R.G. Evans, *Metering and dispensing of powder; the quest for new solid freeforming techniques*. Powder Technology, 2007. 178(1): p. 56-72.
146. Lu, X., Yang, S., Chen, L., and Evans, J. R., *Dry Powder Microfeeding System for Solid Freeform Fabrication*, Solid Freeform Fabrication Symposium, Austin, Texas, The University of Texas. 2006.
147. Lu, X., S. Yang, and J.R.G. Evans, *Studies on ultrasonic microfeeding of fine powders.* Journal of Physics D: Applied Physics, 2006. 39(11): p. 2444.
148. Yashchuk, V. V., Sushkov, A. O., Budker, D., Lee, E. R., Lee, I. T., and Perl, M. L., *Production of dry powder clots using a piezoelectric drop generator*. Review of Scientific Instruments, 2002. 73(6): p. 2331-2335.
149. Das, S., Hollister, S. J., Krebsbach, P. H., and Santosa, J. K., *Solid freeform fabrication of structurally engineered multifunctional devices*. 2009: US.
150. Jiang, Y., Matsusaka, S., Masuda, H., and Qian, Y. (2009). Development of measurement system for powder flowability based on vibrating capillary method., *Development of measurement system for powder flowability based on vibrating capillary method*. Powder Technology, 2009. 188(3): p. 242-247.
151. Pham, D.T. and S.S. Dimov, *Rapid Manufacturing : The Technologies and Applications of Rapid Prototyping and Rapid Tooling*. 2001: Springer-Verlag.
152. Weiss, L. E., Merz, R., Prinz, F. B., Neplotnik, G., Padmanabhan, P., Schultz, L., and Ramaswami, K., *Shape deposition manufacturing of heterogenous structures*. Journal of Manufacturing Systems, 1997. 16: p. 239–248.
153. Cooper, A. G., Kang, S., Kietzman, J. W., Prinz, F. B., Lombardi, J. L., and Weiss, L. E., *Automated fabrication of complex molded parts using Mold Shape Deposition Manufacturing*. Materials & Design, 1999. 20(2–3): p. 83-89.
154. Cutkosky, M. R., and Kim, S., *Design and fabrication of multi-material structures for bioinspired robots*. Physical and Engineering Sciences, 2009. 367: p. 1799–1813.
155. Dollar, A.M. and R.D. Howe, *A robust compliant grasper via shape deposition manufacturing*. IEEE-ASME Transactions on Mechatronics, 2006. 11(2): p. 154-161.
156. Cutkosky, M.R. and S. Kim, *Design and fabrication of multi-material structures for bioinspired robots*. Philosophical Transactions of the Royal Society a-Mathematical Physical and Engineering Sciences, 2009. 367(1894): p. 1799-1813.

157. Weiss, L. E., Prinz, F. B., Neplotnik, G., Padmanabhan, P., Schultz, L., and Merz, R., *Shape Deposition Manufacturing of wearable computers*. Solid Freeform Fabrication Symposium, Austin, Texas, The University of Texas. 1996. p. 31-38.
158. Dollar, A.M., C.R. Wagner, and R.D. Howe, *Embedded sensors for biomimetic robotics via shape deposition manufacturing*. IEEE RAS & EMBS International Conference on Biomedical Robotics and Biomechatronics, 2006: p. 6 pp.-6 pp.6 pp.
159. Binnard, M. and M.R. Cutkosky, *Design by Composition for Layered Manufacturing*. Journal of Mechanical Design, 2000. 122(1): p. 91-101.
160. Ennis, B.J., J. Green, and R. Davies, *The legacy of neglect in the US*. Chemical engineering progress, 1994. 90(4): p. 32-43.
161. Bates, L., The need for industrial education in bulk technology. Bulk Solids Handling, 2006. 26: p. 464-473.
162. Rao, K.K. and P.R. Nott, *An Introduction to Granular Flow*. 2008: Cambridge University Press.
163. Wassgren, C. R., Hunt, M. L., Freese, P. J., Palamara, J., and Brennen, C. E., *Effects of vertical vibration on hopper flows of granular material*. Physics of Fluids (1994-present), 2002. 14(10): p. 3439-3448.
164. Lumay, G., Boschini, F., Traina, K., Bontempi, S., Remy, J. C., Cloots, R., and Vandewalle, N., *Measuring the flowing properties of powders and grains. Powder Technology*, 2012. 224: p. 19-27.
165. Jaeger, H.M., S.R. Nagel, and R.P. Behringer, *Granular solids, liquids, and gases*. Reviews of Modern Physics, 1996. 68(4): p. 1259.
166. Jaeger, H.M., S.R. Nagel, and R.P. Behringer, *The physics of granular materials*. Physics Today, 2008. 49(4): p. 32-38.
167. Areskoug, T., Ed, O., Nilsson, M. and Sundqvist, M., *Consolidation properties of powder formulations*. 2013, Lund University.
168. Woodcock, C. and J. Mason, *Bulk solids handling: an introduction to the practice and technology*. 1988: Springer.
169. Staniforth, J. and M. Aulton, *Powder flow. Pharmaceutics: the science of dosage form design.* 2002: p. 197-210.
170. Schulze, D., *Powders and Bulk Solids: Behavior, Characterization, Storage and Flow*. 2007: Springer.
171. Stanley-Wood, N., *Bulk powder properties: instrumentation and techniques. Bulk Solids Handling: Equipment Selection and Operation.* 2008: p. 1-67.
172. Neumann, B.S., *The flow properties of powders. Advances in pharmaceutical sciences.* 1967. 2: p. 191.
173. Jones, T. and N. Pilpel, *The flow properties of granular magnesia. Journal of Pharmacy and Pharmacology*. 1966. 18(2): p. 81-93.
174. Danish, F.Q. and E. Parrott, *Flow rates of solid particulate pharmaceuticals.* Journal of pharmaceutical sciences, 1971. 60(4): p. 548-554.
175. Pilpel, N., *The flow properties of magnesia. Journal of Pharmacy and Pharmacology.* 1964. 16(11): p. 705-716.

176. Rumpf, H., *The strength of granules and agglomerates*. in: W.A. Knepper (Ed.) Agglomeration. 1962, John Wiley, New York, pp.379-418.
177. Zeng, X.M., G.P. Martin, and C. Marriott, *Particulate Interactions in Dry Powder Formulation for Inhalation*. 2000: Taylor & Francis.
178. Ridgway, K. and R. Rupp, *The mixing of powder layers on a chute: the effect of particle size and shape*. Powder Technology, 1971. 4(4): p. 195-202.
179. Harwood, C. and N. Pilpel, *The flow of granular solids through circular orifices*. Journal of Pharmacy and Pharmacology, 1969. 21(11): p. 721-730.
180. Upadhyaya, G., *Powder metallurgy technology*. Cambridge Int Science Publishing. 1997.
181. Liu, L. X., Marziano, I., Bentham, A. C., Litster, J. D., White, E. T., & Howes, T., *Effect of particle properties on the flowability of ibuprofen powders*. International Journal of Pharmaceutics, 2008. 362(1): p. 109-117.
182. Yu, W., Muteki, K., Zhang, L., and Kim, G., *Prediction of bulk powder flow performance using comprehensive particle size and particle shape distributions.* Journal of pharmaceutical sciences, 2011. 100(1): p. 284-293.
183. Geldart, D., E.C. Abdullah, and A. Verlinden, *Characterisation of dry powders.* Powder Technology, 2009. 190(1–2): p. 70-74.
184. Schwedes, J. and D. Schulze, *Measurement of flow properties of bulk solids*. Powder Technology, 1990. 61(1): p. 59-68.
185. Prescott, J.K. and R.A. Barnum, *On powder flowability*. Pharmaceutical technology, 2000. 24(10): p. 60-84.
186. Schwedes, J., *Review on testers for measuring flow properties of bulk solids*. Granular Matter, 2003. 5(1): p. 1-43.
187. Ortega-Rivas, E., *Unit Operations of Particulate Solids: Theory and Practice*. Taylor & Francis. 2011.
188. Masuda, H., K. Higashitani, and H. Yoshida, *Powder Technology Handbook*, Third Edition. Taylor & Francis. 2006.
189. Jenike, A.W., *Storage and flow of solids.* bulletin no. 123. Bulletin of the University of Utah, 1964. 53(26).
190. Geldart, D., *Types of gas fluidization*. Powder Technology, 1973. 7(5): p. 285-292.
191. Chi-Ying Wong, A., *Characterisation of the flowability of glass beads by bulk densities ratio*. Chemical Engineering Science, 2000. 55(18): p. 3855-3859.
192. Roberts, T. and J. Beddow, *Some effects of particle shape and size upon blinding during sieving*. Powder Technology, 1968. 2(2): p. 121-124.
193. Adler, A., *Flow properties of metal powders*. INT J POWDER MET, 1969. 5(1): p. 7-20.
194. Li, Q., Rudolph, V., Weigl, B., and Earl, A., *Interparticle van der Waals force in powder flowability and compactibility*. International Journal of Pharmaceutics, 2004. 280(1): p. 77-93.

195. McGlinchey, D., *Bulk solids handling: equipment selection and operation*. 2008: Blackwell Pub.
196. Carr, R.L., *Evaluating flow properties of solids*. Chem. Eng, 1965. 72(2): p. 163-168.
197. Aulton, M.E., *Pharmaceutics: The Science of Dosage Form Design*. Churchill Livingstone. 2002.
198. Institution, B.S., *Part 2: Determination of Angle of Repose*. 1970, London: BSI.
199. Carr, R., *Powder and granule properties and mechanics*. 1976: Marcel Dekker, Inc., New York.
200. McGlinchey, D., *Characterisation of Bulk Solids*. 2005: Blackwell.
201. Geldart, D., M. Mallet, and N. Rolfe. *Assessing the flowability of powders using angle of repose*. Powder Handling & Proc. 1990.
202. Roberts, A.W., *Characterisation for hopper and stockpile design.* Characterisation of Bulk Solids, 2005: p. 85-131.
203. Brown, L., *Experiments on the resistance of sand to motion through tubes, with especial reference to its use in the blasting of rocks, made at Fort Adams, Newport harbour, under the direction of col. Totten*. Journal of the Franklin Institute, 1836. 22(2): p. 73-81.
204. Kaza, K. and R. Jackson, *The rate of discharge of coarse granular material from a wedge-shaped mass flow hopper*. Powder Technology, 1982. 33(2): p. 223-237.
205. Tejchman, J., *Confined Granular Flow in Silos: Experimental and Numerical Investigations*. Springer. 2013.
206. Rhodes, M.J., Introduction to Particle Technology. 2008: Wiley.
207. Fitzpatrick, J., S. Barringer, and T. Iqbal, *Flow property measurement of food powders and sensitivity of Jenike's hopper design methodology to the measured values*. Journal of Food Engineering, 2004. 61(3): p. 399-405.
208. Beverloo, W.A., H.A. Leniger, and J. van de Velde, *The flow of granular solids through orifices.* Chemical Engineering Science, 1961. 15(3–4): p. 260-269.
209. To, K., P.-Y. Lai, and H. Pak, *Jamming of granular flow in a two-dimensional hopper*. Physical review letters, 2001. 86(1): p. 71.
210. Zuriguel, I., Garcimartín, A., Maza, D., Pugnaloni, L. A., and Pastor, J. M., *Jamming during the discharge of granular matter from a silo.* Physical Review E, 2005. 71(5): p. 051303.
211. Masuda, T., K. Nishinari, and A. Schadschneider, *Critical Bottleneck Size for Jamless Particle Flows in Two Dimensions*. Physical review letters, 2014. 112(13): p. 138701.
212. Reisner, W., *The behaviour of granular materials in flow out of hoppers*. Powder Technology, 1968. 1(5): p. 257-264.
213. Schwedes, J., *Dimensionierung von Bunkern*. Aufbereitungs-Technik. 1969.
214. Jenike, A., *Gravity Flow of Bulk Solids*. University of Utah Engineering Experiment Station. Bulletin, 1961. 108.

215. Jenike, A.W. and T. Leser, *A flow-no-flow criterion in the gravity flow of powders in converging channels*. 1965.
216. Lozano, C., Lumay, G., Zuriguel, I., Hidalgo, R. C., and Garcimartín, A., *Breaking arches with vibrations: the role of defects*. Physical review letters, 2012. 109(6): p. 068001.
217. Janda, A., Harich, R., Zuriguel, I., Maza, D., Cixous, P., and Garcimartín, A., *Flow-rate fluctuations in the outpouring of grains from a two-dimensional silo*. Physical Review E, 2009. 79(3): p. 031302.
218. Brown, R. and J.C. Richards, *Principles of powder mechanics*. 1970.
219. Brown, R. and J. Richards, *Profile of flow of granules through apertures*. Trans. Inst. Chem. Eng, 1960. 38: p. 243-256.
220. Nedderman, R. M., Tüzün, U., Savage, S. B., and Houlsby, G. T., *The flow of granular materials—I: Discharge rates from hoppers*. Chemical Engineering Science, 1982. 37(11): p. 1597-1609.
221. Tighe, B.P. and M. Sperl, *Pressure and motion of dry sand: translation of Hagen's paper from 1852*. Granular Matter, 2007. 9(3-4): p. 141-144.
222. Nedderman, R.M., *Statics and kinematics of granular materials*. Cambridge University Press. 2005.
223. Zuriguel, I., Pugnaloni, L. A., Garcimartin, A., and Maza, D., *Jamming during the discharge of grains from a silo described as a percolating transition.* Physical Review E, 2003. 68(3): p. 030301.
224. Silos, B., *Draft Design Code for Silos, Bins, Bunkers and Hoppers*. British Materials Handling Board and British Standards Institution, London, 1987.
225. Benyamine, M., Djermane, M., Dalloz-Dubrujeaud, B., and Aussillous, P., Discharge flow of a bidisperse granular media from a silo. Physical Review E, 2014. 90(3): p. 032201.
226. Artega, P. and U. Tüzün, *Flow of binary mixtures of equal-density granules in hoppers—size segregation, flowing density and discharge rates.* Chemical Engineering Science, 1990. 45(1): p. 205-223.
227. Royal, T.A. and J.W. Carson, *Fine powder flow phenomena in bins, hoppers and processing vessels*. Bulk. 2000.
228. Kollmann, T. and J. Tomas. *THE INFLUENCE OF VIBRATIONS ON FLOW PROP-ERTIES OF COHESIVE POWDERS*. Int. Conf. Bulk Materials Storage, Handling and Transportation. 2001.
229. Janda, A., Maza, D., Garcimartín, A., Kolb, E., Lanuza, J., and Clément, E., *Unjamming a granular hopper by vibration*. EPL (Europhysics Letters), 2009. 87(2): p. 24002.
230. Mankoc, C., Garcimartín, A., Zuriguel, I., Maza, D., and Pugnaloni, L. A., *Role of vibrations in the jamming and unjamming of grains discharging from a silo*. Physical Review E, 2009. 80(1): p. 011309.
231. Langston, P. A., Matchett, A. J., Fraige, F. Y., and Dodds, J., *Vibration induced flow in hoppers: continuum and DEM model approaches.* Granular Matter, 2009. 11(2): p. 99-113.
232. Valdes, J.R. and J.C. Santamarina, *Clogging: bridge formation and vibration-based destabilization*. Canadian Geotechnical Journal, 2008. 45(2): p. 177-184.

233. Mori, S. *Vibro-fluidization of group-c particles and its industrial application*. AIChE Symp. Ser. 1990.
234. Jaraiz, E., S. Kimura, and O. Levenspiel, *Vibrating beds of fine particles: estimation of interparticle forces from expansion and pressure drop experiments*. Powder Technology, 1992. 72(1): p. 23-30.
235. Noda, K., Y. Mawatari, and S. Uchida, *Flow patterns of fine particles in a vibrated fluidized bed under atmospheric or reduced pressure*. Powder Technology, 1998. 99(1): p. 11-14.
236. Roberts, A.W. and O. Scott, *An investigation into the effects of sinusoidal and random vibrations on the strength and flow properties of bulk solids*. Powder Technology, 1978. 21(1): p. 45-53.
237. Arnold, P. and A. Kaaden, *Reducing hopper wall friction by mechanical vibration.* Powder Technology, 1977. 16(1): p. 63-66.
238. Fayed, M. and L. Otten, Handbook of Powder Science & Technology. 1997: Springer US.
239. Roberts, A., *Vibration of fine powders and its application*, Handbook of Powder Science & Technology. 1997, Springer. p. 146-201.
240. Xu, C. and J. Zhu, *Parametric study of fine particle fluidization under mechanical vibration.* Powder Technology, 2006. 161(2): p. 135-144.
241. Seville, J., U. Tüzün, and R. Clift, *Processing of particulate solids*. Blackie academic & professional London. 1997.
242. Mott, M. and J. Evans, *Zirconia/alumina functionally graded material made by ceramic ink jet printing*. Materials Science and Engineering: A, 1999. 271(1): p. 344-352.
243. Exner, H., Horn, M., Streek, A., Ullmann, F., Hartwig, L., Regenfuß, P., and Ebert, R., *Laser micro sintering: A new method to generate metal and ceramic parts of high resolution with sub-micrometer powder*. Virtual and Physical Prototyping, 2008. 3(1): p. 3-11.
244. Regenfuss, P., Streek, A., Hartwig, L., Klötzer, S., Brabant, T., Horn, M.,Ebert, R. and Exner, H., *Principles of laser micro sintering.* Rapid Prototyping Journal, 2007. 13(4): p. 204-212.
245. Yang, S.F. and J.R. Evans., *Preparing 3D functional gradients for SLS*. in Materials Science Forum. 2005: Trans Tech Publ.
246. Mumtaz, K.A. and N. Hopkinson, *Laser melting functionally graded composition of Waspaloy® and Zirconia powders.* Journal of materials science, 2007. 42(18): p. 7647-7656.
247. Liu, Z. H., Zhang, D. Q., Sing, S. L., Chua, C. K., and Loh, L. E., *Interfacial Characterisation of SLM Parts in Multi Material Processing: Metallurgical Diffusion between 316L Stainless Steel and C18400 Copper Alloy*. Materials Characterization, 2014.
248. Al-Jamal, O., S. Hinduja, and L. Li, *Characteristics of the bond in Cu–H13 tool steel parts fabricated using SLM*. CIRP Annals-Manufacturing Technology, 2008. 57(1): p. 239-242.
249. Kruth, J. P., Wang, X., Laoui, T., and Froyen, L., *Lasers and materials in selective laser sintering*. Assembly Automation, 2003. 23(4): p. 357-371.
250. Kumar, S. and J.-P. Kruth, *Composites by rapid prototyping technology*. Materials & Design, 2010. 31(2): p. 850-856.

251. Kruth, J. P., Levy, G., Klocke, F., and Childs, T. H. C., *Consolidation phenomena in laser and powder-bed based layered manufacturing*. CIRP Annals-Manufacturing Technology, 2007. 56(2): p. 730-759.
252. Regenfuss, P., R. Ebert, and H. Exner, *Laser Micro Sintering–a Versatile Instrument for the Generation of Microparts*. Laser Technik Journal, 2007. 4(1): p. 26-31.
253. Matsusaka, S., K. Yamamoto, and H. Masuda, *Micro-feeding of a fine powder using a vibrating capillary tube.* Advanced Powder Technology, 1996. 7(2): p. 141-151.
254. Li, X., H. Choi, and Y. Yang, *Micro rapid prototyping system for micro components.* Thin Solid Films, 2002. 420: p. 515-523.
255. Yang, S. and J.R. Evans, *Computer control of powder flow for solid freeforming by acoustic modulation.* Powder Technology, 2003. 133(1): p. 251-254.
256. Yang, S. and J.R. Evans, *A dry powder jet printer for dispensing and combinatorial research*. Powder Technology, 2004. 142(2): p. 219-222.
257. Yang, S. and J.R. Evans, *Acoustic control of powder dispensing in open tubes.* Powder Technology, 2004. 139(1): p. 55-60.
258. Yang, S. and J.R. Evans, Acoustic initiation of powder flow in capillaries. Chemical Engineering Science, 2005. 60(2): p. 413-421.
259. Yang, S. and J.R. Evans, *A multi-component powder dispensing system for three dimensional functional gradients.* Materials Science and Engineering: A, 2004. 379(1): p. 351-359.
260. Lu, X., S. Yang, and J.R. Evans, *Dose uniformity of fine powders in ultrasonic microfeeding*. Powder Technology, 2007. 175(2): p. 63-72.
261. Lu, X., S. Yang, and J.R. Evans, Microfeeding with different ultrasonic nozzle designs. Ultrasonics, 2009. 49(6): p. 514-521.
262. Qi, L., Zeng, X., Zhou, J., Luo, J., and Chao, Y., *Stable micro-feeding of fine powders using a capillary with ultrasonic vibration.* Powder Technology, 2011. 214(2): p. 237-242.
263. Chen, X., K. Seyfang, and H. Steckel, *Development of a micro dosing system for fine powder using a vibrating capillary. Part 1: The investigation of factors influencing on the dosing performance*. International Journal of Pharmaceutics, 2012. 433(1): p. 34-41.
264. Roper, D. A., Good, B. L., McCauley, R., Yarlagadda, S., Smith, J., Good, A., Pa, P. and Mirotznik, M. S., *Additive manufacturing of graded dielectrics.* Smart Materials and Structures, 2014. 23(4): p. 045029.
265. Yang, S. and J. Evans, *Metering and dispensing of powder; the quest for new solid freeforming techniques*. Powder Technology, 2007. 178(1): p. 56-72.
266. Stichel, T., Laumer, T., Baumüller, T., Amend, P., and Roth, S., *Powder Layer Preparation Using Vibration-controlled Capillary Steel Nozzles for Additive Manufacturing*. Physics Procedia, 2014. 56: p. 157-166.
267. Lu, X., Yang, S., Chen, L., and Evans, J. R., *Dry powder microfeeding system for solid freeform fabrication*. Solid Freeform Fabrication Symposium, Austin, Texas, The University of Texas. 2006.

268. Yang, S., M. Mohebi, and J. Evans, *A novel solid freeforming method using simultaneous part and mould construction*. Rapid Prototyping Journal, 2008. 14(1): p. 35-43.
269. Yang, S., *Apparatus and method for dispensing powders*. U.S. Patent No. 6,336,480. 8 Jan. 2002.
270. Evans, J.R.G., L. Xuesong, and Y. Shoufeng, *Dose uniformity of fine powders in ultrasonic microfeeding.* Powder Technology, 2007. 175(2): p. 63-72.
271. Anbar, M., *Cavitation during Impact of Liquid Water on Water: Geochemical Implications.* Science (New York, NY), 1968. 161(3848): p. 1343-1344.
272. Lee, E.R., *Microdrop Generation*. Taylor & Francis. 2010.
273. Storey, R.A. and I. Ymén, *Solid State Characterization of Pharmaceuticals*. Wiley. 2011.
274. Zimon, A.D., *Adhesion of dust and powder*. Springer Science & Business Media. 2012.
275. Sandler, N., Reiche, K., Heinämäki, J., and Yliruusi, J., *Effect of moisture on powder flow properties of theophylline.* Pharmaceutics, 2010. 2(3): p. 275-290.
276. Ketkar, A. and D. Keller Jr, *Adhesion of micron-sized limestone particles to a massive coal substrate.* The Journal of Adhesion, 1975. 7(3): p. 235-251.
277. Lu, X., S. Yang, and J.R. Evans, Ultrasound-assisted microfeeding of fine powders. Particuology, 2008. 6(1): p. 2-8.
278. Li, H., Mechanics of arching in a moving-bed standpipe with interstitial gas flow. Powder Technology, 1994. 78(2): p. 179-187.
279. Jing, S. and H. Li, An experimental study on the mechanics of arching in hoppers connected to a moving bed with negative pressure gradient. Powder Technology, 1998. 95(2): p. 143-151.
280. Tang, J. and R. Behringer, *How granular materials jam in a hopper*. Chaos-Woodbury, 2011. 21(4): p. 041107.
281. Oldal, I., Keppler, I., Csizmadia, B., and Fenyvesi, L., *Outflow properties of silos: The effect of arching*. Advanced Powder Technology, 2012. 23(3): p. 290-297.
282. Wang, W. and L. Li, *High-quality high-material-usage multiple-layer laser deposition of nickel alloys using sonic or ultrasonic vibration powder feeding.* Proceedings of the Institution of Mechanical Engineers, Part B: Journal of Engineering Manufacture, 2011. 225(1): p. 130-139.
283. Harnby, N., A. Hawkins, and D. Vandame, *The use of bulk density determination as a means of typifying the flow characteristics of loosely compacted powders under conditions of variable relative humidity*. Chemical Engineering Science, 1987. 42(4): p. 879-888.
284. Gray, W.A., *Packing of solid particles*. 1968.
285. Chen, X., K. Seyfang, and H. Steckel, *Integration of an in-line dose verification into a micro-dosing system for fine powders*. Pharmazeutische Industrie, 2011. 73(8): p. 1508-+.

286. Schulze, D., *Powders and Bulk Solids: Behavior, Characterization, Storage and Flow*. Springer. 2008.
287. Nedderman, R.M. and C. Laohakul, *The thickness of the shear zone of flowing granular materials.* Powder Technology, 1980. 25(1): p. 91-100.
288. Loverich, J.J., *Development of a new high specific power piezoelectric actuator*. The Pennsylvania State University. 2004.
289. Bradley, M., R. Berry, and R. Farnish, *Methods for design of hoppers. Silos, bins and bunkers for reliable gravity flow, for pharmaceutical, food, mineral and other applications*. 2011.
290. Mills, D., *Pneumatic Conveying Design Guide*. Elsevier Science. 2003.
291. Ludovico, A.D., A. Angelastro, and S.L. Campanelli, *Experimental Analysis of the Direct Laser Metal Deposition Process*. INTECH Open Access Publisher. 2010.
292. Castrejon-Pita, J. R., Baxter, W. R. S., Morgan, J., Temple, S., Martin, G. D., and Hutchings, I. M., *Future, opportunities and challenges of inkjet technologies*. Atomization and Sprays, 2013. 23(6).